Pablo José Fuentealba Durand

Intrinsic and Synaptic Membrane Properties of Neurons in the Thalamic Reticular Nucleus

Thèse présentée à la Faculté des études supérieures de l'Université Laval

dans le cadre du programme de doctorat en neurobiologie

pour l'obtention du grade de Philosophiae Doctor (Ph.D.)

FACULTÉ DE MÉDECINE

UNIVERSITÉ LAVAL

QUÉBEC

Novembre 2004

RESUMÉ

Le noyau réticulaire thalamique (RE) est une structure qui engendre des fuseaux, une oscillation bioélectrique de marque pendant les stades précoces du sommeil. De multiples propriétés neuronales, intrinsèques et synaptiques, sont impliquées dans la génération, la propagation, le maintien et la terminaison des ondes en fuseaux. D'un autre côté, ce rythme constitue un état spécial de l'activité du réseau qui est généré par le réseau lui-même et affecte les propriétés cellulaires du noyau RE. Cette étude se concentre sur ces sujets: comment les propriétés cellulaires et les propriétés du réseau sont inter-reliées et interagissent pour engendrer les ondes fuseaux dans les neurones du RE et leurs cibles, les neurones thalamocorticaux.

La présente thèse fournit de nouvelles évidences montrant le rôle fondamental joué par les neurones du noyau RE dans la genèse des ondes en fuseaux, dû aux synapses chimiques établies par ces neurones. La propagation et la synchronisation de l'activité sont modulées par les synapses électriques entre les neurones réticulaires thalamiques, mais aussi par les composantes dépolarisantes secondaires des réponses synaptiques évoquées par le cortex. De plus, la forme générale et la terminaison des oscillations thalamiques sont probablement contrôlées en grande partie par les neurones du RE, lesquels expriment une conductance intrinsèque leurs procurant une membrane avec un comportement bistable.

Finalement, les oscillations thalamiques en fuseaux sont aussi capables de moduler les propriétés membranaires et l'activité des neurones individuels du RE.

ABSTRACT

The thalamic reticular nucleus (RE) is a key structure related to spindles, a hallmark bioelectrical oscillation during early stages of sleep. Multiple neuronal properties, both intrinsic and synaptic, are implicated in the generation, propagation, maintenance and termination of spindle waves. On the other hand, this rhythm constitutes a special state of network activity, which is generated within, and affects single-cell properties of the RE nucleus. This study is focused on these topics: how cellular and network properties are interrelated and interact to generate spindle waves in the pacemaking RE neurons and their targets, thalamocortical neurons.

The present thesis provides new evidence showing the fundamental role played by the RE nucleus in the generation of spindle waves, due to chemical synapses established by its neurons. The propagation and synchronization of activity is modulated by electrical synapses between thalamic reticular neurons, but also by the secondary depolarizing component of cortically-evoked synaptic responses. Additionally, the general shaping and probably the termination of thalamic oscillations could be controlled to a great extent by RE neurons, which express an intrinsic conductance endowing them with membrane bistable behaviour. Finally, thalamic spindle oscillations are also able to modulate the membrane properties and activities of individual RE neurons.

SUMMARY

Thalamic reticular (RE) neurons, recorded and stained intracellularly *in vivo*, displayed spontaneously occurring spikelets, characteristic of central neurons coupled electrotonically via gap junctions. They were significantly different from excitatory postsynaptic potentials (EPSPs) and also distinct from synaptically generated fast prepotentials. Spikelets were strongly reduced by halothane, a blocker of gap junctions. Multi-site extracellular recordings performed before, during and after administration of halothane demonstrated a role for electrical coupling in the synchronization of spindling activity within the RE nucleus. Finally, computational models of RE neurons predicted that gap junctions between these neurons could mediate the spread of low-frequency activity at great distances.

A subgroup (20%) of RE neurons revealed the presence of membrane bistability, which consisted of two alternate membrane potentials, separated by ~17-20 mV. It was strongly voltage-dependent and only expressed under resting conditions. Addition of QX-314 in the recording micropipette either abolished or disrupted membrane bistability. Thalamocortical cells presented various patterns of spindling that reflected the membrane bistability in RE neurons. Finally, computer simulations predicted a role for RE neurons' membrane bistability in inducing various patterns of spindling in target thalamocortical cells.

To assess the consequences of spindle oscillations on the RE nucleus, recordings were performed during periods of intense synaptic activity as represented by spindle waves. RE neurons presented low-pass filter properties, strongly dumping frequencies higher than 10 Hz, the main component of spindle waves. During spindles, membrane potential was depolarized, membrane fluctuations increased in one order of magnitude, and the apparent input resistance decreased up to 80% in a cyclic way. Both synaptic and intrinsic responsiveness were enhanced during active network states.

We analyzed both the characteristics and possible mechanisms underlying a secondary component of the cortically elicited depolarization in RE neurons. Cortical stimulation evoked fixed and short-latency EPSPs. The evoked EPSPs included a secondary depolarizing component, which occurred as an all-or-none event at ~5 ms after the peak of the initial component that was voltage-dependent and sensitive to QX-314 in the recording micropipette. This late component affected the integrative properties of RE neurons, including their spiking output and temporal summation of incoming cortical inputs.

A subgroup of RE neurons (30%) presented prolonged hyperpolarizing potentials preceding spindles. These hyperpolarizations were present just before the onset of spontaneously occurring spindle waves, and could also be evoked by corticothalamic volleys. A drop in the apparent input resistance was associated with these hyperpolarizing potentials, precluding disfacilitation processes. The reversal potential was with the activation of slow K^+ conductances. QX-314 decreased both the amplitude and incidence

of hyperpolarizations. Simultaneous extracellular and intracellular recordings in the RE nucleus demonstrated that some RE neurons discharged during the hyperpolarizations. These data support the idea that spindles are initiated in the pacemaking RE nucleus.

ACKNOWLEDGEMENTS

The following thesis is presented in the form of a collection of scientific articles, either submitted or accepted for publication. The general introduction describes the theoretical context and experimental strategies of the studies described in the articles. The articles have been submitted to different scientific journals, and therefore the format of bibliographical citations changes from one to another. However, the other aspects concerning the presentation of results have been kept consistent. A general discussion of the results finalizes the thesis with the presentation of a model which integrates them in a coherent mode. The bibliography used for both introduction and discussion, is presented at the very end of the manuscript.

The thesis is mostly related to the pacemaking activity of RE nucleus in the generation of thalamic oscillations. However, at the end of the manuscript two studies related to neocortical neurons and their integrative properties have been also included.

I would like to use this occasion to express my gratitude to my thesis supervisor Dr. Mircea Steriade for the opportunity of working in his laboratory. Without his critics, discussions, corrections and support the present study would not have been possible.

I also would like to show my gratitude to Dr. Igor Timofeev for his help, especially for the experimental techniques and his scientific advises.

Finally, I would like to thank Mr. Pierre Guiguère for his technical and moral support in every moment.

This thesis is the result of a close collaboration during a period of over three years between Dr. Mircea Steriade, Dr. Igor Timofeev and the author. I would like also to express my gratitude to Dr. Sylvain Crochet, Dr. Terrence J. Sejnowski and Dr. Maxim Bazhenov, co-authors in some of the studies.

I would like to take the opportunity also to thank the organisms which provided financial support for the development of this project: Canadian Institute for Health Research, Human Frontier Research Program, National Institute of Neurological Disorders and Stroke, and Fonds de la Recherche en Santé de Québec.

Following, is the list of scientific articles where I have participated during the progress of my Ph.D. program:

1. **Fuentealba, P.,** Crochet, S., Timofeev, I. and Steriade, M. Synaptic interactions between thalamic and cortical inputs onto cortical neurons *in vivo*. *Journal of Neurophysiology* 91:1990-1998, 2004.
2. **Fuentealba, P.,** Crochet, S., Timofeev, I. Bazhenov, M., Sejnowski, T.J. and Steriade, M. Experimental evidence and modeling studies support a synchronizing role for electrical coupling in the cat thalamic reticular neurons *in vivo. European Journal of Neuroscience* 20(1): 111-119, 2004.

3. **Fuentealba, P.,** Timofeev, I. and Steriade, M. Prolonged hyperpolarizing potentials preceding spindles in thalamic reticular neurons. *Proceedings of the National Academy of Science USA* 101(26): 9816-9821, 2004.
4. Crochet, S., **Fuentealba, P.,** Timofeev, I. and Steriade, M. Selective amplification of neocortical neuronal output by fast prepotentials *in vivo*. *Cerebral Cortex (in press).*
5. **Fuentealba, P.,** Timofeev, I., Bazhenov, M., Sejnowski, T.J. and Steriade, M. Membrane bistability in thalamic reticular neurones during spindle oscillations. *Journal of Neurophysiology* (*in press*).
6. **Fuentealba, P.,** Crochet, S. and Steriade, M. The cortically-evoked secondary depolarization affects the integrative properties of thalamic reticular neurons. *European Journal of Neuroscience* (*in press*).
7. **Fuentealba, P.,** Crochet, S. and Steriade, M. Thalamic oscillations modulate activity in thalamic reticular neurons. Thalamus & Related Systems (*submitted).*

LIST OF FIGURES

1. INTRODUCTION

RESULTS

2. Electrical Synapses and their Role in Network Oscillations

3. Instrinsic Membrane Bistability and its Role in Network Oscillations

4. Membrane Properties and their Modulation by Network Activity

5. Synaptic Membrane Responsiveness and its Integrative Properties

6. Intrinsic Chemical Synapses and their Role in Network Oscillations

LIST OF ABBREVIATIONS

ADP	afterdepolarization
AHP	afterhyperpolarization
AMPA	alpha-amino-3-hydroxy-5-methyl-4-isoxazole propionate
CL	centrolateral
CX	cortex
DC	direct current
EEG	electroencephalogram
EMG	electromyogram
EOG	electro-oculogram
EPSP	excitatory postsynaptic potential
FRB	fast rhythmic bursting
FPP	fast prepotential
FS	fast spiking
GABA	gamma-amino butyric acid
Hz	Hertz
I_{CAN}	non-specific cationinc current
I_H	H-potassium current
$I_{Na(p)}$	persistent sodium current
I_T	low-threshold calcium current
IB	intrinsically bursting
IPSP	inhibitory postsynaptic potential
LG	lateral geniculate
LP	lateroposterior
LTS	low-threshold spike
NMDA	N-methyl-D-aspartate
PG	perigeniculate
PPS	paired-pulse stimulation
RE	thalamic reticular
REM	rapid eye movement
R_{in}	apparent input resistance
RS	regular spiking
SWS	slow-wave sleep
TC	thalamocortical
TH	thalamus
VL	ventrolateral
V_m	membrane potential
VM	ventral medial

TABLE OF CONTENTS

1. INTRODUCTION

The thalamus and neocortex maintain a continuous dialogue through a vast number of complex connections (Jones, 1985; Steriade et al., 1990; Guillery, 1995; Steriade et al., 1997). Depending on the interactions established in the network different states of vigilance will be generated, such as wakefulness and sleep (Steriade et al., 1990; McCormick and Bal, 1997). The neural mechanisms that give rise to changes from one conscious state to another operate in the thalamocortical network. During wakefulness, sensory inputs gain access to the cortex only after substantial processing in the thalamus (Steriade et al., 1990) and, when falling asleep, the thalamus functionally disconnects the cortex from ascending sensory inputs and generates slow rhythms characteristic of sleep (Steriade et al., 1990).

A key structure involved in all these mechanisms taking place in the thalamocortical network is the thalamic reticular (RE) nucleus. For long years regarded as a diffusely organized structure, having global rather than localized actions on thalamocortical pathways (Scheibel and Scheibel, 1966), the RE nucleus is known today to be divided into several distinct sectors, each related to a particular functional group of thalamocortical pathways (Jones, 1985; Crabtree, 1989, 1992, 1996); and showing a crucial role in promoting sleep and waking activity (Steriade et al., 1990).

1.1. Anatomy of the RE nucleus

The RE nucleus is a derivative of the ventral thalamus (Rose, 1950), which is entirely composed of GABAergic cells [rodent (Houser et al., 1980), primate (Hendrickson et al., 1983), carnivore (Oertel et al., 1983), marsupial (Penny et al., 1984)], and occupies a unique place in the thalamus. It is a relatively thin sheet of cells that surrounds the anterior, lateral and to some extent ventral surfaces of the dorsal thalamus, separated by the external medullary lamina (Hendry et al., 1988) (Figs. 1.1, 1.2). Because of its anatomical position, the RE nucleus is traversed by most axons passing between the dorsal thalamus and cortex, giving the nucleus its reticulated appearance and name. Indeed, the RE nucleus shows no obvious stratification of the cells and most of their dendrites cover the full thickness of the nucleus (Jones, 1975a). The cell population is relatively homogeneous, although there is a tendency for larger cells to be located posteriorly (Jones, 1985; Clemence and Mitrofanis, 1992). In carnivores, a portion of the RE nucleus closely located to the surface of the dorsal lateral geniculate (LGNd) nucleus is called the perigeniculate nucleus (PG) (Hendry et al., 1988). Its cells are smaller than those of the rest of the RE nucleus, but otherwise identical.

Synaptic inputs to the RE nucleus

The major sources of afferent inputs to the RE nucleus are the collaterals of thalamocortical, but especially corticothalamic fibers (Fig. 1.3), all of which pass through

the RE nucleus on the way to and from the cerebral cortex (Jones, 1975a; Liu and Jones, 1999). It is likely that thalamostriatal and pallidothalamic fibers also contribute collaterals to the RE nucleus (Jones, 1975a; Cornwall et al., 1990; Deschênes et al., 1996), but this is not documented for all species. The collateral thalamocortical and corticothalamic inputs display an anatomical topography in the distribution of their terminals in the RE nucleus (Shosaku et al., 1984; Shosaku, 1985; Crabtree, 1992, 1996). This topography is related to the topology of individual dorsal thalamic nuclei. Fibers passing between a particular dorsal thalamic nucleus and the cortical area with which it is connected traverse a restricted region of the RE nucleus which is different from that traversed by fibers passing between a neighboring thalamic nucleus and its cortical area. Hence, a sector of the RE nucleus is dedicated to each dorsal thalamic nucleus (Jones, 1975b; Montero et al., 1977; Shosaku et al., 1984; Ohara and Lieberman, 1985). Correspondingly, the cells of a sector of the RE nucleus related to a sensory relay nucleus, take many receptive field characteristics of the relay cells in that nucleus (Cleland et al., 1971; Dubin and Cleland, 1977; Shosaku et al., 1984; Yen et al., 1985; Jones and Sillito, 1994). Where sectors are dedicated to two different sensory relay nuclei, the RE cells display mixed receptive fields (Sugitani, 1979; Shosaku and Sumitomo, 1983).

Other afferent inputs to the RE nucleus arise in the brain stem and basal forebrain. In the brainstem the major sources are cholinergic, noradrenergic and serotononergic nuclei (Swanson and Hartman, 1975; Edley and Graybiel, 1983; Woolf and Butcher, 1986; Paré et al., 1988; Raczkowski and Fitzpatrick, 1989). Basal forebrain afferents

arise mainly in GABAergic cells associated with the globus pallidus and the magnocellular, basal nucleus of Meynert (Nauta, 1979; Levey et al., 1987; Steriade et al., 1987b; Cornwall et al., 1990). The cholinergic cells in these regions do not seem to project to the RE nucleus (Bickford et al., 1994). The pretectum and rostral midbrain reticular formation also provide afferents (Edwards and de Olmos, 1976; Benevento et al., 1977; Berman, 1977). Those from the pretectum mainly arise in the nucleus of the optic tract and are GABAergic (Cucchiaro et al., 1993). They appear to be mainly branches of axons projecting to the LGNd (Uhlrich and Manning, 1995).

Sectors in the RE nucleus

A sector of the RE nucleus is defined as a region that i) receives projections from a particular dorsal thalamic nucleus and the cortical area that is reciprocally connected to that nucleus and ii) sends projections back to the dorsal thalamic nucleus from which it receives projections (Jones, 1975a; Steriade et al., 1984) (Fig. 1.1). Several functionally related cortical areas can send projections to the same RE sector and one RE sector can receive projections from and send projections to several functionally related dorsal thalamic nuclei (Crabtree, 1999). The projections of single cells from a given RE sector usually have restricted terminal fields within a dorsal thalamic nucleus (Pinault and Deschênes, 1998a) and, together with the thalamoreticular projections, these reticulothalamic projections usually form open-loop rather than closed-loop circuits (Pinault and Deschênes, 1998b).

Within a sector of the RE nucleus related to a particular dorsal thalamic nucleus, there is a topographic distribution of the terminations of thalamocortical and corticothalamic fiber collaterals. The collaterals are relatively short (Yen et al., 1985; Agmon et al., 1995; Bourassa et al., 1995), and this would tend to preserve the localized character of terminations when groups of fibers are labeled as a group.

Anatomical tracing studies show that the labeling of terminals resulting in the RE nucleus from anterograde or retrograde labeling of thalamocortical or corticothalamic fibers originating from a single focus in a sensory thalamic nucleus or cortical area is also focal. The position of the focus of terminals moves systematically within the RE nucleus, following the topographical map found in the thalamic nucleus or cortical area, as injections are placed in different regions (Montero et al., 1977; Agmon et al., 1995). Similar foci of labeling, found after labeling corticothalamic terminations, tend to form a series of overlapping slabs oriented in the plane of the RE nucleus (Jones, 1975b; Crabtree, 1992; Bourassa et al., 1995). In many sectors, the RE neurons projecting to the relevant dorsal thalamic nucleus, as labeled by retrograde tracers, show a comparable organization in slabs (Shosaku et al., 1984; Shosaku, 1985; Crabtree, 1992, 1996).

A similar arrangement has been reported for corticothalamic terminations in the visual (Crabtree and Killackey, 1989; Harting et al., 1991), motor (Cicirata et al., 1990), auditory (Conley et al., 1991) and limbic (Cornwall et al., 1990; Lozsadi, 1995) sectors, and topographic maps have been described from physiological studies (Shosaku and Sumitomo, 1983; Shosaku et al., 1984). Within a particular sector, corticothalamic and

thalamocortical collateral terminations related to primary and secondary cortical areas may occupy different domains. For example, the collateral terminations of fibers connecting the LGNd and striate cortex and of those connecting the pulvinar and extrastriate cortex occupy different compartments of the visual sector of the RE nucleus (Conley and Diamond, 1990). The zone related to the pulvinar may not be topographically organized. A comparable pattern of organization is found in the auditory sector (Conley et al., 1991), but there may be greater overlap in the collateral terminals of fibers related to the primary and secondary somatosensory areas of cortex in the somatosensory sector (Crabtree, 1992, 1996). Projections in non-sensory sectors may be even more diffuse (Conley et al., 1991; Lozsadi, 1994, 1995).

Anatomically, the thalamocortical and corticothalamic projections are topographically organized, but the extensive overlap of the dendrites of RE neurons makes it unlikely that the maps are very precise, and this is confirmed by the receptive field properties of neurons in the sensory sectors of the RE nucleus (Steriade et al., 1997). In the somatosensory sector of the cat, for example, neurons have large receptive fields covering much of a limb and are not modality specific, responding best to taps, quite unlike cells in the ventral posterior nucleus and somatosensory cortex (Yen et al., 1985). In rats, the cells in the somatosensory sector are similar to ventral posterior cells in responding to stimulation of a single vibrissa, probably reflecting the concentration of collateral inputs from relay cells in a single ventral posterior barreloid in a portion of the somatosensory sector. However, unlike the ventral posterior cells, the RE neurons show no direction selectivity (Sugitani, 1979; Shosaku, 1985), probably indicating the

convergence of inputs from many cells in the barreloid. In the visual sector of the RE nucleus, cells with on-off center receptive fields are typical (Hale et al., 1982) and indicative of convergence from two classes of geniculate cell. The cells have large, diffuse receptive fields (Uhlrich et al., 1991) which are binocular (Dubin and Cleland, 1977), but can show some degree of ocular dominance, probably reflecting concentrated inputs from neighboring relay cells in the same geniculate lamina. In cats, the cells respond to visual stimuli after localized retinal lesions have abolished excitatory responses of relay cells in the topographically related projection column lying immediately beneath them (Eysel et al., 1986). This has been interpreted as lack of fine grain topography in the RE nucleus.

Thus, the sensory sectors of the RE nucleus have many similar organizational features. Each of these sectors occupies a discrete and defined position in the RE nucleus and receives excitatory afferents from a particular set of functionally related areas of the cerebral cortex and nuclei from the dorsal thalamus. Furthermore, each sector contains zones that are related to different cortical areas and to different dorsal thalamic nuclei. However, differences can be seen among the sensory sectors to the degree to which the compartments overlap or, conversely, to the degree to which they are segregated. In addition, each sector receives convergent inputs from both the cortex and dorsal thalamus, which is particularly evident from the receptive field properties of sensory RE neurons. Thus, the receptive fields of these cells would have components that reflect the properties of different sources of inputs. Moreover, each sensory sector sends inhibitory

projections back to the functionally related dorsal thalamic nuclei from where it receives inputs.

Projections from the RE nucleus

The axons arising from RE neurons, after giving off one or two collaterals in the nucleus (Scheibel and Scheibel, 1966; Yen et al., 1985; Liu and Jones, 1999) enter the dorsal thalamus and terminate (Fig. 1.4). Intranuclear collaterals may not be present in rat (Pinault et al., 1995a). The dorsal thalamus is the principal projection target of the RE nucleus, although midbrain projections have been reported (Parent and Steriade, 1984). The projection to the dorsal thalamus tends to be organized topographically, following both the arrangement of sectors defined by collateral terminations of thalamocortical and corticothalamic fibers in the RE nucleus and the topography within these terminations (Cox et al., 1996). Thus, a particular sector of the RE nucleus projects back to the nucleus or nuclei from which it receives its collateral thalamocortical input, with relatively little overlap into adjacent nuclei (Jones, 1975b; Yen et al., 1985; Conley et al., 1991; Cox et al., 1996). Projections to the intralaminar nuclei and to relay nuclei other than the principal sensory nuclei originate from more extensive regions of the RE nucleus than those to the relay nuclei (Steriade et al., 1984) and they may be less topographically organized (Cox et al., 1996; Crabtree, 1996).

With one exception, all dorsal thalamic nuclei are reported to receive a return projection from the RE nucleus (Jones, 1975b; Harting et al., 1991; Lozsadi, 1995;

Crabtree, 1996). The exception is the anterior nucleus in cats (Steriade et al., 1984), which has been correlated with the lack of spindle discharges reported in those nuclei (Paré et al., 1987). The anterior nuclei of other species do appear to receive RE nucleus projections (Shibata, 1992; Lozsadi, 1994; Kultas-Ilinsky et al., 1995).

Individual reticulothalamic axons can branch extensively (Yen et al., 1985), but those which project to sensory relay nuclei tend to follow the topography of the nucleus. In the ventral posterior nucleus of rats, fibers end in short aggregations of branches confined to individual barreloids representing single whiskers (Pinault et al., 1995a; Cox et al., 1996), although some fibers may have more widespread distributions. In the projection of the visual sector of the RE nucleus to the LGNd in the rat, the axons are distributed along trajectories resembling projection lines in the LGNd (Pinault et al., 1995a).

From the PG part of the RE nucleus of the cat, single axons projecting into the LGNd neurons end in a dense, localized terminal ramification in the A or A1 laminae, depending on the ocular dominance exhibited by the PG cell, but branches are given to the other A laminae as well (Uhlrich et al., 1991). The width of the localized ramification is similar to that of the terminal ramifications of a retinogeniculate axon (500 μm), suggesting coupling to the retinotopically organized visual input, although this must be likely diffuse due to the large receptive fields of the PG cells. RE nucleus axons projecting to certain dorsal thalamic nuclei, such as the posterior nucleus of the rat, may

have more widespread branches in those nuclei than in the principal sensory relay nuclei (Pinault et al., 1995a; Cox et al., 1996).

1.2. Neurons of the RE nucleus

The neurons of the RE nucleus are characterized by a relatively small number of long dendrites with few branches that spread over the dorsal thalamus (Fig. 1.4). In places where the RE is thin, the cells are particularly elongated and can be packaged when compressed between fiber fasciculi (Jones, 1975a). Where the RE nucleus is thicker, as on the anterior surface of the thalamus and in the RE nucleus of rodents, the cells tend to be radially symmetrical and, in all parts of the nucleus, dendrites branches can cover the full thickness of the nucleus (Yen et al., 1985). Superficially, the dendrites of RE neurons overlap extensively, especially in the dorso-ventral and antero-posterior directions (Yen et al., 1985; Steriade et al., 1997).

In some species, the secondary or tertiary dendritic branches of RE neurons possess appendages containing vesicles that form synapses on the dendrites of neighboring cells. These presynaptic dendritic appendages are relatively common in cats (Deschênes et al., 1985; Yen et al., 1985; Pinault and Deschênes, 1998a), present but rare in monkeys (Williamson et al., 1993), and reportedly absent in rats (Ohara and Lieberman, 1985).

RE neurons are relatively large, with somal diameters of 20-50 μm (Yen et al., 1985). There is some variation in size in most species; cells in anterior parts tend to be smaller than those in posterior and ventral regions (Jones, 1975a). In general, the cells are ovoid, with long, smooth and relatively few dendritic branches emerging from the poles of the soma, although some reports indicate axonal origins in the dendrites (Pinault et al., 1997). RE neurons tend to be flattened over the surface of the dorsal thalamus, and the dendritic field is commonly discoidal (Scheibel and Scheibel, 1966). Cells on the anterior surface of the dorsal thalamus are flat in the frontal plane. Those on the lateral and ventral surfaces are flattened in the parasagittal or horizontal plane. The degree of flattening depends on the relative thickness of each region of the RE nucleus. Thus, the flattest RE neurons with the most elongated dendritic fields are found laterally where the nucleus is thinnest, and thicker cells with symmetrical dendritic fields are found dorsally and anteriorly where the nucleus is thickest (Jones, 1985). It is possible that these morphological variations are adaptations to fit the dendritic field into available space (Steriade et al., 1997). On the other hand, they may reflect different patterns of innervation, especially by thalamocortical fibers (Steriade et al., 1997).

Even if from the morphological point of view, RE neurons seem to be a homogeneous group, there is evidence for functional differences, which might suggest a certain degree of specialization in some groups. There are, as yet, no morphological correlates of the two populations of RE nucleus described with different bursting properties (Contreras et al., 1992), one of which typically generates low-threshold spikes and is able to switch from tonic to burst firing, the other apparently lacking the low-

threshold calcium conductance and firing only tonically (Contreras et al., 1992). A functional heterogeneity of RE neurons has also been characterized in detail (Brunton and Charpak, 1997).

The axons of RE neurons in the cat are relatively thin (~1.5 μm), but myelinated. They pass directly into the dorsal thalamus. In the RE nucleus, it gives off two or three short, unmyelinated collaterals which end in boutons terminals close to the cell body of origin (Yen et al., 1985; Mulle et al., 1986; Uhlrich et al., 1991; Pinault et al., 1997). These boutons likely form many of the terminals containing flattened synaptic vesicles and ending in symmetrical synapses observed under electronic microscopy (Ide, 1982; Ohara and Lieberman, 1985; Yen et al., 1985; Williamson et al., 1994), although in appropriate sectors of the nucleus some of these probably also arise from axons of pallidal and basal forebrain origin (Asanuma and Porter, 1990; Asanuma, 1994). The presence of intranuclear collaterals has been denied for RE neurons in rats by some authors (Pinault et al., 1995a, b), but reported by others (Spreafico et al., 1988; Lubke, 1993).

On entering the dorsal thalamus, the axon of RE neurons, ramifies mainly in the nucleus related to the sector of the RE nucleus in which the neuron is located (Fig. 1.4). Studies based on juxtacellular injection of small populations of the RE nucleus (Liu et al., 1995; Pinault et al., 1995a, b; Pinault and Deschênes, 1998a) or PG nucleus neurons (Cucchiaro et al., 1991), or injections of single PG (Uhlrich et al., 1991) or RE (Pinault and Deschênes, 1998a) neurons, indicate that the axon branches within a dorsal thalamic

nucleus tend to be concentrated in one region in a pattern that reflects the topographic relation between a sector of the RE nucleus and its related dorsal thalamic nucleus (Montero et al., 1977; Hale et al., 1982; Conley and Diamond, 1990; Crabtree, 1992). It has also been demonstrated that projections of RE neurons innervate ranges from a compact, focal projection to a widespread, diffuse one; encompassing in this way large areas (Cox et al., 1996). Small groups of short branches are given off at intervals and terminal boutons are concentrated on these, although boutons are also observed on the parent axon between the branches (Liu et al., 1995; Pinault et al., 1995a, b).

RE neurons in all species studied, including those in the PG nucleus of the cat, are GABAergic (Montero et al., 1977; Houser et al., 1980; Fitzpatrick et al., 1984; Yen et al., 1985). This, and their projection into the dorsal thalamus, makes them a second population of thalamic inhibitory interneurons. For most dorsal thalamic nuclei in rodents, lagomorphs, bats and marsupials, they are essentially the only inhibitory interneurons. Among other substances expressed in RE neurons are parvalbumin, the CAT301 antigen, and certain neuropeptides such as somatostatin and neuropeptide Y (Oertel et al., 1983; Molinari et al., 1987; Morris, 1989; Conley et al., 1991; Clemence and Mitrofanis, 1992).

A population of GABAergic neurons that are larger than the intrinsic interneurons of the principal laminae of the cat LGNd is found in the interlaminar zones between the laminae of this nucleus (Robson and Martin-Elkins, 1985; Rinvik et al., 1987). sThe dendritic fields are aligned across the orientation of the projection columns of the LGN

nucleus, the cells appears to be innervated by collaterals of geniculocortical relay cells (Bal et al., 1995a) rather than by retinal terminals and, at the electronic microscopy level, they resemble PG cells rather than intrinsic interneurons (Montero, 1989). Physiologically, they also resemble PG neurons, rather than other thalamic neurons (Bal et al., 1995a, b; McCormick et al., 1995) and they are strongly excited by serotonin, a feature of PG cells but not of intrinsic interneurons (Bal et al., 1995a). They may therefore represent a population of cells displaced from the PG nucleus, just as the PG nucleus is itself part of the RE nucleus (Steriade et al., 1997).

Electrophysiological properties of RE neurons

RE neurons have some similarities with thalamocortical cells, which consist in the bursting and tonic discharge modes present in both of them during different states of vigilance. Thus, bursting mode is exhibited during EEG-synchronized sleep, while tonic discharge is detected during waking and rapid eye movement sleep (Mukhametov et al., 1970; Steriade and Wyzinski, 1972; Steriade et al., 1986). The two firing modes depend on the membrane potential of the cell (Contreras et al., 1992; Bal and McCormick, 1993; Gentet and Ulrich, 2003). At depolarized membrane potentials (positive to -65 mV), intracellular injection of a positive current pulse results in the activation of a train of action potentials (Bal and McCormick, 1993). In contrast, intracellular injection of the same current pulse at hyperpolarized membrane potentials (negative to -65 mV) results in the generation of a high-frequency (300-500 Hz) burst of action potentials (Bal and McCormick, 1993). Barbiturate anesthesia depresses the cortical network activity and

turns the membrane potential of RE neurons to hyperpolarized levels, favoring the generation of spike-bursts (Fig. 1.5). Such high-frequency bursts are generated, as in thalamocortical neurons, through the activation of low-threshold calcium currents (T-current) (Huguenard and Prince, 1992; Huguenard, 1996)

The bursts of action potentials generated in RE neurons are different from those taking place in thalamocortical cells (Domich et al., 1986; Steriade et al., 1986; Bal and McCormick, 1993), the main difference being the duration and the internal structure of the burst. A quantitative analysis of bursts fired in thalamic neurons during natural sleep showed that about 65% of cortically projecting ventrolateral and rostral interlaminar neurons displayed 3-5 action potentials per burst, which lasted 5-20 ms. On the other hand, more than 90% of bursts in rostrolateral RE neurons were longer than 50 ms and contained generally 5 or more spikes (Domich et al., 1986; Steriade et al., 1986). The intrinsic burst structure was also different in these two thalamic cell classes. While spike-bursts of thalamocortical neurons typically showed only a progressive increase in interspike intervals, RE neurons displayed a decrease followed by an increase in those intervals. This particular mode of discharge has been called the accelerando-decelerando pattern of RE neurons (Domich et al., 1986; Steriade et al., 1986), and seems to rely on the dendritic location of the T-current in RE neurons (Destexhe et al., 1996).

Another difference between RE and thalamocortical neurons is the characteristics of the single spike mode of action potential generation. The inhibitory neurons from the RE nucleus can generate trains of spikes at frequencies as high as 500 Hz and exhibit a

relatively steeper *f*-I (frequency of discharge versus injected current) curve (Bal and McCormick, 1993), while thalamocortical neurons typically fire at frequencies lower than 250 Hz and exhibit less steep *f*-I relations (Bal and McCormick, 1993).

Intrinsic oscillatory behaviour of RE neurons

Neurons from the RE nucleus exhibit a prominent tendency to generate rhythmic oscillations in the 10 Hz-band range (Fig. 1.5). *In vitro* studies show that intracellular injection of a negative current pulse is typically followed by the generation of a rebound LTS and burst of action potentials. Following this LTS is an afterhyperpolarization (AHP), which is followed typically by a second LTS, and a later AHP (Bal and McCormick, 1993). The number of cycles which are generated and the frequency of the oscillation is a function of the membrane potential (Bal and McCormick, 1993). Depolarization of RE neurons with intracellular current injection results in an increase in the frequency of rhythmic burst discharge. Thus, rhythmic discharges can occur at frequencies between 0.5 and 12 Hz in RE neurons, depending upon membrane potential. Intracellular injection of current is not able to generate such cyclic behavior in studies performed *in vivo*; however the electrical activation of corticothalamic fibers generates a similar effect (Contreras and Steriade, 1995).

Detailed analysis of the ionic mechanisms by which RE neurons generate these rhythmic oscillations reveal that the rhythmic burst firing is mediated by the interaction between T-current and calcium-activated potassium-currents ($K_{(Ca)}$-currents) (Avanzini et

al., 1989; Bal and McCormick, 1993); the latter ones are blocked by extracellular application of apamin (Avanzini et al., 1989; Bal and McCormick, 1993). After the blockage of $K_{(Ca)}$-current with apamin, a large afterdepolarization (ADP) is generated following the LTS (Bal and McCormick, 1993). The ionic mechanisms of the slow ADP were investigated by ion substitution experiments. The results indicated that the slow ADP is likely to be carried by a calcium-activated non-selective cationic current (CAN-current) (Swandulla and Lux, 1985; Partridge and Swandulla, 1988). Based on these results a model was proposed for the rhythmic burst activity followed by tonic discharges in RE neurons. Brief hyperpolarization of these neurons is associated with removal of inactivation of T-current to a sufficient extent to result in the generation of a rebound LTS. The subsequent increase in intracellular calcium, especially from the burst of action potentials, results in the activation of a CAN-current. Inactivation of T-current, as well as activation of potassium currents, results in the repolarization of the membrane potential and the generation of an ADP. During this rhythmic burst firing, the activation of CAN-current increases. Together with decreases in the ability of the interaction of T-current and $K_{(Ca)}$-current to generate rhythmic oscillations, the membrane potential eventually depolarizes, resulting in the generation of a tail of tonic action potentials (Bal and McCormick, 1993).

RE neurons generate LTSs at relatively depolarized membrane potentials and there is only a few millivolts between the bursting and tonic modes of action potential discharge (Bal and McCormick, 1993). This feature of RE neurons may result in part from the unique properties of the T-current in these cells, which exhibits an activation

curve depolarized in comparison to that of thalamocortical neurons (Huguenard and Prince, 1992; Huguenard, 1996). An additional possibility is that the T-current displays unusual voltage dependence at the level of the soma due to the expression of T-channels in the dendrites (Destexhe et al., 1996). The capability to generate LTSs at more depolarized levels is likely to be important for the generation of thalamic oscillations for a double reason. First, the arrival of barrages of EPSPs from activity in thalamocortical cells would be able to trigger LTSs at relatively depolarized levels (Bal and McCormick, 1993; von Krosigk et al., 1993); and second, the propagation of slow activities by electrical synapses might mediate the generation of LTSs at relatively depolarized levels (Long et al., 2004).

Intracellular recordings in RE neurons *in vivo* also reveal in a small group of cells (10%), small-amplitude (3-7 mV) events which seem to be different from EPSPs and electrotonic potentials (Contreras et al., 1993). Although the origin of these events remains elusive, they may represent regenerative events originated distally in the dendritic arbor, and therefore contribute to the integrative properties of RE neurons. The presumed dendritic spikes can be triggered by intracellular current injection, by synaptic activation of excitatory inputs or by the depolarizing waves of spindle sequences (Contreras et al., 1993). They also occur spontaneously, as single events or bursts (400 Hz). Multiple functional roles of the putative dendritic spikes have been proposed, including somatic depolarization, triggering of dendritic low-threshold spikes and conducting depolarizing potentials to more distal dendrites (Contreras et al., 1993).

1.3. Physiology of the RE nucleus and spindle oscillations

On the basis of its connectivity, the RE nucleus occupies a strategic situation in the thalamocortical system, and therefore it is in a position to gate the flow of signals between thalamus and cortex (Steriade et al., 1990; Guillery et al., 1998). Indeed, the RE nucleus has been implicated in modulation of sensory transmission through the dorsal thalamus (Scheibel and Scheibel, 1967; Singer, 1977), enhancer of specific sensory transmission through the dorsal thalamus (Crick, 1984; Warren and Jones, 1994; Hartings et al., 2000; Temereanca and Simons, 2004), regulator of receptive field properties of dorsal thalamic neurons (Sillito and Kemp, 1983; Villa, 1990), attention (Crick, 1984; Guillery et al., 1998), the development of connections between the thalamus and the neorcortex (Mitrofanis and Baker, 1993; Mitrofanis and Guillery, 1993), and the generation of rhythmic activity during sleep and seizure states (Steriade et al., 1990; Steriade et al., 1997). These diverse functions are not mutually exclusive and require numerous cellular mechanisms and very specific anatomical features, but one characteristic that should be common to all of them is some kind of the synchronization of neuronal activity. From these referred functions, the one of rhythmic electrical activity is one of the most studied and best understood (Steriade et al., 1990; Steriade et al., 1993b; McCormick and Bal, 1997; Steriade et al., 1997). This paradigmatic electrical activity, the spindle oscillations, is the subject matter of the present study and therefore will be described in detail in this section.

The genesis of sleep spindle oscillations

The electrical activity of the brain at sleep onset takes the form of relatively low-frequency (7-14 Hz) oscillations (Fig. 1.6), termed spindles because of the spindle shape of the oscillation envelope; and they are also characteristic of barbiturate anesthesia (Fig. 1.5). These waves can be recorded over the skull, but they originate in the thalamus, partly as a consequence of changes in brainstem and basal forebrain neuronal activity (Domich et al., 1986; Steriade et al., 1986).

Spindles are the distinct EEG correlate of sleep onset and the only rhythm, during the transition from wake to sleep, which involves the synchronous activity of a large number of thalamic neurons and of their cortical targets (Contreras and Steriade, 1996; Contreras et al., 1997), so that it can be recorded on the scalp. Only at later stages of resting sleep do waves with lower frequency appear on the EEG, such as delta and the slow oscillation (Steriade et al., 1982; Steriade et al., 1986; Amzica and Steriade, 1995, 1997).

The hypothesis that the RE nucleus is a pacemaker of spindle oscillations was formulated in a study reporting the absence of spindles in thalamocortical systems after disconnection from the RE nucleus (Steriade et al., 1985). This idea received confirmation when it was shown the persistence of spindles in the deafferented rostral pole of RE nucleus (Steriade et al., 1987a). Additional evidence in the same line comes from intracellular recordings and computational models showing that when RE neurons

are hyperpolarized below the chloride reversal potential, synaptic excitation mediated by $GABA_A$ receptors can lead to LTSs crowned by sodium spikes (Bazhenov et al., 1999). This mechanism is able to produce propagating patterns of spike-burst activity, which also develop into self-sustained oscillations (Fig. 1.7). Such a proposal has also been supported by modeling studies showing that spiking-bursting activity in the RE nucleus might initiate sequences of spindle oscillations in thalamic networks (Destexhe et al., 1994a, b; Bazhenov et al., 2000).

The capability of a burst of action potentials in a RE/PG neuron to generate a rebound LTS and a burst of action potentials in thalamocortical/LGNd neurons, which then returns to the same RE neuron as a barrage of EPSPs, has also been proposed as the basic mechanism for the initiation of spindle oscillations (von Krosigk et al., 1993) (Figs. 1.8,1.9). The spindle waves in the ferret LGNd *in vitro* result from the interaction of LGNd and PG neurons in a manner that is predicted by their disynaptic connections. The activation of a burst discharge in a PG neuron results in the generation of an IPSP in a LGNd cell. This IPSP removes inactivation of the T-current, and the repolarizing phase of the IPSP activates this current, giving rise to a LTS and a burst of action potentials. It is this burst of action potentials in LGNd cells that subsequently activates once again the PG neurons. The time required for the completion of this loop explains the frequency range of spindles (McCormick and Bal, 1997).

Spreading and synchronization of spindle oscillations

Spindle oscillations are synchronized within large thalamocortical territories (Contreras and Steriade, 1996; Contreras et al., 1997; Timofeev et al., 2001). This is shown by their appearance on the EEG activity recorded over widespread areas on both hemispheres (Fig. 1.6). The mechanisms of synchronization process are most likely multifold. They include synchronization among pacemaking RE neurons (Destexhe et al., 1994a; Bazhenov et al., 1999; Bazhenov et al., 2000) (Fig. 1.7), reciprocal operations in the recurrent circuit between reticular and thalamocortical neurons (von Krosigk et al., 1993) (Fig. 1.8), possibly the contralateral thalamic projections of the RE nucleus (Paré and Steriade, 1993), and potentiation of spindle genesis by corticothalamic volleys (Contreras and Steriade, 1996; Contreras et al., 1997).

During spindles, the rising phase leading to spike-bursts in RE neurons is preceded by high frequency events of small amplitude, presumably EPSPs arising from bursts from thalamocortical neurons (Mulle et al., 1986). These EPSPs are mediated, at least partially, by non-NMDA receptors, since application of AMPA/kainite receptor antagonists results in complete block of both spontaneous and evoked spindle waves (Bal et al., 1995b). Additionally, recent studies in slices have shown that NMDA components of cortically evoked responses in RE neurons are negligible, likely due to the lack of expression of the corresponding receptor in those synapses (Gentet and Ulrich, 2004).

In simple intrathalamic circuits, as in slices, it is possible to obtain spindle waves (Kim et al., 1997; Lee and McCormick, 1997; Sanchez-Vives and McCormick, 1997). Due to their sensitivity to be activated in the burst mode, RE neurons may produce a

spike-burst which results in the hyperpolarization of a number of thalamocortical cells, some of which may rebound in response to the depolarizing phase of the IPSPs (Kim et al., 1997). During these IPSPs, RE neurons are also being hyperpolarized from the activation of $K_{(Ca)}$-current, and the next burst is probably enhanced due to the increase deinactivation of the T-current (Huguenard and Prince, 1992; Huguenard, 1996). In addition, the spread of projections from thalamic relay nuclei to the RE nucleus result in the activation of additional RE neurons that were not activated during the initial bursts (Timofeev et al., 2001). This mechanism is proposed to explain the waxing of spindles due to increasing recruitment and increased synchronization of more and more thalamic neurons, both relay and RE.

Another possible mechanism for the synchronization of thalamocortical activities exerted by the RE nucleus is the electrical coupling by gap junctions (Landisman et al., 2002; Long et al., 2004) (Fig. 1.10). It has been shown that many RE neurons are interconnected by electrical synapses. The properties of these electrical interactions are similar to most electrical synapses that have been studied in vertebrate nervous systems: i) coupling is symmetric and current passes equally well in both directions, ii) there is no obvious rapid gating of the coupling conductance that depends on transjunctional voltage, iii) electrical signals of high frequency are attenuated and filtered and iv) coupling depends on the expression of a connexin protein, Cx 36 (Landisman et al., 2002).

Electrical synapses can synchronize activity in RE neurons (Landisman et al., 2002; Long et al., 2004) (Fig. 1.11). The evidence suggests that the relatively strong

filtering properties of electrical connections between RE neurons favor the synchronization of low frequency events, such as LTS and slower oscillations, but excludes fast events as spikes (Landisman et al., 2002). This means that electrical synapses might synchronize oscillations in the range of spindles, which are mediated by LTSs.

The rhythmicity of spike-bursts fired by RE neurons during spindles and the fact that their discharges extend over the whole period of spindle sequences explain the relation between RE spike-bursts superimposed over a depolarizing envelope (Mulle et al., 1986; Contreras et al., 1993), whereas the cyclic IPSPs of thalamocortical cells develop over a waxing-and-waning hyperpolarization (Steriade et al., 1993b; von Krosigk et al., 1993). The depolarization of RE neurons during spindles exhibits two periods of temporal integration: one which is time-locked to the generation of each event of the spindle sequence (spindle wavelets) and another that is related to the general shape of the spindle as a whole (depolarizing plateau). The prolonged depolarizing envelope of spindle oscillation recorded from RE neurons *in vivo* (Mulle et al., 1986; Contreras et al., 1993; Contreras et al., 1996a) is absent in the PG cells recorded from ferret slices, a condition under which RE neurons undergo during spindles a progressive hyperpolarization (von Krosigk et al., 1993; Bal et al., 1995a; Kim et al., 1997; Kim and McCormick, 1998). This difference may be explained by several factors, such as the fact that thalamic slices are deprived of brainstem modulatory systems and corticothalamic depolarizing inputs (Steriade, 2001), a condition that may also account for the absence of spindles in the isolated RE neurons *in vitro*. It is also possible that PG cells have some

distinct properties when compared to neurons from the rostral pole and lateral districts of the nucleus, as suggested by the shorter duration of their spike-bursts and the absence of tonic discharge following rhythmic spike-bursts during spindles (Hirsch et al., 1982). It has been suggested that the intracellularly recorded RE neurons *in vivo* may not exhibit a slow hyperpolarization, as seen *in vitro*, owing to the lower input resistance, compared to that obtained in slices (Bal et al., 1995a, b). The possibility that the depolarizing envelope of spindle sequences *in vivo* may be due to the impalement is precluded by the demonstration that the extracellularly recorded discharges of RE cells during either natural sleep (Domich et al., 1986; Steriade et al., 1986) or anesthesia (Contreras and Steriade, 1995; Steriade and Contreras, 1995) consist of rhythmic spike-bursts followed by a tonic tail of action potentials, extending throughout the duration of a spindle sequence. These findings in an extracellular position, that precludes a compromised integrity of membrane input resistance, are clearly indicative of the depolarization of RE neurons during spindles.

Besides their dependence on synaptic inputs, the patterns of spindles in intracellularly recorded RE neurons also depend on their membrane potential, as was also observed in thalamocortical neurons (Steriade et al., 1993a). Changes in the membrane potential of RE neurons by current injection influence both the individual wavelets of EPSPs during a spontaneous spindle sequence and the associated depolarizing envelope that increases in amplitude with slight hyperpolarization, up to -80 or -85 mV, and decreases with depolarization (Contreras and Steriade, 1996). This behavior is similar for spontaneously occurring and cortical-elicited spindles. Neither the frequency of

oscillation nor the duration of spindle sequence changes with these fluctuations in the membrane potential. The constant frequency of spindles within a broad range of membrane potentials indicates that the intrinsic oscillatory properties of RE neurons are overwhelmed by network operations during this type of oscillation (Contreras and Steriade, 1996; Contreras et al., 1996b). Further hyperpolarizations, however, bringing the membrane potentials at levels more negative than -85 mV, have the effect of decreasing the amplitude of both the spindling wavelets and the depolarizing plateau (Contreras and Steriade, 1995). One possible explanation for this is the decrease in the apparent input resistance of the cell by up to 50% resulting from inward rectification (Bal and McCormick, 1993; Contreras et al., 1993).

Besides the conventional projections from the RE nucleus to the ipsilateral dorsal thalamus, the contralateral thalamic projections of this nucleus may also be implicated in the synchronization of spindles. Retrograde and anterograde tracing studies have shown that RE neurons project contralaterally to a number of thalamic nuclei (Paré and Steriade, 1993). The cross talk between the two thalami was also shown to involve projections from the rostral pole of the reticular nucleus to the contralateral side (Paré and Steriade, 1993). These projections are not topographically organized and they are minor compared to the ipsilateral projections. About 15% of the RE input to intralaminar nuclei is from the contralateral side (Paré and Steriade, 1993).

Activation of corticothalamic pathways is more efficient in eliciting spindle oscillations than stimulation applied to prethalamic pathways. This is so even with

stimulation of the contralateral cortex to prevent antidromic activation of thalamocortical axons. The role played by corticothalamic volleys in spindle oscillations is demonstrated by using synchronous stimuli applied to the cerebral cortex and also by taking advantage of the slow oscillation (<1 Hz) whose components include a sharp negative potential in the cortical depth, reflecting the synchronous depolarizations and spike trains in corticothalamic neurons (Contreras and Steriade, 1995) (Fig. 1.12).

The cortically evoked spindles in RE neurons decrease in amplitude as well as in duration by diminishing the intensity of the applied stimuli. The amplitude of the depolarizing envelope of spindles is also decreased progressively by diminishing the amount of stimulating current (Contreras and Steriade, 1995). The changes in the intensity of cortical stimulation do not alter the frequency of the evoked oscillatory response in RE neurons. By decreasing the intensity of cortical stimulation, the evoked spindle sequence starts earlier because the prolonged hyperpolarization that follows the early excitation in RE neurons and precedes the initiation of the oscillatory response is shorter (Contreras and Steriade, 1995). The variations in the durations of spindle sequences parallel the durations of the preceding hyperpolarizations, which closely correspond to the temporal course of the depth positive cortical EEG wave reflecting synchronous hyperpolarizations in cortical neurons. This indicates that populations of cortical and RE neurons undergo hyperpolarizations of similar durations and are thus synchronized at the onset of the spindle afterdischarge. The phase relations, during spontaneously occurring spindle sequences, between cortical and RE cells are clearly visible by recording both of these neurons (Figs. 1.5,1.12). Intracellularly recorded

cortical neurons oscillate with spike-bursts in phase with the depth negative EEG waves, as well as with the spike-bursts of simultaneously recorded RE neurons (Figs. 1.5,1.12). The averaged oscillations demonstrate significant correlation between cortical and RE activities (Contreras and Steriade, 1995).

The power of cortical volleys to trigger the oscillatory pattern of RE cells also results from their effectiveness in synchronizing RE neurons that may otherwise oscillate independently. Even though simultaneously recorded RE neurons may display only weak synchronization in the spindle frequency range, cortical stimuli induce stronger spindles that become synchronous between the two cells (Contreras and Steriade, 1995).

The effect of cortical pathways on spindle synchronization depends on the different patterns assumed by the sleep oscillation. The waxing and waning of spindle waves depend on different degrees of synchronization in thalamic and cortical networks that vary with the global state of the brain. Thus, the background activity in the oscillatory network will depend on various anesthetics used or the depth of sleep (Domich et al., 1986; Contreras and Steriade, 1995, 1996).

The difference between the waxing and waning patterns of spindles is attributable to variations in the timing of inputs within the oscillatory network, in relation to the background activity upon which these inputs are superimposed. With low spontaneous activity, as under barbiturate anesthesia, the spindle threshold is low, with the consequence that any input reaching thalamic cells initially triggers spike-bursts in a

small number of elements that would eventually lead to a complete spindle sequence (Contreras and Steriade, 1996). In fact, in thalamic slices, where background activity is very low, a burst of a single thalamic neuron can generate a whole spindle sequence (Kim et al., 1995). Thus, under conditions of a low level of background activity, the initial waxing of spindles would depend on a progressive recruitment and synchronization of thalamic and cortical neurons.

Conversely, when the spontaneous activity of thalamocortical networks is high, the threshold for spindle generation is higher and coherent rhythms are only reached when highly synchronized activities are superimposed on background activity from the very onset of the oscillation, thus giving rise to mostly waning spindle waves (Contreras and Steriade, 1995). In such case, the higher threshold of spindles makes waxing process less likely. Such highly synchronized inputs are provided by corticothalamic volleys that arise in an overwhelming proportion of regular spiking and intrinsically bursting cortical neurons after the prolonged hyperpolarization characteristic of the slow oscillation (<1 Hz) of neocortical neurons. The phase relations between thalamic and cortical neurons are attributed to distributed excitatory signals from thalamocortical to cortical and RE neurons. Consequently, cortical neurons provide a powerful drive to potentiate the genesis of spindles in the networks of RE neurons (Contreras and Steriade, 1995, 1996).

Termination of spindle oscillations

In addition to the waxing of the spindle wave, these oscillations also wane, so that after approximately half of the duration of the spindle wave, fewer neurons discharge and each neuron discharges less intensely until the oscillation ceases (Contreras and Steriade, 1996; Timofeev et al., 2001). The waning of spindle waves is followed by a relative refractory period during which the threshold for the initiation of another wave is markedly increased (Kim et al., 1995). For example, extracellular electrical stimulation, or depolarization of a single PG neuron, can initiate a spindle wave that then propagates through the thalamic slice *in vitro* away from the point of initiation. Following the generation of a spindle wave, application of the extracellular stimulus does not generate a full spindle wave or the propagation of such. As the time since the generation of the last spindle wave increases, the ability of the network to generate another spindle wave recovers, such that after ~10 seconds, an additional spindle wave may be generated that then propagates through the slice (Kim et al., 1995). This however, is not the case *in vivo*, since in those preparations spindle waves can take place every 2-3 s (Domich et al., 1986; Steriade et al., 1986).

The spontaneous cessation of synchronized spindle oscillations is generated at least in part through the progressive activation of the hyperpolarization-activated cation current (H-current) (Bal and McCormick, 1996) (Fig. 1.14). This persistent activation of H-current results in a relative refractory period during which the propensity to generate synchronized oscillations is markedly reduced. Each spindle wave is followed by a 1-4 mV ADP, the duration of which matches the duration of the *in vitro* refractory period (5-20 s). Intracellular injection of repetitive hyperpolarizing current pulses, which activate

H-current, also resulted in the same ADP, and spindle waves that occurred during this induced ADP were associated with a marked decrease in the amplitude of the rebound LTSs. In addition, the ability of a burst of action potentials in a single PG neuron to generate rebound burst firing in thalamocortical cells is markedly depressed immediately following the generation of a spindle wave, and this depression recovers with the same time course as the decrease in ADP (Bal and McCormick, 1996).

Although the ADP is relatively small (1-4 mV), intracellular injection of current in thalamocortical cells reveals that it is large enough to reduce the amplitude or suppresses the occurrence of rebound LTS in these neurons. The selective abolition of the slow ADP, those that follow the intracellular injection of hyperpolarizing pulses and those that follow network oscillations, by extracellular application of cesium, indicates that this ADP is mediated by the persistent activation of H-current (Bal and McCormick, 1996). The application of cesium not only resulted in the abolition of slow ADP, but also of the spindle wave refractory period, resulting in synchronized 6-10 Hz oscillations that occurred continuously without the typical waxing and waning associated with normal spindle waves.

Therefore, spindle waves are associated with the persistent activation of H-current, which then reduces the responsiveness of these cells to IPSPs by increasing the membrane conductance and by depolarizing thalamocortical cells toward the reversal potential of H-current (~-35 mV, (McCormick and Pape, 1990)). Most likely, with each hyperpolarization and rebound burst, more and more H-current is persistently activated,

resulting in the input conductance of the neuron and depolarization of the membrane potential.

It has been proposed that the progressive activation of H-current results in a progressive decrease in the amplitude of rebound burst firing in thalamocortical neurons, which then results in a decrease in the amplitude of the barrages of EPSPs arriving in the GABAergic PG neurons. Probably, this decrease in excitation of PG neurons is then reflected as a decrease in the action potential discharge of these cells as a population, resulting in a decrease in the amplitude of the IPSPs initiated in the thalamocortical cell during the next cycle of the oscillation (Bal and McCormick, 1996). In this manner, the interaction between PG and LGNd cells that underlies these synchronized oscillations may progressively fail, leading to the cessation of the network oscillation. Following the cessation of the oscillation, only the persistent activation of H-current remains; resulting in the generation of the ADP and the relative refractory period.

Additionally, the termination of spindles may be mediated by other factors. Repetitive stimulation of the dorsal thalamus with low intensity pulse-trains at spindle frequencies induces decremental responses in RE neurons (Timofeev and Steriade, 1998) (Fig. 1.15). This mechanism might mediate a depression of inhibition induced by rhythmic volleys from the RE neurons to thalamocortical neurons. Since the primary source of spindle activity is located within RE nucleus, the relative role of H-current and depressed inhibition in thalamocortical neurons has been proposed not to be fundamental in the termination of spindle waves *in vivo* (Timofeev et al., 2001).

Another mechanism for the termination of spindles depends on the desynchronization of activity, based on dissimilarity of intrinsic responses in different cortical and thalamocortical neurons (Fig. 1.16). There are several sources of desynchronization that facilitate spindle termination (Timofeev et al., 2001). First, LTSs are generated with different delays from the onset of arriving IPSPs. The asynchronous burst firing of thalamocortical neurons keeps the membrane potential of RE neurons at relatively depolarized levels, so preventing the deinactivation of T-current and diminishing the probability of burst firing. Barrages of EPSPs from prethalamic relay stations (like the cerebellum) may produce a small, but long-lasting depolarization and decreased input resistance of thalamocortical neurons that could desynchronize the thalamocortical network and disrupt thalamic oscillations (Bazhenov et al., 2000). Because the trains of prethalamic EPSPs would occur only randomly, the most important source of spindle desynchronization, leading to the decrease in their duration, is probably long-lasting spike-trains from neocortical neurons. Several mechanisms may be involved: first, intrinsically bursting neurons fire bursts that may significantly outlast the duration of thalamically generated EPSPs. Second, slightly depolarized fast rhythmic bursting neurons could fire high-frequency, non-accommodating trains of spikes throughout the spindle. Those bursting neurons would recruit other cortical neurons into an excited state that is out-of-phase with the thalamic neurons. Third, strong depolarizing cortical inputs onto thalamic (primarily RE) neurons will prevent the generation of LTSs and thus will lead to the spindle termination (Timofeev et al., 2001).

Consequences of spindle oscillations in RE neurons

Early theoretical studies proposed that cortical network activity might affect the integrative properties of neurons in the nervous system (Barret, 1975). Such proposal has received in the past years support from both experimental data and computational simulations which showed that in fact, integrative properties of pyramidal neurons are strongly modulated by the ongoing network state of activity. This issue has been studied especially for the cortex with computational models (Ho and Destexhe, 2000; Destexhe et al., 2001; Fellous et al., 2003), through the generation of different artificial states of background noise *in vitro* (Stacey and Durand, 2001; McCormick et al., 2003; Mitchell and Silver, 2003), and through the activation of synaptic potentials or local suppression of network activity *in vivo* (Timofeev et al., 1996; Destexhe and Paré, 1999). Changes in background synaptic activities may underlie the generation of persistent neuronal discharges, but also may influence neuronal excitability and responsiveness to other synaptic inputs (Destexhe et al., 2003). In fact, increases or decreases in background synaptic activity may mediate the influence of feed-back pathways or local networks on the responsiveness of single neurons (Destexhe et al., 2003).

These conditions of regulation which are valid for the neocortex are likely to be also applicable to the RE neurons, were the ongoing synaptic background activity powerfully modulates membrane properties at single-cell level.

1.4. Conclusion

As it has been shown it the previous sections, the physiology of the thalamic RE is devoted to a great extent to the generation of intrinsic thalamic rhythms characteristic of sleep stages. The involvement of the RE nucleus is multiple including generation, synchronization, spreading and termination of thalamic oscillations. Even though the current state of knowledge about thalamic oscillations is well developed, many questions remain unclear. For example, there is yet an ongoing debate about the origin of spindle oscillations. While some authors propose the thalamic RE to be the necessary and sufficient source for this rhythm (Steriade et al., 1987a; Bazhenov et al., 1999; Bazhenov et al., 2000), others maintain the necessity of dialogue between the RE nucleus and dorsal relay nuclei (von Krosigk et al., 1993; Bal et al., 1995a, b; McCormick and Bal, 1997).

To answer these and other topics related to the function of RE nucleus during spindle thalamic oscillations, the present thesis was carried on. For this, intracellular recordings of electrophysiological activity were performed in the RE nucleus (but also in the neocortex and thalamic relay nuclei) of anesthetised animals. In all cases neurons were identified by their electrophysiological characteristic activities, and in many occasions stained and reconstructed to provide further insights on their morphological features.

The results of the study are grouped in five different topics, though all of them are closely related. At the end, two studies related to the integrative properties of neocortical neurons have also been included. The data obtained from experimental research will be presented in the next section in the following order:

1. Electrical synapses and their role in network oscillations.
2. Instrinsic membrane bistability and its role in network oscillations.
3. Membrane properties and their modulation by network activity.
4. Synaptic membrane responsiveness and its integrative properties.
5. Intrinsic chemical synapses and their role in network oscillations.
6. Neuronal integration of synaptic inputs in the cortex.
7. Modulation of neuronal output by dendritic potentials in the cortex.

The last two chapters (6 and 7) have no relation with the studies performed in the RE nucleus, but have been added as proof of work since they are part of the thesis results. Therefore, they will not be mentioned in the Introduction or in the Discussion.

1.5. Figures

Figure 1.1. Frontal view of the RE nucleus. Anterior section of the dorsal thalamus from cat, displaying the somatosensory sector of RE nucleus, internal capsula and dorsal thalamus. The dotted line shows the limits of the RE nucleus and the stained cell at the bottom is a thalamocortical cell recorded and loaded with neurobiotin (Timofeev and Steriade; unpublished observations).

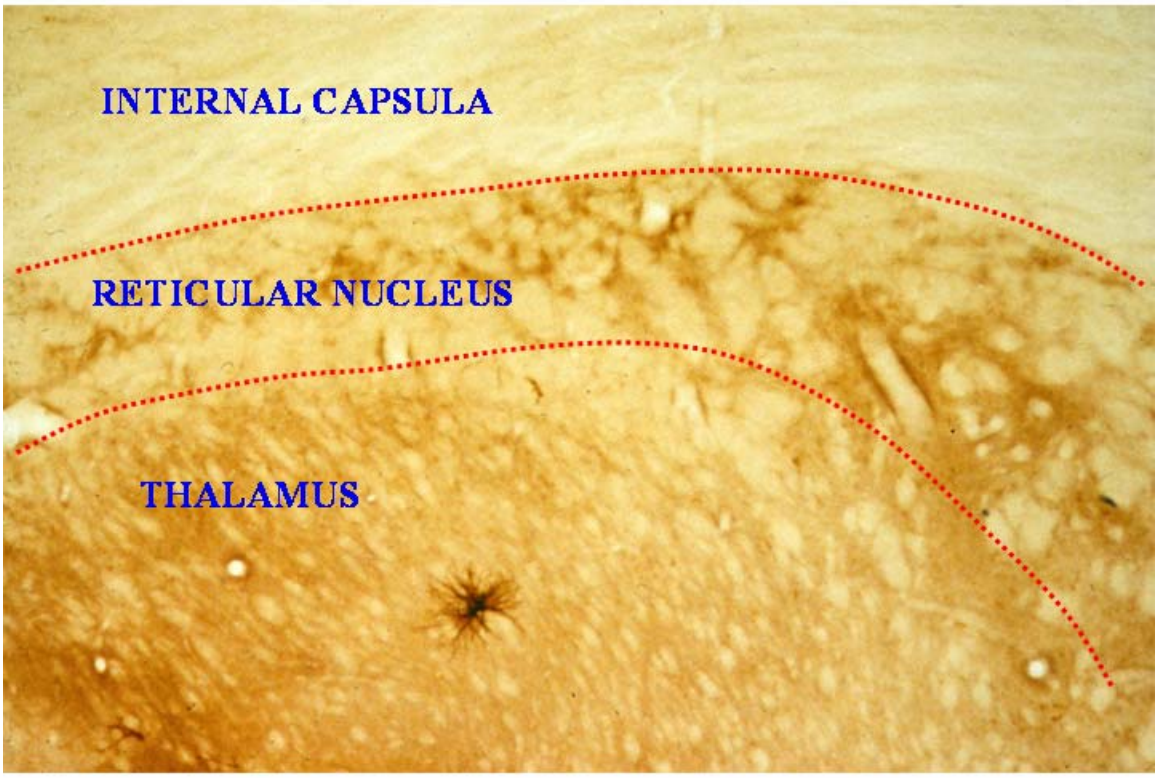
INTERNAL CAPSULA
RETICULAR NUCLEUS
THALAMUS

Figure 1.2. Schematic drawing through the rostrocaudal extent of the RE. The graphic illustrates the location of 111 biocytin- or Neurobiotin-filled RE neurons from rat with a well identified origin of the axon. The *white dots* indicate 12 neurons, the axons of which gave rise to intrinsic collaterals. The *negative numbers* correspond to the anteroposterior distances (in mm) between the bregma and the frontal RE sections (each 0.2 mm apart). *A*, Anterior; *D*, dorsal; *L*, lateral. (Pinault et al., 1997).

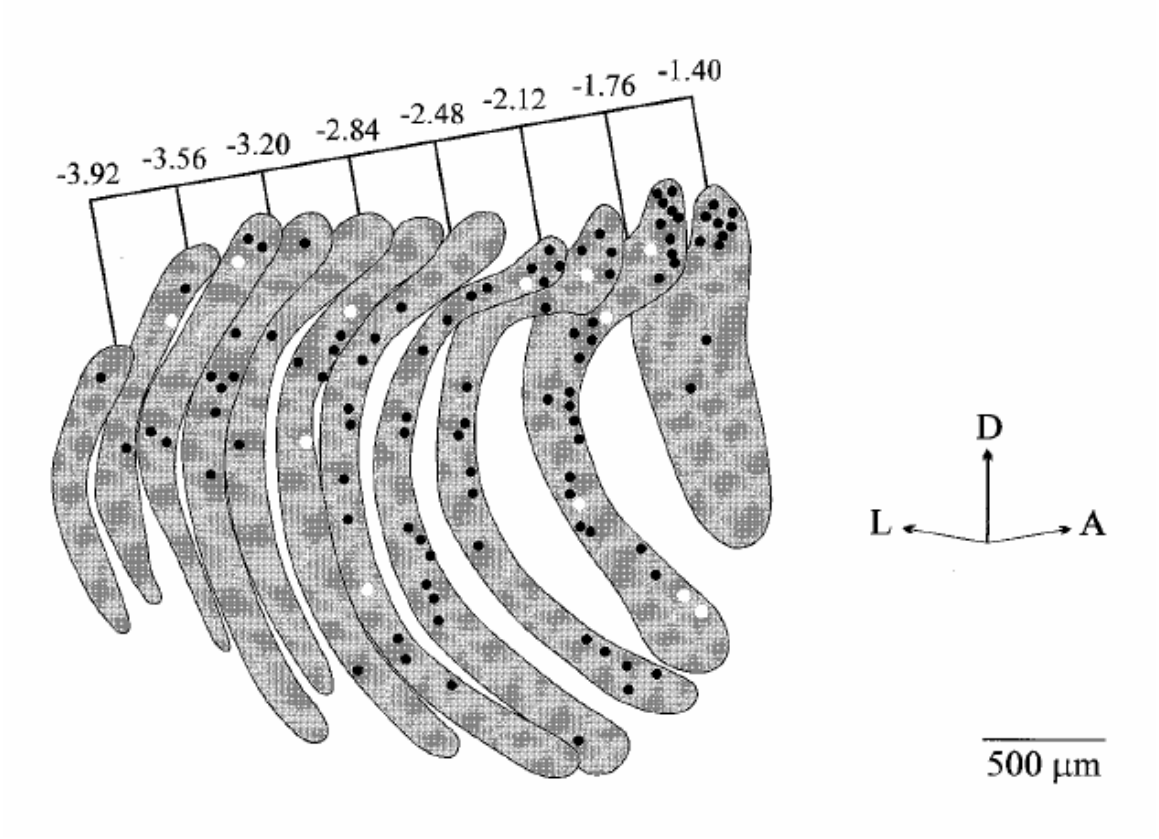
-3.92
-3.56
-3.20
-2.84
-2.48
-2.12
-1.76
-1.40
D
L
A
500 μm

Figure 1.3. Synaptic inputs to the RE nucleus. (A) Schematic distribution of synapses of various types innervating the RE nucleus. Inset: quantitative distribution of GABAergic (GA), thalamocortical collateral (LT) and corticothalamic (ST) terminals on soma, proximal and distal dendrites of a labeled cell in the RE nucleus of a rat. (B) Electron micrographs of two sections from a series through a corticothalamic terminal (T) labeled by transported PhAL and synapsin (arrows) on the dendrite of a neuron in the RE of a rat, labeled for GABA by immunogold particles. Scale bar, 1 mm. (C) EPSPs induced in a RE cell in a mouse thalamocortical slice. Each panel consists of three superimposed traces from whole-cell recordings before, during and after application of NMDA-(APV) and AMPA-(CNQX)-receptor antagonists. Arrow indicates trace recorded during application of the antagonists. The single arrowheads in the middle and lower traces indicate increased afterhyperpolarization (middle panel) and overlap of remaining slow EPSP and after hyperpolarization (lower panel). The double arrowhead in the lower panel indicates early EPSP that is blocked by CNQX. (Jones, 2002).

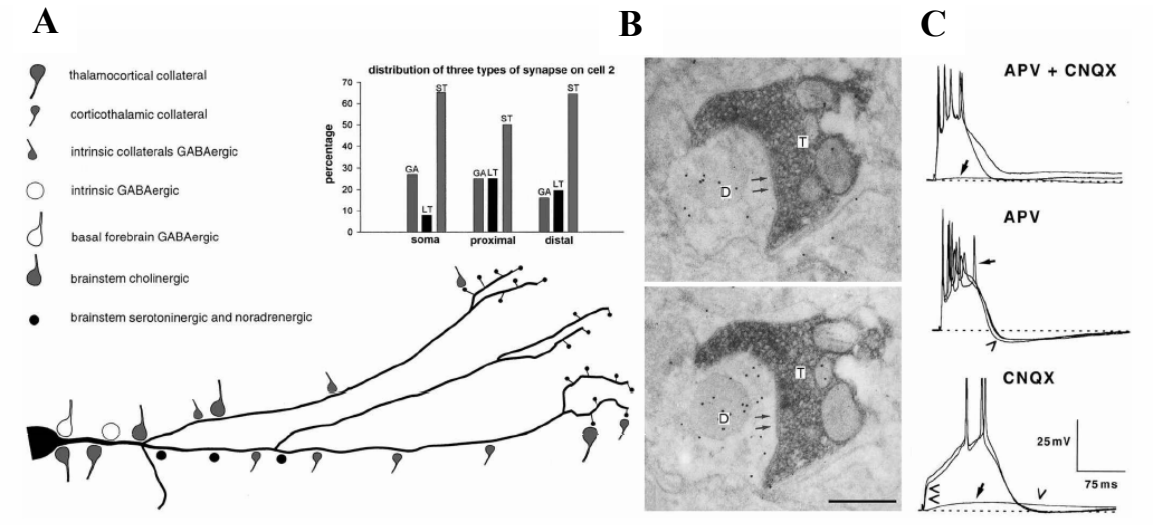
A
B
C
thalamocortical collateral
corticothalamic collateral
intrinsic collaterals GABAergic
intrinsic GABAergic
basal forebrain GABAergic
brainstem cholinergic
brainstem serotoninergic and noradrenergic
distribution of three types of synapse on cell 2
percentage
soma
proximal
distal
GA
LT
GALT
ST
T
D
APV + CNQX
APV
CNQX
25 mV
75 ms
V

Figure 1.4. Morphology of neurons in the RE nucleus. A tracer-filled RE neuron from rat with two axons, which were the continuation of a dendrite. (A) Dorsal view of its somatodendritic complex and axonal projections. The *framed areas* (*a*, *b*) are shown at higher magnification in the corresponding photomicrographs. This neuron had two thick axons, one giving rise to an axonal arbor into the lateral posterior thalamic nucleus (*LP*) and the other terminating in the lateral dorsal thalamic nucleus (*LD*). These two axons, one of which (*a*) was thicker than the other (*b*), still had swellings when traveling in the thalamus (*a, b*). (B) Lateral view of the somatodendritic complex and of the initial course of the two axons, both being the continuation of a common distal dendrite. (C) Shown is the perikaryon and the axons-bearing dendrite, separately. The *arrowheads* indicate the presumed onset of the two axons. The *arrow* in *C'* points to the dendrite bearing the two axons. Scale bars: *b*, 10 mm (also valid for *a*); *C'*, 20 mm. *A*, Anterior; *D*, dorsal; *M*, medial. (Pinault et al., 1997).

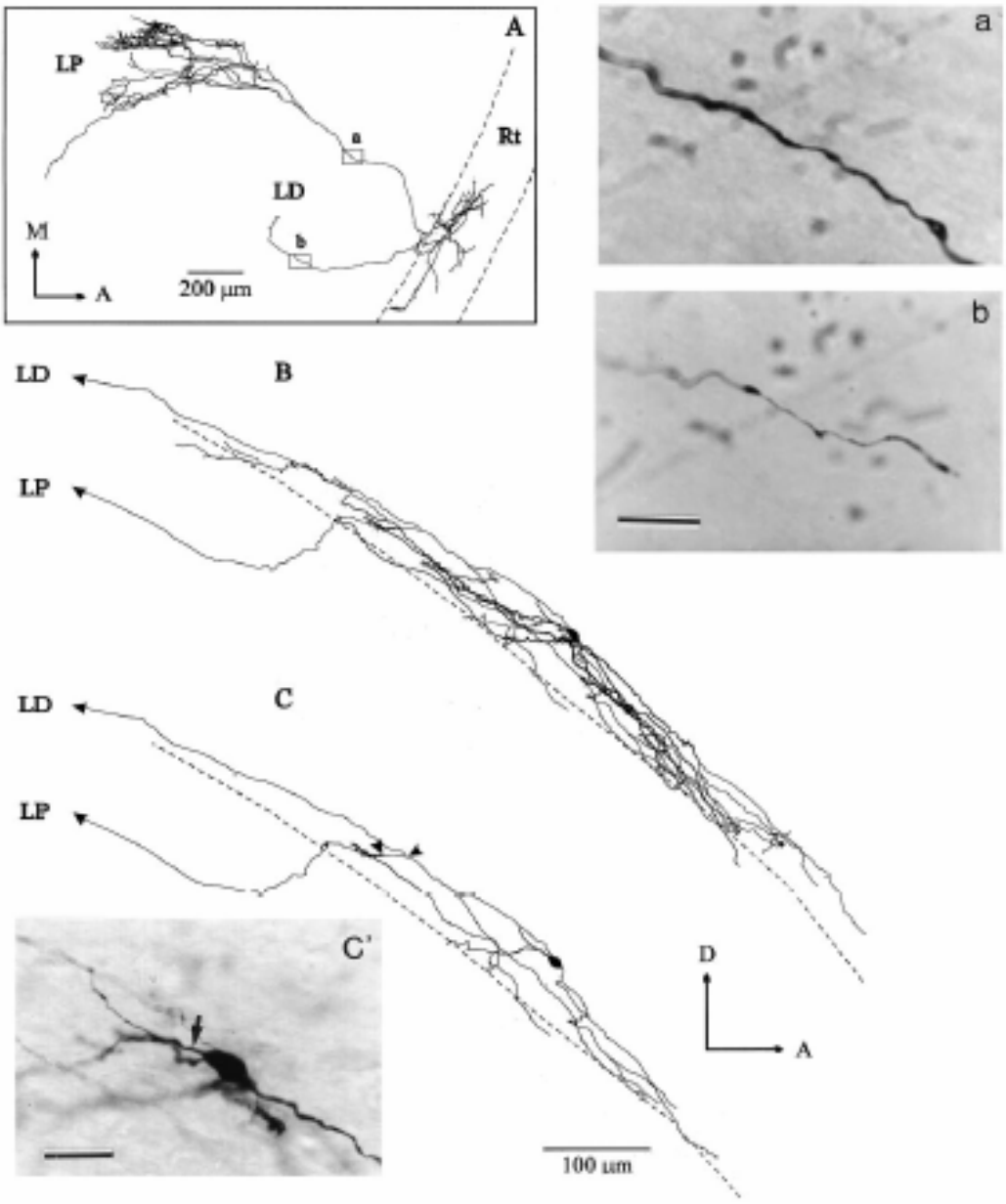
A
LP
a
Rt
LD
b
M
A
200 µm
a
b
LD
B
LP
LD
C
LP
C'
D
A
100 µm

Figure 1.5. Spindle oscillations in the cortex and RE nucleus. (A) Simultaneous intracellular recordings from a cortical neuron (CX, area 4) and a thalamic reticular neuron (RE, rostral) *in vivo*, barbiturate anesthesia. Note the synchronization of both intracellular activities and also the cortical EEG (area 4), however the spindle always starts in the RE nucleus (B) Electrical stimulation of thalamic ventrolateral (VL) nucleus identifies the cortical cell as a corticothalamic neuron, therefore pyramidal, due to the antidromic action potential generated followed by synaptic activation. The same VL stimulation generates a short, fixed latency EPSP in the RE neuron preceded by a small artifact (asterisk), due to the capacitive coupling between both intracellular recordings. Note the latency of the artifact in the RE neuron to correspond to the peak of the antidromic action potential in the cortical pyramidal cell (1.4 ms). Therefore, both neurons belong to the same functional thalamocortical circuit, involving VL-RE-area 4. (Fuentealba, Timofeev and Steriade; unpublished observations).

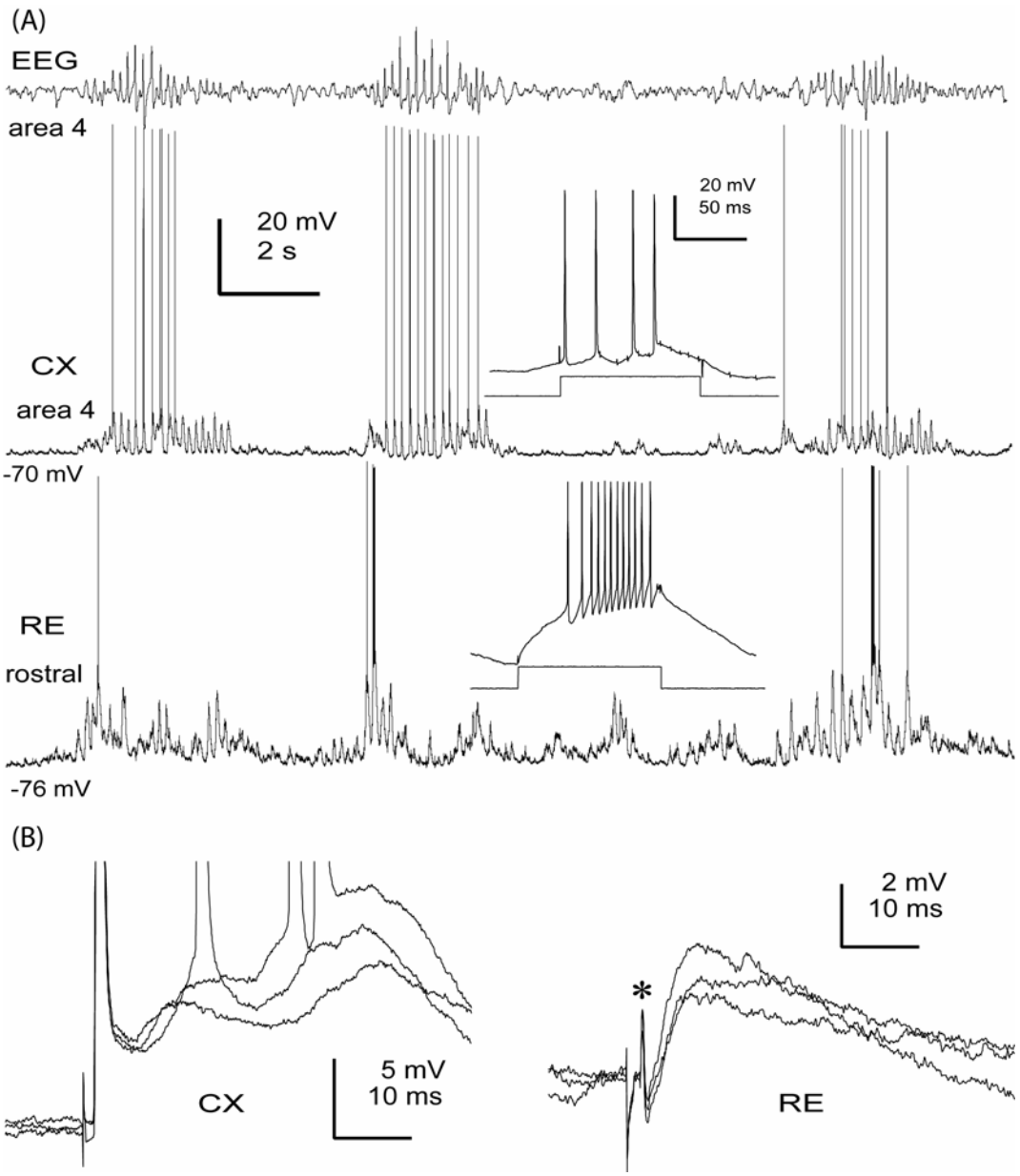
(A)
EEG
area 4
20 mV
2 s
20 mV
50 ms
CX
area 4
-70 mV
RE
rostral
-76 mV
(B)
5 mV
10 ms
CX
2 mV
10 ms
*
RE

Figure 1.6. Cortical spindles are coherent oscillations during natural sleep. In the *top panel* (*HUMAN*), spindles were recorded from six standard EEG derivations (indicated in the schematic at *right*, *arrowheads*) in a normal subject during sleep stage 2. Cross-correlations of individual spindle sequences (n = 15) were calculated between C3-A2 and each one of the other channels. Averaged correlations (*CROSS*) showed rhythmicity at 14 Hz and central peak values between 0.7 and 0.9. *Bottom panel* (*CAT*) shows EEG from a chronically implanted naturally sleeping animal. EEG was recorded from six tungsten electrodes separated by 1 mm, inserted in the depth of the suprasylvian gyrus (*Ssylv*), represented by *dots 1–6* in the scheme at *right*; also in the scheme are represented the ectosylvian (*Ecto.*) and the marginal (*Marg.*) gyri [anterior (*Ant.*) and posterior (*Post.*) are indicated]. The same procedure as for the human EEG was used to obtain the averaged cross-correlations depicted at *right* (*CROSS*), showing correlation at 14 Hz with central peaks between 0.75 and 0.9. (Contreras et al., 1997).

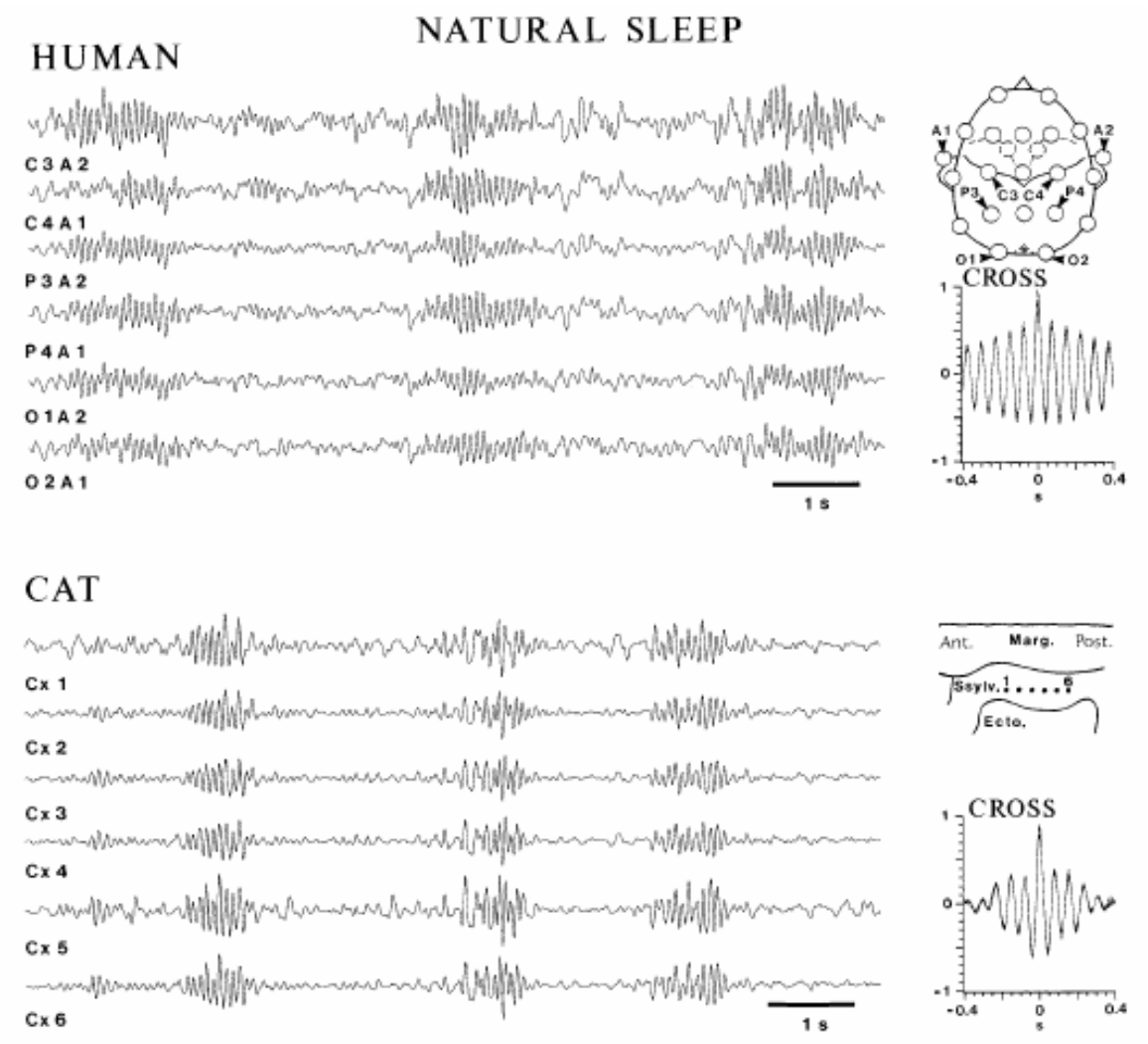
NATURAL SLEEP
HUMAN
C3 A2
C4 A1
P3 A2
P4 A1
O1 A2
O2 A1
1 s
A1
A2
P3
C3 C4
P4
O1
O2
CROSS
1
0
-1
-0.4
0
0.4
s
CAT
Cx 1
Cx 2
Cx 3
Cx 4
Cx 5
Cx 6
1 s
Ant.
Marg.
Post.
Ssylv.
Ecto.
CROSS
1
0
-1
-0.4
0
0.4
s

Figure 1.7. Spreading of activity in computer-simulated networks of RE neurons. (A) Velocity of the traveling wave in a one dimensional network. a, velocity of propagation as a function of $GABA_A$ conductance. N is the radii of connections. For N>6 and $gGABA_A$>0.2 μS, the speed of propagation showed only a weak dependence on $GABA_A$ receptor coupling and radius of RE-RE connections. The solid curves are the nonlinear fits of the calculated data. b, localized activity patterns propagating with different speed. $gGABA_A$=0.1 μS, N=2 (left) and $gGABA_A$=0.4 μS, N=7 (right). (B) Localized patterns of activity in a two dimensional network model. a, the maximal conductance for low-threshold calcium current in reticular cells was g_T=2.2 mS/cm^2. Initial stimulation of one cell at t=0 led a cylindrical wave traveling through the network with a constant velocity. b, g_T=2.45 mS/cm^2. Increasing the maximal conductance for low-threshold calcium current led to self-sustained patterns of activity in the form of a rotating spiral wave. (Bazhenov et al., 1999).

A

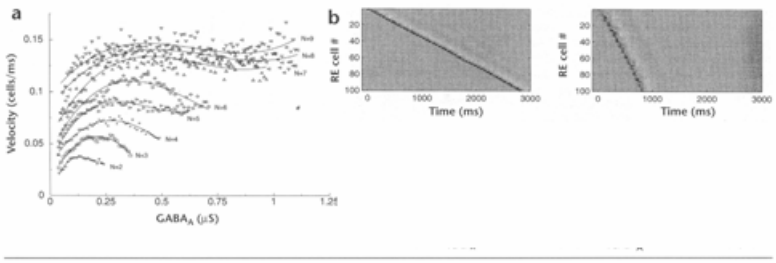
a
Velocity (cells/ms)
GABA$_A$ (μS)
b
RE cell #
Time (ms)
RE cell #
Time (ms)

B

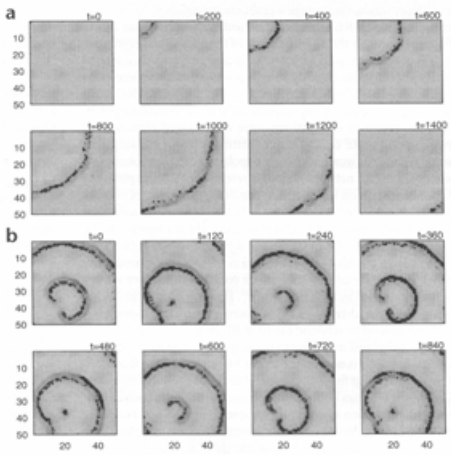
a
b

Figure 1.8. Synaptic interactions between thalamocortical and PG cells. (*A*–*C*) Activation of a PG neuron that monosynaptically innervates a thalamic relay cell results in IPSPs. Generation of a tonic train of action potentials in the PG neuron through the intracellular injection of a current pulse results in a barrage of IPSPs in the thalamocortical cell but does not result in a rebound LTS. In contrast, activation of the PG neuron in the burst firing mode results in a larger IPSP and a rebound LTS in the thalamocortical neuron. (*D*–*F*) Monosynaptic connections between thalamocortical and PG neurons. Generation of a single spike in the thalamocortical neuron results in a prolonged single EPSP in the PG cell. Generation of a burst of action potentials results in a barrage of EPSPs that exhibit temporal summation. (McCormick and Bal, 1997).

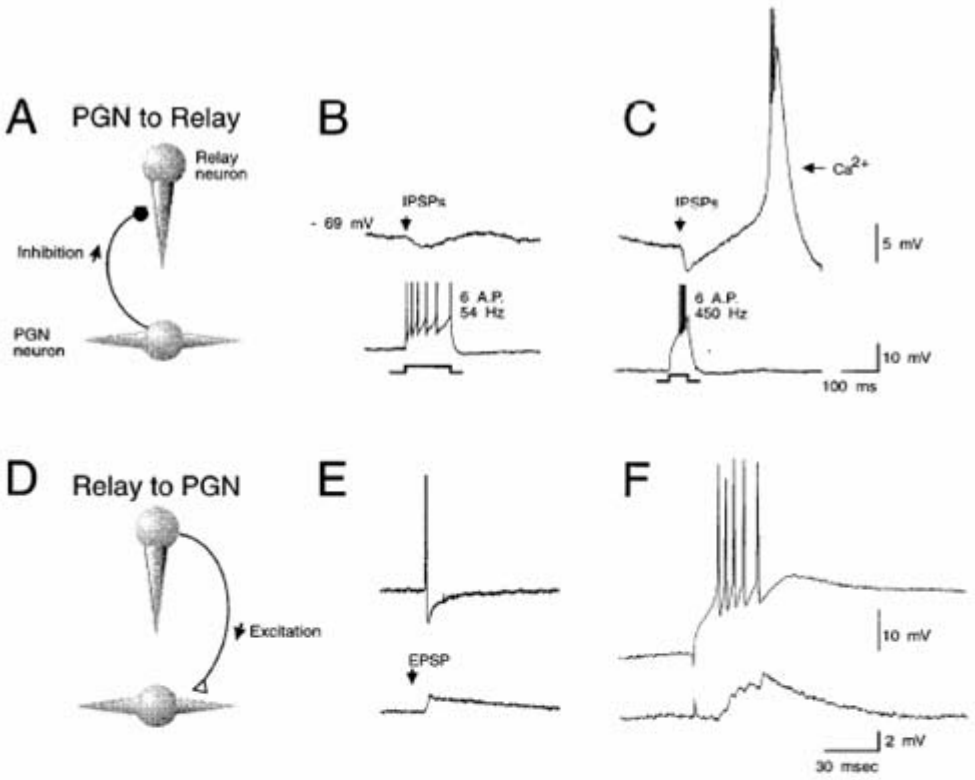
A
PGN to Relay
Relay neuron
Inhibition
PGN neuron
B
- 69 mV
IPSPs
6 A.P.
54 Hz
C
IPSPs
Ca^{2+}
5 mV
6 A.P.
450 Hz
10 mV
100 ms
D
Relay to PGN
Excitation
E
EPSP
F
10 mV
2 mV
30 msec

Figure 1.9. Spindle waves and the interaction between RE or PG cells and thalamocortical cells during spindle wave generation. (*A*) Field potential recording in cat intralaminar central lateral thalamic nucleus. Filtering of the field potential recording reveals spindle waves. (Paré et al., 1987). (*B*) Spindle waves are generated *in vitro* by an interaction between PG neurons and relay neurons such that PG neurons inhibit a number of relay neurons, some of which rebound burst following each IPSP. These rebound bursts activate LTSs and action potential bursts in PG neurons. (McCormick and Bal, 1997).

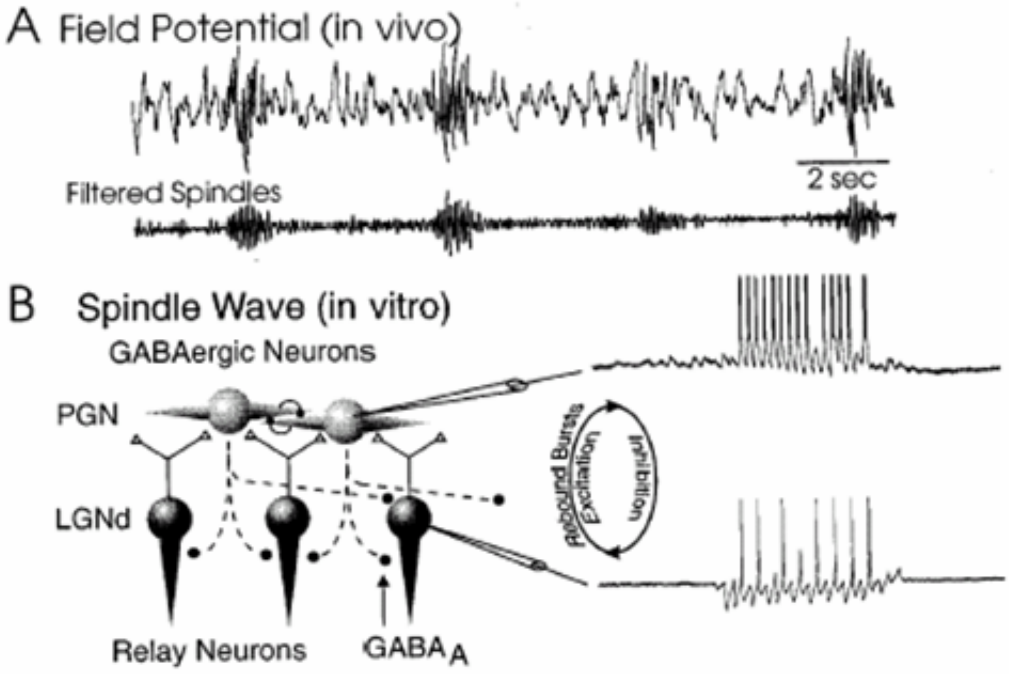
A Field Potential (in vivo)
2 sec
Filtered Spindles
B Spindle Wave (in vitro)
GABAergic Neurons
PGN
LGNd
Rebound Burst
Excitation
Inhibition
Relay Neurons
GABA A

Figure 1.10. Electrical coupling between rat RE neurons. (A) Intracellular current steps (200 pA) to evoke responses in cell 1 induced attenuated voltage changes in cell 2 (*left traces*) (coupling coefficient of 0.1). Tracings on the *right* are from the same cell pair, but, in this case, current steps were delivered to cell 2. (B) Close-up of a single presynaptic spike and the averaged spikelet it induced in the soma of a coupled neighboring cell. (C) Close-up of the rebound burst generated by cell 2 in *A* (*right*) and the coupling potential corresponding to it in cell 1. (Landisman et al., 2002).

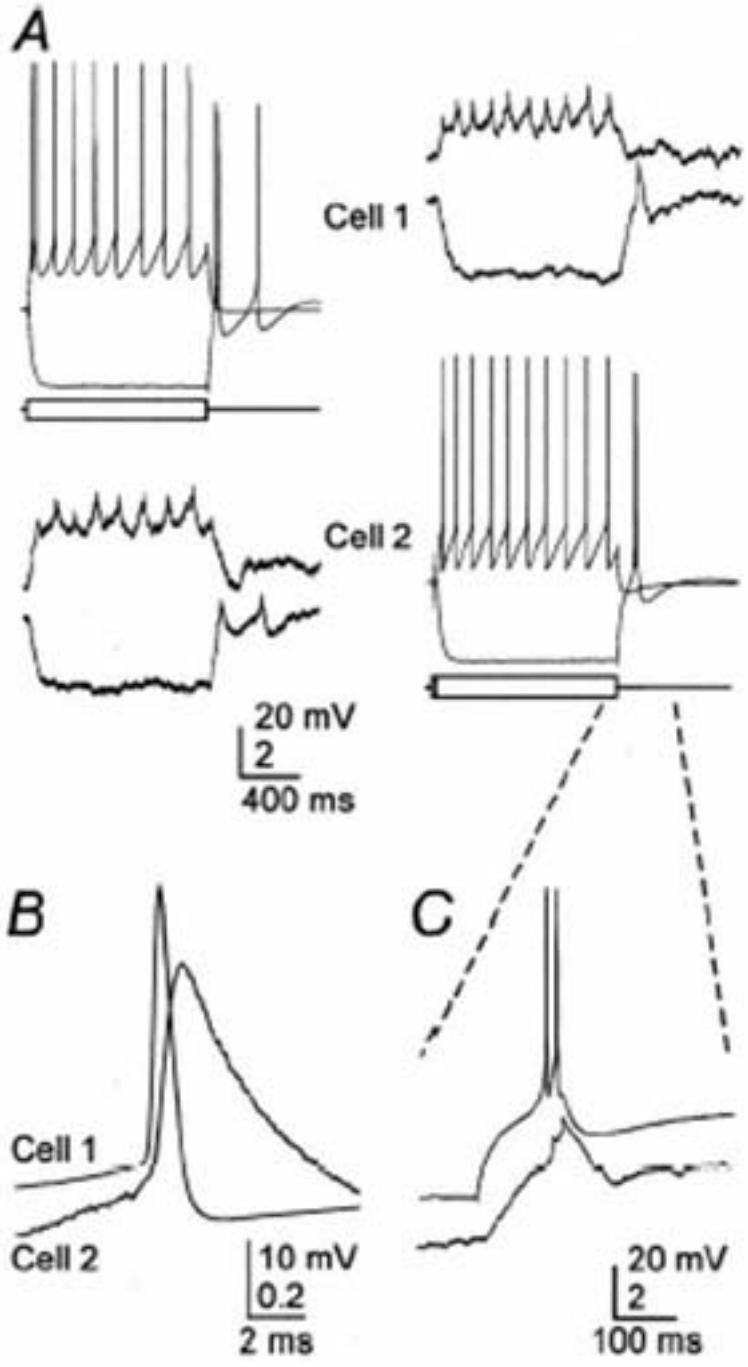
A
Cell 1
Cell 2
20 mV
2
400 ms
B
Cell 1
Cell 2
10 mV
0.2
2 ms
C
20 mV
2
100 ms

Figure 1.11. Subthreshold rhythms can synchronize spikes in RE neurons. (A) A hyperpolarized pair of RE cells that show strongly synchronous and rhythmic subthreshold activity in response to ACPD application, as reflected in the corresponding crosscorrelogram (values for each bin were normalized by the mean number of spikes per bin). (B) ACPD-induced spike synchrony in the absence of hyperpolarizing holding current. Action potentials are truncated in these traces. (C) Paired recordings during ACPD-induced rhythms. Initially both cells generated well synchronized subthreshold rhythms; as cells depolarized slightly, cell 1 began to spike. Rhythmic spikes in cell 1 were consistently well correlated with the peaks of the subthreshold rhythms in cell 2. (Long et al., 2004).

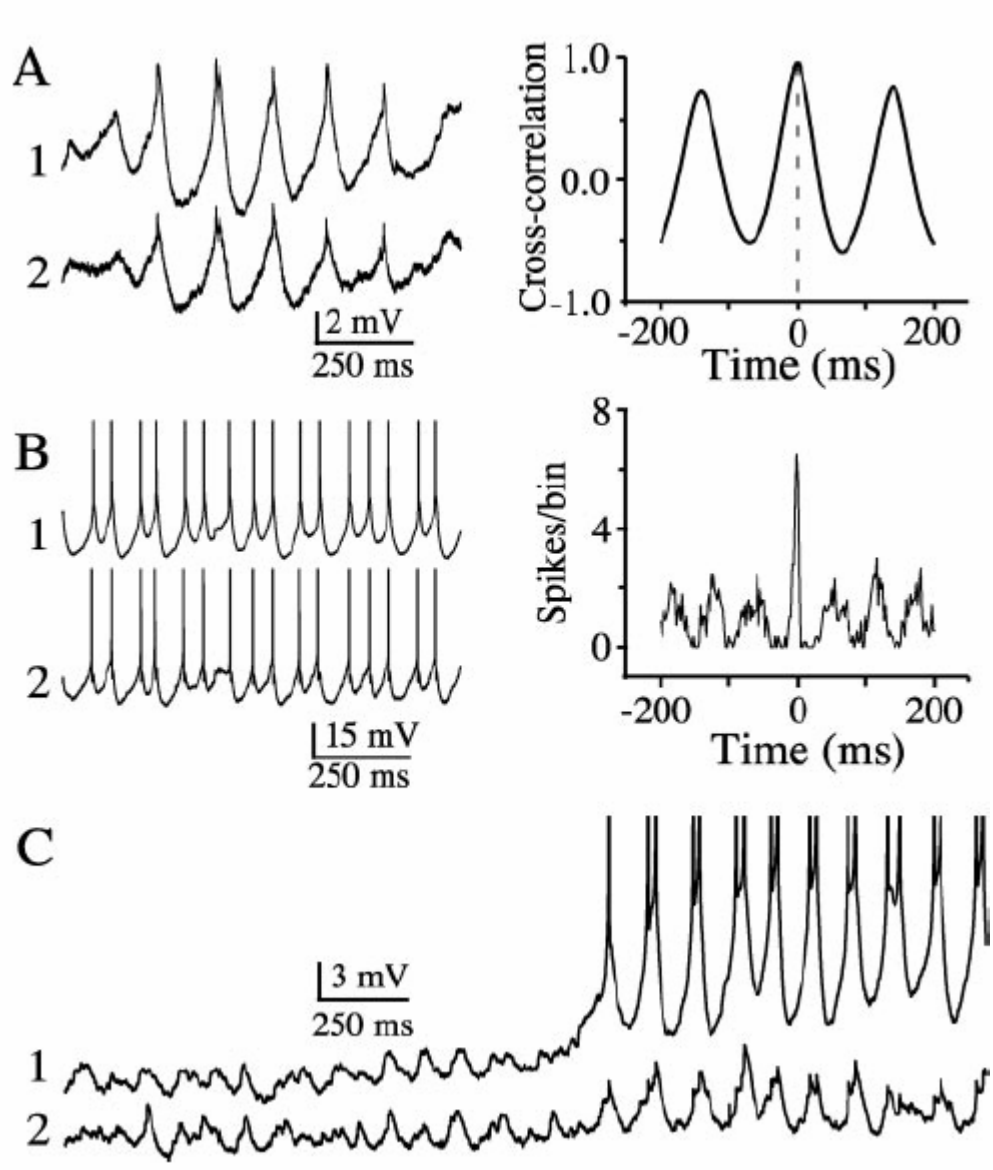
A
1
2
2 mV
250 ms
Cross-correlation
1.0
0.0
-1.0
-200
0
200
Time (ms)
B
1
2
15 mV
250 ms
Spikes/bin
8
4
0
-200
0
200
Time (ms)
C
3 mV
250 ms
1
2

Figure 1.12. Phase relations between spindling in cortical EEG and intracellularly recorded RE neurons. EEG from motor area 4, reticular neurons from the rostrolateral sector. Ketamine-xylazine anesthesia. (A) The filtering of EEG waves (0.3-100 Hz) enhanced the spindling oscillation and diminished the slow components of the EEG. Panels A1-3 show three different spontaneous spindle sequences. The oscillatory behavior within the frequency range of spindles was preceded by a cellular hyperpolarization that corresponded to a depth-positive EEG wave. In A4, expanded first burst of the oscillation depicted in A1. (B) A single response of a reticular neuron to cortical stimulation is shown for a relatively depolarized membrane potential, together with the EEG from the surface and depth of the motor cortex. The cell oscillated in phase with the depth-negative EEG waves that reverse polarity at the surface. (Contreras and Steriade, 1995).

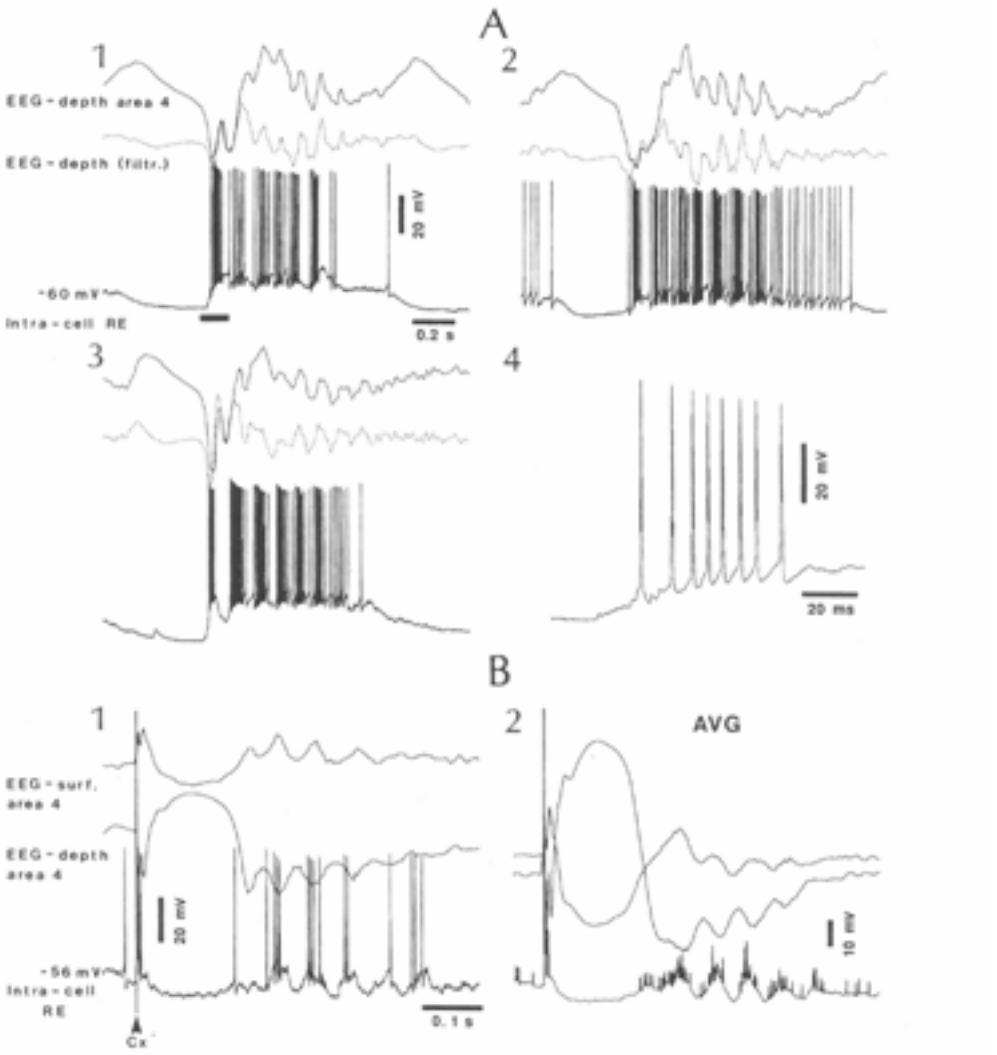
A
1
EEG - depth area 4
EEG - depth (filtr.)
20 mV
-60 mV
Intra - cell RE
0.2 s
2
3
4
20 mV
20 ms
B
1
EEG - surf. area 4
EEG - depth area 4
20 mV
-56 mV
Intra - cell RE
A
Cx
0.1 s
2
AVG
10 mV

Figure 1.13. Cortical and RE neurons oscillate in phase during spindles. A cortical neuron was recorded intracellularly from cat motor cortex, simultaneously with EEG from the depth of cortical area 4 and a rostrolateral RE cell. Ketamine-xylazine anesthesia. In the left panel, the three traces show spontaneous spindle sequences, aligned by the first depth-negative of cortical EEG and displaced vertically for clarity. By using the same alignment point, the right panel shows an average calculated from 10 spontaneous spindle sequences and the perievent histogram (bin = 5 ms) for the reticular neuron. (Contreras and Steriade, 1995).

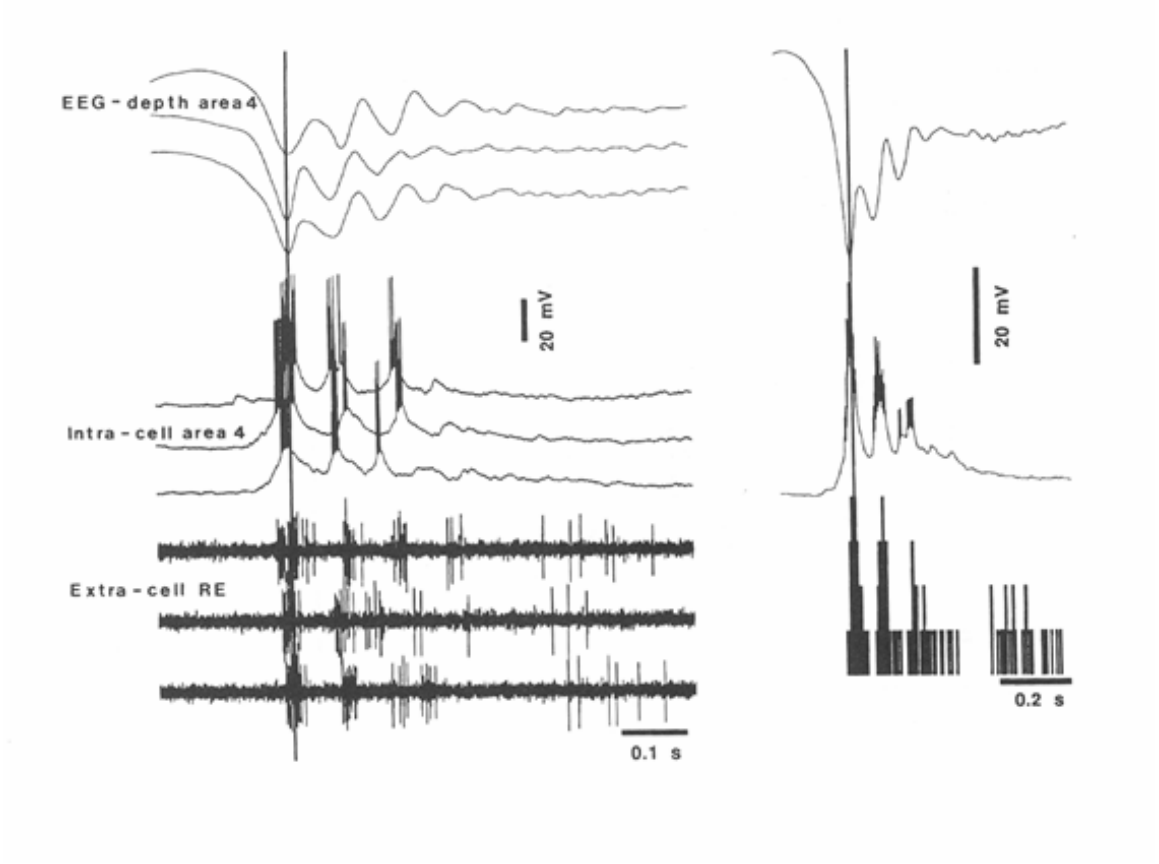
EEG - depth area 4
20 mV
Intra - cell area 4
Extra - cell RE
0.1 s
20 mV
0.2 s

Figure 1.14. Persistent activation of the hyperpolarization-activated cation current I_h generates the slow afterdepolarization. (A) Intracellular injection of repetitive (4 Hz) short-duration (120 ms) hyperpolarizing current pulses results in the generation of a slow afterdepolarization (ADP). Local application of Cs^+ (20 mM in micropipette) completely, and reversibly, blocks this afterdepolarization. (B) and (C) Expansion of electrotonic response to intracellular injection of hyperpolarizing current pulses, illustrating the effects of Cs^+. The main effect was a block of the depolarizing sag that accompanies hyperpolarization, indicating block of Ih. (D) and (E) Intracellular injection of a depolarizing current pulse to deactivate I_h also results in a block of the ADP. (D) Intracellular injection of repetitive hyperpolarizing current pulses is followed by an ADP. (E) Depolarization of the neuron during this ADP results in a reduction or abolition of the afterdepolarization. The full extent of the voltage deviations during the hyperpolarizing current pulses are not illustrated. (Bal and McCormick, 1996).

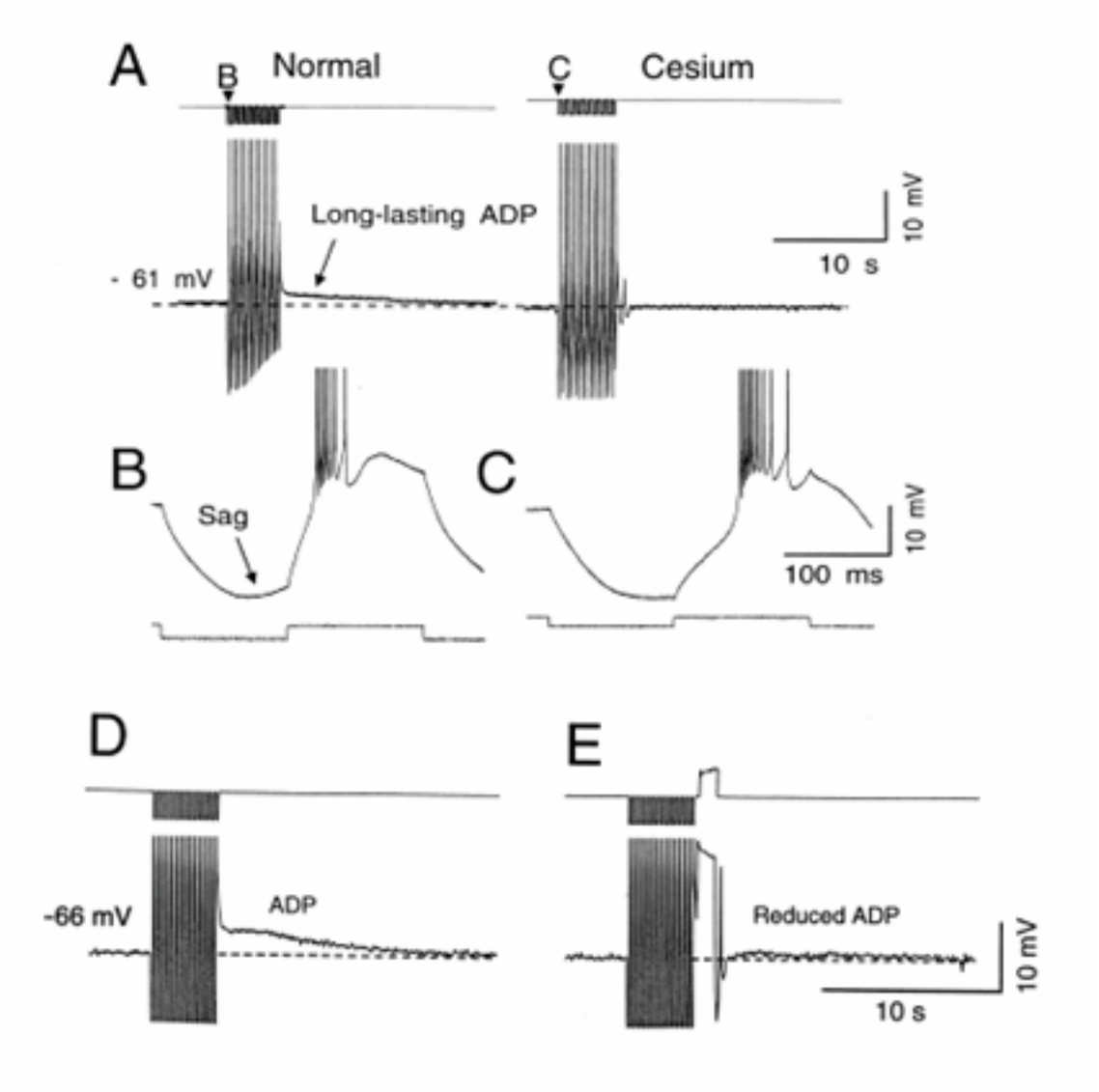
A
B
Normal
C
Cesium
Long-lasting ADP
- 61 mV
10 mV
10 s
B
Sag
C
10 mV
100 ms
D
-66 mV
ADP
E
Reduced ADP
10 mV
10 s

Figure 1.15. Intensity-dependency of decremental and incremental intracellular responses of rostral RE neuron to repetitive (10 Hz) VL stimuli. (A) lower speed; responses to all 5 stimuli in a pulse train at 10 Hz. (B) higher speed; responses to 1st and 2nd and 4th and 5th stimuli, respectively. Decremental responses were observed with stimuli at 15–30% of maximal intensity. Incremental responses occurred at high intensities (70–100%). At half intensity (50%) there was virtually no change in the number of spikes evoked by the 5 stimuli in the pulse train. (Timofeev and Steriade, 1998).

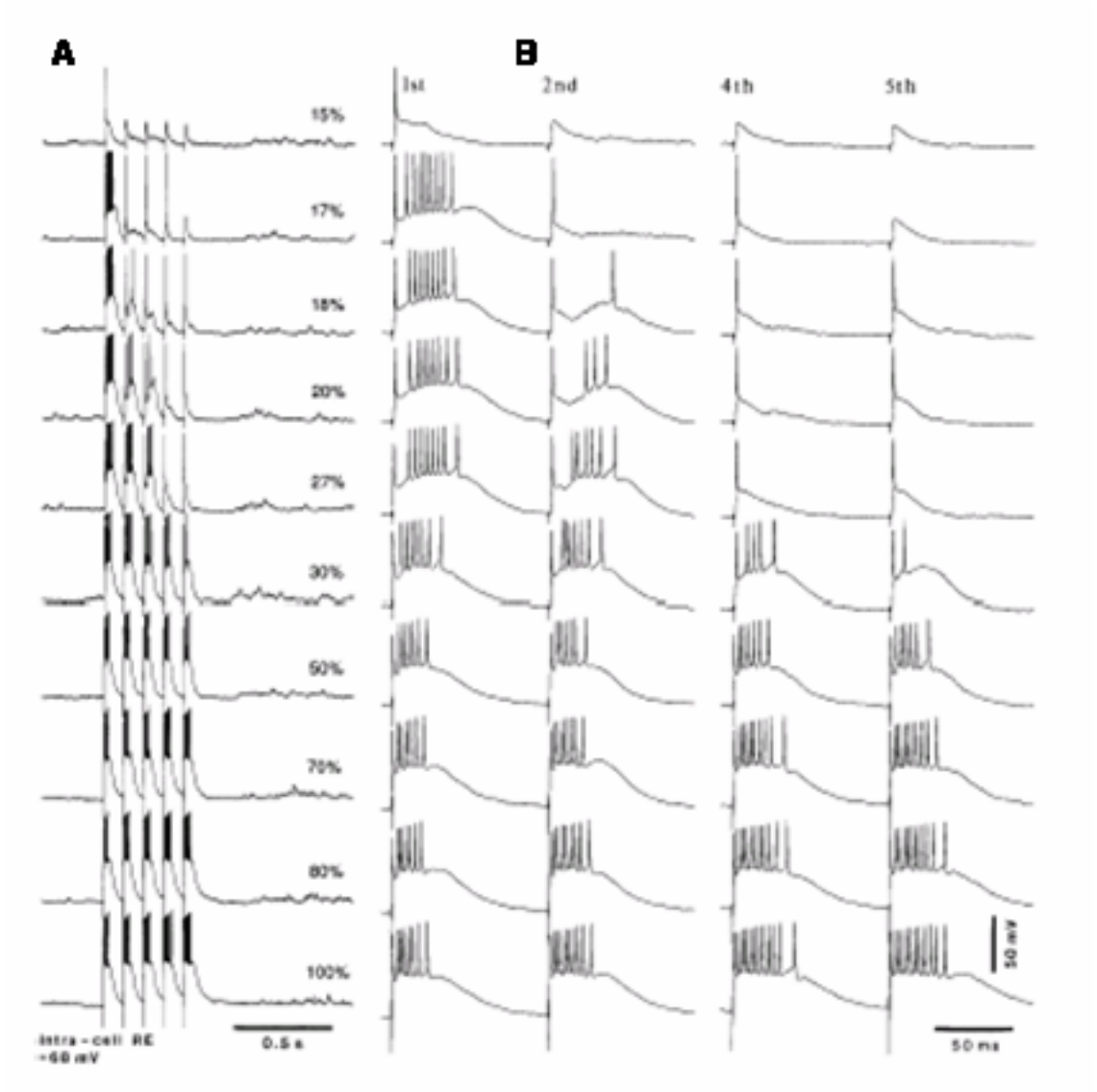
A
B
1st
2nd
4th
5th
15%
17%
18%
20%
27%
30%
50%
70%
80%
100%
Intra-cell RE
-68 mV
0.5 s
50 mV
50 ms

Figure 1.16. LTSs in thalamocortical neurons are graded in amplitude and time to peak. Intracellular recordings *in vivo*, ketamine–xylazine anesthesia, decorticated animal. (A) LTS responses generated at a termination of 100 ms hyperpolarizing current pulses. Note stability and graded nature of responses as a function of applied current pulse (left) and great fluctuations in time and amplitude at threshold hyperpolarization (right). Plots below indicate graded responses in voltage (B) and time-to-peak (C). Conditioning membrane potential is the membrane potential just before the end of the current pulse. Amplitude of maximal depolarization is calculated from baseline membrane potential. Time-to-peak is the time from the end of current pulse to the maximal depolarization excluding fast spikes. (D) LTS reaches its maximal amplitude first and then the latency to peak decreases. (Timofeev et al., 2001).

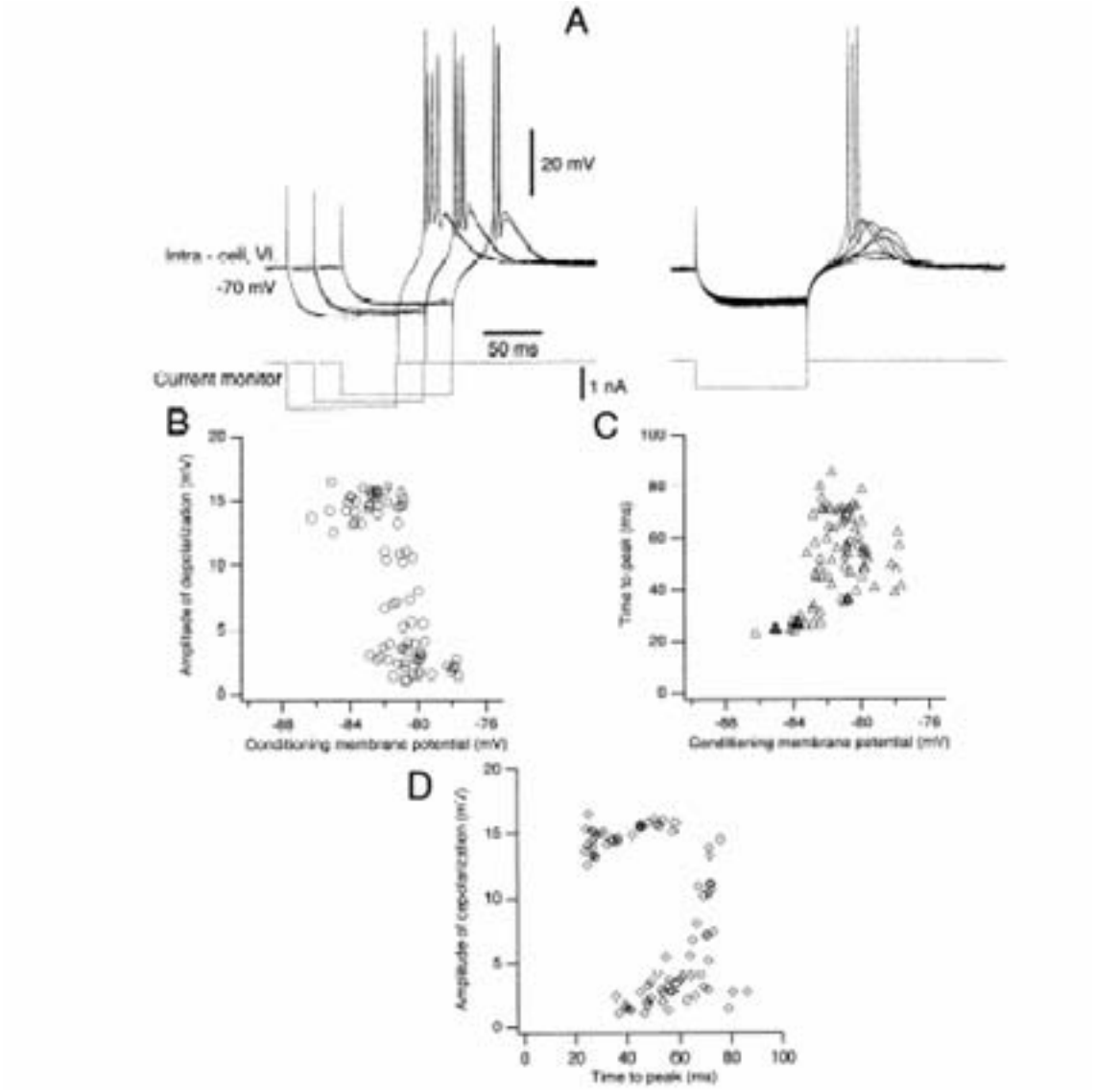
A
20 mV
Intra - cell, Vi
-70 mV
50 ms
Current monitor
1 nA
B
Amplitude of depolarization (mV)
Conditioning membrane potential (mV)
C
Time to peak (ms)
Conditioning membrane potential (mV)
D
Amplitude of depolarization (mV)
Time to peak (ms)

RESULTS

2. Electrical Synapses and their Role in Network Oscillations

EXPERIMENTAL EVIDENCE AND MODELING STUDIES SUPPORT A SYNCHRONIZING ROLE FOR ELECTRICAL COUPLING IN THE CAT THALAMIC RETICULAR NEURONS IN VIVO

Pablo Fuentealba, Sylvain Crochet, Igor Timofeev, Maxim Bazhenov, Terrence J. Sejnowski and Mircea Steriade (2004). *European Journal of Neuroscience* 20(1):111-119.

RESUMÉ

Les neurones thalamiques réticulaires (RE) jouent un rôle crucial dans les rythmes du cerveau. Ici, nous rapportons que les neurones RE de chats adultes, enregistrés et marqués intracellulairement *in vivo*, présentaient des *spikelets* de façon spontanée, ce qui est une caractéristique des neurones centraux qui sont couplés électriquement par des jonctions communicantes (*gap junctions*). Les *spikelets* se produisent spontanément pendant l'oscillation en fuseau, une oscillation dans laquelle les neurones RE jouent un rôle primaire, aussi bien que pendant les périodes d'accalmie entre les fuseaux. Ils étaient significativement différents des potentiels postsynaptiques excitateurs et aussi, ils étaient différents des prépotentiels rapides (FPPs) qui sont vraisemblablement des potentiels d'action dendritiques générés synaptiquement. Les *spikelets* étaient fortement réduits par l'halothane, un inhibiteur des jonctions communicantes. Des enregistrements extracellulaires multiples fait avant, pendant et après une administration d'halothane ont démontré un rôle du couplage électrique dans la synchronisation de l'activité en fuseau à l'intérieur du noyau RE. Finalement, des modèles de simulations par ordinateur ont prédit que les jonctions communicantes entre ces neurones pourraient favoriser la propagation d'activité à basse fréquence sur de longues distances. Ces données expérimentales et de simulations suggèrent qu'un couplage électrique à l'intérieur du noyau RE joue un rôle de premier plan dans la génération et la synchronisation des activités à basses fréquences (fuseaux) dans le thalamus.

ABSTRACT

Thalamic reticular (RE) neurons are crucially implicated in brain rhythms. Here, we report that RE neurons of adult cats, recorded and stained intracellularly *in vivo*, displayed spontaneously occurring spikelets, which are characteristic of central neurons that are coupled electrotonically via gap junctions. Spikelets occurred spontaneously during spindles, an oscillation in which RE neurons play a leading role, as well as during interspindle lulls. They were significantly different from excitatory postsynaptic potentials and also distinct from fast prepotentials that are presumably dendritic spikes generated synaptically. Spikelets were strongly reduced by halothane, a blocker of gap junctions. Multi-site extracellular recordings performed before, during and after administration of halothane demonstrated a role for electrical coupling in the synchronization of spindling activity within the RE nucleus. Finally, computational models of RE neurons predicted that gap junctions between these neurons could mediate the spread of low-frequency activity at great distances. These experimental and modeling data suggest that electrotonic coupling within the RE nucleus plays an important role in the generation and synchronization of low-frequency (spindling) activities in the thalamus.

INTRODUCTION

The GABAergic neurons of the thalamic reticular (RE) nucleus provide inhibitory input to thalamocortical neurons and are crucially involved in the generation of spindles (Steriade *et al.*, 1985, 1987), an oscillation that characterizes early stages of natural slow-wave sleep and barbiturate anesthesia. It was recently shown in slices maintained *in vitro* that RE neurons of rats and mice are electrically coupled and that electrical synapses require Cx36 (Landisman *et al.*, 2002), the predominant type of connexins, proteins that comprise gap junction channels (Condorelli *et al.*, 2000; Rash *et al.*, 2000; Venance *et al.*, 2000). Parallel experiments also revealed dye-coupling in cat dorsal lateral geniculate (dLG) neurons *in vitro*, accompanied by spikelets that survived application of antagonists of fast chemical synaptic transmission and were reversibly blocked by the gap junction blocker carbenoxolone (Hughes *et al.*, 2002). Spikelets are considered to be the electrophysiological correlate of electrotonic coupling via gap junctions (Perez Velazquez & Carlen, 2000).

In addition to interactions through conventional chemical synapses, thalamic neurons use electrical synapses that might promote the synchronization of normal brain rhythms as well as in paroxysmal activities. The RE nucleus has a pivotal role in both these oscillatory types. The synaptic interactions between RE neurons as well as their reciprocal relations with thalamocortical neurons are regarded as the key elements in generating sleep spindles (Steriade *et al.*, 1993) and imposing inhibitory postsynaptic potentials (IPSPs) on thalamocortical neurons during spike-wave seizures (Steriade &

Contreras, 1995; Timofeev *et al.*, 1998; Avanzini *et al.*, 1999). In view of the above-mentioned results from *in vitro* experiments on juvenile animals demonstrating electrical synapses among rat RE neurons, we examined this topic *in vivo*, using intracellular recordings and staining of these inhibitory neurons in the adult cat, as well as computational models. Data showed the presence of spikelets during and outside RE-cells' oscillatory activity, which were significantly different from excitatory postsynaptic potentials (EPSPs) and fast prepotentials (FPPs). These results have been published in abstract form (Fuentealba *et al*., 2002).

METHODS

Animal preparation

Experiments were performed on adult cats (2.5-3.5 kg), deeply anesthetized with pentobarbital (25 mg/kg, i.p.), urethane (1.8 g/kg, i.p.), or ketamine-xylazine (10-15 mg/kg and 2-3 mg/kg, respectively, i.m.). When the cats showed the signs of deep anesthesia, the animals were paralyzed with gallamine triethiodide and artificially ventilated with control of the end-tidal CO_2 concentration at ~3.5%. Body temperature was maintained at 36-38^{o} C. The depth of anesthesia was continuously monitored by EEG and additional doses of anesthetics were administered at the slightest tendency toward low-voltage and fast EEG rhythms. At the end of experiments, animals were given a lethal dose of pentobarbital (50 mg/kg).

Electrophysiological recordings

Current-clamp recordings from thalamic RE neurons were performed using glass micropipettes (DC resistance, 30-60 MΩ). To avoid breaking of recording micropipettes, the cortex and white matter overlying the head of the caudate nucleus were removed by suction. The pipettes entered ~3 mm through the caudate nucleus to reach the rostral pole or the rostrolateral sector of the thalamic RE nucleus. Pipettes were generally filled with 3 M solution of K-acetate and, in some experiments, with KCl or KAc containing 50 mM of QX-314. The stability of intracellular recordings was ensured by cisternal drainage, bilateral pneumothorax, hip suspension, and by filling the hole over the thalamus with 4% agar solution. A high-impedance amplifier with active bridge circuitry was used to

record and inject current inside the cells. Most intracellular recordings included in the database lasted for periods longer than 30 min. Simultaneous extracellular recording were performed using up to four tungsten electrodes (10-15 MΩ; Frederick Haer, Bowdoinham, WA, USA) inserted through the caudate nucleus, with an inter-electrode distance of ~0.5 mm. Thalamic RE neurons were recognized by their long burst (>50 ms) and the accelerando-decelerando bursting firing pattern (see Fig. 2.7*A*). For data acquisition system, we used Nicolet Vision (Middleton, WI, USA).

Data analysis and computational modeling

The extraction of spikelets and EPSPs was performed automatically using Mini Analysis Program (Synaptosoft). The peaks of events were selected within 3-ms windows, considering only deflections with higher amplitude than 0.6 mV and half duration less than 10 ms. Rising phase was fitted with a single exponential between the 10% to 90% of the peak, while decaying phase was fitted with a single exponential between 90% to 10% of the peak.

Three network models were simulated: *1)* a circuit with two coupled RE neurons; *2)* a one-dimensional chain of 100 RE cells; and *3)* a two-dimensional network of 128x128 RE neurons. In the one-dimensional network the diameter of the connection fan out for RE<->RE electrical coupling was 2 cells. $GABA_A$ synapses were set at distances from 3 to 5 cells randomly, with probability 0.2. Each RE cell was modeled by a single compartment that included fast Na^+ current, fast K^+ current, low-threshold Ca^{2+}-dependent current, and K^+ leak current described by Hodgkin-Huxley kinetics. $GABA_A$

synaptic currents were modeled by first-order activation schemes (Destexhe *et al.*, 1996). Electrical coupling was modeled as $I_{ele} = g_{ele} (V_{pre} - V_{post})$, where g_{ele} is maximal conductance, $V_{pre - post}$ is pre - postsynaptic membrane potential. The voltage- and Ca^{2+}-dependent transition rates for all intrinsic currents and the rate constants for all synaptic kinetic equations are given elsewhere (Bazhenov *et al.*, 1998).

RESULTS

Characteristics of spikelets during spontaneous activity of RE neurons

Intracellular recordings from the rostral pole and rostrolateral sector of the cat RE nucleus (n = 49) showed the characteristic accelerando-decelerando pattern of their long spike-bursts that occurred over the depolarizing envelope of spindle sequences (inset in Fig. 2.1*A*), which are different from the shorter spike-bursts of thalamocortical neurons with progressively longer interspike intervals (Domich *et al.*, 1986; Contreras *et al.*, 1993). Invariably, small-amplitude, short-duration events were observed during spontaneous activity of all recorded RE neurons, regardless of the anesthesia (barbiturate, n = 29; urethane, n = 10; ketamine-xylazine, n = 10). During barbiturate-induced spindling activity, RE neurons displayed prolonged spike-bursts over a depolarizing envelope and spikelets occurred during both spindle sequences and interspindle lulls (Fig. 2.1*A*-*B*). In addition to electrophysiological features that define RE neurons, some neurons located in the rostrolateral sector of the nucleus adjacent to the ventrolateral nucleus were intracellularly stained and showed the typical aspect of RE neurons, with fusiform shape lying parallel to the surface of the dorsal thalamus and very long dendrites (Fig. 2.1*C*).

Generally, spikelets were much smaller (1.03 ± 0.04 mV, range 0.8 to 1.2 mV; n = 25) than action potentials, with a common amplitude ratio of ~1:50 (inset in Fig. 2.1*B*). In some neurons, however, spikelets reached amplitudes up to 3-5 mV (see below, Figs. 2.3*A* and 2.5*A*). Spikelets were fast-rising (0.52 ± 0.1 ms, range 0.3 to 0.7 ms; n = 25) and

fast-decaying (1.8 ms ± 0.3 ms, range 0.8 to 3 ms, n = 25 neurons). The distributions of rise and decay times are shown for a representative RE neuron in Fig. 2.2*B*. Spikelets were voltage-independent for a large range of membrane potentials (Fig. 2.2*C*), thus suggesting their ubiquitous presence under physiological conditions.

Spikelets are different from EPSPs and FPPs

To differentiate spikelets from depolarizing events triggered by synaptic mechanisms, such as EPSPs and FPPs, we first set the threshold for their detection at 0.6 mV, well beyond the maximum value of electronic noise that reached ~0.3-0.4 mV (see Fig. 2.2*C*). When all subthreshold events were considered (action potentials were excluded), the histograms of their amplitudes showed a continuously decreasing distribution from 0.6 to 5 mV (not shown). The duration of depolarizing events was selected at an empirical cutoff of 10 ms to encompass not only spikelets and FPPs but also slower depolarizations, such as EPSPs (see bottom left panel in Fig. 2.3*B*). As spikelets and EPSPs did not show differences in ranges of their amplitudes (0.5-6 mV), the rising and decaying phases were tested in all depolarizing events.

That spikelets and EPSPs were different events resulted from two major features. Firstly, we considered spikelets those events whose rising phase peaked at ~0.5 ms and the decaying phase at ~2 ms, whereas the same phases peaked at ~1 ms and ~4 ms in EPSPs (Fig. 2.3*A*). Thus, spikelets have much faster rising and decaying phases than EPSPs. Secondly, spikelets were unable to elicit full action potentials, even during states of membrane depolarization close to firing threshold, whereas EPSPs led to cell firing at

the same level of depolarization (Fig. 2.3*B*). Modeling studies have suggested that the membrane time constant, τ_m, influences the delay between the onset of a given synaptic input and spike generation (Koch *et al.*, 1996), i.e. the generation of a full action potential is not instantaneous once the threshold is reached. It is then possible that fast events displaying very short durations, such as spikelets, do not generate full action potentials even if they reach the threshold for spike generation.

Spikelets could also be distinguished from fast prepotentials (FPPs), which are usually considered as dendritic spikes triggered by synaptic volleys. Since the initial identification in hippocampal neurons (Spencer & Kandel, 1961), FPPs are characterized by rapid falling phase and initiation at ~5-6 mV below the usual firing level. These synaptic events have been described in RE neurons where they were efficiently triggered by corticothalamic volleys (Contreras *et al.*, 1993) and in thalamocortical neurons (Maekawa & Purpura, 1967; Deschênes *et al.*, 1984; Steriade *et al.*, 1991; Timofeev & Steriade, 1997). In the present experiments, the amplitudes of FPPs were much greater than those of spikelets, and their time-course was also different (see scaled spikelet and FPP in Fig. 2.4*A*). In contrast to spikelets, FPPs were mainly present during periods of membrane depolarization; thus, comparison bottom right plot in Fig. 2.2*C* (spikelets) with bottom left histogram in Fig. 2.4*B* (FPPs) shows that FPPs are virtually absent at membrane potentials more negative than –70 mV. However, similarly to spikelets, the amplitudes of FPPs were not voltage-dependent (bottom right plot in Fig. 2.4*B*).

Similarity between spikelets and firing patterns of RE neurons

RE neurons display two different modes of firing patterns: bursting, with intraburst frequencies up to 300-400 Hz, defining states associated with membrane hyperpolarization, as in natural slow-wave sleep (Steriade *et al.*, 1986) and anesthesia (Contreras et al., 1993) or some types of seizures (Steriade & Contreras, 1995; Timofeev *et al.*, 1998); and tonic, with single spikes at frequencies between 40 and 80 Hz, characteristic for the waking state (Steriade *et al.*, 1986). Figure 2.5 shows two RE neurons recorded in different experiments, one of them displaying spikelets, the other full action potentials. The frequency of clusters formed by spikelets (~350-400 Hz) and that of individual spikelets (~40-50 Hz) in one RE neuron were similar to frequencies of spike-bursts and tonic firing displayed by the other RE neuron. Histograms of inter-event intervals also demonstrate the two firing modes in both neurons, with an early peak at 3-4 ms, reflecting frequencies of spike-bursts and clusters of spikelets (which both predominated during recordings), and widely distributed intervals during the tonic mode, mainly between 10 and 20 ms.

Origin of spikelets

To determine the origin of spikelets, several manipulations were performed. Decortication or addition of QX-314 or KCl in the recording pipette had no effect on the amplitudes or incidence of spikelets (not shown). By contrast, administration of halothane (5%, 2-5 min; n = 4), a gap junction blocker, invariably decreased the incidence of spikelets, without changing their amplitudes and durations (Fig. 2.6). Halothane blocked the occurrence of spindle sequences under barbiturate anesthesia. Its action lasted for 7-8 min, with complete recovery after 10 min. The strongest observed

effect was on spikelets. The ratio between spikelets and EPSPs, recorded during periods of 5 min in all three states (before, during, and after halothane administration) showed a 5-fold decrease from control to halothane, with subsequent recovery to the control value.

Role of gap junctions in synchronization of spindling activity in the thalamus

In order to test a possible role of gap junctions in the synchronization of activity in the RE nucleus, simultaneous dual, triple and quadruple extracellular recordings of RE neurons were performed in decorticated cats under barbiturate anesthesia, and auto- and cross-correlation analyses were carried out before and after the application of halothane (4%, 2-3 min). Decortication was performed to avoid any corticothalamic influences. During the control period (5-10 min), neurons displayed oscillatory activity in the spindle frequency (~10 Hz) (Fig. 2.7*A*). Such activity was highly correlated between the different pairs of cells (Fig. 2.7*A*). Upon the application of halothane (4%, 2-3 min), RE neurons changed their behavior. Instead of the rhythmic firing characteristic of spindle activity, each neuron displayed burst and tonic firing in an apparently random way (Fig. 2.7*B*). Such activity did not represent spindle waves, since 10 Hz-activity disappeared from both auto- and cross-correlograms (Fig. 2.7*B*). Thus, halothane did not seemingly affect the firing rates of RE neurons, but their rhythmicity, in particular that in the frequency range of spindles. Note that some neuronal couples (1-3, 2-4, 1-4) maintained high correlation in the presence of halothane, but only for high frequencies, whereas correlations in the frequency range of spindles was invariably impaired (Fig. 2.7*B*). When halothane administration was stopped, spindling activity recovered slowly in all neurons until the control pattern was completely restored (Fig. 2.7*C*). Not only the spindling frequency

recovered, but also the phase lags between the different neuronal pairs were similar to those in the control (Fig. 2.7*C*). These results suggest a role for electrical coupling in the synchronization of spindle activity in the RE nucleus.

Modeling experiments predict a role for gap junctions in spreading of slow activities in the thalamus

To test a possible effect of gap junction between RE cells, a pair of electrically connected neurons was modeled. When both cells were held at relatively depolarized potentials, a single spike in the presynaptic cell induced a spikelet in the postsynaptic cell, with amplitude matching experimental data (Fig. 2.8*A*, top trace and inset). Hyperpolarization of the presynaptic RE cell de-inactivated T-channels, so the same stimulus induced a low-threshold spike (LTS) followed by a burst of fast action potentials (Fig. 2.8*A*, second trace). This relatively slow process was transmitted better through the electrical synapse and the progressive depolarization of the postsynaptic cell during the spike-burst led to a Na^+ spike (Fig. 2.8*A*, second trace). Finally, when both neurons were hyperpolarized (Fig. 2.8*A*, third trace), the electrical coupling dependent depolarization of the postsynaptic RE neuron triggered an LTS, suggesting that gap junctions may spread activity between connected cells. Intracellular recordings *in vivo* (Fig. 2.8*A*, bottom trace) indeed showed that it was rather common to see after a sequence of spikelets' clusters, the RE neuron to reach the state at which a spike-burst was generated (see inset in Fig. 2.8*A*). We should note that although the amplitude of simulated spikelets was similar to that in experimental data, the time course was different, i.e. the action potentials in the model were wider than in experimental data (Fig. 2.8*A*) because of the properties of

simulated action potentials that generated spikelets. Also, simulated spikelets displayed a prominent hyperpolarizing component after the decaying phase, generated by low-pass filtering of action potentials' afterhyperpolarizing potential, a component that was rarely seen in the present intracellular recordings.

To study the network effect of electrical coupling, a one-dimensional chain of RE neurons was simulated. Gap junctions were introduced between RE neurons within a two-neuron footprint. $GABA_A$ synapses were included between RE neurons more than two cells apart and within a five-cell radius with a sparse $GABA_A$-mediated connectivity with probability 0.2. When an external stimulus was applied to the cells at the end of the chain, a wave of activation propagated with constant velocity (not shown). In a two-dimensional network of RE cells (128x128) interconnected via gap junctions, the same mechanism mediated either plane waves (Fig. 2.8*B*) or self-sustained spiral waves (not shown). Electrical coupling mediated rebound LTS and wave propagation. Inactivation of Ca^{2+}-dependent LTS after burst discharges precipitated the refractory period, so the waves disappeared after collapsing in the middle of the network.

These results suggest that gap junctions can mediate spread of activity not only between electrically connected neurons but also at great distances.

DISCUSSION

Our results show that RE neurons investigated *in vivo* display small but rapidly rising and decaying potentials, termed spikelets in recent *in vitro* studies on RE (Landisman *et al.*, 2002) and thalamocortical (Hughes *et al.*, 2002) neurons, which are a sign of electrotonic coupling. In the absence of definitive dual intracellular recordings from neighboring RE neurons, the evidence indicate that spikelets recorded in our experiments were not synaptically triggered events: *(a)* spikelets displayed much faster rising and decaying phases than EPSPs (Fig. 2.3*A*) and their amplitudes were much lower than those of FPPs (Fig. 2.4); *(b)* spikelets did not trigger action potentials, as already reported in electrotonically coupled inferior olivary neurons (Devor & Yarom, 2002), in contrast to the ability of EPSPs to promote spiking at the same level of membrane potential (Fig. 2.3*B*); *(c)* their frequency in both cluster and single-event modes was virtually identical to those of full action potentials in other RE neurons during these two firing modes (Fig. 2.5); and *(d)* spikelets were blocked by halothane (Fig. 2.6), a gap junction blocker (Draguhn *et al.*, 1998; Moortgat *et al.*, 2000). Additionally, spikelets are not dependent on synaptic inputs from cortex, as is the case of FPPs that are most efficiently triggered by cortico-RE volleys (Contreras *et al.*, 1993), since they occurred without changes in incidence and shape/amplitude in decorticated animals. As well, recordings with KCl-filled micropipettes, to reverse $GABA_A$-receptor-mediated potentials, did not affect their characteristic features.

The time-course and amplitudes of spikelets documented here are very similar to those described in slices from RE nucleus (Landisman *et al.*, 2002). Some differences between the characteristics of presently described spikelets in RE neurons and spikelets recorded *in vitro* from thalamic dLG neurons (Hughes *et al.*, 2002) are as follows: *(a)* in dLG neurons spikelets were present in a subset of cells (17-19%), whereas all 49 of the presently recorded RE neurons displayed such events; *(b)* the amplitudes of dLG spikelets was more than twice as high (range 2-7 mV) as in the presently recorded RE neurons (range 0.8-1.2 mV); and *(c)* with few exceptions the waveform of dLG spikelets was similar to that of conventional PSPs, whereas RE-cells' spikelets displayed significantly faster rising and decaying times than EPSPs. These differences might be ascribed to the large family of connexins, with particular distributions and characteristics (Goodenough *et al.*, 1996).

Although electrotonic coupling has been described in a variety of central structures in mammals, among them neocortex (Galarreta & Hestrin, 1999; Gibson *et al.*, 1999), hippocampus (Draguhn *et al.*, 1998), thalamus (Hughes *et al.*, 2002; Landisman *et al.*, 2002), and inferior olive (Llinás *et al.*, 1974; Lampl & Yarom, 1997; Devor & Yarom, 2002), at least for neocortex it is common in early stages of circuit formation and decreases during later development (Connors *et al.*, 1983; Peinado *et al.*, 1993). Among the exceptions to this rule are the inferior olive in which the morphological correlate of the electrotonic coupling, gap junctions, is present at birth (Bourat & Sotelo, 1983) and RE neurons in which spikelets were recorded in the present experiments on adult cats. In

these two structures, the role of electrotonic coupling may be that of a synchronizing device.

Experimental and modeling studies have shown that electrotonic coupling underlies the rhythmicity of complex spike activity in the olivo-cerebellar pathway (Welsh & Llinás, 1997; Makarenko & Llinás, 1998; Loewenstein *et al.*, 2001). A combination of electrical and chemical synapses among local-circuit basket inhibitory neurons has been proposed to entrain fast rhythms, in the gamma frequency range, in rat neocortex (Tamás *et al.*, 2000), and electrical synapses are also thought to generate gamma oscillations in the hippocampus (Draguhn *et al.*, 1998; Traub *et al.*, 1999a, 1999b).

As to the RE nucleus, besides chemical synapses among these GABAergic neurons, which have been implicated in the generation and synchronization of spindle rhythms in experimental (Steriade *et al.*, 1987) and modeling (Destexhe *et al.*, 1994; Golomb *et al.*, 1994; Bazhenov *et al.*, 1999) studies, electrotonic coupling may be an additional, if not the leading, factor in this synchronizing processes. In fact, the simulations presented here show that activity in the RE nucleus can spread not only between pairs of neighboring electrotonically coupled neurons (Fig. 2.8*A*) but also at greater distances (Fig. 2.8*B*). This spreading activity could not be due to single spikelets because they are not able to trigger action potentials (Fig. 2.3*B*). However, LTSs may be able to activate a neighbor cell and thus contribute to the propagation and synchronization of spindle activity (Fig. 2.7). This could be expected due to the low-pass

properties of gap junctions (Landisman *et al.*, 2002), which strongly filter fast signals (such as action potentials) but not slower signals (as LTSs). In our experiments the incidence of spikelets decreased during halothane application. As to a possible reduction in spikelets' amplitudes, this cannot be discarded but, under normal recording conditions, spikelets already displayed small amplitudes, sometimes close to the level of noise. In the study on electrotonic coupling between RE neurons maintained *in vitro* (Landisman *et al.*, 2002), it was also concluded that, although spike-to-spike synchronization was precluded in all but the most strongly coupled cell groups, electrical synapses may be effective in some normal and paroxysmal rhythmical activities. Besides a role in spreading slow activities in the RE nucleus, predicted by modeling studies (Fig. 2.8), we hypothesized (Fuentealba *et al*., 2002) and the present experimental data (Fig. 2.7) support the idea that electrical coupling may be important for the synchronization of spindle activities.

REFERENCES

Avanzini, G., De Curtis, M., Pape, H.C. & Spreafico, R. (1999) Intrinsic properties of reticular thalamic neurons relevant to genetically determined spike-wave generation. In Delgado-Escucta, A.V., Wilson W.A., Olsen, R.W. & Porter R.J. (eds), *Jasper's Basic Mechanisms of the Epilepsies*, Lippincott - Williams & Wilkins, pp. 297-309.

Bazhenov, M., Timofeev, I., Steriade, M. & Sejnowski T.J. (1998) Cellular and network models for intrathalamic augmenting responses during 10-Hz stimulation. *J. Neurophysiol.* **79**, 2730-2748.

Bazhenov, M., Timofeev, I., Steriade, M. & Sejnowski, T.J. (1999) Self-sustained rhythmic activity in the thalamic reticular nucleus mediated by depolarizing GABAA receptor potentials. *Nat. Neurosci.* **2**, 168-174.

Bourat, F. & Sotelo, C. (1983) Postnatal development of the inferior olivary complex in the rat. I. An electronic microscopic study of the medial accessory olive. *Dev. Brain Res.* **8**, 291-310.

Condorelli, D.F., Belluard, N., Trovato-Salinaro, A. & Mudo, I. (2000) Expression of Cx36 in mammalian neurons. *Brain Res. Rev.* **32**, 72-85.

Connors, B.W., Benardo, L.S. & Prince, D.A. (1983) Coupling between neurons of the developing rat neocortex. *J. Neurosci.* **3**, 773-782.

Contreras, D., Curró Dossi, R. & Steriade, M. (1993) Electrophysiological properties of cat reticular neurones in vivo. *J. Physiol. (Lond.)* **470**, 273-294.

Deschênes, M., Paradis, M., Roy, J.P. & Steriade, M. (1984) Electrophysiology of neurons of lateral thalamic nuclei in cat: resting properteis and burst discharges. *J. Neurophysiol.* **51**, 1196-1219.

Destexhe, A., Contreras, D., Sejnowski, T.J. & Steriade, M. (1994) A model of spindle rhythmicity in the isolated thalamic reticular nucleus. *J. Neurophysiol.* **72**, 803-818.

Destexhe, A., Bal, T., McCormick, D.A. & Sejnowski, T.J. (1996) Ionic mechanisms underlaying synchronized and propagating waves in a model of ferret thalamic slices. *J. Neurophysiol.* **76**, 2049-2070.

Devor, A. & Yarom, Y. (2002) Electrotonic coupling in the inferior olivary nucleus revealed by simultaneous double patch recordings. *J. Neurophysiol.* **87**, 3048-3058.

Domich, L., Oakson, G. & Steriade, M. (1986) Thalamic burst patterns in the naturally sleeping cat: a comparison between cortically projecting and reticularis neurones. *J. Physiol. (Lond.)* **379**, 429-449.

Draguhn, A., Traub, R.D., Schmitz, D. & Jefferys, J.G. (1998) Electrical coupling underlies high-frequency oscillations in the hippocampus in vitro. *Nature* **394**, 189-192.

Fuentealba, P., Crochet, S., Timofeev, I. & Steriade, M. (2002) "Spikelets" in cat thalamic reticular nucleus in vivo. *Soc. Neurosci. Abstr.* **28**, 144.19.

Galarreta, M. & Hestrin, S. (1999) A network of fast-spiking cells in the neocortex connected by electrical synapses. *Nature* **402**, 72-75.

Gibson, J.R., Beierlein, M. & Connors, B.W. (1999) Two networks of electrically coupled inhibitory neurons in neocortex. *Nature* **402**, 75-79.

Golomb, D., Wang, X.J. & Rinzel, J. (1994) Synchronization properties of spindle oscillations in a thalamic reticular nucleus model. *J. Neurophysiol.* **72**, 1109-1126.

Goodenough, D.A., Goliger, J.A. & Paul, D.L. (1996) Connexins, connexons, and intercellular communications. *Ann. Rev. Biochem.* **65**, 475-502.

Hughes, S.W., Blethyn, K.L., Cope, D.W. & Crunelli, V. (2002) Properties and origin of spikelets in thalamocortical neurones in vitro. *Neuroscience* **110**, 395-401.

Koch, C., Rapp, M. & Segev, I. (1996) A brief history of time (constants). *Cereb. Cortex* **6**, 93-101.

Lampl, I. & Yarom, Y. (1997) Subthreshold oscillations and resonant behavior: two manifestations of the same mechanism. *Neuroscience* **78**, 325-341.

Landisman, C.E., Long, M.A., Beierlein, M., Deans, M.R., Paul, D.L. & Connors, B.W. (2002) Electrical synapses in the thalamic reticular nucleus. *J. Neurosci.* **22**, 1002-1009.

Llinás, R., Baker, R. & Sotelo, C. (1974) Electrotonic coupling between neurons in cat inferior olive. *J. Neurophysiol.* **37**, 560-571.

Loewenstein, Y., Yarom, Y. & Sompolinsky, H. (2001) The generation of oscillations in networks of electrically coupled cells. *Proc. Natl. Acad. Sci. USA* **98**, 8095-8100.

Maekawa, K. & Purpura, D.P. (1967) Properties of spontaneous and evoked activities of thalamic ventrobasal neurons. *J. Neurophysiol.* **30**, 360-381.

Makarenko, V. & Llinás, R. (1998) Experimentally determined chaotic phase synchronization in a neuronal system. *Proc. Natl. Acad. Sci. USA* **95**, 15747-15752.

Moortgat, K.T., Bullock, T.H. & Sejnowski, T.J. (2000) Precision of the pacemaker nucleus in a weakly electric fish: Network vs. cellular influences. *J. Neurophysiol*. **83**, 971-983.

Peinado, A., Yuste, R. & Katz, L.C. (1993) Extensive dye coupling between rat neocortical neurons during the period of circuit formation. *Neuron* **10**, 103-114.

Perez-Velazquez, J.L. & Carlen, P.L. (2000) Gap junctions, synchrony and seizures. *Trends Neurosci.* **23**, 68-74.

Rash, J.E., Staines, W.A., Yasumura, T., Patel, D., Furman, C.S., Stelmack, G.L. & Nagy, J.I. (2000) Immunogold evidence that neuronal gap junctions in adult rat brain and spinal cord contain connexin-36 but not connexin-32 or connexin-43. *Proc. Natl. Acad. Sci. USA* **97**, 7573-7578.

Spencer, W.A. & Kandel, E.R. (1961) Electrophysiology of hippocampal neurons. IV. Fast prepotentials. *J. Neurophysiol.* **24**, 272-285.

Steriade, M. & Contreras, D. (1995) Relations between cortical and thalamic cellular events during transition from sleep pattern to paroxysmal activity. *J. Neurosci.* **15**, 623-642.

Steriade, M., Deschênes, M., Domich, L. & Mulle, C. (1985) Abolition of spindle oscillations in thalamic neurons disconnected from nucleus reticularis thalami. *J. Neurophysiol.* **54**, 1473-1497.

Steriade, M., Domich, L. & Oakson, G. (1986) Reticularis thalami neurons revisited: activity changes during shifts in states of vigilance. *J. Neurosci.* **6**, 68-81.

Steriade, M., Domich, L., Oakson, G. & Deschênes, M. (1987) The deafferented reticularis thalami nucleus generates spindle rhythmicity. *J. Neurophysiol.* **57**, 260-273.

Steriade, M., Curró Dossi, R., Paré, D. & Oakson, G. (1991) Fast oscillations (20-40 Hz) in thalamocortical systems and their potentiation by mesopontine cholinergic nuclei in the cat. *Proc. Natl. Acad. Sci. USA* **88**, 4396-4400.

Steriade, M., McCormick, D.A. & Sejnowski, T.J. (1993) Thalamocortical oscillation in the sleeping and aroused brain. *Science* **262**, 679-685.

Tamás, G., Buhl, E.H., Lorincz, A. & Somogyi, P. (2000) Proximally targeted GABAergic synapses and gap junctions synchronize cortical interneurons. *Nat. Neurosci.* **3**, 366-371.

Timofeev, I. & Steriade, M. (1997) Fast (mainly 30-100 Hz) oscillations in the cat cerebellothalamic pathway and their synchronization with cortical potentials. *J. Physiol. (Lond.)* **504**, 153-168.

Timofeev, I., Grenier, F. & Steriade, M. (1998) Spike-wave complexes and fast runs of cortically generated seizures. IV. Paroxysmal fast runs in cortical and thalamic neurons. *J. Neurophysiol.* **80**, 1495-1513.

Traub, R.D., Schmitz, D., Jefferys, J.G.R. & Draguhn, A. (1999a) High-frequency population oscillations are predicted to occur in hippocampal pyramidal neuronal networks interconnected by axoaxonal gap junctions. *Neuroscience* **92**, 407-426.

Traub, R.D., Jefferys, J.G.R. & Whittington, M.A. (1999b) *Fast Oscillations in Cortical Circuits.* The MIT Press, Cambridge (MA).

Venance, L., Rozov, A., Blatow, M., Burnashev, N., Feldmeyer, D. & Monyer, H. (2000) Connexin expression in electrically coupled postnatal rat brain neurons. *Proc. Natl. Acad. Sci. USA* **97**, 10260-10265.

Welsh, J.P. & Llinás, R. (1997) Some organizing principles for the control of movement based on olivocerebellar physiology. *Progr. Brain Res.* **114**, 449-461.

FIGURES

Figure 2.1. Spikelets during spontaneous activity of RE neurons. Barbiturate anesthesia. *A*, Spike-bursts over the depolarizing envelope of spindles. Typical low-threshold spike-burst of RE cell expanded in inset. Epochs marked *1* (at the onset of a spindle sequence) and *2* (during inter-spindle lull) are expanded below and show spikelets (asterisks), i.e. fast-rising and low-amplitude events occurring singly or in clusters. *B*, another RE neuron displaying spikelets (asterisks) occurring in isolation or in clusters. Inset shows the average (n = 500) of spikelets (solid line; calibration bar 0.4 mV), scaled with the average (n = 500) of full action potentials (dotted line; calibration bar 20 mV). C, intracellularly stained (Neurobiotin) RE neuron located in the rostrolateral sector of the nucleus. Photograph (right) and reconstruction (left). Arrowhead indicates the axon to the dorsal thalamus. Calibration bar within the photograph = 0.1 mm for RE neuron in the photograph and 0.15 mm for the reconstructed neuron.

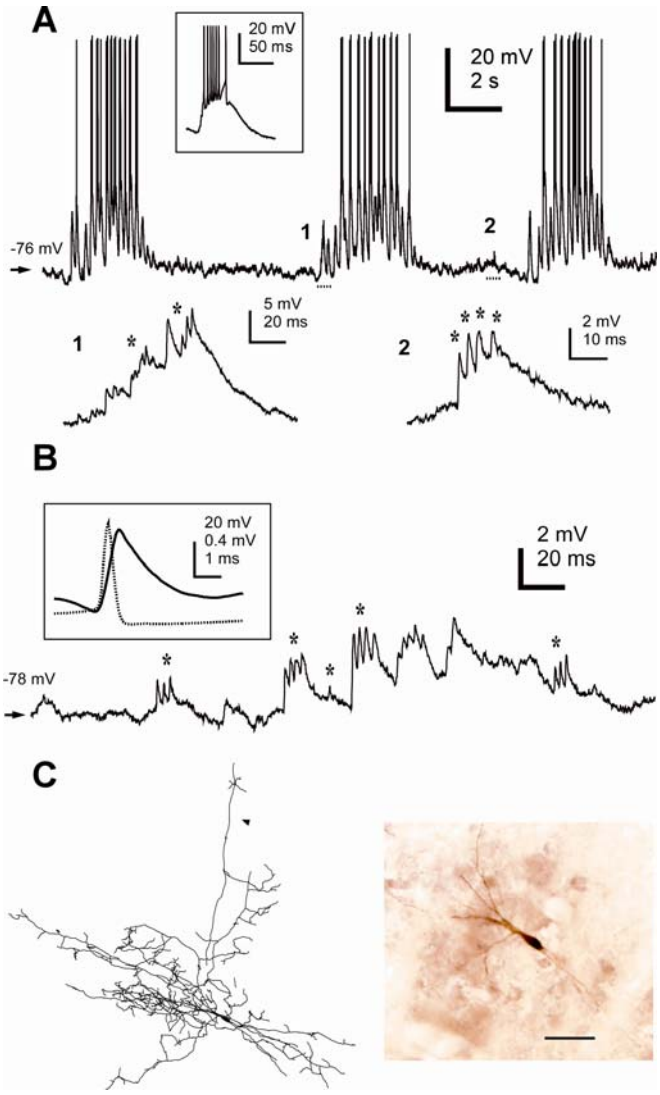
A
20 mV
50 ms
20 mV
2 s
-76 mV
1
2
5 mV
20 ms
2 mV
10 ms
B
20 mV
0.4 mV
1 ms
2 mV
20 ms
-78 mV
C

Figure 2.2. Rise and decay phases, amplitudes, and voltage-independency of spikelets. Barbiturate anesthesia. All panels from the same neuron. *A*, left, superimposition of spikelets in single traces; right, average (n = 500) of spikelets from a single RE neuron. *B*, left and right, histograms of rise time (10-90%) and decay phase (90-10%), respectively, for all spikelets in one neuron. *C*, left histogram shows amplitude distribution of spikelets. Right plot depicts the voltage-independency of spikelets' amplitudes (each point is the average of 10 individual points taken at the same membrane potential; dotted line is the best linear fitting for the group of points).

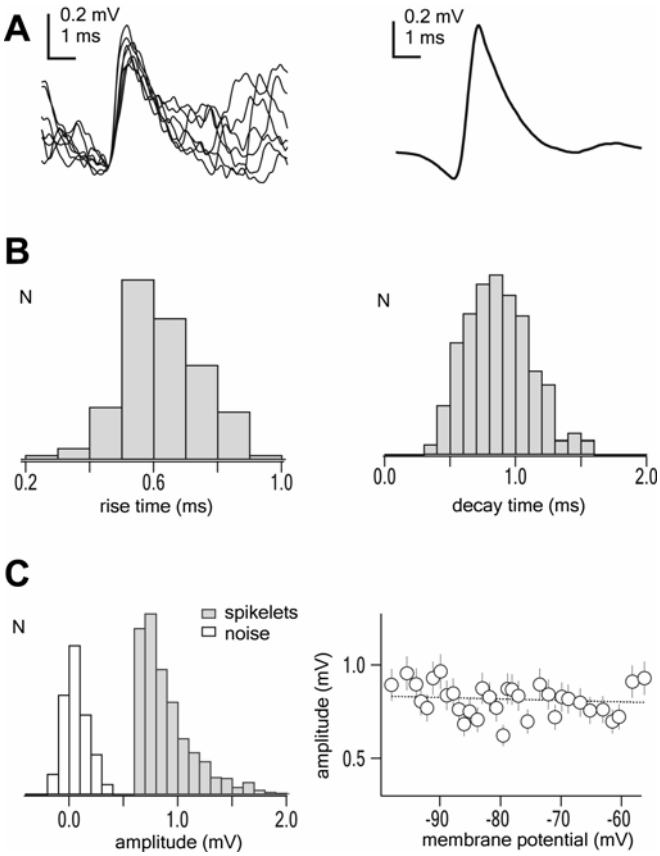
A
0.2 mV
1 ms
0.2 mV
1 ms
B
N
0.2
0.6
1.0
rise time (ms)
N
0.0
1.0
2.0
decay time (ms)
C
N
spikelets
noise
0.0
1.0
2.0
amplitude (mV)
amplitude (mV)
1.0
0.5
-90
-80
-70
-60
membrane potential (mV)

Figure 2.3. Spikelets and EPSPs are different types of depolarizing events. *A*, barbiturate anesthesia. Top three traces, from the same RE neuron, show two types of depolarizations: spikelets (∗) and EPSPs (+). Below, two histograms show the distribution of the rising and decaying phases (left and right, respectively) in the two types of events. *B*, ketamine-xylazine anesthesia, another neuron. Spikelets (∗) are present during the firing of RE cell (spikes truncated). Note different rising phases in spikelets and some EPSPs that give rise to action potentials. Below, superimposed traces from the same neuron showing EPSPs and spikelets (see also text).

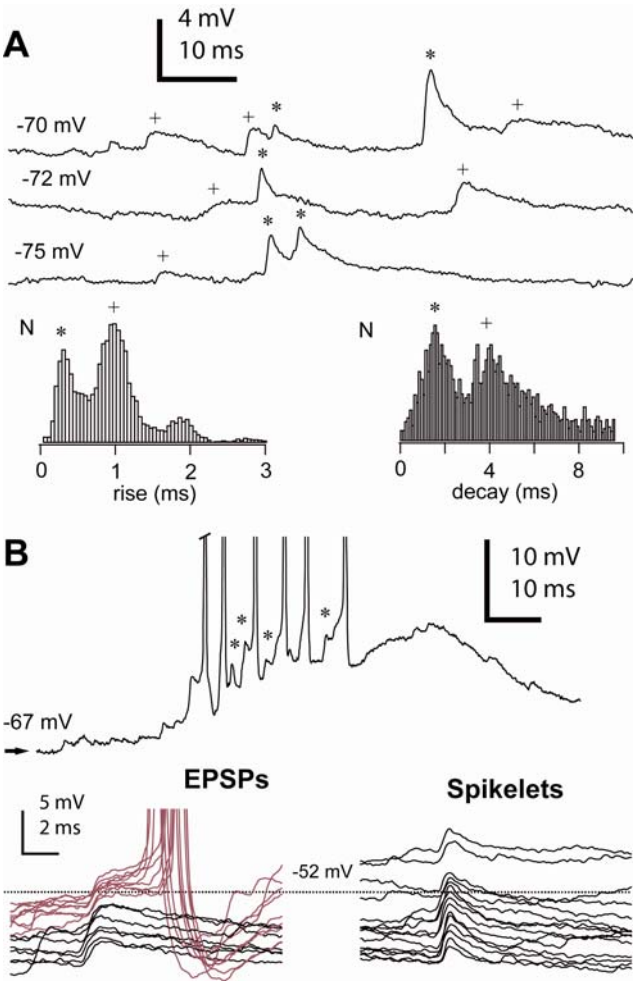
A
4 mV
10 ms
-70 mV
-72 mV
-75 mV
N
0
1
2
3
rise (ms)
N
0
4
8
decay (ms)
B
10 mV
10 ms
-67 mV
EPSPs
Spikelets
5 mV
2 ms
-52 mV

Figure 2.4. Spikelets are also different from FPPs. Ketamine-xylazine anesthesia. *A*, top trace displays FPPs (arrowheads) and spikelets (∗). Action potentials truncated. Below, superimposition of single events (left) and averages (n = 100) showing both FPPs and spikelets (right); the gray trace shows the averaged spikelet scaled (x 5) for comparison. *B*, upper histograms show the rising and decaying phases (left and right, respectively) of FPPs. Bottom left histogram shows the voltage sensitivity of FPPs (compare to bottom right plot in Fig. 2.2 showing the voltage-independence of spikelets). Bottom right histogram shows voltage independency of the amplitude of FPPs. Each point is the average of ten points taken from intervals of 10 mV.

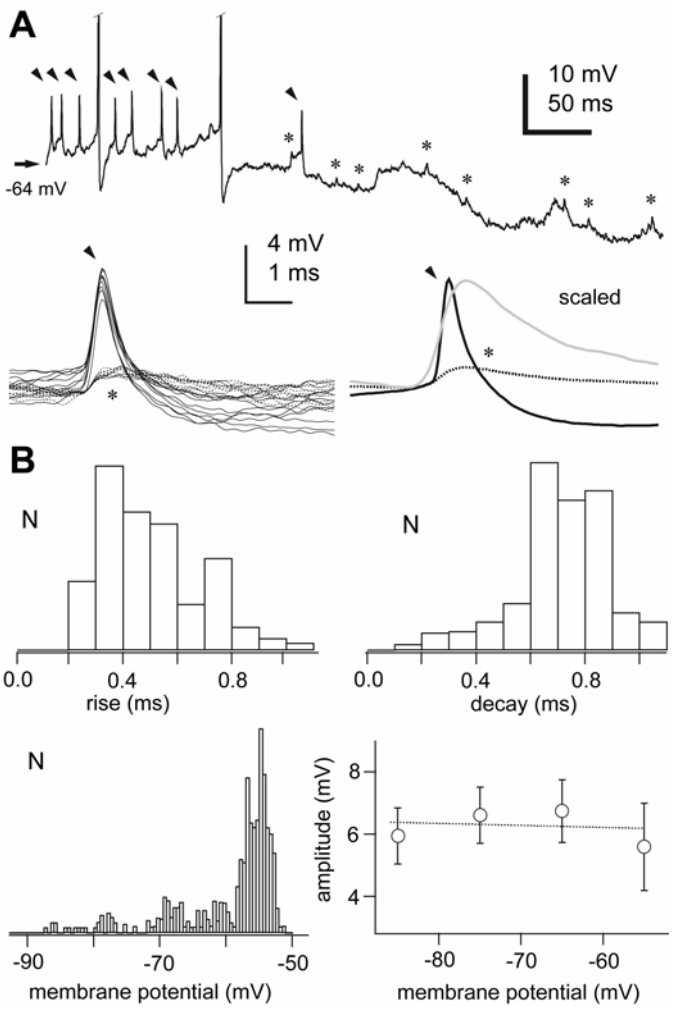
A
10 mV
50 ms
-64 mV
4 mV
1 ms
scaled
B
N
0.0
0.4
0.8
rise (ms)
N
0.0
0.4
0.8
decay (ms)
N
-90
-70
-50
membrane potential (mV)
amplitude (mV)
8
6
4
-80
-70
-60
membrane potential (mV)

Figure 2.5. Similarity between firing pattern of RE neurons and spikelets. Barbiturate anesthesia. *A*, traces displaying spikelets (top) and full action potentials (bottom). Left, clusters of spikelets separated by 2.5 ms and, below, spike-burst (~350 Hz) from another RE neuron (same as the stained cell depicted in Fig. 2.1*C*). Right, individual spikelets and, below, tonic firing with the same frequency (~50 Hz). Same two RE neurons as in the left panel. *B*, histograms with inter-event intervals (IEIs) for spikelets and full action potentials from the two RE neurons, showing mode peaking at 3-4 ms for spike-bursts (gray color in right histogram) and tonic firing in RE neuron firing action potentials, and similar distribution of IEIs in the other RE neuron firing spikelets.

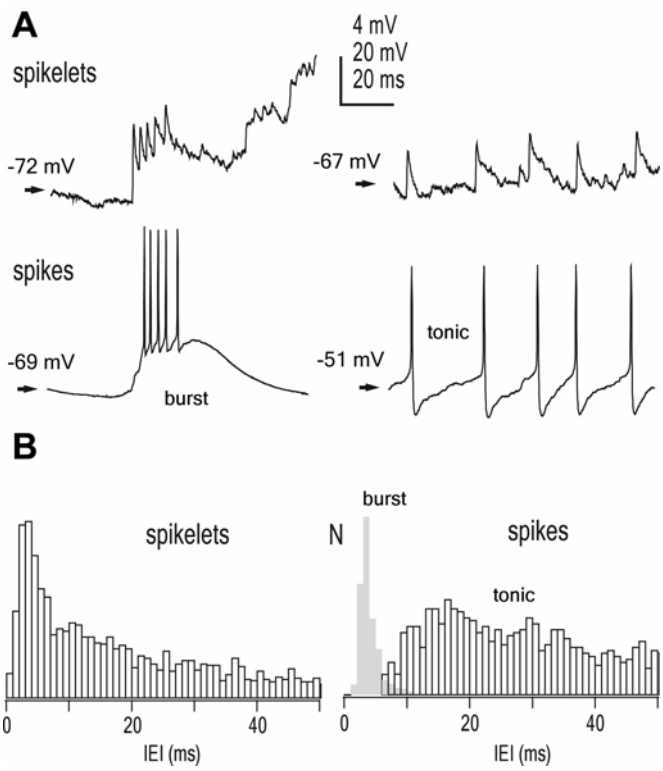
A
4 mV
20 mV
20 ms
spikelets
-72 mV
-67 mV
spikes
-69 mV
burst
-51 mV
tonic
B
spikelets
burst
N
spikes
tonic
0
20
40
IEI (ms)
0
20
40
IEI (ms)

Figure 2.6. Spikelets are strongly reduced or virtually abolished by halothane. Barbiturate anesthesia. Left column, different epochs before (*A*), during halothane administration (*B*), and recovery of initial state after halothane (*C*). Right column, expanded periods from neurons depicted in the left column. Insets: incidence of spikelets (SPK) and EPSPs (left ordinate), and their ratio during a 5-min period of recording (right ordinate), in each of the three states.

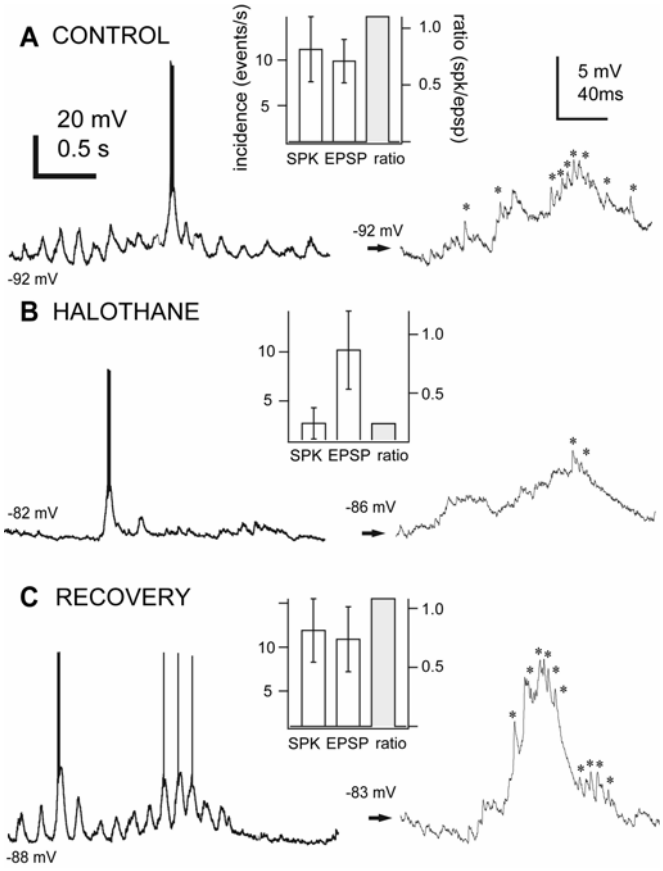
A CONTROL
20 mV
0.5 s
incidence (events/s)
10
5
1.0
0.5
ratio (spk/epsp)
SPK EPSP ratio
5 mV
40ms
-92 mV
-92 mV
B HALOTHANE
10
5
1.0
0.5
SPK EPSP ratio
-82 mV
-86 mV
C RECOVERY
10
5
1.0
0.5
SPK EPSP ratio
-83 mV
-88 mV

Figure 2.7. The role of gap junctions in spindle synchronization. Simultaneous quadruple extracellular recordings of RE neurons were performed in decorticated cats under barbiturate anesthesia. Neighbor electrodes were separated by ~0.5 mm (1 represents the most anteriorly located neuron and 4 the most posterior). RE neurons were identified in each case by their long bursts (>50 ms) and the accelerando-decelerando firing pattern (see inset in *A*, burst extracted from cell 2). *A*, *CONTROL* shows 30 s of normal activity of four RE neurons during barbiturate anesthesia, with recurrent spindles each 2-to-5 s. At the bottom, auto- and cross-correlograms are depicted for 5 min. of recording. Note highly correlated ~10 Hz activity in all cases. *B, HALOTHANE* illustrates the effect of halothane (4%, 2 min.) on RE neurons. Note the loss of correlation between pairs of cells and the absence of activity at 10 Hz. *C, RECOVERY*, when halothane administration stopped, RE neurons recovered the pattern of activity displayed in the control period.

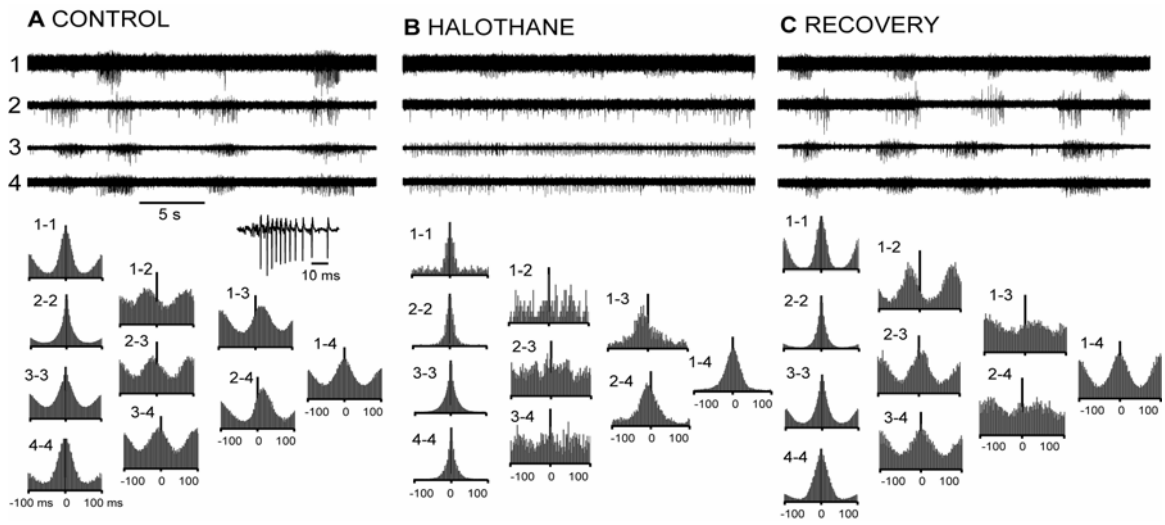
A CONTROL
B HALOTHANE
C RECOVERY
1
2
3
4
5 s
10 ms
1-1
1-2
1-3
1-4
2-2
2-3
2-4
3-3
3-4
4-4
-100 ms 0 100 ms
-100 0 100

Figure 2.8. Role of gap junctions between RE cells in initiating LTS and wave propagation. *A*, model of a pair of reciprocally connected RE cells. Spikelet (see inset) was induced in the postsynaptic cell (red line) by single spike in the presynaptic neuron (black line). Upon hyperpolarization of presynaptic neuron (second trace), a burst of spikes can trigger a single spike in the postsynaptic neuron. When both cells are hyperpolarized (third trace), a burst in the presynaptic cell can induce a delayed spike-burst in the postsynaptic cell. Bottom trace represents intracellular recording of RE neuron *in vivo* (see text). *B*, wave dynamics in two-dimensional network of RE neurons. Two stimuli were applied simultaneously at the comers of a two-dimensional 128x128 network of RE cells interconnected with gap junctions. Firing cells are shown in red, silent neurons indicated by blue.

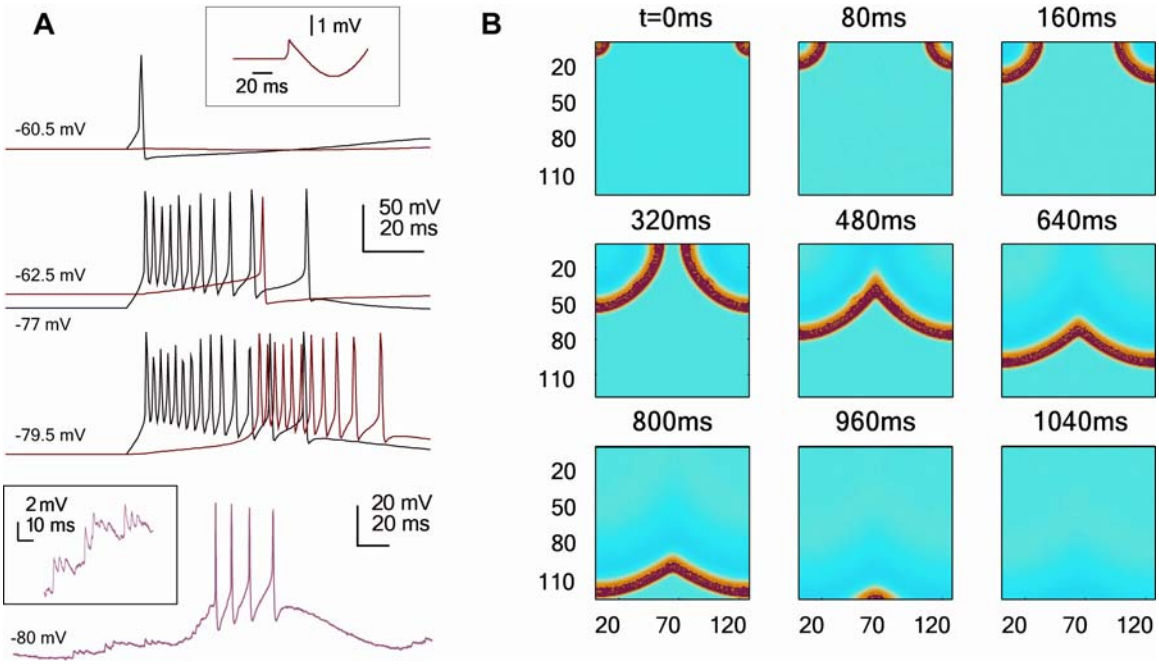
A
1 mV
20 ms
-60.5 mV
50 mV
20 ms
-62.5 mV
-77 mV
-79.5 mV
2 mV
10 ms
20 mV
20 ms
-80 mV
B
t=0ms
80ms
160ms
320ms
480ms
640ms
800ms
960ms
1040ms
20
50
80
110
20
70
120

3. Intrinsic Membrane Bistability and its Role in Network Oscillations

MEMBRANE BISTABILITY IN THALAMIC RETICULAR NEURONS DURING SPINDLE OSCILLATIONS

Pablo Fuentealba, Igor Timofeev, Maxim Bazhenov, Terrence J. Sejnowski, and Mircea Steriade (2004). *Journal of Neurophysiology (in press)*

RESUMÉ

Le noyau thalamique réticulaire (RE) joue un rôle crucial dans la régulation de l'excitabilité des réseaux thalamocorticaux et dans la génération de quelques rythmes du sommeil. Des enregistrements intracellulaires en courant fixe (*current clamp*) de neurones du RE sur des chats sous anesthésie ont révélé la présence d'une bistabilité de la membrane dans ~20% des neurones. Cette bistabilité consistait à une alternance de deux potentiels de membrane séparés par ~17-20 mV. Les neurones RE bistables déchargeaient de façon tonique, avec une modulation des vagues de la première à la dernière séquence en fuseau. La bistabilité était fortement dépendante du voltage et présente uniquement sous des conditions aux repos (i.e. sans injection de courant). Une addition de QX-314 dans les micropipettes d'enregistrement soit abolissait, soit interrompait la bistabilité de la membrane, ce qui suggère que $I_{Na(p)}$ est responsable de sa génération. Les cellules thalamocorticales ont présenté divers patrons de fuseau qui reflétaient la bistabilité de la membrane dans les neurones RE. Finalement, des données expérimentales et des simulations par ordinateurs ont prédit un rôle pour la bistabilité des neurones RE dans l'induction de divers patrons de fuseau dans les cellules thalamocorticales cible. Nous concluons que la bistabilité de la membrane des neurones RE est une propriété intrinsèque, vraisemblablement généré par $I_{Na(p)}$ et modulé par les influences corticales, aussi bien que par un facteur qui détermine différents patrons de rythmes en fuseau dans les neurones thalamocorticaux.

ABSTRACT

The thalamic reticular (RE) nucleus is a major source of inhibition in the thalamus. It plays a crucial role in regulating the excitability of thalamocortical networks and in generating some sleep rhythms. Current clamp intracellular recordings of RE neurons in cats under barbiturate anesthesia revealed the presence of membrane bistability in ~20% of neurons. Bistability consisted of two alternate membrane potentials, separated by ~17-20 mV. While non-bistable (common) RE neurons fired rhythmic spike-bursts during spindles, bistable RE neurons fired tonically, with burst modulation, throughout spindle sequences. Bistability was strongly voltage-dependent and only expressed under resting conditions (i.e. no current injection). The transition from the silent to the active state was a regenerative event that could be activated by brief depolarization, while brief hyperpolarizations could switch the membrane potential from the active to the silent state. These effects outlasted the current pulses. Corticothalamic stimulation could also switch the membrane potential from silent to active states. Addition of QX-314 in the recording micropipette either abolished or disrupted membrane bistability, suggesting $I_{Na(p)}$ to be responsible for its generation. Thalamocortical cells presented various patterns of spindling that reflected the membrane bistability in RE neurons. Finally, experimental data and computer simulations predicted a role for RE neurons' membrane bistability in inducing various patterns of spindling in target thalamocortical cells. We conclude that membrane bistability of RE neurons is an intrinsic property, likely generated by $I_{Na(p)}$ and modulated by cortical influences, as well

as a factor that determines different patterns of spindle rhythms in thalamocortical neurons.

INTRODUCTION

The GABAergic neurons of the thalamic reticular (RE) nucleus play a major role in modulating the flow of information through the dorsal thalamus and in the generation of sleep spindles, a thalamically generated rhythm (Steriade et al. 1990). The RE neurons are reciprocally connected with thalamocortical (TC) cells in dorsal thalamic nuclei (Jones, 1985) and RE neurons exert powerful inhibitory effects on TC neurons of the dorsal thalamus (Thomson, 1988; Contreras and Steriade, 1996; Kim and McCormick, 1998b).

Despite the relative homogeneity of this nucleus, some data have pointed to differential functional features in various types of RE neurons. For example, a subsample (~20%) of RE neurons do not discharge spike-bursts to depolarizing current pulses even when the membrane potential (V_m) reaches –100 mV, nor do they fire rebound spike-bursts after prolonged hyperpolarizations, thus suggesting that such RE neurons do not express T-type Ca^{2+} channels (Contreras et al. 1992). This is indeed the case of ventral lateral geniculate cells (Crunelli et al. 1987) that share a common embryological origin with RE neurons and similarly do not project to the cerebral cortex (Jones, 1985).

Another difference was found between some RE neurons that, during natural slow-wave sleep, fire spike-bursts lasting ~50-100 ms, and other RE neurons that display during the same behavioral state a prolonged (up to 1 or 2 seconds) tonic tail of single action potentials after the spike-bursts (compare Figs. 3.4 and 3.5 in Steriade et al. 1986).

In vitro experiments showed that this prolonged depolarization is due to either a persistent Na^+ current, $I_{Na(p)}$, or a Ca^{2+}-activated nonselective cation current (Kim and McCormick, 1998a). The $I_{Na(p)}$ can generate plateau potentials and membrane bistability (Crill, 1996; Gola et al. 1998) that has been demonstrated in various neuronal types of the spinal cord (Bennett et al. 1998), cerebellum (Llinás and Sugimori, 1980), dorsal thalamus (Williams et al. 1997; Toth et al. 1998; Hughes et al. 1999), neocortex (Schwindt and Crill, 1999), olfactory bulb (Heyward et al. 2001), and hippocampus (Chuang et al. 2000; Fricker and Miles, 2000).

If RE neurons displayed exceedingly long or shorter spike-bursts during spindle oscillations (Steriade et al. 1986), such differences would presumably be reflected in variant types of inhibition-rebound sequences at the level of target thalamocortical neurons. This hypothesis was at the origin of the present study. The intrinsic firing patterns of RE neurons are fundamental toward the understanding of their role in controlling the electrical activity of target TC neurons. We investigated the membrane properties of RE neurons *in vivo* and, in particular, the conditions under which long-lasting depolarizing plateaus and prolonged hyperpolarizations can be elicited by intracellular pulses or synaptic volleys. The results show that a subgroup of RE neurons displays membrane bistability, as indicated by two discrete modes of V_m, with different responsiveness to cortical inputs. Active membrane properties can amplify and extend in time the influence of both depolarizing and hyperpolarizing inputs. The membrane bistability of RE neurons probably plays a role in shaping spindling oscillations.

METHODS

Animal preparation

Experiments were performed on adult cats (2.5-3.5 kg), anaesthetized with pentobarbital (25 mg/kg, i.p.). When the cats showed the signs of deep anesthesia, the animals were paralyzed with gallamine triethiodide and artificially ventilated with control of the end-tidal CO_2 concentration at ~3.5%. Body temperature was maintained at 36-38^{o} C. The depth of anesthesia was continuously monitored by EEG and additional doses of anaesthetic were administered at the slightest tendency toward low-voltage and fast EEG rhythms. At the end of experiments, animals were given a lethal dose of pentobarbital (50 mg/kg i.v.).

Electrophysiological recordings

Current-clamp intracellular recordings from RE neurons (rostral and rostrolateral sector of the nucleus) and TC neurons from the ventrolateral (VL) nucleus were performed using glass micropipettes (DC resistance, 30-60 MΩ). To avoid breaking of recording micropipettes, the cortex and white matter overlying the head of the caudate nucleus were removed by suction. The pipettes entered ~3 mm through the caudate nucleus to reach the thalamic RE nucleus. Pipettes were generally filled with 3 M solution of K-acetate and, in some experiments; with 50 mM of QX-314 (the DC resistance was identical to that of K-acetate-filled pipettes). The stability of intracellular recordings was ensured by cisternal drainage, bilateral pneumothorax, hip suspension,

and by filling the hole over the thalamus with 4% agar solution. A high-impedance amplifier with active bridge circuitry was used to record and inject current inside the cells. Most intracellular recordings included in the database lasted for periods longer than 30 min. Simultaneous extracellular recordings were performed using up to four tungsten electrodes (10-15 MΩ) inserted through the caudate nucleus, with an inter-electrode distance of ~0.5 mm. To determine the membrane potential (V_m) of RE neurons, DC offset was adjusted constantly before and after every recording; and the bridge was also adjusted through intracellular recordings. Once the recording was finished, the recording pipette was withdrew from the recording site (10-20 μm) in order to avoid possible DC offsets due to the extracellular environment close to the neurons and to establish a reference considered as zero (0 mV) for the intracellular recordings.

Cortical activity was monitored in all experiments by EEG recordings from areas 4 and 6, corresponding to intracellularly recorded RE neurons.

Data analysis

All data were analysed under Igor pro 4.0 (Wametrics, Inc.). Since the correct determination for V_m was central for this study, precautions were taken during both experiments and analysis. Action potentials during active states did not affect significantly V_m measurements because of *(a)* the short duration of action potentials in RE neurons (1 ms); and *(b)* very high sampling rate of intracellular recordings (20 kHz), which guarantees a sub-millisecond time resolution. Moreover, preliminary analyses were carried out in digitized filtered waves (0-40 Hz) in order to eliminate spikes from

the intracellularly recorded signals. V_m distributions of such signals proved to be very much similar to the non-filtered signals, and displayed only small shifts in the active peak (2-4 mV) for the cases of resting and hyperpolarized conditions. For depolarized states, in which RE neurons undergo sustained (tonic) discharge, filtered signals showed a narrower V_m distribution when compared to non-filtered signals, with small shifts to depolarized values (2-4 mV). Therefore, most analyses were performed directly on non-filtered waves.

Computer simulations

In modeling studies, we examined single-compartment models of RE and TC cells which included voltage- and Ca^{2+}-dependent currents described by Hodgkin-Huxley kinetics. For both RE and TC cells we considered a fast Na^+ current, I_{Na}, a fast K^+ current, I_K, a low-threshold Ca^{2+}-dependent current, I_T (Huguenard and McCormick, 1992; Huguenard, 1996), and a K^+ leak current, $I_{KL} = G_{KL}(V-E_{KL})$ A model of hyperpolarization-activated cation current I_H (McCormick and Pape, 1990), taking into account both voltage and Ca^{2+} dependencies (Destexhe et al. 1996b) was also included in TC cells. A persistent Na^+ current, $I_{Na(p)}$, was included to RE cells to model bistability of the responses. For $I_{Na(p)}$, $I_{Na(p)} = G_{Na(p)}m(V -50)$, $dm/dt = (m_\infty - m)/0.2$, $m_\infty = 1/(1 + \exp(-(V +42)/5))$ (Alzheimer et al. 1993). The expressions for voltage- and Ca^{2+}-dependent transition rates for all currents are given in Bazhenov et al. (1998, 2000).

$GABA_A$ and AMPA synaptic currents were modeled by first-order activation schemes (Destexhe et al. 1994). $GABA_B$ receptors were modeled by a higher-order

reaction scheme that took into account activation of K^+ channels by G-proteins (Dutar and Nicoll, 1988; Destexhe et al. 1994, 1996b). The equations for all synaptic currents are given in Bazhenov et al. (1998, 2000).

A thalamic network was also modeled, and consisted of a one-dimensional two-layer array of *M* RE and *M* TC neurons, where *M* was varied between 20 and 64. In most of the simulations the connection fan out was ±3 cells for $GABA_A$ mediated RE-RE synapses; ±3 cell for AMPA mediated TC-RE synapses; ±3 cells for $GABA_A$ and $GABA_B$ mediated RE-TC synapses. Other radii of synaptic interconnections were used to test the sensitivity of the results.

RESULTS

All neurons recorded intracellularly (n = 57) and extracellularly (n = 13) within the rostral pole and rostrolateral sector of the RE nucleus were identified by accelerando-decelerando spike-bursts (see insets in Fig. 3.1*A* for intracellular, and Fig. 3.4 for extracellular, recordings). The accelerando-decelerando pattern refers to the initially increasing, but rapidly decreasing inter-spike intervals that occur within every single burst of action potentials in RE neurons. This is the typical firing pattern of RE neurons' spike-bursts during spindling, as described during natural slow-wave sleep (Domich et al. 1986; Steriade et al. 1986), as well as intracellularly in anesthetized animals (Contreras et al. 1993).

Differences between bistable and non-bistable RE neurons

A subgroup of intracellularly recorded neurons (23%, 13 of 57) displayed a sustained depolarization during EEG spindles (Fig. 3.1*A*, left). This plateau potential was initiated at the beginning of each spindle sequence and persisted during its whole duration. At variance, the remaining RE neurons fired spike-bursts interrupted by clear-cut hyperpolarizing potentials (Fig. 3.1*A*, right), as described in previous studies on RE neurons. Histograms of V_m distribution showed two discrete peaks in the former group of RE cells (at ~-80 mV and ~-56 mV for the left neuron in Fig. 3.1*A*), representing the sustained depolarization during spindles and the silent phase, whereas only one peak was detected in the remaining RE neurons (Fig. 3.1*B*). Thus, neurons displaying two, discrete peaks in their V_m distribution were defined as revealing membrane bistability (see

Heyward et al. 2001). Autocorrelograms of action potentials fired by non-bistable neurons displayed clear lags of about 110 ms (Fig. 3.1*C*), consistent with firing in the frequency range of spindles (~9 Hz). At variance, bistable neurons showed much less pronounced peaks and troughs (Fig 3.1*C*).

Bistability was a graded property since it displayed a variable range of values between resting and active periods. Figure 3.1*D* shows the V_m distributions for 3 different RE neurons. All these bistable neurons were at a resting V_m of ~-80 mV; however, the second peak differed for each cell, not only in its position but also in its relative amplitude (arrows, Fig. 3.1*D*). Bistable cells spontaneously generated two discrete V_ms (Fig. 3.1*E*): *(a)* the first one represented the active state, with relatively depolarized V_m (-60.8 ± 3.1 mV), coincident with spindle activity and around the threshold for action potential generation; *(b)* the second was a silent state, with a relatively hyperpolarized V_m (-77.7 ± 2.7 mV), occurring during interspindle lulls. The difference between the two states was 16.8 ± 3.5 mV (range 13-22 mV, $n = 9$; Fig. 3.1*E*). By contrast, non-bistable cells displayed the well-known waxing and waning pattern of spindle oscillation (see Fig. 3.1*A*, right) and their V_m distribution presented a single peak at ~-80 mV (see Fig. 3.1*B*).

Morphological reconstruction of some bistable neurons showed typical features of RE neurons, with fusiform shape lying parallel to the surface of the dorsal thalamus and very long dendrites (Fig. 3.1*F*-*G*), suggesting no morphological differences between bistable and non-bistable neurons.

Consistent with the idea of a graded property, transitions between non-bistable and bistable behaviors were seen in some RE neurons (n = 7). In those cases, spindle oscillations started as typical waxing waves of low-threshold spikes (LTSs) and bursts of fast action potentials, which later switched to a sustained plateau potential, characteristic of membrane bistability. This suggests that so-called bistable and non-bistable neurons may not represent two different categories of RE cells, but this dissimilar behavior should reside in the differential expression of some intrinsic properties that RE neurons express in some circumstances (not shown).

Similarly to spontaneously generated spindles, bistability was seen in cortically elicited spindles. Histograms of V_m distributions during evoked spindling showed that only bistable RE neurons displayed a clear-cut two-peak pattern of membrane bistability, and autocorrelograms of action potentials showed that bistable neurons did not consistently discharge in the frequency range of spindles (Fig. 3.2).

Voltage dependency of membrane bistability

We assessed the voltage dependence of bistability in RE neurons (n = 6) (Fig. 3.3). The V_m distributions represent the proportion of time spent at each V_m (excluding action potentials) in resting condition (with no current injection) and during the injection of negative or positive steady current through the pipette. *(a)* During resting (0 nA), the distribution was bimodal, with two peaks reflecting the silent state (-79 mV, i.e. interspindle lulls) and the active state (-62 mV, i.e. spindles) (Fig. 3.3*B*). *(b)* Positive

current injection (+0.2 nA) abolished bistability, and generated sustained firing with no repolarization to the resting state (Fig. 3.3*A*). The V_m distribution showed a single peak (at -59 mV), which rapidly decayed up to -70 mV; more negative values of V_m were virtually absent. *(c)* With injection of negative current (-0.2 nA), the bimodal distribution of V_m was also abolished, and a single peak remained (-89 mV), falling sharply up to -80 mV and decaying smoothly at more positive values (Fig. 3.3*C*). The abolition of bistability could be reached with current injections as small as -0.1 nA (not shown).

Thus, injection of different levels of steady current showed that bistability was exclusively displayed under the resting condition, i.e. when no current was injected. The V_m of bistable neurons was asymmetrically affected, depending on the sign of the injected current. Negative current produced a hyperpolarization with higher amplitude than the depolarization induced by the same amount of current with opposite sign (Fig. 3.3*D*). This supposed an asymmetric change in input resistance (R_{in}) measured from the resting V_m. Actually, in a sample of 6 bistable RE neurons, the R_{in} was four-fold higher for hyperpolarized values of V_m than for the depolarized ones (25.3 ± 6.2 MΩ and 6.4 ± 4.0 MΩ respectively). On the other hand, R_{in} was linearly related to V_m in non-bistable neurons (not shown). Comparing R_{in} between non-bistable and bistable neurons (during periods of negative DC), showed no significant difference (25.3 ± 6.2 MΩ and 31.5 ± 8.5 MΩ, for bistable and non-bistable groups, respectively; $p>0.5$). An inverse relation was found for the mean firing frequency. Even though the R_{in} was lower during states associated with membrane depolarization, tiny changes in injected current produced large changes in firing frequency (Fig. 3.3*E*). In fact, the gain in firing frequency was much

higher for depolarized membrane values compared to changes in the hyperpolarized values (84.7 ± 69.3 Hz/nA and 18.7 ± 11.6 Hz/nA, respectively; $p<0.05$; $n = 6$). These results indicate that membrane bistability in RE neurons is strongly voltage dependent, which would be consistent with the generation of bistability by intrinsic mechanisms.

To investigate whether bistability was an artefact arising from intracellular recordings, simultaneous extracellular recordings of two or more RE neurons were performed ($n = 13$). Figure 3.4 shows one of those experiments in which two RE neurons were recorded simultaneously and identified by their spike-bursts with accelerando-decelerando firing patterns. Differences in firing patterns during spontaneous spindles between the two cells could be firstly seen by visual inspection. While one neuron only fired rhythmic spike-bursts (*cell 1*), the other neuron also displayed tonic tails of discharges following the bursts (*cell 2*). Tonic tail refers to low-frequency spikes (typically <100 Hz) generated by some RE neurons, which fire in single mode towards the end of spindle waves. Two other cells presented similar features as *cell 2* (then, 3 out of the total 13), with initial spike-bursts followed by tonic tails. Plots of instantaneous firing frequency during spindles showed that *cell 1* exclusively discharged high-frequency bursts (>300 Hz) during the spindle period, whereas *cell 2* fired slower bursts (~200 Hz) followed by tonic firing up to 100 Hz (Fig. 3.4*C*). Consistent with these results, the interspike interval (ISI) histogram for a long period of spontaneous activity showed for non-bistable neurons, like *cell 1*, a narrow distribution that peaked at 3 ms (~350 Hz) and decayed rapidly up to ~10 ms (100 Hz), indicative that tonic firing was virtually absent (inset, Fig. 3.4*C*). A much wider ISI distribution was seen for neurons

like *cell 2*, which peaked at 4 ms (250 Hz) and decayed smoothly up to 40 ms (25 Hz), which reflected the tonic firing (inset, Fig. 3.4*C*). The same analysis carried out for extracellular recordings was applied for intracellular recordings, showing that only bistable neurons displayed an important component of tonic firing in their discharge pattern (data not shown).

Intrinsic mechanisms generate bistability

The idea that intrinsic mechanisms are implicated in the generation of bistability was supported by experiments showing that current pulses (200 ms, 1 nA) were able to activate the plateau potential characteristic for bistability, with very similar kinetics to the spontaneous one. The initiation of bistability induced by current pulses was twice faster when compared to the spontaneous one, as shown by the exponential fitting to the rising phase of the plateau potential (τ of activation, ~21 ms and ~48 ms, respectively; n = 3, not shown).

The artificial generation of membrane bistability by injection of current pulses of different durations and amplitudes was investigated in 9 bistable RE neurons held at different values of V_m. Intracellular current pulses were applied at low frequencies (0.3-to-1 Hz). Depolarizing current pulses (2 nA) applied at rest (0 nA) were able to generate an initial burst of action potentials, followed by tonic spikes that outlasted the current pulse (Fig. 3.5*A*-*B*). Under steady hyperpolarization (-2 nA), the depolarizing current pulses failed to elicit an outlasting plateau potential, even though the pulse amplitude was greatly increased (Fig. 3.5*C*-*D*). The same failure was obtained by using shorter current

pulses (Fig. 3.5*E*). The plot in Fig. 3.5*F* summarizes these results, showing the duration of the plateau potential outlasting the response evoked by the current pulse at the resting V_m (-80 mV), the absence of such a plateau under steady hyperpolarization (reaching -90 mV), as well as an intermediate level with plateau potential outlasting the duration of the current pulse, though not as long as in the resting (V_m, -85 mV).

Similarly to the initiation of the active state, the termination of the active period could be ascribed to intrinsic mechanisms. Thus, brief current pulses were able to mimic termination of active states. The termination of the active states was fitted with an exponential function. The average (n = 10) of such fitting functions showed that termination evoked by current pulses was twice faster than spontaneous termination (τ of inactivation 75 ms and 131 ms, respectively; n = 3), similarly to what was found for the activation process (not shown). The presence of such a mechanism for termination of plateau potentials suggests that this active state is maintained by voltage dependent mechanisms, which can be deactivated by hyperpolarization.

After a relatively long silent period (~2 s), a brief positive current pulse was able to evoke an active period (Fig. 3.6, top) very similar to the one generated following a relatively short silent period (~0.4 s) (Fig. 3.6*A*, middle). Similar results were found in other two neurons. The plot at the bottom of Fig. 3.6*A* shows no relation between the duration of the preceding silent period and the duration of the active period generated by the current pulse. Current pulses that were not able to produce an outlasting active state

were considered as failures. There was also no relation between the duration of the preceding silent period and the likelihood of failure (bottom plot in Fig. 3.6*A*).

Brief negative current pulses, which *were* able to terminate the active state, were effective regardless of the duration of the preceding active state, as either short or long-lasting plateaus could be equally shunted (Fig. 3.6*B*). Similar results were found in other two neurons. The probability for a given current pulse (100 ms, 2 nA) to terminate an active state was considerably high (80%) (bottom plot in Fig. 3.6*B*). However, there was a relation between the duration of shunting produced by the hyperpolarizing current pulse and the preceding active period. Long-lasting active periods (>3 s) were shunted for longer periods than short-lasting (<2 s) active states (936.7 ± 370.4 ms and 412.5 ± 247.5 ms, respectively; $p<0.01$). Similarly to the initiation of active periods, the likelihood of shunting failures was not dependent on the duration of the preceding active period (bottom plot in Fig. 3.6*B*).

Absence of bistability in RE neurons recorded with QX-314

To elucidate some of the ionic mechanisms underlying the origin of bistability, and given the antecedent that TTX blocks plateau potentials in RE neurons (Kim and Mccormick, 1998a), intracellular recordings were performed with QX-314 (50 mM) in the micropipette. From the pool or recorded neurons (n = 19), only in one case was it possible to recognize bistable membrane behavior (see Discussion). In that case, the RE neuron displayed clear plateau potentials, consisting of burst and tonic discharges during the early period of the recording (Fig. 3.7*A*). The V_m of this neuron presented the

characteristics of bistability, with a double peak in the distribution histogram (*early* in Fig. 3.7*B*). After a few minutes, QX-314 started to diffuse and action potentials decreased both in amplitude and frequency. As time elapsed, not only spike generation was affected, but also the expression of the plateau potential (Fig. 3.7). The decrease in the sustained depolarization during spindles was reflected as a change in the V_m distribution of the cell, since the secondary peak of active states was abolished (*late* in Fig. 3.7*B*). Measuring the area of depolarization during spindle periods showed a three-fold decrease in the presence of QX-314 in the recording pipette, after 40 minutes of recording (40993.1 ± 18607.2 mV*ms and 13499.2 ± 3548.8 mV*ms, $p<0.05$, 2 min and 40 min; respectively; Fig. 3.7*C*).

In other neurons, we were not able to detect bistable behavior during the early period of recordings with QX-filled pipettes. Therefore, we compared the depolarization area during the spindle sequences in bistable neurons and in some of the neurons recorded with QX-314 ($n = 5$). At hyperpolarized V_ms, the areas of depolarization during spindles were very similar in bistable and QX-314-recorded neurons (10.1 ± 1.4 and 9 ± 1.5 normalized units, respectively); however, when neurons were at the resting V_m, bistable cells displayed their characteristic active states increasing considerably the depolarization area, two-fold larger than in recordings with QX-314 (16.6 ± 2 and 8 ± 1.3 normalized units, respectively; $p = 0.0001$; not shown). These results suggest that QX-314 either abolishes or disrupts bistability in RE neurons.

Membrane bistability of RE neurons modulates their synaptic responsiveness

Responses to stimulation of the internal capsule where compared during silent and active states in bistable RE neurons (n = 5). During silent states, corticofugal volleys elicited short-latency, subthreshold EPSPs, with little variability in amplitude. During active states, the V_m was depolarized by about ~20 mV and responses to stimulation, crowned by action potentials, where of two types: either short and fixed-latency spikes or EPSPs that elicited spikes with much longer and variable latencies (Fig. 3.8*A*-*C*). By raising the stimulation strength, action potentials could be elicited even during the silent state **(**not shown). The threshold intensities for spike generation were quantified for silent as well as for active states. The half-maximal probability of spike generation was reached at a stimulation intensity of 130 μA for the active period and 164 μA during the silent state (Fig. 3.8*D*). This shows that stimulus intensities that are sufficient to produce spikes during the active state did not evoke action potentials in the silent state. Thus, the active state represents a condition of increased responsiveness to synaptic inputs.

Various spindling patterns in thalamocortical neurons may reflect non-bistable or bistable activity patterns of RE neurons

The main output of the RE nucleus is to the dorsal thalamus, whose neurons receive a powerful, cyclic inhibition from GABAergic RE neurons during spindles (Steriade et al. 1990, 1993). In order to assess a possible effect of membrane bistability in RE neurons on spindle waves, we performed intracellular recordings from TC cells (n = 21), identified by their short spike-bursts (<30 ms) and their characteristic sequence of IPSPs during spindle waves (Fig. 3.9*A*).

Visual inspection revealed the presence of a sub-group of neurons (14%, 3 of 21) displaying different types of spindles, compared to all other neurons. One of those cells (*cell 2* in Fig. 3.9) is shown for comparison with a typical TC neuron (*cell 1* in Fig. 3.9). As known, during spindles most TC neurons (like *cell 1*) display regular and powerful IPSPs, due to the inhibitory action of RE neurons during spindles, which hyperpolarize the neuronal membrane, thus de-inactivating the I_T that, in turn, may generate a burst of action potentials. Such canonical TC neurons initiate rebound bursts after the initial three-four IPSPs during spindle periods (Fig. 3.9*B*). On the other hand, neurons like *cell 2* presented irregular sequences of IPSPs superimposed on a tonic hyperpolarization during spindles; a spike-burst was not present before the second half of the spindle sequence and such bursts usually occurred toward the very end of the spindle (Fig. 3.9*C*).

In fact, the frequency spectrum of the signals extracted by fast Fourier transform analysis showed spindles in the frequency range of ~7-10 Hz to be much more represented in thalamocortical neurons like *cell 1* than in neurons like *cell 2* (Fig. 3.9), consistent with the irregularity seen in IPSPs occurring during spindles in *cell 2*. Spindle-related IPSPs were selected and their intervals of incidence measured. Histograms of inter-event intervals (IEIs) in thalamocortical *cell 1* showed that IPSPs during spindles were mostly distributed in the 130-150 ms interval, consistent with the spindle frequency at ~7 Hz (Fig. 3.9*E*). At variance, thalamocortical neurons like *cell 2* presented a tail shifted to shorter intervals (asterisk in Fig. 3.9*E*), indicating the presence of faster activities in some thalamocortical neurons. Indeed, intracellular recordings of neurons like *cell 2* revealed the presence of small-amplitude events, presumably IPSPs, during

spindle waves, reflecting higher frequencies (~20 Hz) than the expected frequency at 7-10 Hz for these periods (see arrowheads in inset, Fig. 3.9*C*). Since the IPSPs in thalamocortical neurons during spindles are generated by RE neurons, these results suggest that at least two functional groups of neurons in the RE nucleus produce diverse patterns of IPSP-rebound sequences in thalamocortical neurons.

Computer simulations predict a role for membrane bistability of RE neurons in modulating thalamic oscillations

Since intracellular recordings with QX-314 abolished bistable behavior in RE neurons, we hypothesized that $I_{Na(p)}$ could contribute to the generation of prolonged depolarizing states in those neurons. To test this possibility, the role $I_{Na(p)}$ was further studied in computer simulations. In a first stage, RE neurons were modeled in order to determine if inclusion of $I_{Na(p)}$ in their repertoire was enough to produce membrane bistability; and furthermore, if such behavior would have an impact on oscillations in TC neurons. Then, thalamic networks containing RE and TC neurons were modeled.

Computer simulations of typical RE neurons displayed an initial high-frequency spike-burst followed by a lower-frequency train of action potentials upon stimulation with a positive current pulse (Fig. 3.10*A*, non-bistable). Inclusion of $I_{Na(p)}$ in the same model was able to generate a sustained firing pattern, which outlasted the duration of the current pulse (Fig. 3.10*A*, bistable), a typical feature of membrane bistability in these cells (see previous figures). As $I_{Na(p)}$ had a strong effect in the initial bursting response of RE neurons (not shown), the values for I_T were decreased in those neurons, including the

$I_{Na(p)}$ (Fig. 3.10*A*). This way, another characteristic of bistable RE neurons was mimicked: the slightly lower frequency discharges compared to typical non-bistable RE neurons (plot in Fig. 3.10*A*; see also Fig. 3.4). Activation and deactivation of the plateau potential, distinctive of membrane bistability, were also seen in RE neurons modeled with the inclusion of $I_{Na(p)}$. Stimulation with a brief positive current pulse to RE neurons in resting conditions induced transition to the active, depolarized state, which outlasted the duration of the stimulus and remained indefinitely in the model (bottom black trace, Fig. 3.10*A*). Such an active state or plateau potential could be terminated by the injection of the same current pulse, but with opposite sign (bottom grey trace, Fig. 3.10*A*). In this situation, V_m returned to initial resting conditions.

Next, we modeled a thalamic network consisting of RE and TC neurons. To mimic the proportion found in experiments, only a few RE neurons presented $I_{Na(p)}$ and, thus, membrane bistability (see Methods). Thalamic oscillations presented different patterns in TC neurons, depending on the presence or absence of membrane bistability in RE neurons. For the majority of RE neurons, bursting within spindle frequency was evident during active oscillatory periods (Fig. 3.10*B*, two upper traces). On the other hand, bistable RE neurons exhibited prolonged firing, by far exceeding the durations of individual LTSs (~60 ms) (Fig. 3.10*B*, two lower traces), consistent with a low correlation with spindle-frequency activities (see Fig. 3.1). These different patterns of activity in RE neurons had a differential effect of target TC neurons, depending on the connectivity in the reciprocal network. Note that TC cells receive projections from multiple RE neurons; therefore, the final effect on spindling pattern was a combination

between those multiple inhibitory inputs. Accordingly, TC neurons receiving preferentially projections from non-bistable RE neurons displayed robust, regular oscillations, with rebound spike-bursts in most cases (Fig. 3.10*B*, two upper traces). Conversely, TC cells receiving inputs mainly from bistable RE neurons showed irregular rhythms, associated with very low rebound discharges (Fig. 3.10*B*, two lower traces; compare to experimental data in Fig. 3.9*C*). In fact, the spatial-temporal pattern of activity in the modeled thalamic network showed a few TC neurons that were hyperpolarized and did not fire during the active periods of this type of thalamic oscillations (not shown).

DISCUSSION

The main results of the present study are as follows. *(a)* About 23% of cat RE neurons displayed membrane bistability during spindles *in vivo*. The bistability consisted of two discrete V_m levels: an active state (plateau potential) and a silent state, separated by ~17 mV. *(b)* The membrane bistability only occurred at the resting V_m, was an intrinsic property of RE neurons, and was modulated by synaptic activity. *(c)* Bistability did not appear in neurons recorded with QX-314. *(d)* Bistable and non-bistable RE neurons could determine different patterns of spindling in target thalamocortical neurons. *(e)* Computer simulation supported the idea that membrane bistability in RE neurons is generated by the activation of $I_{Na(p)}$ and that such bistable activity is able to modulate the pattern of thalamic spindle oscillations.

The active state in bistable RE neurons has the characteristics of plateau potentials**.** Such behavior could be generated either by intrinsic membrane properties or a particular synaptic activity in the thalamocortical network. The membrane bistability here reported seems to be intrinsically generated, as is the case described in multiple structures in the central nervous system (see Introduction). That membrane bistability is an intrinsic, voltage-dependent property of RE neurons was indicated by its presence only at the resting V_m, through induction of prolonged depolarizing plateaus by brief intracellular current pulses, and by termination of these plateaus by hyperpolarizing current pulses. Our results indicate that intrinsic mechanisms are involved in the generation, maintenance, and termination of active states during membrane bistability. While the

active state represents a depolarized plateau potential that may be de-activated by hyperpolarization, the silent state is maintained until sufficient depolarization occurs to initiate an active depolarization toward the active state. The transition from the silent to the active state proceeds exponentially. The present data showed that small-amplitude EPSPs are ineffective in spike generation during the silent state. However, when EPSPs are strong enough, they give rise to action potentials even during the silent state (data not shown), and the transition to an active state may occur.

The two different modes of V_m bistability are associated with different degrees of neuronal responsiveness. The active state is around the threshold for action potential generation, while the silent state is subthreshold. A broader range of depolarizing inputs' amplitudes may be processed during the silent state, without the generation of a short-latency and stereotyped spike, than in the active state. On the other hand, small-amplitude EPSPs, which are ineffective during the silent state, may well trigger action potentials during the active state. When excitatory inputs occurring during the silent state are strong enough, transition to the active state might occur. Such transition amplifies the voltage change produced by transient depolarizing signals.

Actually, corticofugal volleys elicit complex depolarizing responses in RE neurons, composed by several EPSPs followed by all-or-none events resembling dendritic spikes or, in less numerous RE neurons, presumably unitary dendritic spikes (Contreras et al. 1993). The dendritic spikes may contribute to the generation of spindle oscillations by boosting distal inputs and depolarizing the soma as well as by triggering

dendritic low-threshold spikes (Huguenard and Prince, 1992; Destexhe et al. 1996c; Huguenard, 1996) that are crucial in the generation of spindle oscillations. Thus, although an intrinsic membrane property, bistability may strongly be modulated by synaptic activity.

Intracellular recordings of RE neurons *in vivo* present technical problems due to instability. In the majority of cases, the initial period of recording (3-5 min) is unstable, presenting continuous changes in the V_m. To maintain the neuron, this period was necessarily performed under negative current injection. Since membrane bistability is present only at resting conditions, and is abolished by current injection in the pipette, it was not possible to detect bistable behavior in neurons recorded under QX-314. During the few minutes that are necessary to stabilize the recording, QX-314 is already acting on its target conductances. This is the probable reason to explain the fact that upon current removal, and resting conditions recovered, bistable behavior was not seen in most neurons recorded with QX-314-filled pipettes. The only neuron in which bistability was seen under QX-314 conditions (see Fig. 3.7) was stable from the very early period of recordings (1-2 min) and both action potentials and plateau potentials were rapidly affected.

The marked effect of QX-314 suggests that generation of bistability requires activation of voltage-gated Na^+ channels. However, QX-314 also blocks low- and high-voltage activated Ca^{2+} currents (Talbot and Sayer, 1996), K^+ currents (Svoboda et al. 1997; Paré and Lang, 1998) as well as hyperpolarization-activated currents (Perkins and

Wong, 1995). Therefore, the relative contribution of Na^+ and other QX-314-sensitive channels in generating bistability is not yet clear. Still, TTX bath application in perigeniculate (RE) thalamic slices blocked plateau potentials, suggesting that $I_{Na(p)}$ may generate such activities (Kim and McCormick, 1998a). Furthermore, computer simulations of RE neurons predicted that by the inclusion of $I_{Na(p)}$, otherwise typical RE neurons became bistable. Thus, the ionic basis of bistability in RE neurons seem to be different than those in TC neurons, where a steady-state residual ("window") component of I_T is responsible for signal amplification and bistable behavior (Williams et al. 1997).

Membrane bistability in a subgroup of RE neurons may play an important role in different patterns of spindles displayed by thalamocortical neurons. *In vivo* (Steriade et al. 1985; Timofeev and Steriade, 1996) and *in vitro* (Bal et al. 1995a,b) intracellular studies have revealed the cellular mechanisms responsible for spindle generation, demonstrating that prolonged, rhythmic IPSPs in TC cells during spindles are time-locked and generated by spike-bursts fired by RE neurons. Consequently, any change in the bursting pattern of RE neurons would affect their targets, thalamic relay neurons. Intracellular recordings of TC cells showed at least two different patterns during spontaneously occurring spindles. Although simultaneous recordings of RE and TC neurons have not been performed in the present experiments, the two patterns displayed by *cell 1* and *cell 2* in Fig. 3.9 may be related to the actions exerted by non-bistable and bistable RE neurons, respectively. Indeed, non-bistable neurons fired stronger bursts, with higher intra-bursts frequencies, which are assumed to generate deeper and longer IPSPs in TC neurons, giving rise to the usual frequency range of spindles under barbiturate anesthesia, ~7-10 Hz. By contrast,

IPSPs with lower amplitudes and higher frequency, up to 20 Hz (see inset in Fig. 3.9*C*) are likely to be mainly generated by single action potentials in RE neurons, as they occur during the depolarizing plateau in bistable cells. In either case, the crucial role of RE neurons in initiating spindles, even in the absence of feed-back excitatory effects from TC neurons, is shown by the absence of rebound bursts with fast action potentials after the first three or four IPSPs in relay cells (Timofeev et al. 2001). Supporting these results, computational models of thalamic networks, including bistable RE neurons, showed a significant shaping of thalamic oscillations in TC neurons by bistable RE neurons. While spindles are initiated in the RE nucleus (Steriade et al. 1987), this oscillation is maintained by reciprocal actions between RE and TC neurons (Steriade et al. 1993; von Krosigk et al. 1993; Bal et al. 1995a,b).

REFERENCES

Alzheimer C, Schwindt PC, and Crill WE. Modal gating of Na^+ channels as a mechanism of persistent Na^+ current in pyramidal neurons from rat and cat sensorimotor cortex. *J Neurosci* 13: 660-673, 1993.

Bal T, von Krosigk M, and McCormick DA. Synaptic and membrane mechanisms underlying synchronized oscillations in the ferret lateral geniculate nucleus *in vitro*. *J Physiol* 483: 641-663, 1995a.

Bal T, von Krosigk M, and McCormick DA. Role of the ferret perigeniculate nucleus in the generation of synchronized oscillations *in vitro*. *J Physiol* 483: 665-685, 1995b.

Bazhenov M, Timofeev I, Steriade M, and Sejnowski TJ. Cellular and network models for intrathalamic augmenting responses during 10-hz stimulation. *J Neurophysiol* 79: 2730-2748, 1998.

Bazhenov M, Timofeev I, Steriade M, and Sejnowski TJ. Patterns of spiking-bursting activity in the thalamic reticular nucleus initiate sequences of spindle oscillations in thalamic network. *J Neurophysiol* 84: 1076-1087, 2000.

Bennett DJ, Hultborn H, Fedirchuk B, and Gorassini M. Synaptic activation of plateaus in hindlimb motoneurons of decerebrate cats. *J Neurophysiol* 80: 2023-2037, 1998.

Chuang SC, Bianchi R, and Wong RK. Group I mGluR activation turns on a voltage-gated inward current in hippocampal pyramidal cells. *J Neurophysiol* 83: 2844-2853, 2000.

Contreras D, Curró Dossi R, and Steriade M. Bursting and tonic discharges in two classes of reticular thalamic neurons *in vivo*. *J Neurophysiol* 68: 973-977, 1992.

Contreras D, Curró Dossi R, and Steriade M. Electrophysiological properties of cat reticular thalamic neurons *in vivo*. *J Physiol* 470: 273-294, 1993.

Contreras D and Steriade M. Spindle oscillation: the role of corticothalamic feedback in a thalamically generated rhythm. *J Physiol* 490: 159-179, 1996.

Crill WE. Persistent sodium current in mammalian central neurons. *Annu Rev Physiol* 58: 349-362, 1996.

Crunelli V, Kelly JS, Leresche N, and Pirchio M. The ventral and dorsal lateral geniculate nucleus of the rat: intracellular recordings in vitro. *J Physiol* 384: 587-601, 1987.

Destexhe A, Mainen ZF, and Sejnowski TJ. Synthesis of models for excitable membranes, synaptic transmission and neuromodulation using a common kinetic formalism. *J Comput Neurosci* 1: 195-230, 1994.

Destexhe A, Bal T, McCormick DA, and Sejnowski TJ. Ionic mechanisms underlying synchronized oscillations and propagating waves in a model of ferret thalamic slices. *J Neurophysiol* 76: 2049-2070, 1996a.

Destexhe A, Bal T, McCormick DA, and Sejnowski TJ. Ionic mechanisms underlying synchronized and propagating waves in a model of ferret thalamic slices. *J Neurophysiol* 76: 2049-2070, 1996b.

Destexhe A, Contreras D, Steriade M, and Huguenard JR *In vivo*, *in vitro* and computational analysis of dendritic calcium currents in thalamic reticular neurons. *J Neurosci* 16: 169-185, 1996c.

Domich L, Oakson G, and Steriade M. Thalamic burst patterns in the naturally sleeping cat: a comparison between cortically projecting and reticularis neurons. *J Physiol* 379: 429-449, 1986.

Dutar P and Nicoll RA. A physiological role for $GABA_B$ receptors in the central nervous system. *Nature* 332: 156-158, 1988.

Fricker D and Miles R. EPSP amplification and the precision of spike timing in hippocampal neurons. *Neuron* 28: 559-569, 2000.

Gola M, Delmas P, and Chagneux H. Encoding properties induced by a persistent voltage-gated muscarinic sodium current in rabbit sympathetic neurons. *J Physiol* 510: 387-399, 1998.

Heyward P, Ennis M, Keller A, and Shipley MT Membrane bistability in olfactory bulb mitral cells. *J Neurosci* 21: 5311-5320, 2001.

Hughes SW, Cope DW, Toth TI, Williams SR, and Crunelli V All thalamocortical neurons possess a T-type Ca^{2+} "window" current that enables the expression of bistability-mediated activities. *J Physiol* 517: 805-815, 1999.

Huguenard JR. Low-threshold calcium currents in central nervous system neurons. *Ann Rev Physiol* 58: 329-348, 1996.

Huguenard JR and Prince DA. A novel T-type current underlies prolonged Ca^{2+}-dependent burst firing in GABAergic neurons of rat thalamic reticular nucleus. *J Neurosci* 12: 3804-3817, 1992.

Huguenard JR and McCormick DA. Simulation of the currents involved in rhythmic oscillations in thalamic relay neurons. *J Neurophysiol* 68: 1373-1383, 1992.

Jones EG. *The Thalamus*. Plenum, New York, 1985.

Kim U and McCormick DA. Functional and ionic properties of a slow afterhyperpolarization in ferret perigeniculate neurons in vitro. *J Neurophysiology* 80: 1222-1235, 1998a.

Kim U and McCormick DA. The functional influence of burst and tonic firing mode on synaptic interactions in the thalamus. *J Neurosci* 18: 9500-9516, 1998b.

Llinás R and Sugimori M. Electrophysiological properties of in vitro Purkinje cell somata in mammalian cerebellar slices. *J Physiol* 305: 171-195, 1980.

McCormick DA and Pape HC. Properties of a hyperpolarization-activated cation current and its role in rhythmic oscillation in thalamic relay neurons. *J Physiol* 431: 291-318, 1990.

Paré D and Lang EJ. Calcium electrogenesis in neocortical pyramidal neurons in vivo. *Eur J Neurosci* 10: 3164-3170, 1998.

Perkins KL and Wong RK. Intracellular QX-314 blocks the hyperpolarization-activated inward current I_q in hippocampal CA1 pyramidal cells. *J Neurophysiol* 73: 911-915, 1995.

Schwindt P and Crill W. Mechanisms underlying burst and regular spiking evoked by dendritic depolarization of layer 5 cortical pyramidal neurons. *J Neurophysiol* 81: 1341-1354, 1999.

Steriade M, Deschênes M, Domich L, and Mulle C. Abolition of spindle oscillations in thalamic neurons disconnected from nucleus reticularis thalami. *J Neurophysiol* 54: 1473-1497, 1985.

Steriade M, Domich L, and Oakson G. Reticularis thalami neurons revisited: activity changes during shifts in states of vigilance. *J Neurosci* 6: 68-81, 1986.

Steriade M, Domich L, Oakson G, and Deschênes M. The deafferented reticularis thalami nucleus generates spindle rhythmicity. *J Neurophysiol* 57: 260-273, 1987.

Steriade M, Jones EG, and Llinás RR. *Thalamic Oscillations and Signaling.* Wiley-Interscience, New York, 1990.

Steriade M, McCormick DA and Sejnowski TJ. Thalamocortical oscillation in the sleeping and aroused brain. *Science* 262: 679-685, 1993.

Svoboda K, Denk W, Kleinfeld D and Tank DW. In vivo dendritic calcium dynamics in neocortical pyramidal neurons. *Nature* 385: 161-165, 1997.

Talbot MJ and Sayer RJ. Intracellular QX-314 inhibits calcium currents in hippocampal CA1 pyramidal neurons. *J Neurophysiol* 76: 2120-2124, 1996.

Timofeeev I and Steriade M. Low-frequency rhythms in the thalamus of intact-cortex and decorticated cats. *J Neurophysiol* 76: 4152-4168, 1996.

Timofeev I, Bazhenov M, Sejnowski TJ, and Steriade M. Contribution of intrinsic and synaptic factors in the desynchronization of thalamic oscillatory activity. *Thalamus & Related Systems* 1: 53-69, 2001.

Thomson AM. Inhibitory postsynaptic potentials evoked in thalamic neurons by stimulation of the reticularis nucleus evoke slow spikes in isolated rat brain slices. *Neuroscience* 25: 491-502, 1988.

Toth TI, Hughes SW and Crunelli V. Analysis and biophysical interpretation of bistable behavior in thalamocortical neurons. *Neuroscience* 87: 519-523, 1998.

Von Krosigk M, Bal T, and McCormick DA. Cellular mechanisms of a synchronized oscillation in the thalamus. *Science* 261: 361-364, 1993.

Williams SR, Toth TI, Turner JP, Hughes SW, and Crunelli V. The "window" component of the low threshold Ca^{2+} current produces input signal amplification and bistability in cat and rat thalamocortical neurons. *J Physiol* 505: 689-705, 1997.

FIGURES

Figure 3.1. Membrane bistability in RE neurons during spontaneously occurring spindles. *A*, cortical EEG and intracellular recordings from two RE neurons**.** Typical low-threshold spike-bursts of each of these RE cells are expanded in insets; scale is same for both neurons. Bistable neuron displayed sustained depolarizations throughout spindle waves. Non-bistable neuron fired spike-bursts, separated by phasic hyperpolarizations, during spindling. Scale bars: 50 ms, 20 mV. *B*, histograms of V_m distribution from bistable and non-bistable cells in *A*, taken from a 5-minute period of spontaneous activity. Only bistable neurons presented bimodal V_m distributions. Bin size, 1 mV. *C*, autocorrelograms of action potentials for the same periods used in *B*. Non-bistable cells discharged in the spindle frequency (~9 Hz), showing clear peaks at ~±110 ms delay, whereas bistable cells showed less marked correlation with spindle frequency. Bin size, 1 ms. *D*, Bistability is a graded property. Different bistable RE neurons (represented by different gray tones) displayed diverse patterns of V_m distributions, but all showed two discrete peaks though at different positions. Note the constancy of the first peak (*silent*) and the variable position of the second peak (*active*, arrows). Bin size, 1 mV. *E*, Silent and active states during membrane bistability presented different membrane potentials (mean ± SD, $n = 9$); * $p<0.001$. *F*, intracellularly stained (Neurobiotin) bistable RE neuron located in the rostral sector of the nucleus. Photograph (*right*) and reconstruction (*left*). Arrowhead indicates the axon to the dorsal thalamus. Calibration bar = 20 μm for RE neuron in the photograph and 100 μm for the reconstructed RE neuron. *G*, microphotograph of the section where the cellular soma was recovered. Reconstruction

shows the relative position of the neuron. Arrowheads point to the rostrolateral sector of the RE nucleus. Asterisk marks the stimulating electrode in the IC. Abbreviations: AV, anteroventral nucleus; CA, caudate nucleus; IC, internal capsule; LV, lateral ventricle; RE, reticular nucleus; VA, ventroanterior nucleus. Scale bar: 500 μm.

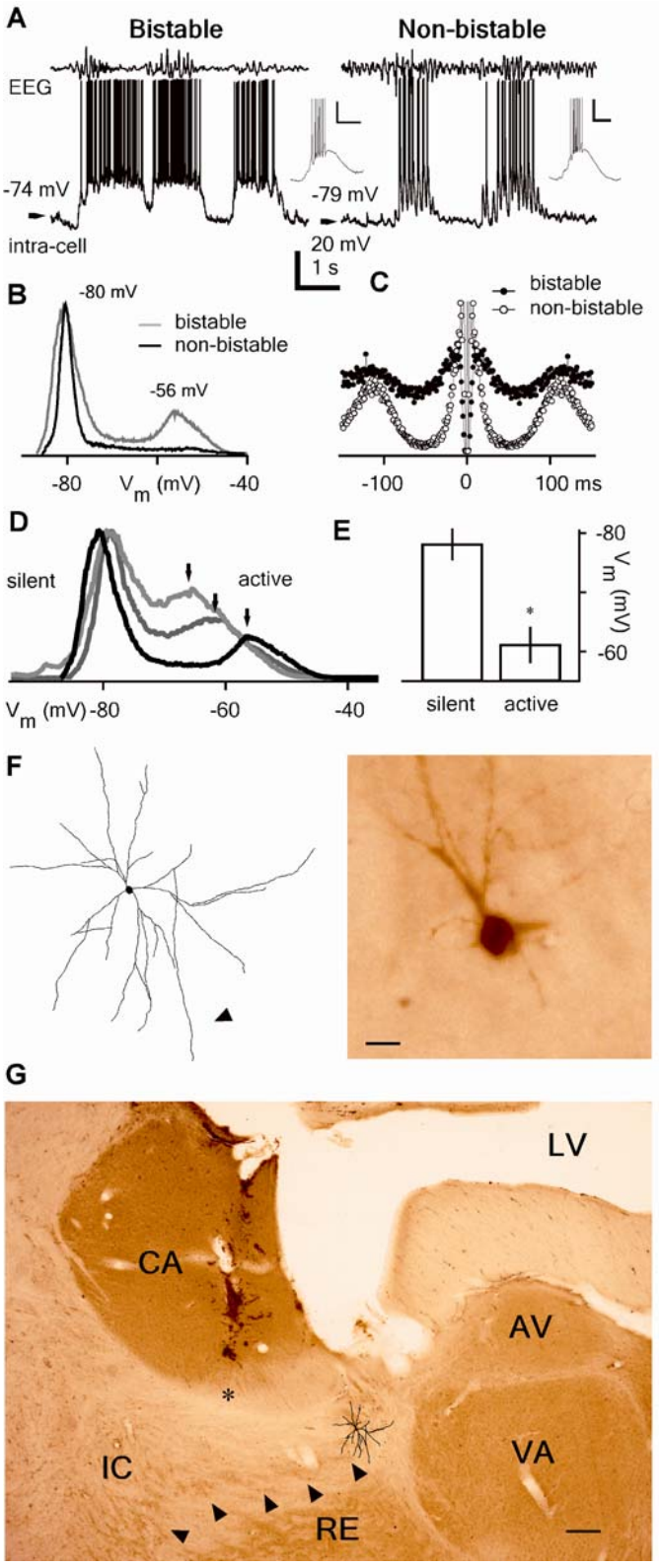
A
Bistable
Non-bistable
EEG
-74 mV
intra-cell
-79 mV
20 mV
1 s
B
-80 mV
bistable
non-bistable
-56 mV
-80
V_m (mV)
-40
C
bistable
non-bistable
-100
0
100 ms
D
silent
active
V_m (mV) -80
-60
-40
E
-80
V_m (mV)
-60
silent
active
F
G
LV
CA
AV
IC
VA
RE

Figure 3.2. Membrane bistability can be triggered by corticothalamic inputs. *A*, intracellular recordings of two RE neurons, displaying spindles triggered by electrical stimulation of the internal capsule. One of them presents a plateau potential (bistable), while the other neuron shows a typical sequence of spike-bursts during spindling. *B*, autocorrelograms of action potentials in both neurons; bin size, 1 ms.

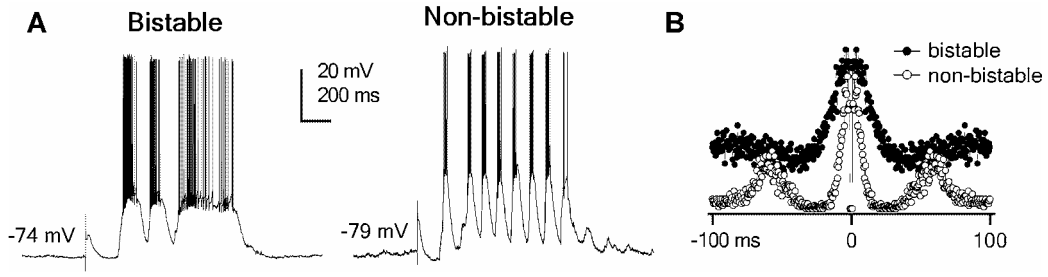
A
Bistable
Non-bistable
20 mV
200 ms
-74 mV
-79 mV
B
bistable
non-bistable
-100 ms
0
100

Figure 3.3. Membrane bistability is voltage-dependent. Intracellular recording (left column, *A*-*C*) and histograms of V_m distributions (right column) for a RE neuron held at different levels of DC. *A,* positive current injection (+0.2 nA) depolarized the V_m to –64 mV and caused a sustained, tonic firing (left). Only a single mode was present in such cases for V_m distribution (right). *B,* without current (0 nA, -79 mV), it was possible to distinguish a bimodal V_m distribution (right). *C,* negative current injection (-0.2 nA, -90, mV) was equally efficient in abolishing bistability (right), even though firing occurred during spindles (left). *D,* summary plot of the relation between injected current (DC) and the resulting membrane potential (V_m). The resting level (0 nA) is the only two-point case in the V_m axis (-79 mV and -62 mV) and constitutes an asymmetric axis for the apparent input resistance, R_{in} (7 MΩ for positive DC and 22 MΩ for negative DC). *E,* summary plot of the relation between injected current (DC) and mean firing frequency of the cell. The resting level marks an asymmetric axis for the gain in firing frequency (56 Hz/nA for positive DC and 10 Hz/nA for negative DC). R_{in} and gain in firing frequency were calculated as the slope for the linear fitting in *D* and *E*, respectively. Each V_m point is the mean of a Gaussian fitting to the histogram (3-minute period of intracellular recording) for each DC value. Histograms' bin size, 1 mV.

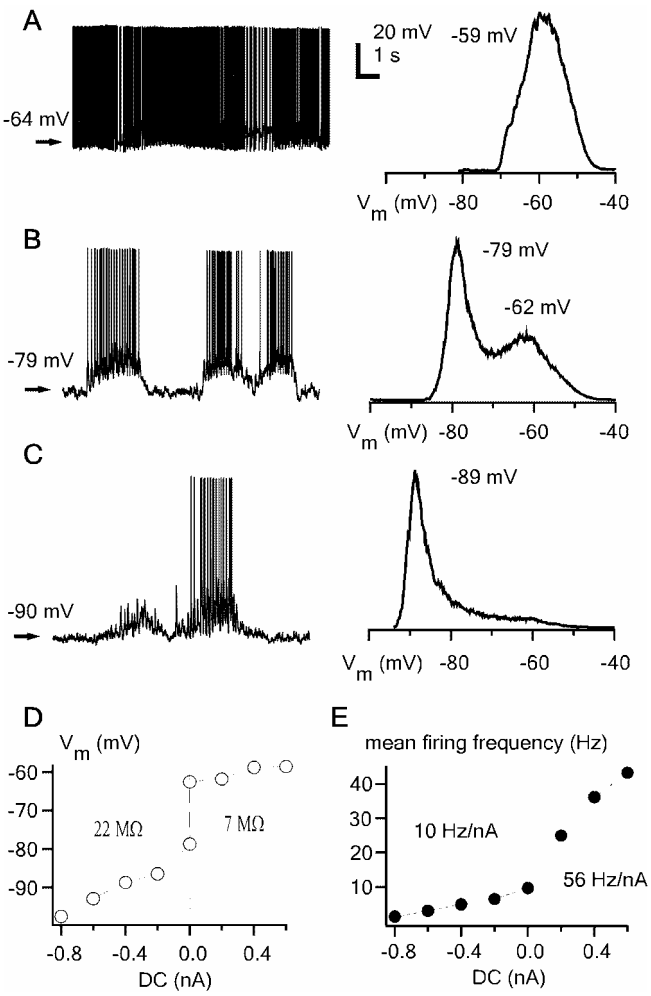
A
-64 mV
20 mV
1 s
-59 mV
V_m (mV) -80 -60 -40
B
-79 mV
-79 mV
-62 mV
V_m (mV) -80 -60 -40
C
-90 mV
-89 mV
V_m (mV) -80 -60 -40
D
V_m (mV)
-60
-70
-80
-90
22 MΩ
7 MΩ
-0.8 -0.4 0.0 0.4
DC (nA)
E
mean firing frequency (Hz)
40
30
20
10
10 Hz/nA
56 Hz/nA
-0.8 -0.4 0.0 0.4
DC (nA)

Figure 3.4. Simultaneous extracellular recordings of non-bistable and bistable RE neurons show different firing patterns during spindles. To avoid corticofugal influences, recordings were made in decorticated cats. *A,* dual extracellular recordings of RE neurons (*cell 1* and *cell 2*). *B,* one spindle period chosen from the above panel, for each RE neuron. Visual inspection reveals the presence of tonic firing in *cell 2* (right). Spike-bursts displaying the accelerando-decelerando pattern identified both RE neurons (see arrows and insets in *B*). *C,* semi-logarithmic plot for firing frequency in *cell 1* and *cell 2* during spindle sequences shown in *B*. Note tonic spikes (~20-100 Hz) only in *cell 2*. Inset plot depicts inter-spike intervals for a 5-minute period of recording during spontaneous activity in each cell; bin size, 1 ms.

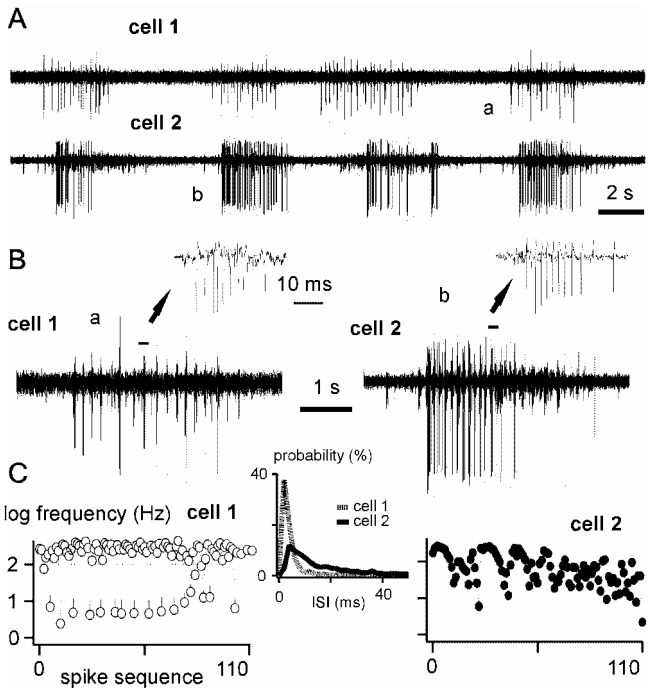
A
cell 1
a
cell 2
b
2 s
B
10 ms
cell 1
a
b
cell 2
1 s
C
log frequency (Hz)
cell 1
2
1
0
0
spike sequence
110
probability (%)
40
0
cell 1
cell 2
0
ISI (ms)
40
cell 2
0
110

Figure 3.5. Active states in membrane bistability evoked by depolarizing current pulses in RE neurons are graded and voltage-dependent. *A,* current pulse (200 ms, 2 nA) generated an outlasting active state at rest (0 nA). *B,* shorter current pulses (50 ms, 2 nA) were also able to elicit outlasting active states, but of shorter duration. *C-D*, hyperpolarization (–2 nA), bringing the V_m to –90 mV, abolished the ability of current pulses to generate outlasting active state in the same neuron, even though their amplitudes were increased (+2, +2.4, +2.7, and +3 nA). *E*, very short current pulses (10 ms, 30 ms) were not able to elicit active responses under slight hyperpolarization (DC –1 nA). Short current pulses (50 ms) could trigger a spike occasionally. *F*, summary plot for the current pulse duration versus the duration of the evoked plateau outlasting the stimulus. note graded properties for intermediate levels of membrane polarization (-85 mV).

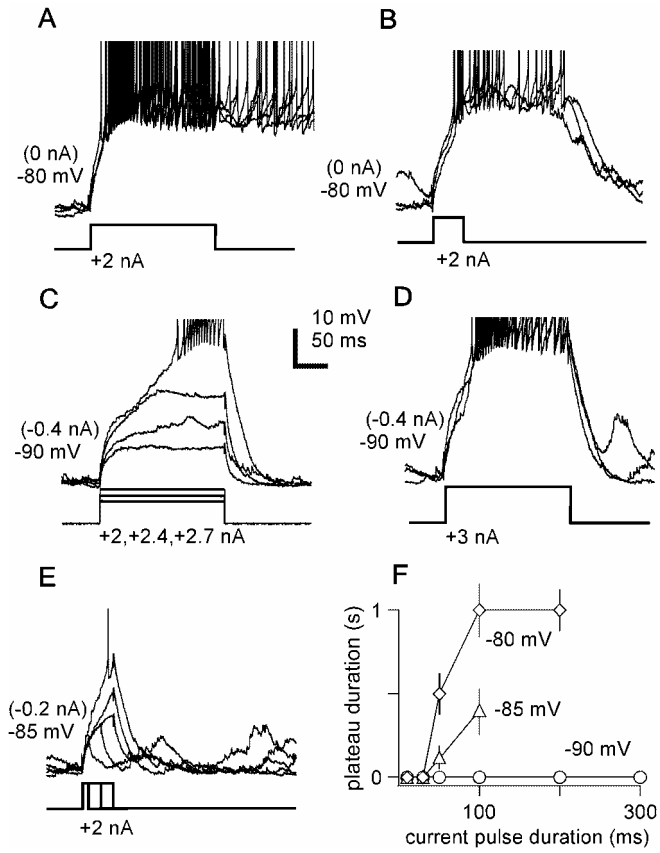
A
(0 nA)
-80 mV
+2 nA
B
(0 nA)
-80 mV
+2 nA
C
10 mV
50 ms
(-0.4 nA)
-90 mV
+2,+2.4,+2.7 nA
D
(-0.4 nA)
-90 mV
+3 nA
E
(-0.2 nA)
-85 mV
+2 nA
F
plateau duration (s)
1
0
-80 mV
-85 mV
-90 mV
100
300
current pulse duration (ms)

Figure 3.6. Intrinsic membrane properties are involved in the generation, maintenance, and termination of active states in membrane bistability. *A,* depolarizing current pulses (200 ms, +2 nA) were able to generate active states, characteristic of membrane bistability in RE neurons, independent on the duration of the previous silent period (bottom plot). Note that failures in generating an active state were also independent on the history of the cell. *B,* hyperpolarizing current pulses (200 ms, -1 and -2 nA) were effective in shunting the active states. Note (bottom plot) that long-lasting active periods (>3s) were shunted for longer periods than short lasting (<2s) active periods; and failures were independent on the ongoing active state duration.

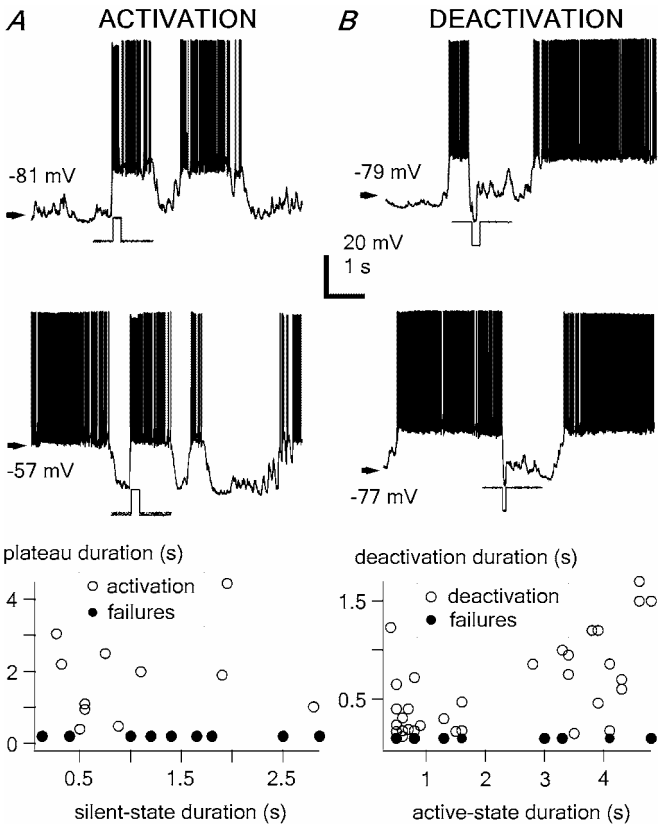
A
ACTIVATION
B
DEACTIVATION
-81 mV
-79 mV
20 mV
1 s
-57 mV
-77 mV
plateau duration (s)
activation
failures
4
2
0
0.5
1.5
2.5
silent-state duration (s)
deactivation duration (s)
deactivation
failures
1.5
0.5
1
2
3
4
active-state duration (s)

Figure 3.7. Ionic basis of membrane bistability. *A*, RE neuron recorded with QX-314-filled pipette (50 mM) shown at two different periods of recording: early (2 min) and late (40 min). *B*, V_m distribution for the two periods of recording. Bin size, 1 mV. *C*, average (n = 20) of spindle oscillations for the two (early and late) periods of recording shows a neat decrease in plateau potentials during the late period. Spikes were removed by filtering digitized signals (< 100 Hz).

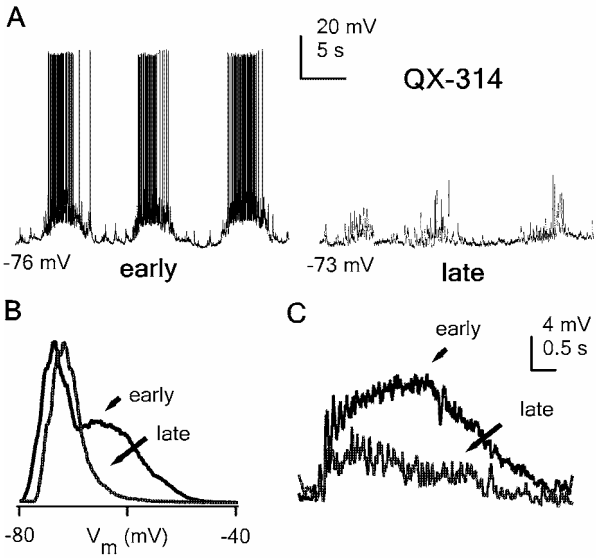
A
20 mV
5 s
QX-314
-76 mV
early
-73 mV
late
B
early
late
-80
V_m (mV)
-40
C
early
4 mV
0.5 s
late

Figure 3.8. Membrane bistability modulates synaptic responsiveness of RE neurons. *A,* intracellular recording of RE neuron displaying both silent and active periods, as stimulated from the internal capsule (140 μA, 1 Hz). *B*, superimposed responses (n = 5) during silent states, consisting on short-latency and low-variability EPSPs. *C*, superimposed responses (n = 5) during active states, consisting on short-latency, fixed spikes (arrowhead) and spikes with variable latencies (asterisk). *D*, summary plot for the stimulation intensity and the probability of evoking and action potential. Note a shift in the curve for active states, which require lower stimulation intensities. Spike probability was calculated as the fraction of stimuli that elicited an action potential.

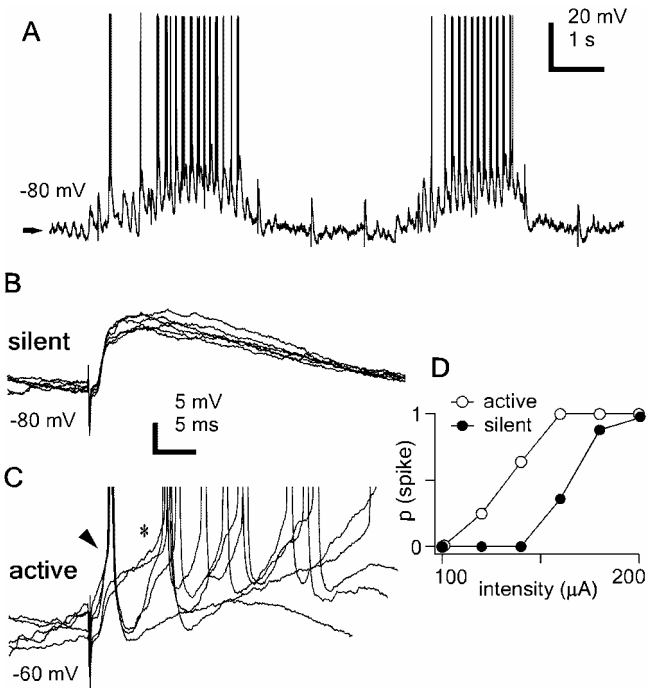
A
20 mV
1 s
-80 mV
B
silent
-80 mV
5 mV
5 ms
C
active
*
-60 mV
D
active
silent
1
0
p (spike)
100
200
intensity (μA)

Figure 3.9. Different spindling patterns in thalamocortical cells reflect various firing patterns in RE neurons. *A,* intracellular recordings of two TC neurons (VL nucleus) during spindle activity. *B-C,* three different spindle sequences for each of the above cells. Note highly regular activity and early rebound bursting in *cell 1*. Inset in *cell 2* shows three IPSPs (arrows) at much higher frequency (~20 Hz) than the usual frequency range of spindles (see text). *D,* average of frequency spectrums of spindle periods (n = 10, mean ± SD) in both *cell 1* and *cell 2* neurons. Bin size, 1 Hz. Note a clear peak around 7 Hz for *cell 1*. *E,* histograms of inter-event intervals (IEI) for presumably IPSPs (n = 400) in both *cell 1* and *cell 2* during spindle waves. Bin size, 10 ms. Note the presence of a tail at short intervals (<100 ms) for *cell 2* (asterisk).

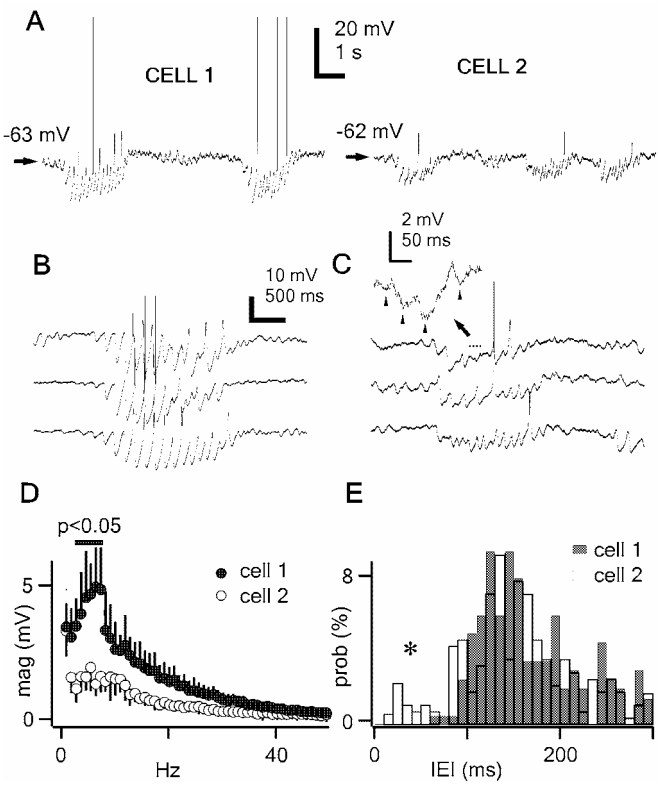
A
20 mV
1 s
CELL 1
CELL 2
-63 mV
-62 mV
B
10 mV
500 ms
C
2 mV
50 ms
D
p<0.05
cell 1
cell 2
mag (mV)
5
0
0
40
Hz
E
cell 1
cell 2
prob (%)
8
0
*
0
200
IEI (ms)

Figure 3.10. Computational models predict that membrane bistability of RE neurons modulates patterns of spindle oscillations in TC neuron. *A,* single-compartment models of bistable and non-bistable RE neurons. Bistability was obtained by inclusion of $I_{Na(p)}$ in non-bistable neurons. Non-bistable g_T = 3 mS/cm^2, $I_{Na(p)}$ = 0.3 mS/cm^2, bistable g_T = 0.75 mS/cm^2, $g_{Na(p)}$ = 0.6 mS/cm^2 for higher traces; g_T = 1 mS/cm^2, $g_{Na(p)}$ = 0.6 mS/cm^2 for lower traces. Resting V_m -80 mV. Right plot reflects inter-spike intervals for both types of cells, notice non-bistable neurons to fire at higher frequencies. *B,* RE and TC neurons during active periods in a simulated thalamic network (26 RE cells and 26 TC cells). See also text.

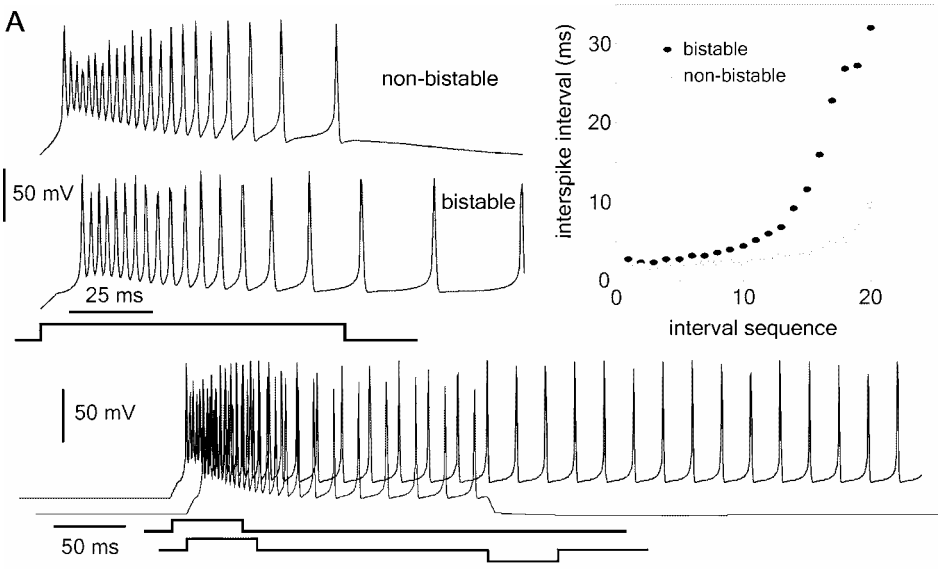
A
non-bistable
50 mV
bistable
25 ms
interspike interval (ms)
30
20
10
0
0
10
20
bistable
non-bistable
interval sequence
50 mV
50 ms

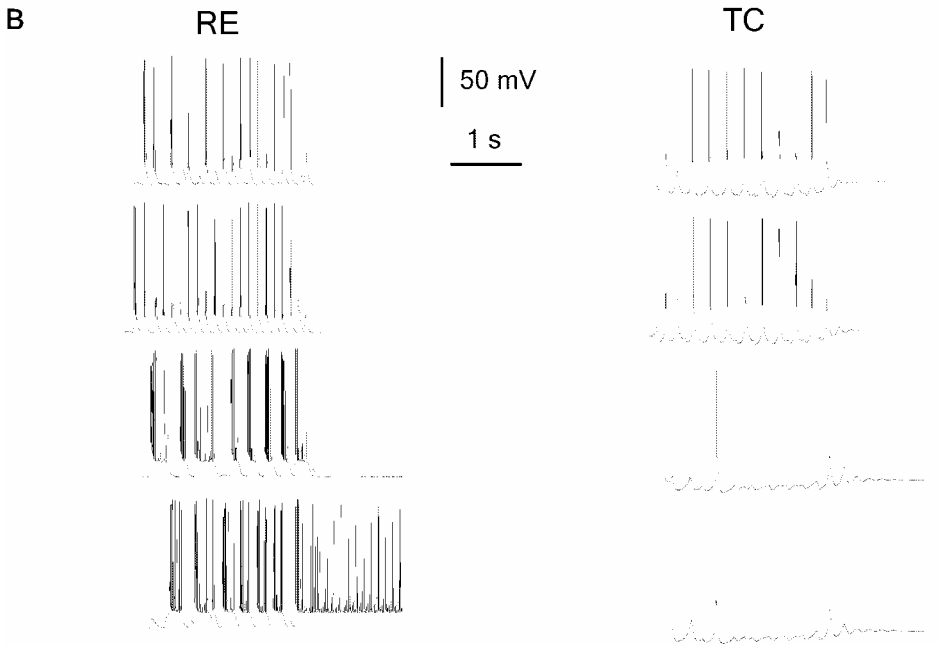
B
RE
TC
50 mV
1 s

4. Membrane Properties and their Modulation by Network Activity

THALAMIC OSCILLATIONS MODULATE MEMBRANE PROPERTIES OF THALAMIC RETICULAR NEURONS

Pablo Fuentealba, Sylvain Crochet and Mircea Steriade (2004). *Thalamus & Related Systems (submitted)*

RESUMÉ

Les oscillations en fuseau sont générées dans des circuits intrathalamiques, surtout par l'action du noyau réticulaire thalamique (RE). Afin d'évaluer les conséquences de cette oscillation sur les neurones RE, nous avons effectué des enregistrements intracellulaires *in vivo* sur des chats anesthésiés pendant les périodes d'activité synaptique intenses, représenté par les ondes en fuseaux, en comparaison avec les périodes silencieuses (périodes d'accalmie entre les fuseaux) qui correspondent à une hyperpolarisation d'environ –75 mV. Pendant les fuseaux, l'activation massive du courrant-T générait de puissantes décharges à seuil bas (LTSs) qui ont changé le potentiel de membrane (V_m) des cellules du RE par 10-20 mV et augmenté leurs fluctuations de la membrane par un ordre de magnitude (de 1-3 mV à 10 mV). Également, la génération des LTSs a diminué la résistance apparente d'entrée (R_{in}) par ~80% pour environ 20-30 ms, de façon cyclique. Les changements dans les propriétés de base de la membrane ont prouvé qu'ils étaient fonctionnellement significatifs pour les neurones RE, puisque les réponses synaptiques et intrinsèques étaient augmentées pendant l'état actif du réseau. Par conséquent, les réponses synaptiques testées par la stimulation des voies afférentes (corticothalamique et thalamo-RE) ont montré une augmentation des décharges. Les mêmes résultats ont été trouvés pour les réponses intrinsèques en utilisant des pulses de courant positifs et négatifs aussi bien que des courants sinusoïdes. Les vagues de décharges, responsables de la génération des changements décris ci-haut, ont prouvé être un patron de décharge très puissant et très fiable dans les neurones RE.

ABSTRACT

Spindle oscillation is generated in intrathalamic circuits, especially by the action of thalamic reticular (RE) nucleus that acts as its pacemaker. To assess the consequences of this oscillation on RE neurones, we performed *in vivo* intracellular recordings in anesthetized cats during periods of intense synaptic activity, represented by spindle waves, compared to silent periods (interspindle lulls) that corresponded to a hyperpolarization of about -75 mV. During spindles, the massive activation of T-current generated powerful low-threshold spikes (LTSs) that changed the membrane potential (V_m) of RE cells by 10-20 mV and increased their membrane fluctuations by one order of magnitude (from 1-3 mV to 10 mV). Besides, the generation of LTSs decreased the apparent input resistance (R_{in}) by ~80% for about 20-30 ms, in a cyclic way. The changes in basic membrane properties proved to be functionally significant for RE neurones, since both synaptic and intrinsic responsiveness were enhanced during active network states. Thus, synaptic responses tested by stimulating afferent (corticothalamic and thalamo-RE) pathways displayed increased spiking. The same result was found for intrinsic responses using positive and negative current pulses, as well as sinusoidal wave currents. Bursting discharges, responsible for the generation of the above described changes, proved to be a very robust and reliable firing pattern in RE neurones.

INTRODUCTION

Thalamic reticular (RE) neurones are crucially implicated in the generation of spindle oscillations (Steriade *et al.* 1987; Fuentealba *et al.* 2004b), a hallmark brain rhythm of light sleep. The synchronization of this sleep oscillation over widespread territories of thalamocortical systems depends on corticothalamic projections (Contreras *et al.* 1996a, 1997). In RE neurones recorded *in vivo*, spindles are characterized by sequences of rhythmic (7-14 Hz) spike-bursts, superimposed over a depolarizing envelope. These active periods are separated by epochs of neuronal silence, called interspindle lulls. Although waxing-and-waning spindles typically appear during sleep, a behavioral state in which external signals are obliterated at the thalamic level, this oscillation and its experimental model (augmenting responses) are operational in producing synaptic plasticity, which is expressed by enhancement of neuronal responsiveness during and outlasting spindle sequences (Castro-Alamancos & Connors, 1996; Steriade *et al.*, 1998; Timofeev *et al.* 2002; reviewed in Steriade & Timofeev, 2003).

In the present experiments, we addressed the question of differences in membrane properties and responsiveness of RE neurons during the two, active and silent, states associated with spindle oscillations. Data show that both synaptic and intrinsic responses are increased in RE neurones during the active period of spindles and that bursting discharge is very robust and reliable firing pattern in RE neurones. These changes may be

important for the integrative properties of pacemaking RE neurons during a network operation in which both thalamocortical and corticothalamic neurons are implicated.

METHODS

Preparation

Experiments were performed on adult cats (2.5-3.5 kg), anesthetised with pentobarbital (25 mg/kg, i.p.). When the cats showed the signs of deep anaesthesia, the animals were paralyzed with gallamine triethiodide (20 mg kg^{-1}) and artificially ventilated with control of the end-tidal CO_2 concentration at ~3.5%. The depth of anesthesia was continuously monitored by EEG and additional doses of anesthetic were administered at the slightest tendency toward low-voltage and fast EEG rhythms. Body temperature was maintained at 36-38^{o} C and the heartbeat was monitored and kept constant (acceptable range, 90-110 beats min^{-1}). Glucose saline (5% glucose, 10 ml I.P.) was given every 3-4 hours during the experiments, which lasted for 10 to 12 hours. At the end of experiments, animals were given a lethal dose of pentobarbital (50 mg/kg). All experimental procedures were performed according to national and international guidelines, and were approved by the committee for animal care at Laval University.

Recording and stimulation

Current-clamp intracellular recordings from RE neurones (rostral and rostrolateral sector of the nucleus) were performed using glass micropipettes (DC resistance, 30-60 MΩ). To avoid breaking of recording micropipettes, the cortex and white matter overlying the head of the caudate nucleus were removed by suction. The pipettes entered ~3 mm through the caudate nucleus to reach the thalamic RE nucleus. Pipettes were generally filled with 3 M solution of K-acetate and, in some experiments, with 50 mM of

QX-314. The stability of intracellular recordings was ensured by cisternal drainage, bilateral pneumothorax, hip suspension, and by filling the hole over the thalamus with 4% agar solution. A high-impedance amplifier with active bridge circuitry was used to record and inject current inside the cells. Most intracellular recordings included in the database lasted for periods longer than 30 min.

Electrical stimulation of afferent axons (originating in cortex or in the dorsal thalamus) was performed by descending one or two bipolar stimulating electrodes to the internal capsule (anterior +13, lateral +3.5, depth +1) and applying extracellular current pulses (0.2 ms, 0.2-0.6 mA, 0.33-1 Hz). The recording micropipettes were placed 0.5-1 mm posterior to the stimulation focus.

Data Analysis

All data analysis was performed under Igor Pro 4.0 (Wametrics. Inc.). Values are expressed as mean ± SD, and *t*-tests were used to assess statistical differences when necessary. Differences were considered as significant at $p<0.05$.

RESULTS

Database and neuronal identification

Intracellular recordings from RE neurones were performed in the rostral pole and rostrolateral sector of the nucleus. All cells (n = 25) were identified by the characteristic accelerando-decelerando pattern of their spike-bursts (inset, Fig. 4.1*A*) that occurred during spindle sequences. Resting membrane potentials (V_ms) were more negative than -70 mV in all cases (-76 ± 3.2 mV). At such V_ms, T-current are de-inactivated and RE neurones fire bursts of action potentials (Huguenard & Prince, 1992; Huguenard, 1996). Therefore, all recorded neurones were able to generate spontaneously low-threshold spikes (LTSs) during spindle oscillations occurring in the network. This is the case shown in Fig. 4.1, where a neurone was recorded at a V_m of -78 mV, and produced long spike-bursts (>50 ms; inset in Fig. 4.1*A*) during spindle sequences.

RE neurones during active and silent states of spindle oscillations

Previous intracellular studies of RE neurones *in vivo* have shown that spindle oscillations are widely synchronized through corticothalamic reciprocal pathways (Contreras *et al.* 1996a, 1997). Periods of intracellular activity reflect the synchronous activity of large neuronal populations, especially during sleep or anesthesia (Steriade *et al.* 1993a). During barbiturate anesthesia, a potent spindle-inductor, RE neurones typically displayed active periods consistent of waxing and waning waves with long spike-bursts, alternating with long silent periods (Fig. 4.1*A*), as previously described (Contreras & Steriade, 1996).

Histograms of V_m showed approximately symmetric distribution and a clear single-peak at hyperpolarized values, a sign of dominance of the prolonged, silent states under resting membrane conditions (n = 10; Fig. 4.1*B*). The power spectral densities of intracellular signals were computed in the absence of action potentials (filtered or hyperpolarized) and demonstrated the predominance of low-frequency activities (<10 Hz) in RE neurones. Power spectrum distributions were broadband and behaved as a negative power of frequency, as expected for low-pass filtered noise (Fig. 4.1*B*). However, a small component of spindle frequencies was also present (asterisk, Fig. 4.1*B*). When silent and active periods were separated and their V_m values compared, a large difference of 10-20 mV between active and silent states was evident in intracellular activity (inset, Fig. 4.1*B*).

The major difference was found in membrane fluctuations occurring in the two different, silent and active, states (Fig. 4.1*C*-*D*). In order to determine the degree of membrane fluctuations in intracellular recordings, neurones were initially hyperpolarized by current injection through the pipette to avoid action potential discharge (Fig. 4.1*C*). Even at greatly hyperpolarized levels of V_m (-110 mV) some neurones were occasionally able to generate powerful LTSs, which reached the threshold for spike generation (not shown). In those cases, action potentials were truncated close to the threshold (-50 mV) to avoid overestimation of membrane fluctuations. Comparing the standard deviation (SD) of the V_m during active and silent states it was evident that its variability during active states was almost one order of magnitude higher than during silent periods. In fact, during quiet periods membrane fluctuations reached 1-3 mV, while active periods

showed variations in the order of 10 mV (Fig. 4.1*D*). Powerful LTSs dominate intracellular activity of RE neurones during spindle waves, and they are likely responsible for the large membrane fluctuations since their amplitude was commonly in the order of 10 mV, but could also reach 50 mV (Fig. 4.1*D*). To determine whether background synaptic activity other than LTSs was enhanced during active periods in RE neurones, the first derivative of intracellular recordings was calculated (Fig. 4.1*C*). This way, the contribution of slow signals, as is the case of LTSs, was removed and only fast potentials (action potentials excluded) were evaluated (compare *silent* and *active* in Fig. 4.1*C*). Under such conditions, active periods presented a standard deviation (SD) two-fold compared to silent epochs, suggesting that fast synaptic activity was also enhanced during spindle waves in RE neurones (Fig. 4.1*D*).

In order to calculate the apparent input resistance (R_{in}) of RE neurones in our experimental conditions and to evaluate the impact of V_m on membrane fluctuations, we recorded spontaneous activity of RE neurones held at different values of V_m by injecting steady current (DC) through the recording pipette (n = 4). Intracellular activity was recorded for 2-3 min. for each DC level, and active and silent states were separated. In all cases, the V_m histograms for silent states showed sharp and symmetric normal distributions (Fig. 4.2*A*-*C*). Conversely, active states were characterized by a broad, bimodal distribution at hyperpolarized V_m values, which was abolished during depolarization (Fig. 4.2*A*-*C*). These histogram distributions also allowed detection of larger V_m fluctuations during active states. Plotting the V_m as a function of the steady current injected, a linear relation between the parameters was evident, being the slope of

the linear fittings the R_{in} of RE neurones' membranes (Fig. 4.2*D*). When the average of V_m distributions was used to built the I-V curve, similar values for R_{in} were obtained for silent periods and spindle waves (27.2 ± 4 MΩ and 25.6 ± 5.3 MΩ, for active and silent states, respectively; $p>0.5$, $n = 4$). Nevertheless, when the secondary peak of active states was used for the calculus (asterisks in Fig. 4.2*A*-*B*), a two- to three-fold decrease in R_{in} was observed for active membrane states compared to silent ones (9.7 ± 3.2 MΩ). As shown for resting conditions (Fig. 4.1*D*), membrane fluctuations were one order of magnitude higher during spindle waves than during quiet periods. However, this difference became smaller as neurones were depolarized by positive current injection (Fig. 4.2*E*). On the other hand, membrane fluctuations displayed a minimal dependence on injected current for negative values, remaining practically constant (Fig. 4.2*E*). As depolarization took place, V_m distributions became wider for silent states, though maintaining the same symmetric, sharp appearance (Fig. 4.2*C*). This was correlated with a substantial increase in the coefficient of variation (CV) of the distributions (Fig. 4.2*F*). On the other hand, the CV did change significantly for the distributions of active states (Fig. 4.2*F*).

To estimate the effect of powerful, cyclic LTSs occurring during spindles on R_{in} in RE neurones, LTSs were selected from intracellular recordings performed at different levels of steady current injected through the pipette (Fig. 4.2*G*). Calculation of R_{in} at high time-resolution (20 kHz) showed a strong decrease produced by LTSs during spindle waves. Such a decrease in R_{in} was as high as 80% and lasted for 20-30 ms (Fig. 4.2*H*). This large drop was also very fast since after ~10 ms of LTSs onset the R_{in} fell to 50% of

the original value. At variance, ~50 ms were necessary for the recovery of R_{in} to control levels (Fig. 4.2*H*). Plotting the holding V_m of the recorded neurones against the amplitude of the LTS showed a linear relation between them, and an average reversal potential (V_{rev}) of ~-40 mV (-43.2 ± 3.5 mV, n = 5; Fig. 4.2*I*). Therefore, spindle oscillations produced a discontinuous but cyclic drop in R_{in} of RE neurones, which could not be detected if spindles were considered as a whole event. The drop in R_{in} produced during spindles was clearly due to the potent LTSs.

Impact of network activity on synaptic responsiveness during active states

The above results show that RE neurones display dissimilar cellular properties during different states of network activity. To study how these changes might affect the activity of RE neurones, we stimulated electrically corticothalamic and/or thalamocortical fibers in the internal capsule (n = 6). Stimulation was applied at different intensities to determine the threshold for minimal responses, spike, and spindle generation. In all cases, stimulation intensity was adjusted to elicit short-latency LTSs from resting conditions, generally crowned by spike-bursts (Fig. 4.3*A*-*B*). Stimuli were applied randomly at low frequencies (0.33-1 Hz) and later on sorted depending on the state of neuronal activity. Responses during active network states, e. g. spindle waves, were significantly different from those during silent states, e. g. interspindle lulls. Only stimuli applied within the same range of V_m were considered. Even under such conditions, responsiveness during active states was increased when compared to silent periods. The number of spikes generated by each response was significantly higher during active states when compared to silent states, even though the V_m preceding stimulation was similar (-85.6 ± 2.7 mV

and -81 ± 6.5 mV, for silent and active, respectively; p>0.5; Fig. 4.3*A*-*D*). Not only the number of spikes per response was higher, but also the duration of the action potential response was longer during active network states (Fig. 4.3*C*). Spikes remained up to 20 ms when stimulation was applied during silent states, while action potentials continued up to 40-50 ms during active states (Fig. 4.3*C*). Besides, comparisons between evoked and spontaneous LTSs also showed other differences. During silent states, spontaneous LTSs failed to evoke spikes in ~20% of cases (Fig. 4.3*D*); however, in active network states, LTSs were always crowned by at least one action potential, but in most cases with 4-5 spikes (Fig. 4.3*D*).

Since LTSs are predominant and modulate membrane properties during spindle oscillations, we studied the effect of synaptic activation during different phases of LTSs. Neurons were stimulated from the internal capsule, responses were sorted on the basis of the epoch during which LTSs were elicited (Fig. 4.3*E*-*H*), and compared to spontaneously occurring LTSs (Fig. 4.3*D*). Spontaneously occurring spike-bursts crowned the majority of cycles during spindle oscillations (Fig. 4.3*A*), with a relatively moderate number of spikes per LTS (3.1 ± 2.1, n = 100), which were distributed in a normal way over the duration of LTSs (Fig. 4.3*D*).

When synaptic activation preceded the beginning of a spindle cycle (as in case *2*, Fig. 4.3*A*), a full spike-burst was evoked, with a spike distribution differing from the control (silent state, case *1*), with the majority of action potentials fired early on the LTS (Fig. 4.3*C*, *F*). As stimulation fell during the rising phase of the LTS, no further spiking-

response compared to the spontaneous cases was evident, suggesting the abolition of the effect of synaptic activation (Fig. 4.3*G*). During the peak of the LTS, synaptic activation increased the number of evoked spikes for only a short period (~10 ms, Fig. 4.3*H*). During the decaying phase of the LTS, synaptic activation was powerful enough to generate a new response, with bursting characteristics (Fig. 4.3*I*). Plotting these results in sequence showed the cycle of responsiveness during LTSs in RE neurons (Fig. 4.3*J*). Thus, during the rising phase of the LTS the spiking response is minimal, while it is maximal during the decaying phase of the LTS.

Intrinsic membrane properties during active network states

The increased synaptic responsiveness of RE neurones during the active state with spindle waves could be due to at least two non-exclusive factors: on one hand, a complex network effect operated by the thalamocortical recurrent circuitry and, on the other hand, a change in intrinsic membrane properties of RE neurones. In order to test the latter possibility, positive current pulses were applied through the recording pipette ($n = 5$). The intracellular injection of depolarizing current pulses applied during active states revealed that spindle waves, and the barrages of synaptic activity that underlie them, are associated with a substantial increase in neuronal responsiveness, as quantified by the action potential response (Fig. 4.4*A*). As for the case of synaptic responses, only intrinsic responses obtained during similar V_m values were analyzed for the active and silent states (-70.1 ± 4.9 mV and -74.8 ± 2.2 mV, respectively; $p>0.5$). Current pulses applied during active states were more efficient in triggering action potentials, though similar V_m values were attained (Fig. 4.4*B*-*C*). Accordingly, the latencies for the first evoked spike were

significantly shorter during active membrane states, when compared to silent ones (Fig. 4.4*B*-*C*).

T-current are greatly represented in dendrites of RE neurones, and strongly determine their firing properties (Mulle *et al.* 1986; Huguenard & Prince, 1992; Contreras *et al.* 1993; Destexhe *et al.* 1996; Huguenard, 1996). To test the functional state of these intrinsic currents, prolonged negative current pulses (>100 ms) were applied during intracellular recordings (n = 4) in order to de-inactivate T-current and induce rebound LTSs. Once again, important differences were found between silent and active network states. Current pulses that were subthreshold for LTS generation during silent periods were able to elicit active responses during spindle waves (Fig. 4.4*D*). The higher probability of generating an active response was associated with an increased number of spikes in the response (Fig. 4.4*E*-*F*).

Next, membrane properties of RE neurones were assessed by injecting a sinusoidal waveform current through the pipette (n = 3). Under such conditions, action potential responses were considerably increased during active network states. During silent states, the intracellular injection of the sine wave yielded no or maximum one action potential (case *2* in Fig. 4.5*A*-*B*). However, during active states, action potentials were generated throughout a greater extent of the depolarizing phase (case *1* in Fig. 4.5*A*-*B*), resulting in a better representation of the amplitude-time course of the sine wave input by the action potential discharge (Fig. 4.5*C*). This was related to a large increase in the CV during active states (~150%). We injected sinusoidal waves of different frequencies

and constant amplitude in RE cells. The same results were consistently found for most frequencies examined, as both the number of evoked spikes per cycle and the probability of triggering and action potential were higher during spindle waves compared to silent periods (Fig. 4.5*D*-*E*). RE neurons did not display any kind of frequency tuning or preferred frequency for discharge. Instead, they behaved as common low-pass band filters. Accordingly, the probability of spike discharge was severely decreased for high frequencies (>10 Hz) during the silent states (Fig. 4.5*E*)

Low-pass filter properties of cellular membranes in RE neurones

Due to their molecular properties, plasmatic membranes of most neurones in the nervous systems act as low-pass filters (Rall, 1995). The power spectral densities showed above confirmed that RE neurones act as low-pass filters. To go further, the filtering properties of RE neurones were studied by passing through the pipette sinusoidal waves of different frequencies (1-40 Hz) at constant amplitude (1 nA peak-to-peak) (Fig. 4.6*A*). Only traces from silent periods were analyzed to avoid any contamination effect of active responses (such as action potentials). The relation between the input current and the membrane response was quantified by cross-correlations between the injected sine wave current and the intracellular recorded neurone (Fig. 4.6*B*). Peak cross-correlations and time-shifts were then compared for the studied frequencies. Both of these parameters showed a frequency-dependent decrease (Fig. 4.6*C*). Thus, the amplitude of membrane responses was strongly attenuated as frequency increased, reaching 50% attenuation at 10 Hz (Fig. 4.6*D*), the main component of spindle oscillations. We also calculated the slopes of the rising and decaying phases of the signals and plotted as function of the frequency

of the injected sinusoidal current (Fig. 4.6*E-F*). This procedure demonstrated that, while the rate of the input increased linearly, the rate of the output followed an exponential kinetics, showing saturation for high frequencies (>10 Hz); this was the case for both rising and decaying phases of the signals (Fig. 4.6*E-F*). Therefore, the attenuation observed in the transfer of signals in RE neurones' membranes was related to their limited capacity to follow signals at high frequencies (>10 Hz). The same procedure was applied to investigate membrane responses during active network states. Though the same general kinetic behaviour was found, i.e. exponential, active states presented rates slightly faster (by ~10%) at high frequencies (>10 Hz) for both rising and decaying phases (not shown).

Responses of RE neurones to sinusoidal waves of different amplitudes (0.5-1.5 nA peak-to-peak) were then studied, and compared for the silent and active network states (Fig. 4.7*A-C*). The frequency of sinusoidal injected current was fixed at a value of 10 Hz, given that this corresponds to 50% attenuation of signal transfer in RE neurones. By examining the response of RE neurones to sine waves of different amplitudes it became evident that active states were associated with a higher excitability, owing to a decrease in the amount of current needed to elicit action potentials (Fig. 4.7*D*). This difference did not reside in different passive membrane responses, since membrane deflections produced during active states were slightly, though not significantly, smaller than those occurring during silent states (Fig. 4.7*E*). An additional effect of the active state on the membrane response to sinusoidal wave currents was a shift in the cross-correlation peak to earlier times, a phase advance; for all sine wave amplitudes it was

seen higher correlation between injected sine wave current and intracellular recordings during silent states (Fig. 4.7*F*-*G*).

Bursting properties of RE neurones

During spindle oscillation, LTSs generated by T-current dominate the firing pattern of RE neurones. Given the significance of such events for the functional properties of RE neurones, we studied their modulation during spindle oscillations. Spontaneously occurring spindles were recorded in RE neurones held at different levels of V_m by injecting current through the recording pipette (n = 8) (Fig. 4.8). At resting conditions, RE neurones displayed recurrent spike-bursts, at a frequency of ~10 Hz, each burst being composed by 2-6 spikes (Fig. 4.8*A*). The quantification of time-relations between yielded action potentials showed a clear-cut peak at short inter-spike intervals (~6 ms), showing that discharge activity occurred into the bursting mode (Fig. 4.8*A*-*C*). Autocorrelograms for actions potentials showed oscillatory behavior for the neurones held at resting V_m, with secondary peaks at ~±110 ms, typical of spindle waves (10-14 Hz). As negative current was injected through the pipette and the recorded neurones were hyperpolarized, similar behavior was observed, except for an increase in the degree of autocorrelation (not shown). As neurones were depolarized by positive current injection, the discharge pattern started to change: although spike-bursts were still distinguished, single spikes appeared afterwards (Fig. 4.8*B*). As depolarization was enhanced, more and more tonic spikes were evident, but bursting discharges could still be detected and interspike intervals displayed two, discrete peaks: one for bursting discharges (~6 ms) and another for tonic spikes (~25 ms) (Fig. 4.8*C*). Plotting the current passed through the

pipette against the frequency of discharges showed that intra-burst frequencies were quite constant for the whole tested range of injected current, proving bursting discharges to be a very robust intrinsic property of RE neurones (Fig. 4.8*D*). At variance, tonic action potentials appeared only at resting conditions, and their frequency increased linearly as depolarization was enhanced (Fig. 4.8*D*). To quantify the oscillatory behavior of RE neurones at different levels of injected current, a "rhythmicity index" was defined as the peak-to-peak amplitude adjacent to the central peak of the autocorrelogram for action potentials; the index thus ranges from 0 (non-rhythmic) to 1 (perfectly rhythmic). Rhythmic discharge of action potentials in RE neurones was evident at hyperpolarized membrane states, decreasing rapidly with depolarization. At positive values of injected current, rhythmicity fell near to zero (Fig. 4.8*E*). This behavior was related to the emergence of tonic action potentials with depolarization, which quickly increased as positive currents were injected.

DISCUSSION

The results of this study demonstrate that membrane properties of neurones in the RE nucleus, are modulated by spindle waves, a network oscillatory activity generated in the same nucleus, but maintained by complex cortico-thalamo-cortical interactions (Steriade et al., 1997). The main findings of the present work are as follows: *(a)* basic membrane properties of RE neurones are affected during active network states, such as spindle waves; *(b)* both synaptic and intrinsic responsiveness are increased in RE neurones during spindles; *(c)* active responses, including firing of action potentials, but not passive membrane responses, are increased during spindle oscillations; and *(d)* bursting discharge is very robust and reliable firing pattern in RE neurones.

The present experiments have shown that spindle oscillations modulate basic membrane properties of RE neurones during spindle waves, including: average depolarization of V_m (10-20 mV), increased membrane fluctuations (1-3 mV to 10 mV), and decreased R_{in} (up to 80%). All these were mainly due to the sequential activation of powerful LTSs. Membrane fluctuations were increased by almost one order of magnitude during spindle waves. However, this effect was not entirely due to LTSs occurring during spindles, since fast activities, such as EPSPs and spikelets (Kim *et al.* 1997; Landisman *et al.* 2002; Fuentealba *et al.* 2004), were also enhanced.

Synaptic background activity is able to affect the responses to synaptic inputs. This has been studied in the cortex with computational models (Ho & Destexhe, 2000;

Destexhe *et al.* 2001; Fellous *et al.* 2003), through the generation of different artificial states of background noise *in vitro* (Stacey & Durand, 2001; McCormick *et al.* 2003; Mitchell & Silver 2003), and through the activation of synaptic potentials or local suppression of network activity *in vivo* (Timofeev *et al.* 1996; Destexhe & Paré, 1999). These studies showed that membrane depolarization and small to moderate membrane fluctuations may facilitate the responsiveness to synaptic inputs, especially those of low amplitude. Here, we have showed that volleys of synaptic activity can result in significant changes in neuronal excitability and responsiveness in RE neurones.

Spindle waves are thalamically generated and synchronized by complex network operations, including cortical inputs (Contreras & Steriade, 1996; Contreras *et al.* 1996a). Although spindle rhythms are almost simultaneous in different thalamocortical systems (Contreras *et al.* 1997), it has been shown that not all neocortical neurones follow faithfully spindle oscillations, most notably intrinsically-bursting neurones (Steriade *et al.* 1993b). Moreover, RE neurones receive most of their synaptic inputs from cortex, which contributes with up to 70% of the inputs to RE neurones (Liu & Jones, 1999), and dorsal thalamus. Therefore, it is likely that during spindle oscillations in thalamocortical networks, RE neurones are not only receiving phase-locked, powerful, rebound bursts from thalamocortical neurones, but also an important fraction of inputs from cortical neurones which arrive out of phase and generate a state of increased synaptic background activity. RE neurones are also coupled by gap junctions (Landisman *et al.* 2002). These membrane proteins generate electrical continuity between coupled cells and therefore might also play a role in enhancing synaptic background during active network states,

such as spindle oscillations (Fuentealba *et al.* 2004a; Long *et al.*, 2004). Changes in membrane fluctuations will not only affect the number of action potentials, but also their timing. In fact, the average histogram of the spike response is more representative of the amplitude and time course of the sine wave currents injected.

During periods of irregular fast EEG activity, as seen during the active state of ketamine-xylazine anesthesia (depolarizing phase of the slow oscillation), neocortical neurones display depolarized values of V_m, low input resistance, experience continuous membrane fluctuations, and fire spontaneously at rest (Steriade *et al.* 1993b; Contreras *et al.* 1996b). This condition has been referred as a "high-conductance state" of cortical networks (Destexhe *et al.* 2003); however, natural wakefulness is associated with stable and high input resistance of cortical neurons because of the action of activating neuromodulators (Steriade *et al.* 2001). *In vitro* studies as well as computational models have provided evidence that networks of cortical neurones are able to generate and sustain prolonged periods of activity, and such network activity may influence the responsiveness of single cortical cells to arriving inputs (Destexhe *et al.* 2003). In contrast to ketamine-xylazine, barbiturate anesthesia produces a state of reduced cortical activity in which cortical neurones fire at very low rates. Conductance analyses show that barbiturates induce a state of lower global conductance compared with ketamine-xylazine and waking states. Our present results suggest that, in contrast to cortical networks, spindle waves induced by barbiturates represent an active network, high conductance state in the RE nucleus. Actually, spindle oscillations are associated with an average membrane depolarization, increased membrane fluctuations, and decreased R_{in} in RE

neurones. Then, spindles should not to be compared with cortical high conductance states, since many differences are to be mentioned; among them, the temporal discontinuity of changes during spindles. Another disparity is that active network states in the cortex are generated by both excitatory and inhibitory interacting conductances; in contrast, spindle waves in RE neurones have the form of powerful depolarizing LTSs, which are activated at hyperpolarized values of V_m (<-65 mV) (Gentet & Ulrich, 2003), either by excitatory or reversed inhibitory inputs (Bazhenov *et al.*, 1999).

Active network states, such as spindles in RE neurons, imply a series of consequences for integrative properties of neurones. One of them is that responsiveness of neurones is markedly different in the presence of fluctuating background synaptic activity. Due to the presence of membrane potential fluctuations, cortical neurones respond stochastically to a given stimulus, and their behavior is best described by probability functions (Ho & Destexhe, 2000). Another effect of active network states is on temporal processing. The reduction of the space constant in states of high conductance is accompanied by a marked reduction in the membrane time constant (Destexhe *et al.* 2003). In our experimental data active responses were also faster to injected positive current pulses. The reduced time constant should favor finer temporal discrimination of distant synaptic inputs. Modeling studies have predicted that cortical neurones can resolve higher frequency inputs in active membrane states than when silent (Destexhe *et al.* 2003). It is expected that a similar case might be found in RE neurones, though evidence should be provided by future experiments.

The volleys of synaptic activity that underlie spindle waves were associated with multiple changes in RE neurones which were mostly due to the activation of LTSs. Thus, our results suggest that regulation of T-current is a fundamental element in the modulation of responsiveness in RE neurones. The bursting mode of RE neurones, which is closely linked to LTS generation, proved to be very consistent and faithful for a wide range of V_m conditions. In fact, bursts of action potentials displayed practically the same frequency, while tonic spikes showed a clear dependence on the injected current.

REFERENCES

Bazhenov M, Timofeev I, Steriade M & Sejnowski TJ. (1999). Self-sustained rhythmic activity in the thalamic reticular nucleus mediated by depolarizing $GABA_A$ receptor potentials. *Nat Neurosci* **2,** 168-174.

Castro-Alamancos, M.A. & Connors, B.W. (1996) Cellular mechanisms of the augmenting response: short-term plasticity in a thalamocortical pathway. *J Neurosci* **16**, 7742-7756.

Contreras D, Curró Dossi R & Steriade M. (1993). Electrophysiological properties of cat reticular thalamic neurones in vivo. *J Physiol* **470,** 273-294.

Contreras D & Steriade M. (1996). Spindle oscillation in cats: the role of corticothalamic feedback in a thalamically generated rhythm. *J Physiol* **490,** 159-179.

Contreras D, Destexhe A, Sejnowski TJ & Steriade M. (1996a) Control of spatiotemporal coherence of a thalamic oscillation by corticothalamic feedback. *Science* **274**, 771-774.

Contreras D, Timofeev I & Steriade M (1996b) Mechanisms of long-lasting hyperpolarizations underlying slow sleep oscillations in cat corticothalamic networks. *J Physiol* **494**, 251-264.

Contreras D, Destexhe A, Sejnowski TJ & Steriade M. (1997). Spatiotemporal patterns of spindle oscillations in cortex and thalamus. *J Neurosci* **17,** 1179-1196.

Destexhe A, Contreras D, Steriade M, Sejnowski TJ & Huguenard JR. (1996). *In vivo*, *in vitro*, and computational analysis of dendritic calcium currents in thalamic reticular neurons. *J Neurosci* **16,** 169-185.

Destexhe A & Paré D. (1999). Impact of network activity on the integrative properties of neocortical pyramidal neurons in vivo. *J Neurophysiol* **81,** 1531-1547.

Destexhe A, Rudolph M, Fellous JM & Sejnowski TJ. (2001). Fluctuating synaptic conductances recreate in vivo-like activity in neocortical neurons. *Neuroscience* **107,** 13-24.

Destexhe A, Rudolph M & Paré D. (2003). The high-conductance state of neocortical neurons in vivo. *Nat Rev Neurosci* **4,** 739-751.

Fellous JM, Rudolph M, Destexhe A & Sejnowski TJ. (2003). Synaptic background noise controls the input/output characteristics of single cells in an in vitro model of in vivo activity. *Neuroscience* **122,** 811-829.

Fuentealba P, Crochet S, Timofeev I, Bazhenov M, Sejnowski TJ & Steriade M (2004a). Experimental evidence and modeling studies support a synchronizing role for electrical coupling in the cat thalamic reticular nucleus *in vivo*. *Eur J Neurosci*, in press.

Fuentealba P, Timofeev I & Steriade M (2004b). Prolonged hyperpolarizing potentials precede spindle oscillations in the thalamic reticular nucleus. *Proc Natl Acad Sci USA*, in press.

Gentet LJ & Ulrich D. (2003). Strong, reliable and precise synaptic connections between thalamic relay cells and neurones of the nucleus reticularis in juvenile rats. *J Physiol* **546,** 801-811.

Ho N & Destexhe A. (2000). Synaptic background activity enhances the responsiveness of neocortical pyramidal neurons. *J Neurophysiol* **84,** 1488-1496.

Huguenard JR & Prince DA. (1992). A novel T-type current underlies prolonged Ca^{2+}-dependent burst firing in GABAergic neurons of rat thalamic reticular nucleus. *J Neurosci* **12,** 3804-3817.

Huguenard JR. (1996). Low-threshold calcium currents in central nervous system neurons. *Annu Rev Physiol* **58,** 329-348.

Kim U, Sanchez-Vives MV & McCormick DA. (1997). Functional dynamics of GABAergic inhibition in the thalamus. *Science* **278,** 130-134.

Landisman CE, Long MA, Beierlein M, Deans MR, Paul DL & Connors BW. (2002). Electrical synapses in the thalamic reticular nucleus. *J Neurosci* **22,** 1002-1009.

Liu XB & Jones EG. (1999). Predominance of corticothalamic synaptic inputs to thalamic reticular nucleus neurons in the rat. *J Comp Neurol* **414,** 67-79.

Long MA, Landisman CE & Connors BW. (2004). Small clusters of electrically coupled neurons generate synchronous rhythms in the thalamic reticular nucleus. *J Neurosci* **24,** 341-349.

McCormick DA, Shu Y, Hasenstaub A, Sanchez-Vives M, Badoual M & Bal T. (2003). Persistent cortical activity: mechanisms of generation and effects on neuronal excitability. *Cereb Cortex* **13,** 1219-1231.

Mitchell SJ & Silver RA. (2003). Shunting inhibition modulates neuronal gain during synaptic excitation. *Neuron* **38,** 433-445.

Mulle C, Madariaga A & Deschênes M. (1986). Morphology and electrophysiological properties of reticularis thalami neurons in cat: in vivo study of a thalamic pacemaker. *J Neurosci* **6,** 2134-2145.

Rall W. (1995). *The Theoretical Foundation of Dendritic Function*. MIT Press, MA.

Stacey WC & Durand DM. (2001). Synaptic noise improves detection of subthreshold signals in hippocampal CA1 neurons. *J Neurophysiol* **86,** 1104-1112.

Steriade M, Domich L & Oakson G. (1986). Reticularis thalami neurons revisited: activity changes during shifts in states of vigilance. *J Neurosci* **6,** 68-81.

Steriade M, Domich L, Oakson G & Deschênes M (1987). The deafferented reticularis thalami nucleus generates spindle rhythmicity. *J Neurophysiol* **57**, 260-273.

Steriade M, Contreras D, Curró Dossi R & Nuñez A. (1993a). The slow (< 1 Hz) oscillation in reticular thalamic and thalamocortical neurons: scenario of sleep rhythm generation in interacting thalamic and neocortical networks. *J Neurosci* **13,** 3284-3299.

Steriade M, Nuñez A & Amzica F. (1993b). Intracellular analysis of relations between the slow (<1 Hz) neocortical oscillation and other sleep rhythms of the electroencephalogram. *J Neurosci* **13,** 3266-3283.

Steriade M, Jones EG & McCormick DA. (1997). *Thalamus*, vol. 1. Elsevier Science Ltd., Oxford.

Steriade M & Timofeev I (2003). Neuronal plasticity in thalamocortical networks during sleep and waking oscillations. *Neuron* **37**, 563-576.

Steriade M, Timofeev I, Grenier F & Dürmüller N (1998). Role of thalamic and cortical neurons in augmenting responses: dual intracellular recordings *in vivo*. *J Neurosci* **18**, 6425-6443.

Steriade M, Timofeev I & Grenier F. (2001). Natural waking and sleep states: a view from inside neocortical neurons. *J Neurophysiol* **85,** 1969-1985.

Timofeev I, Contreras D & Steriade M. (1996). Synaptic responsiveness of cortical and thalamic neurones during various phases of slow sleep oscillation in cat. *J Physiol* **494,** 265-278.

Timofeev I, Grenier F, Bazhenov M, Houweling AR, Sejnowski TJ & Steriade M (2002). Short- and medium-term plasticity associated with augmenting responses in cortical slabs and spindles in intact cortex of cats *in vivo*. *J Physiol* **542**, 583-598.

FIGURES

Figure 4.1. Silent and active states in RE neurones during spindle oscillations

A, a neurone recorded at rest in the rostral pole of the RE nucleus. Note alternate states of spike-bursts activity (active) and quiescence (silent) characteristic of spindle waves. Inset, typical burst of action potentials displaying accelerando-decelerando pattern. B, histogram of V_m distribution (left) and power spectral density (right) for the previous neurone. Inset, average (n = 20 periods) value of V_m for silent and active periods. Spikes were truncated close to the threshold (~-50 mV) to build up the histogram and calculate average V_m. Thick grey line in power spectrum represents the best fitting to high frequencies (>10 Hz) with a power law (f^k, k≈2.9); asterisk points to a bump at 10 Hz, due to spindle oscillations. Data points are collected from an intracellular recording of 3 min. at resting conditions. Binsize 0.2 mV and 0.25 Hz, for histogram and power spectrum, respectively. C, left, period of spindle waves in the same RE neurone as A, but hyperpolarized by negative current injection (-1 nA) to avoid action potential discharge. Below, derivative of the previous period. Silent and active indicate episodes expanded in middle and right panels, respectively. Dotted lines in derivative traces indicate 0 mV. D, standard deviation (SD) of the membrane potential for the intracellular recording (left) and its derivative (middle) across different states of activity. Points represent mean ± SD over 20 periods. Right, distribution of amplitudes of LTSs (n = 200). Note the presence of large-amplitude LTSs (~50 mV). Binsize 5 mV.

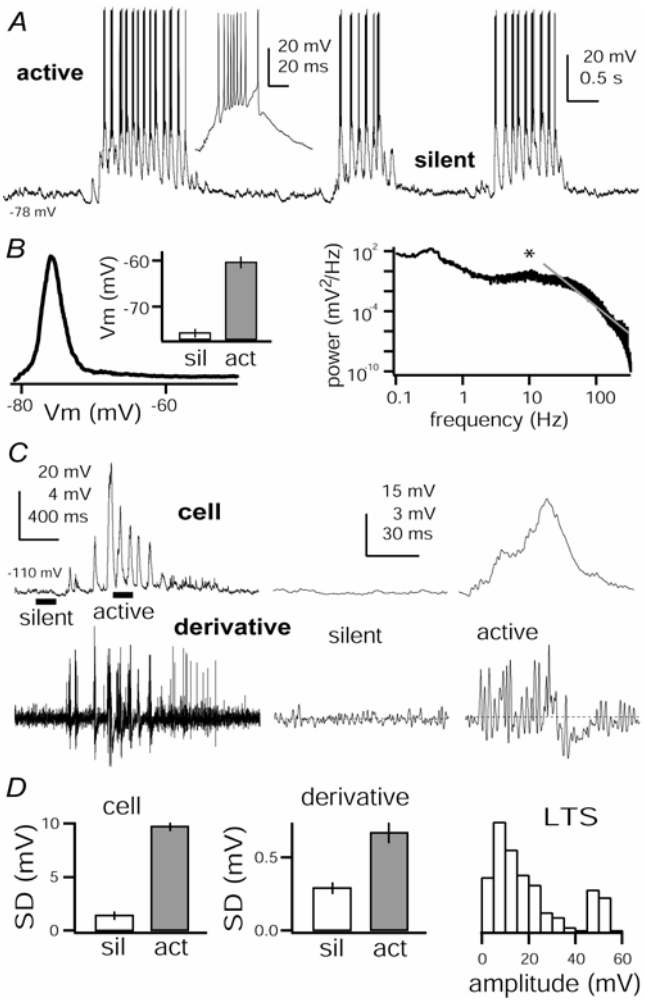
A
active
20 mV
20 ms
20 mV
0.5 s
silent
-78 mV
B
Vm (mV)
-60
-70
sil
act
-80
Vm (mV)
-60
power (mV²/Hz)
10²
10⁴
10¹⁰
*
0.1
1
10
100
frequency (Hz)
C
20 mV
4 mV
400 ms
cell
15 mV
3 mV
30 ms
-110 mV
silent
active
derivative
silent
active
D
cell
SD (mV)
10
5
0
sil
act
derivative
SD (mV)
0.5
0.0
sil
act
LTS
0
20
40
60
amplitude (mV)

Figure 4.2. Changes in R_{in} and synaptic background during spindle oscillations

A-C, a RE neurone recorded at different levels of V_m by steady current (DC) injection through the pipette. Left column shows periods of intracellular activity during spindle waves and right column displays cumulative histograms of V_m distribution for active (thick line) and silent (grey area) periods (n = 30) of intracellular activity. Asterisks point to secondary peaks during active states. Spikes were truncated close to the threshold (~-50 mV) to build up histograms. Each DC level was recorded during 1-2 min. Binsize 0.2 mV. D, summary plot for the V_m dependency on the injected current (DC). V_m was measured as the peak of the normal distribution for the silent periods (empty circles). For the active periods it was used the secondary peak (asterisks) and the total average (filled circles). Solid and dotted lines represent linear fittings ($r>0.9$) for the three sets of points used. Slopes of linear fittings represent the apparent input resistance (R_{in}) for each condition: 31.6 ± 1.5 MΩ in silent states (empty circles), 29.0 ± 2.8 MΩ and 14.3 ± 3.2 MΩ for active states (measured as the average or the secondary peak, filled circles and asterisks, respectively). E, summary plot for the membrane fluctuations (SD) dependency on the injected current (DC). Membrane fluctuations were measured as the standard deviation during silent (empty circles) and active (filled circles) periods. Points represent mean ± SD over 30 periods. F, summary plot for the coefficient of variation (CV) dependency on the injected current (DC). CV was measured as the SD-to-mean ratio. G, averages (n =10) of LTSs occurring during spindle waves recorded at different DC levels. Action potentials were truncated in single traces. H, time-course of changes in R_{in} during LTSs. Each point represents the linear fitting to the I-V curve for LTSs presented in F and other three DC levels. Binsize 0.05 ms. I, reversal potential (V_{rev}) for LTSs presented

in H calculated as the intersection of the linear fitting with the abscise axis. V_{rev} = -40.3 mV.

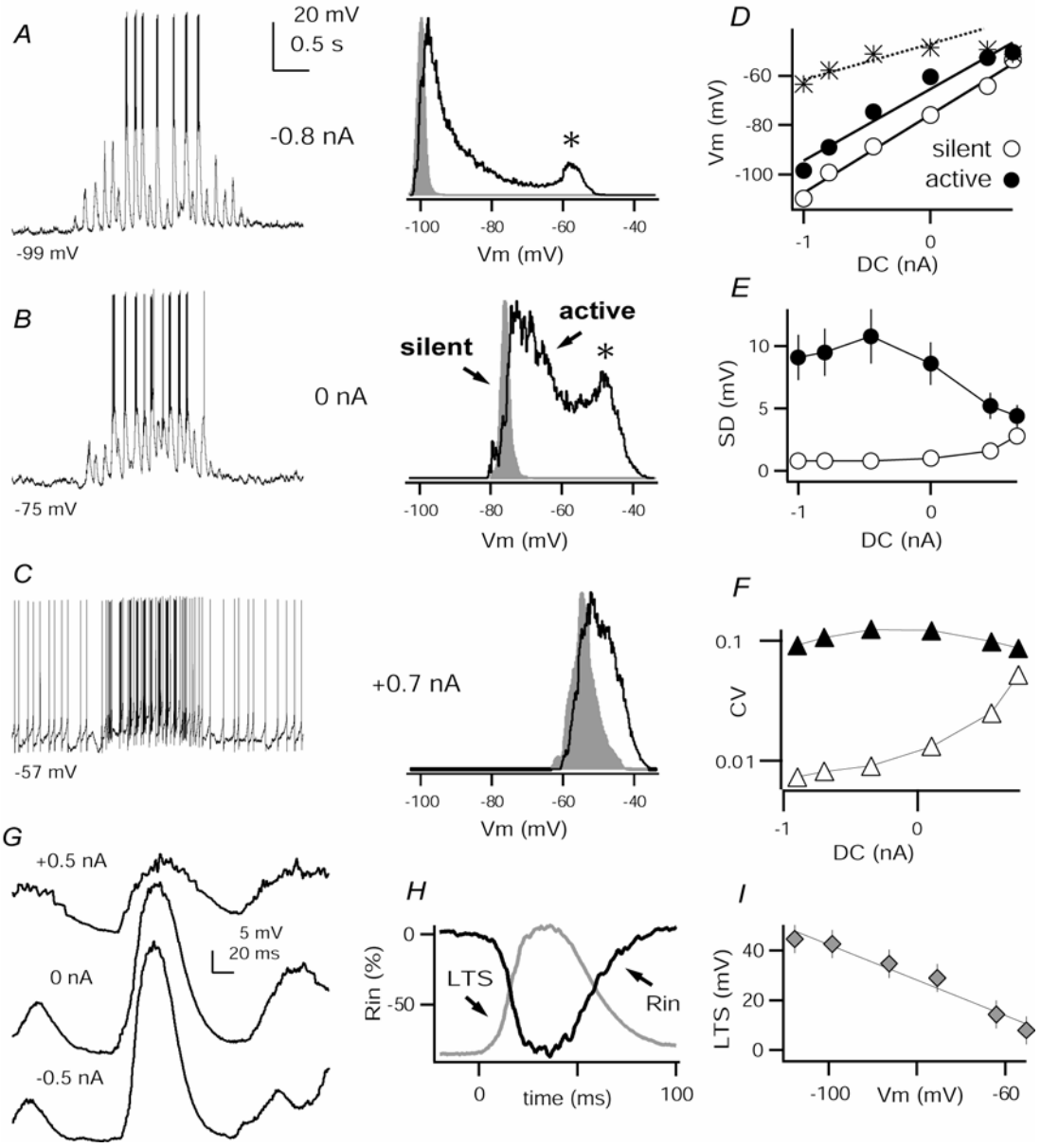
A
20 mV
0.5 s
-0.8 nA
-99 mV
B
0 nA
-75 mV
C
-57 mV
+0.7 nA
Vm (mV)
silent
active
D
Vm (mV)
silent
active
DC (nA)
E
SD (mV)
DC (nA)
F
CV
DC (nA)
G
+0.5 nA
5 mV
20 ms
0 nA
-0.5 nA
H
Rin (%)
LTS
Rin
time (ms)
I
LTS (mV)
Vm (mV)

Figure 4.3. Synaptic responsiveness is increased during spindle waves

A, a RE neurone recorded at rest as stimuli were applied to internal capsule (0.5 Hz). Two stimuli applied to internal capsule during silent (1) and active (2) states. B, responses from previous neurone to stimuli applied at different network states. C, plots for the number of action potentials per burst (top) and the cumulative probability of peri-stimulus intervals (bottom) during different network states. Binsize 1 ms. * $p<0.05$. D, histograms for the distributions of number of action potentials per LTS (spikes), occurring either spontaneously (spontaneous) or evoked (silent and active). Gray bars indicate cases were no action potential took place (20% and 22%, for spontaneous and silent; respectively), and arrowheads point to the mean value for each distribution (spontaneous, 2.5; silent, 1.9; active, 4.5). Histograms were built from 50 LTSs each. E, overlay of spontaneous LTSs (top, n = 3) and spike count (bottom, n = 10). Binsize 10 ms. F-I, effect of corticothalamic stimulation during different epochs of the LTS: rest (F), rising phase (G), peak (H), and decaying phase (I). Intracellular recordings and spike counts as in E. The value of V_m when stimulation was applied is indicated at left in each case. J, summary plot for the effect of synaptic activation at different periods of the LTS. Solid bottom line represents the envelope of the averaged spontaneous LTSs (n = 100), while superimposed empty squares indicate the average V_m (n = 10) when stimulation was applied. Note decaying and rising phases to display similar values of V_m. The number of evoked spikes was calculated as the difference between LTSs during synaptic activation (F-I) and spontaneous ones (E). The coefficient of variation (CV) is expressed as the percentage of the CV for spontaneous LTSs.

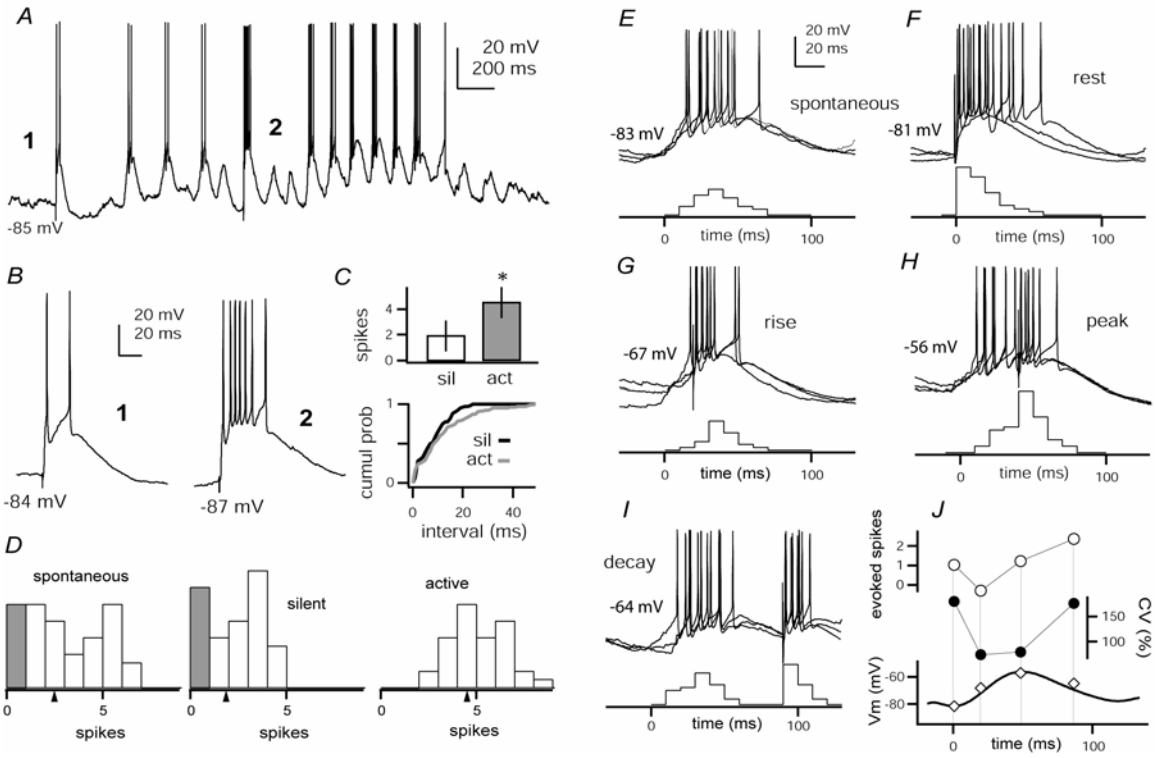
A
20 mV
200 ms
1
2
-85 mV
B
20 mV
20 ms
1
2
-84 mV
-87 mV
C
*
spikes
4
2
0
sil
act
cumul prob
1
0
sil
act
0
20
40
interval (ms)
D
spontaneous
silent
active
0
5
spikes
E
20 mV
20 ms
spontaneous
-83 mV
0
time (ms)
100
F
rest
-81 mV
G
rise
-67 mV
H
peak
-56 mV
I
decay
-64 mV
J
evoked spikes
2
1
0
150
100
CV (%)
Vm (mV)
-60
-80

Figure 4.4. Responses to current pulses are enhanced during spindle oscillations

A, a RE neurone from the rostral pole recorded at rest. Positive current pulses (+1 nA, 100 ms) were applied during both silent and active membrane states. B, responses from previous neurone to current pulses applied at different network states. C, plots for the number of action potentials per pulse (top) and the latency of the first spike (bottom) during different network states, calculated over 15 current pulses for each state. D, another RE neurone from the rostral pole recorded at rest. Negative current pulses (-1 nA, 200 ms) were applied during both silent and active membrane states. E, responses from previous neurone to current pulses applied at different network states. F, plots for the number of action potentials per rebound burst (top) and probability of triggering a rebound-burst (bottom) during different network states. Calculated over 20 current pulses for each state. * $p<0.05$.

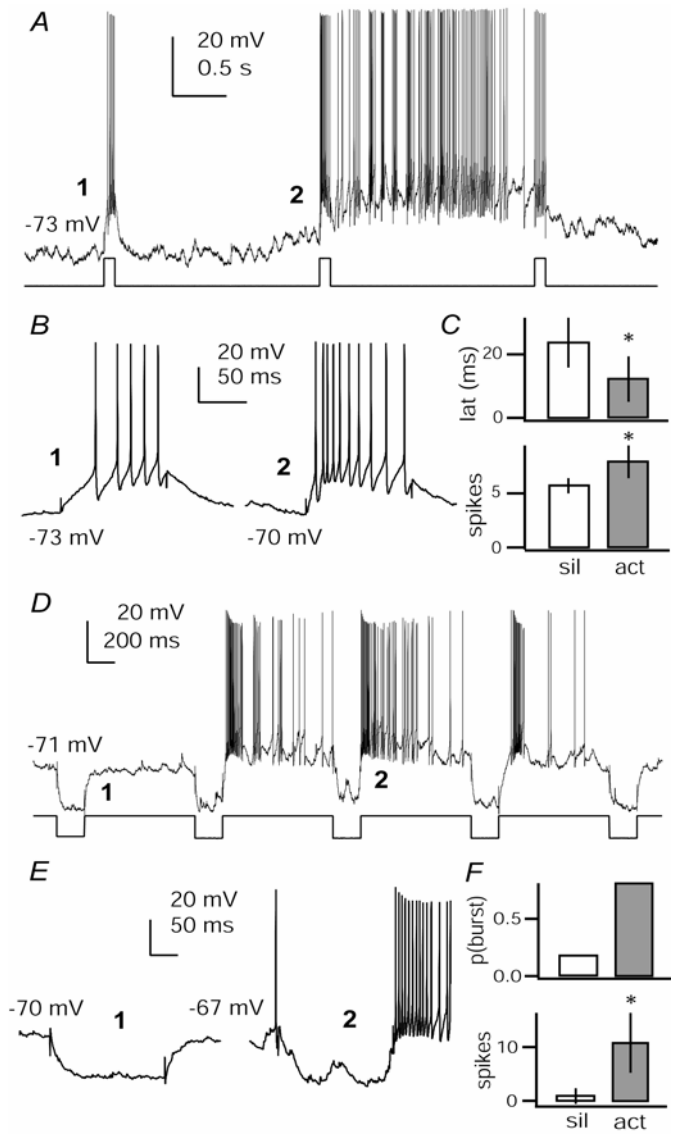
A
20 mV
0.5 s
1
2
-73 mV
B
20 mV
50 ms
1
2
-73 mV
-70 mV
C
lat (ms)
20
0
*
spikes
5
0
*
sil
act
D
20 mV
200 ms
-71 mV
1
2
E
20 mV
50 ms
-70 mV
1
-67 mV
2
F
p(burst)
0.5
0.0
spikes
10
0
*
sil
act

Figure 4.5. Responses to sinusoidal current waves are enhanced during spindle oscillations

A, a RE neurone from the rostral pole recorded at rest while sinewave current is injected through the pipette (1 nA peak-to-peak, 10 Hz). B, responses from previous neurone to current cycles during different network states. C, the plot shows the peri-stimulus histogram of the action potential response to the sinewave injection during different membrane states (n = 100 cycles). The coefficient of variation was increased from 2.6 to 4.0. Binsize 1 ms. D-E, plots for the number of action potentials per cycle (D) and the probability of triggering a spike (E) as function of the frequency of the sinusoidal wave injected. In D points are presented as mean ± SD of measurements (n=50-500 cycles). Probability of action potential was calculated as the fraction of cycles where at least one action potential was present.

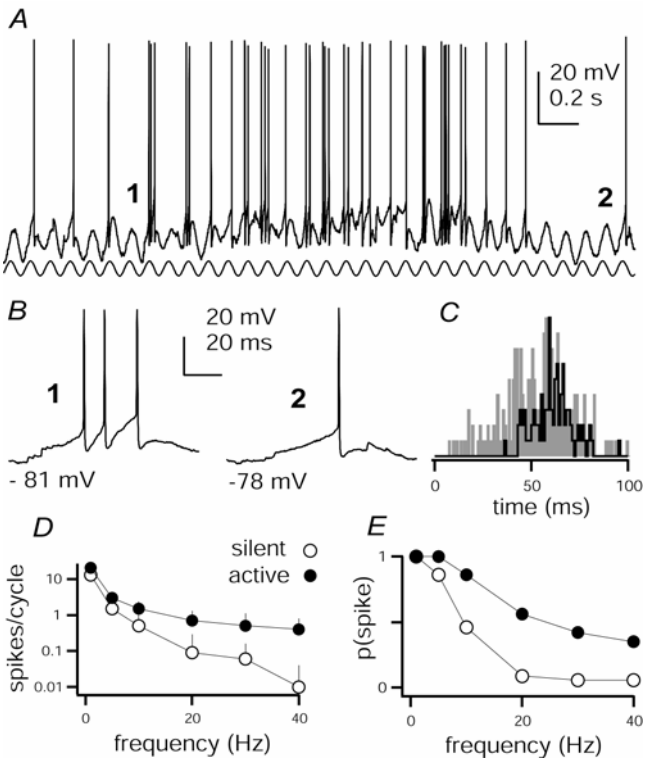
A
20 mV
0.2 s
1
2
B
20 mV
20 ms
1
2
- 81 mV
-78 mV
C
0
50
100
time (ms)
D
silent
active
spikes/cycle
10
1
0.1
0.01
0
20
40
frequency (Hz)
E
p(spike)
1
0
0
20
40
frequency (Hz)

Figure 4.6. Frequency dependence of signal transfer in RE neurones

A, Membrane responses from a RE neurone during silent states (top trace) to sinewave current injection (1 nA peak-to-peak) at two different frequencies (bottom trace). B, Cross-correlation for the two pairs of signals presented previously, for a period of 30 s. Binsize 1 ms. C, peak cross-correlations and phase shifts in membrane responses as a function of sinewave current injected. D, Normalized attenuation of sinusoidal signals across RE membranes as a function of signal frequency. Attenuation was defined as the ratio of peak-to-peak amplitude in membrane responses, normalized to the 1 Hz attenuation and expressed as percentage. E-F, slopes of signals as a function of frequency, for the rising (E) and decaying (F) phases of the injected current (filled triangles, input) and voltage passive responses (empty triangles, output). Slopes of injected current (input) were best fitted with linear functions ($r = 0.99$), while those of voltage responses (output) with exponential functions ($\chi^2 = 0.001$). Note output slope to saturate at high frequencies (>10 Hz). Insets, slopes were calculated as the maximum in the derivative of the best sigmoid fitting to the signal. Scale in E-F, nA/ms and mV/ms, for input and output; respectively. Data points are mean ± SD of measurements from 100 cycles.

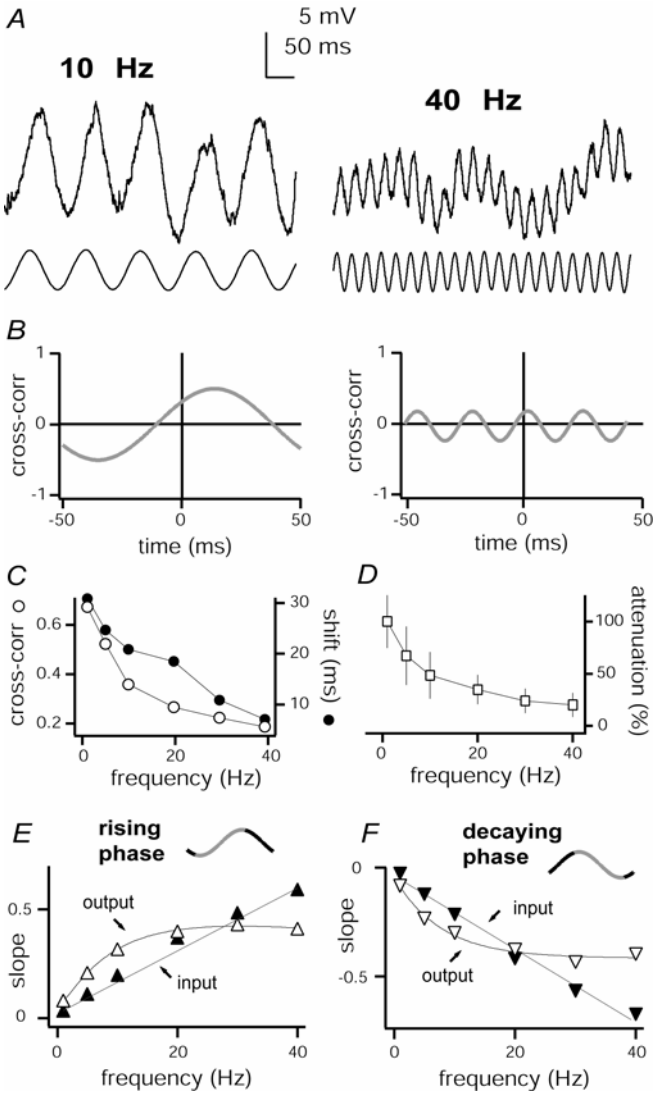
A
5 mV
50 ms
10 Hz
40 Hz
B
cross-corr
time (ms)
C
cross-corr o
shift (ms) •
frequency (Hz)
D
attenuation (%)
frequency (Hz)
E
rising phase
output
input
slope
frequency (Hz)
F
decaying phase
input
output
slope
frequency (Hz)

Figure 4.7. Amplitude dependence of membrane responses in RE neurones

A-C, membrane responses from a RE cell during different network states to sinewave current injection (10 Hz) of different amplitudes. A, 0.5 nA; B, 0.75 nA; C, 1.5 nA. D-E, plots for the probability of action potential generation (D) and response amplitude (E) as a function of sinewave current amplitude. In E points are presented as mean ± SD of measurements. F-G, plots for the peak cross-correlation (F) and phase-shift (G) as a function of sinewave current amplitude. Black and white symbols represent active and silent network states, respectively. All data points are extracted from 100 cycles.

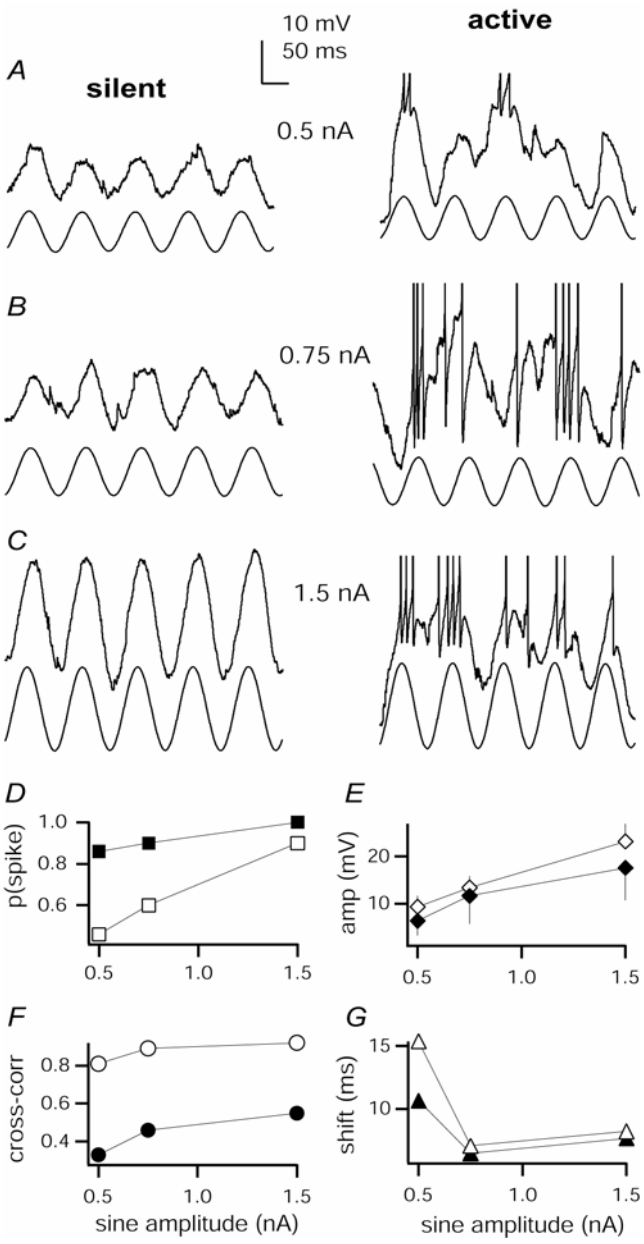
A
silent
10 mV
50 ms
active
0.5 nA
B
0.75 nA
C
1.5 nA
D
p(spike)
1.0
0.8
0.6
0.5
1.0
1.5
E
amp (mV)
20
10
0.5
1.0
1.5
F
cross-corr
0.8
0.6
0.4
0.5
1.0
1.5
sine amplitude (nA)
G
shift (ms)
15
10
0.5
1.0
1.5
sine amplitude (nA)

Figure 4.8. Spike-bursts represent a strong, consistent discharge mode in RE neurones

A-C, left column, action potential discharges during spindle oscillations of a RE neurone held at different values of V_m by injection of DC. A, 0 nA; B, +0.2 nA; C, +0.4 nA. Right column, histograms of inter-spike intervals and auto-correlograms for spikes (inset) for the previous periods. Asterisks denote tonic spikes in the intracellular recordings and their location in the histograms of inter-spike intervals. Binsize 1 ms, for histograms and auto-correlograms. D, discharge frequencies for bursting (filled circles) and tonic spikes (empty circles) as a function of the steady current injected. Points were calculated as the reciprocal of the peak in the histograms of A-C. E, rhythmicity (filled triangles) and fraction of tonic action potentials (empty circles) as a function of the steady current injected. Note an inverse relation for these parameters. Rhythmicity index was defined as the peak-to-peak amplitude adjacent to the central peak of the auto-correlogram for action potentials. Tonic fraction was defined as the ratio between the number of action potentials fired in tonic mode (ISI 20-90 ms) and the total number of action potentials for every level of DC.

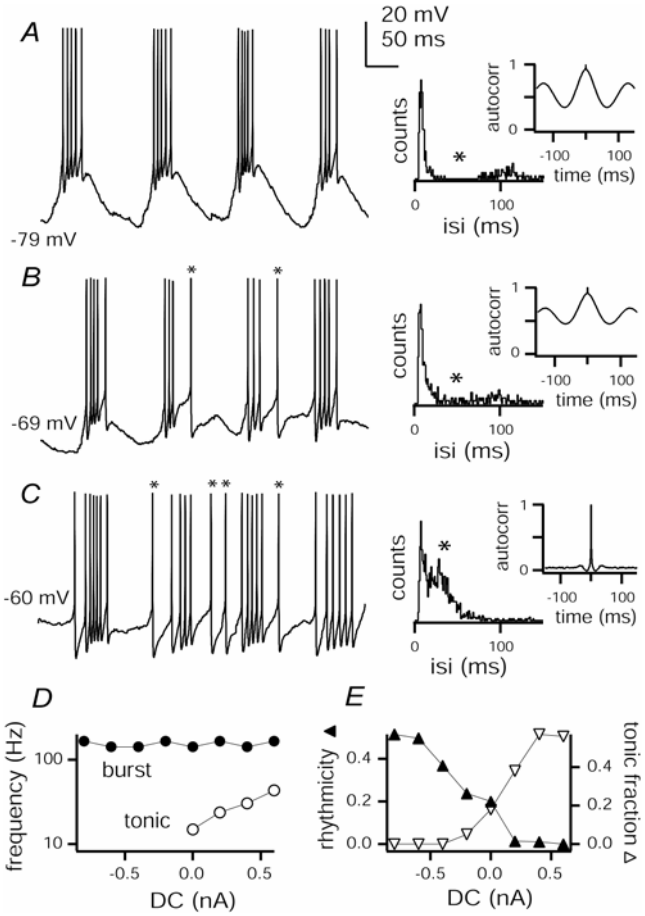
A
20 mV
50 ms
-79 mV
counts
autocorr
time (ms)
isi (ms)
B
-69 mV
C
-60 mV
D
frequency (Hz)
burst
tonic
DC (nA)
E
rhythmicity
tonic fraction Δ
DC (nA)

5. Synaptic Membrane Responsiveness and its Integrative Properties

THE CORTICALLY EVOKED SECONDARY DEPOLARIZATION AFFECTS THE INTEGRATIVE PROPERTIES OF THALAMIC RETICULAR NEURONS

Pablo Fuentealba, Sylvain Crochet, and Mircea Steriade (2004). *European Journal of Neuroscience (in press)*

RESUMÉ

Les terminaisons corticothalamiques sur les neurones thalamiques réticulaires (RE) comptent pour la plupart des synapses provenant des voies afférentes sur ce noyau. Étant donné la suprématie des entrées corticales, nous avons analysé ici les caractéristiques et les mécanismes possibles sous-jacents à une composante secondaire de dépolarisations provoquées corticalement dans les neurones RE, enregistré sur des chats sous anesthésie. Une stimulation électrique des axones corticothalamiques dans la capsule interne a provoqué des potentiels postsynaptiques excitateurs (EPSPs) à latence fixe et courte qui, en augmentant l'intensité de la stimulation et à des niveaux hyperpolarisés (< -70 mV), se sont développés en décharges à seuil bas (LTSs) et en oscillations en fuseaux. Le seuil pour les oscillations en fuseaux était de 60% plus haut que ce qui est requis pour provoquer des EPSPs minimaux. Les EPSPs provoqués comportaient une composante dépolarisante secondaire qui se produisait comme un événement tout ou rien à ~5 ms après le pic de la composante initiale et était dépendante du voltage, i.e. plus présente entre –70 mV et –85 mV alors qu'elle était grandement réduite ou absente à des niveaux plus hyperpolarisés. La composante dépolarisante secondaire était sensible au QX-314 dans les micropipettes d'enregistrements. Nous suggérons que la composante secondaire des EPSPs provoqués corticalement dans les neurones RE est due à l'activation des courants-T avec une contribution probable du courant persistant Na^+. Cette composante tardive affectait les propriétés intégratives des neurones RE, incluant leurs décharges et la sommation temporale des entrées corticales.

ABSTRACT

Corticothalamic terminals on thalamic reticular (RE) neurons account for most synapses from afferent pathways onto this nucleus and these inputs are more powerful than those from axon collaterals of thalamocortical (TC) neurons. Given the supremacy of cortical inputs, we analyzed here the characteristics and possible mechanisms underlying a secondary component of the cortically elicited depolarization in RE neurons, recorded in cats under barbiturate anesthesia. Electrical stimulation of corticothalamic axons in the internal capsule evoked fixed and short-latency excitatory postsynaptic potentials (EPSPs) that, by increasing stimulation intensity and at hyperpolarized levels (< -70 mV), developed into low-threshold spikes (LTSs) and spindle oscillations. The threshold for spindle oscillations was just 60% higher than that required for evoking minimal EPSPs. The evoked EPSPs included a secondary depolarizing component, which occurred as an all-or-none event at ~5 ms after the peak of the initial component and was voltage–dependent, i.e. most prominent between -70 mV and -85 mV, while being greatly reduced or absent at more hyperpolarized levels. The secondary depolarizing component was sensitive to QX-314 in the recording micropipette. We suggest that the secondary component of cortically evoked EPSPs in RE neurons is due to the dendritic activation of T-current, with a probable contribution of the persistent Na^+ current. This late component affected the integrative properties of RE neurons, including their spiking output and temporal summation of incoming cortical inputs.

INTRODUCTION

The thalamic reticular (RE) nucleus is entirely composed of neurons releasing γ-aminobutyric acid (GABA), which project to the dorsal thalamus and are crucially implicated in the generation of sleep spindle oscillations (Steriade *et al.*, 1990). The major extrinsic synaptic inputs of these neurons arise from axons of layer VI cortical pyramidal neurons and axon collaterals of thalamocortical (TC) neurons (Jones, 1985). Intrinsic synapses are both chemical (Deschênes *et al.*, 1985; Yen *et al.*, 1985) and electrical (Landisman *et al.*, 2002). Of all external sources of synaptic contacts, the cortex is the most important as corticothalamic terminals on RE cells in the somatosensory sector of the nucleus account for ~65-70% of synapses, whereas synapses of TC origin account for 20-25% and GABAergic synapses for 15-20% (Liu & Jones, 1999). Differences in the strength of corticothalamic connections to RE and TC cells, as expressed by three-fold larger unitary excitatory postsynaptic currents in RE neurons, are correlated with about three times higher numbers of GluR4 receptor subunits at the RE synapse (Golshani *et al.*, 2001). The small terminals from corticothalamic collaterals have a single small postsynaptic density, which appears to reflect the presence of a single vesicle release site, and are distributed in approximately equal numbers over both proximal and distal dendrites at RE neurons (Liu *et al.*, 2001).

The RE neurons display two firing modes: tonic discharges at relatively depolarized levels of membrane potential (V_m), as in brain-active behavioral states, and

prolonged spike-bursts during oscillations characteristic for natural slow-wave sleep (Steriade *et al.*, 1986, Steriade *et al.*, 1990). These spike-bursts are made of fast Na^+ action potentials that crown a low-threshold spike (LTS) generated by the transient Ca^{2+} current, I_T, which is de-inactivated by membrane hyperpolarization (Mulle *et al.*, 1986; Llinás & Geijo-Barrientos, 1988; Huguenard & Prince, 1992; Contreras *et al.*, 1993). The distal dendritic origin of RE-cells' LTSs has been shown experimentally and in computational studies (Huguenard & Prince, 1992; Destexhe *et al.*, 1996). While the dendritically generated I_T in RE neurons is mainly implicated in the induction of low-frequency sleep spindle oscillations (Steriade *et al.*, 1987; Steriade *et al.*, 1990), activation of a distinct Ca^{2+} current, P/Q-type, generates high-frequency (20-80 Hz) oscillations in the dendrites of TC neurons (Pedroarena & Llinás, 1997).

In previous studies we have shown that corticothalamic stimulation elicits powerful EPSPs in RE neurons, which develop into spike-bursts and spindle oscillations in the thalamocortical network (Contreras & Steriade, 1996). The present study was undertaken to further characterize the secondary depolarizing component of cortically evoked EPSP in RE neurons (Contreras *et al.*, 1993) by analyzing its voltage-dependency and sensitivity to QX-314, since this component is of importance for the integrative properties of RE neurons.

METHODS

Preparation

Experiments were performed on adult cats (2.5-3.5 kg), anesthetized with pentobarbital (25 mg/kg, i.p.). When the cats showed the signs of deep anaesthesia, they were paralyzed with gallamine triethiodide and artificially ventilated with control of the end-tidal CO_2 concentration at ~3.5%. Body temperature was maintained at 36-38^{o} C. The depth of anesthesia was continuously monitored by EEG and additional doses of anesthetic were administered at the slightest tendency toward low-voltage and fast EEG rhythms. At the end of experiments, animals were given a lethal dose of pentobarbital (50 mg/kg).

Recording and stimulation

Current-clamp intracellular recordings from the rostral and rostrolateral sector of the RE nucleus were performed using sharp electrodes, glass micropipettes (DC resistance, 30-60 MΩ). To avoid breaking of recording micropipettes, the cortex and white matter overlying the head of the caudate nucleus were removed by suction. The pipettes entered ~3 mm through the caudate nucleus to reach the RE nucleus. Pipettes were generally filled with 3 M solution of K-acetate and, in some experiments, 50 mM of QX-314 was added. The stability of intracellular recordings was ensured by cisternal drainage, bilateral pneumothorax, hip suspension, and by filling the hole over the thalamus with 4% agar solution. A high-impedance amplifier with active bridge circuitry

was used to record and inject current inside the cells. Most intracellular recordings included in the database lasted for periods longer than 30 min.

Electrical stimulation of corticothalamic fibers was performed by descending one or two bipolar stimulating electrodes to the internal capsule (anterior +13, lateral +3.5, depth +1) and applying extracellular current pulses (0.2 ms, 50-600 μA, 0.5-1 Hz). In all cases, the threshold intensity for EPSP's generation was determined. Due to the all-or-none nature of the secondary component of responses at threshold intensities, most experiments were done with intensities 10-30% over the threshold in order to study the secondary component.

Data analysis

All analyses were performed using Igor Pro 4.0 (Wavemetrics. Inc.). Values are expressed as mean ± S.D., and t-tests were used to assess statistical differences.

RESULTS

Intracellular recordings from RE neurons were performed in the rostral pole and rostrolateral sector of the nucleus. All cells (n = 32) were identified by the characteristic accelerando-decelerando pattern of their spike-bursts (inset in Fig. 5.1*A*), which occurred during spindle sequences. Resting V_ms were more negative than -70 mV in all cases (-75 ± 4 mV). At such V_ms, T-current are de-inactivated (Llinás, 1988; Llinás & Geijo-Barrientos, 1988; Huguenard & Prince, 1992) and RE neurons fire bursts of action potentials during spontaneously occurring spindles (Fig. 5.1*A*).

EPSPs evoked by stimulation of corticothalamic fibers

RE neurons were activated by electrical stimulation of corticothalamic fibers in the internal capsule (Fig. 5.1, *B*-*C*). In all cases, stimulation evoked a short-latency EPSP. Stimulation intensity was adjusted in order to obtain a minimal response. For the neuron depicted in Fig. 5.1, low intensities (≤110 μA) failed to evoke any response. Increasing stimulation intensity produced responses from 120 μA, considered the threshold. Thus, EPSPs of small amplitude (3.4 ± 1.4 mV, n = 30), as recorded at somatic level and resting V_m, and short duration (~30 ms) were elicited with threshold stimulation intensity of 120 μA (left panels in Fig. 5.1, *B*-*C*). Such EPSPs were not followed by long-latency responses. Since there were no additional excitatory or inhibitory components, and the latency was short and fixed, these evoked EPSPs were considered to be monosynaptic. In the same cell, increasing stimulation intensity to 180 μA induced two effects: *i)* the short-latency EPSP gave rise to an LTS crowned by spike-bursts at the same resting V_m as that

at which lower intensity stimulation evoked a simple EPSP (middle superimposition within the right column in Fig. 5.1*C*), while at more depolarized or hyperpolarized levels (upper and lower superimpositions in Fig. 5.1*C*) the EPSPs gave rise to single action potentials or displayed increased amplitude, respectively; and *ii)* spindle oscillation was generated in all cases (Fig. 5.1*B*). The threshold for spindle generation, a network phenomenon, was just ~60% higher than the threshold for EPSP. These results were consistently seen in all other neurons.

Progressively increasing the strength of stimulation enhanced both the amplitude and depolarization area of evoked responses (traces *a-c* in Fig. 5.2*A*). When stimulation intensity was strong enough, LTSs were triggered from the resting V_m (-80 mV in the neuron depicted in Fig. 5.2*A*) and were followed by either a single, delayed spike (trace *d* in Fig. 5.2*A*) or a burst of spikes (trace *e* in Fig. 5.2*A*). The relation between rising stimulation intensity and increased firing probability of RE neurons was well fitted with a sigmoid function ($p_{0.5}$ reached at 150 μA; upper plot in Fig. 5.2*A*), proving a non-linear dependence of spike probability on stimulation intensity. However, both amplitude and area of EPSP displayed a positive linear relation to stimulation intensity, since both were well fitted by a linear function (lower plot in Fig. 5.2*A*). In the majority of cases (7 out of 9 neurons), stimulation inducing spindles was also able to evoke consistent discharges crowning the initial EPSP (Fig. 5.1*A*), suggesting a critical correlation between firing of RE neurons and spindle generation.

Evoked EPSPs display a secondary depolarizing component

Most EPSPs evoked by stimulation at threshold intensity displayed a secondary depolarizing component that frequently occurred as an all-or-none event. One example is the neuron depicted in Figure 5.2*B* (responses were recorded at the same V_m and evoked by stimuli with the same parameters). At the resting V_m (-76 mV) the cortically evoked EPSP displayed a short-latency, fast rising EPSP that was present in all cases (component *a*), but was associated in the majority of cases (70%) with a later, depolarizing component (component *b*). The latter response considerably increased **(**~75%) the depolarization area of the EPSP (from 62 to 109 mV*ms, Fig. 5.2*B*).

Effects of QX-314 on evoked EPSPs

Dendrites of most neurons are provided with a plethora of voltage-gated ionic channels (Llinás, 1975). This property allows dendrites to control synaptic amplitude and its conduction to the soma. The dendritic ionic channels may produce supralinear, sublinear or linear summation of arriving inputs. To evaluate the effect of active conductances on evoked EPSPs in RE neurons, recordings were performed in the presence of QX-314. QX-314 decreased the amplitude and depolarization area of evoked EPSPs (n = 7). The effect of QX-314 was mainly exerted on the late component of the response (Fig. 5.3*A*). The amplitude of the first component and area of the secondary component of the EPSPs, comparing the beginning of recording (control) and after seven minutes under QX-314, were 8.1 ± 1.1 mV and 207.3 ± 23.8 mV*ms, and 7.3 ± 2.3 mV and 171.2 ± 38.6 mV*ms, respectively. QX-314 is generally used for its property as a blocker of fast and persistent Na^+ currents (Yeh, 1978; Crill, 1996); however, it also blocks low- and high-voltage activated Ca^{2+} currents (Talbot & Sayer, 1996), K^+ currents

(Svoboda *et al.*, 1997; Paré & Lang, 1998), and hyperpolarization-activated currents (Perkins & Wong, 1995).

Voltage dependence of the secondary depolarizing component and the effect of QX-314

In a set of neurons (n = 7), evoked EPSPs were recorded at rest and at different values of V_m, obtained by current injection through the pipette (Fig. 5.3*B*). V_m depolarization from rest (-78 mV, second trace in left panel of Fig. 5.3*B*) to –73 mV increased the depolarization area of EPSPs, mainly by enhancing the secondary depolarizing component, whereas the amplitude of the early component remained nearly invariable. At more negative values of the V_m (-88 mV to –106 mV), the presence of the secondary depolarizing component was markedly diminished, while the amplitude of the first response remained virtually the same (left panel in Fig. 5.3*B*). Measurements of both early and late components showed that a linear relation was kept in both cases; while the amplitude of the early component remained almost invariable, the area of the secondary depolarizing component increased linearly with depolarization (Fig. 5.3*C*).

QX-314 decreased both the amplitude and area of cortically evoked EPSPs in a voltage dependent way (n = 4). The RE neuron depicted in Fig. 5.3*B* (right panel) was recorded during 30 min in QX-314 (50 mM). After an initial period of 2-3 min, full action potentials decreased in both amplitude and incidence, showing an effect of QX-314 on fast Na^+ currents (not shown). At rest (-83 mV), cortically evoked EPSPs showed rather small amplitude (~5 mV), but no secondary depolarizing component was evident

(right panel in Fig. 5.3*B*). Contrary to control recordings (with K^+-acetate), EPSPs recorded under QX-314 displayed decreased amplitude and area of depolarization as the V_m became more positive.

Figure 5.3*C* presents the pooled results for various neurons recorded under either control conditions (K^+-acetate, n = 7) or QX-314 (**n** = 4). For all cases recorded under QX-314, a voltage dependent decrease in both amplitude and area of evoked EPSPs was found (Fig. 5.3*C*). QX-314 started to exert its effect at about -80 mV, a value close to the resting V_m for RE neurons, and the effect increased as V_m depolarized.

Properties of suprathreshold synaptic responses

Since in most cases the resting V_m was quite hyperpolarized (around -75 mV or even more negative), EPSPs were generally subthreshold for spike generation. Increasing stimulation intensity frequently led to spike generation, but those usually crowned the LTSs (see Fig. 5.2*A*). Depolarizing the V_m by steady current injection through the pipette was another way to elicit suprathreshold responses. In such cases, the early and late components of evoked EPSPs showed differential contributions to neuronal output (n = 11). The RE neuron depicted in Fig. 5.4 was recorded at a resting V_m (-80 mV) at which evoked EPSPs were not able to trigger action potentials (not shown). However, as the neuron was depolarized, spikes were triggered in response to cortically evoked EPSPs. At -73 mV, spikes were triggered by the secondary depolarizing component (*b*), while the early component (*a*) remained subthreshold (Fig. 5.4*A*). Only starting at -65 mV was the early component able to trigger spikes (dotted line). The probability of spike generation

was plotted for both early and late components of the response as a function of V_m, and both were well fitted with a sigmoid function (Fig. 5.4*B*). The secondary component of the response was able to trigger full action potentials at more hyperpolarized V_m values than the early component. In fact, the $V_{0.5}$ for the early component was about -64 mV, and about -72 mV for the secondary component (Fig. 5.4*B*). Thus, the secondary depolarizing component of evoked EPSPs was able to boost the neuronal output of RE neurons at a more negative V_m.

The boosting properties of the secondary component were correlated with a faster rising phase as V_m was depolarized (Fig. 5.4*A*). Plotting the slow rising slope of the secondary depolarizing component against the holding V_m showed an increasing slope with depolarization. Such relation was well fitted with a single exponential function, which describes the dynamics of the process (Fig. 5.4*B*). In contrast, the early component of the EPSP presented a very fast, though only slightly voltage dependent rising slope (Fig. 5.4*B*).

The variable rising slope of the secondary component was expressed as a wide range (3-25 ms) of variable latencies in spike generation, standing in contrast to a short, fixed latency for the early component (Fig. 5.4*A*). Plotting the spike latency as a function of V_m showed an inverse relation compared to the rising slope for the secondary depolarizing component, meaning a progressive decrease as the neuronal membrane was depolarized (Fig. 5.4*B*). Such relation was well fitted with a single, decaying exponential,

while the early component displayed an almost independent relation of spike-latency to V_m (Fig. 5.4*B*).

These results show that the early and late components of evoked EPSPs have differential contributions in the neuronal output. The early component generates stereotyped spikes at short, fixed latencies, at relatively depolarized values (around -65 mV), while the secondary depolarizing component triggers spikes with widely variable latencies at more hyperpolarized values (around -72 mV).

Temporal summation of evoked EPSPs

The temporal summation of cortical inputs was assessed by high frequency stimulation (50-100 Hz) of corticothalamic fibers in the internal capsule (n = 8). The temporal summation of EPSPs was high and voltage-dependent. Figure 5.5 shows a RE neuron that was stimulated with 5 pulses at 10-ms time- intervals, at different V_ms. Only at V_ms close to -80 mV or more positive, was the summation effect observed (Fig. 5.5*A*). At rest (-82 mV), slight summation was detected, which increased with V_m depolarization. Plotting the ratio between the last (fifth) and first EPSP against the holding V_m, showed a maximal (200%) summation (Fig. 5.5*B*). Around -76 mV the responses to the pulse-train ended with a spike in the last stimulus (Fig. 5.5*A*). Increasing the membrane depolarization shifted the initiation of spikes to earlier EPSPs in the train in a linear fashion. Thus, in this example, at -76 mV only the last EPSP was able to trigger a spike, while at -53 mV the first EPSP triggers a full action potential (Fig. 5.5*B*).

DISCUSSION

Our results indicate that synaptic connections made by corticothalamic fibers onto RE neurons display some remarkable features: *(a)* the stimulation intensity threshold for spindle generation, a network phenomenon, was just ~60% higher than the threshold for short-latency and small-amplitude, monosynaptic EPSP; *(b)* evoked EPSPs frequently displayed a secondary depolarizing component, which was voltage dependent and sensitive to intracellular application of QX-314; *(c)* both rising phase and amplitude of early components of evoked responses were also affected by QX-314; and *(d)* the secondary depolarizing component of evoked EPSPs influenced the neuronal output and temporal summation of cortical inputs.

The neocortex and thalamus engage in a continuous dialogue that is maintained by corticothalamic and thalamocortical fibers, which connect them in a recurrent circuit. Although the stimulating electrode within the internal capsule likely activated not only corticothalamic fibers but also antidromically invaded some thalamocortical axons, with possibly axon reflex excitation of RE neurons, the number of corticothalamic axons is one order of magnitude higher than that of thalamocortical ones. Thus, we consider that the evoked EPSPs were mainly due to the activation of corticothalamic fibers and the contribution of thalamocortical fibers was minimal.

In the present experiments, stimulation was adjusted for minimal intensity and we could determine that the threshold for evoking spindle oscillations was only 40% higher

than for EPSPs. Increasing stimulation intensity showed that both the amplitude and depolarization area of the response rose in a linear way. However, the probability of discharge seemed to be governed by a sigmoid function. Spindle oscillations are known to be a network phenomenon initiated in the RE nucleus and maintained by the recurrent intrathalamic circuit (Steriade *et al.*, 1993). Thus, firing in RE neurons is necessary to generate the oscillation, which explains the close relation between the threshold for EPSP generation and spindle activation. At hyperpolarized resting V_m (around -75 mV), as displayed by RE neurons recorded in present experiments, the T-current is fully de-inactivated and therefore LTSs can be generated (Huguenard, 1996). Actually, all recorded neurons displayed spontaneous bursting behavior during spindle oscillations. The graded nature of LTSs in RE neurons was well characterized *in vivo* (Contreras *et al.*, 1993) and depends on the distal dendritic localization of T-channels (Huguenard & Prince, 1992; Destexhe *et al.*, 1996) coupled with the constant synaptic bombardment of dendritic arbors by network activity (Contreras *et al.*, 1993).

We detected a secondary depolarizing component in evoked EPSPs of RE neurons, as was also previously reported (Contreras *et al.*, 1993). In the present study, this component occasionally occurred as an all-or-none event, appearing ~5 ms after the peak of the response, in cases of small amplitude EPSPs. Higher amplitude EPSPs presented always a secondary depolarizing component. The secondary depolarizing component of the EPSP was voltage dependent, as it was present at V_ms as hyperpolarized as -100 mV, linearly increased with depolarization, and gave rise to action potentials as the V_m was close to firing threshold. Besides its voltage dependency, the

secondary depolarizing component was sensitive to QX-314 in the recording pipette. The effect of QX-314 was also voltage dependent since it did not affect responses at voltages more negative than -80 mV. QX-314 is a blocker of many conductances (see **RESULTS**). However, given the hyperpolarized V_m at which QX-314 exerted its effect, the secondary depolarizing component was probably due to the dendritic activation of T-current. The secondary component of evoked responses seems to be important for the integrative properties of RE neurons since it modulated both the neuronal output and its precise timing. Indeed, the secondary component was able to boost spike generation in RE neurons at V_ms more negative by 5-10 mV and to generate single or multiple spikes within a variable time window, as compared to stereotyped spikes generated by the peak of the early component of EPSPs when it reached the threshold. Consistent with an integrative role of the secondary depolarization, high-frequency stimulation induced temporal summation of evoked responses in a voltage dependent manner. These properties are related to the previously characterized gradual nature of bursting responses in RE cells (Contreras *et al.*, 1993).

The presence and contribution of persistent Na^+ currents cannot be discarded since its range of activation is close to the threshold for spike generation (5-10 mV below) and it is also blocked by QX-314 (Crill, 1996). Besides, studies in inhibitory neurons from the hippocampus have demonstrated the presence and importance of active dendritic Na^+ conductances (Martina *et al.*, 2000). It is thus possible that a joint contribution of Ca^{2+} and Na^+ dendritic currents acts in RE neurons for integration of cortical inputs.

Another effect of QX-314 on evoked responses was the two- to three-fold decrease in the rising slope (not shown). The rising phase of any active response depends on both its location in the dendritic tree and the active conductances that regulate its conduction to the soma (Magee, 2000). In the present experiments, electrical stimulation of corticothalamic fibers frequently elicited fast-rising responses (5-10 mV/ms slope) in RE neurons. Recent experiments have shown that cortically evoked EPSPs are mainly AMPA-receptor-dependent, with a negligible element of NMDA-receptor response, which is virtually absent at hyperpolarized levels of V_m (-70 mV) (Gentet & Ulrich, 2004; see also Pedroarena & Llinás, 1997). Even though the effect of QX-314 on the rising phase was not voltage dependent, a clear reduction was seen at different voltages in all cases, suggesting an additive contribution of active conductances to the AMPA component in the response.

In short, then, the voltage dependent dendritic channel distribution in RE neurons provides them with important properties for integration of cortical inputs. We suggest that, in comparison with the effects these inputs exert on TC neurons, at which level dendritic currents generate high-frequency rhythms (Pedroarena & Llinás, 1997) that define brain alertness, the parallel activation of RE-cells' dendrites by synchronized cortical volleys produces low-frequency oscillations (Steriade *et al.*, 1990; Contreras *et al.*, 1993; Contreras & Steriade, 1996) that characterize the disconnected state of slow-wave sleep. Moreover, during cortically generated spike-wave seizures, the powerful activation of GABAergic RE neurons leads to the inhibition of TC neurons (Steriade,

2003), their steady hyperpolarization with increased membrane conductance and, consequently, the obliteration of incoming messages en route to the cortex.

REFERENCES

Contreras, D., Curró Dossi, R. & Steriade, M. (1993) Electrophysiological properties of cat reticular thalamic neurones in vivo. *J. Physiol.*, **470**, 273-294.

Contreras, D. & Steriade, M. (1996) Spindle oscillation in cats: the role of corticothalamic feedback in a thalamically generated rhythm. *J. Physiol.*, **490**, 159-179.

Crill, W.E. (1996) Persistent sodium current in mammalian central neurons. *Annu. Rev. Physiol.*, **58**, 349-362.

Deschênes, M., Madariaga-Domich, A. & Steriade, M. (1985) Dendrodendritic synapses in the cat reticularis thalami nucleus: a structural basis for thalamic spindle synchronization. *Brain Res.*, **334**, 165-168.

Destexhe, A., Contreras, D., Steriade, M., Sejnowski, T.J. & Huguenard, J.R. (1996) In vivo, in vitro, and computational analysis of dendritic calcium currents in thalamic reticular neurons. *J. Neurosci.*, **16**, 169-185.

Gentet, L.J. & Ulrich, D. (2004) Electrophysiological characterization of synaptic connections between layer VI cortical cells and neurons of the nucleus reticularis thalami in juvenile rats. *Eur. J. Neurosci.*, **19**, 625-633.

Golshani, P., Liu, X.B. & Jones, E.G. (2001) Differences in quantal amplitude reflect GluR4- subunit number at corticothalamic synapses on two populations of thalamic neurons. *Proc. Natl. Acad. Sci. U S A*, **98**, 4172-4177.

Huguenard, J.R. (1996) Low-threshold calcium currents in central nervous system neurons. *Annu. Rev. Physiol.*, **58**, 329-348.

Huguenard, J.R. & Prince, D.A. (1992) A novel T-type current underlies prolonged Ca(2+)-dependent burst firing in GABAergic neurons of rat thalamic reticular nucleus. *J. Neurosci.*, **12**, 3804-3817.

Jones, E.G. (1985) *The Thalamus*. Plenum, New York.

Landisman, C.E., Long, M.A., Beierlein, M., Deans, M.R., Paul, D.L. & Connors, B.W. (2002) Electrical synapses in the thalamic reticular nucleus. *J. Neurosci.*, **22**, 1002-1009.

Liu, X.B., Bolea, S., Golshani, P. & Jones, E.G. (2001) Differentiation of corticothalamic and thalamocortical collateral synapses on mouse reticular nucleus neurons by EPSC amplitude and AMPA-receptor subunit composition. *Thalamus & Related Systems*, **1**, 15.

Liu, X.B. & Jones, E.G. (1999) Predominance of corticothalamic synaptic inputs to thalamic reticular nucleus neurons in the rat. *J. Comp. Neurol.*, **414**, 67-79.

Llinás, R. (1975) Electroresponsive properties of dendrites in central neurons. *Adv. Neurol.*, **12**, 1-13.

Llinás, R. (1988) The intrinsic electrophysiological properties of mammalian neurons: insights into central nervous system function. *Science*, **242**, 1654-1664.

Llinás, R. & Geijo-Barrientos, E. (1988) *Cellular Thalamic Mechanisms*. Elsevier, Amsterdam.

Magee, J.C. (2000) Dendritic integration of excitatory synaptic input. *Nat. Rev. Neurosci.*, **1**, 181-190.

Martina, M., Vida, I. & Jonas, P. (2000) Distal initiation and active propagation of action potentials in interneuron dendrites. *Science*, **287**, 295-300.

Mulle, C., Madariaga, A. & Deschênes, M. (1986) Morphology and electrophysiological properties of reticularis thalami neurons in cat: in vivo study of a thalamic pacemaker. *J. Neurosci.*, **6**, 2134-2145.

Paré, D. & Lang, E.J. (1998) Calcium electrogenesis in neocortical pyramidal neurons in vivo. *Eur. J. Neurosci.*, **10**, 3164-3170.

Pedroarena, C. & Llinás, R. (1997) Dendritic calcium conductances generate high-frequency oscillation in thalamocortical neurons. *Proc. Natl. Acad. Sci. U S A*, **94**, 724-728.

Perkins, K.L. & Wong, R.K. (1995) Intracellular QX-314 blocks the hyperpolarization-activated inward current Iq in hippocampal CA1 pyramidal cells. *J. Neurophysiol.*, **73**, 911-915.

Steriade, M. (2003) *Neuronal Substrates of Sleep and Epilepsy*. Cambridge University Press, Cambridge, UK.

Steriade, M., Domich, L. & Oakson, G. (1986) Reticularis thalami neurons revisited: activity changes during shifts in states of vigilance. *J. Neurosci.*, **6**, 68-81.

Steriade, M., Domich, L., Oakson, G. & Deschênes, M. (1987) The deafferented reticular thalamic nucleus generates spindle rhythmicity. *J. Neurophysiol.*, **57**, 260-273.

Steriade, M., Jones, E.G. & Llinás, R. (1990) *Thalamic oscillations and signaling.* Wiley-Interscience, New York.

Steriade, M., McCormick, D.A. & Sejnowski, T.J. (1993) Thalamocortical oscillations in the sleeping and aroused brain. *Science*, **262**, 679-685.

Svoboda, K., Denk, W., Kleinfeld, D. & Tank, D.W. (1997) In vivo dendritic calcium dynamics in neocortical pyramidal neurons. *Nature*, **385**, 161-165.

Talbot, M.J. & Sayer, R.J. (1996) Intracellular QX-314 inhibits calcium currents in hippocampal CA1 pyramidal neurons. *J. Neurophysiol.*, **76**, 2120-2124.

Yeh, J.Z. (1978) Sodium inactivation mechanism modulates QX-314 block of sodium channels in squid axons. *Biophys. J.*, **24**, 569-574.

Yen, C.T., Conley, M., Hendry, S.H. & Jones, E.G. (1985) The morphology of physiologically identified GABAergic neurons in the somatic sensory part of the thalamic reticular nucleus in the cat. *J. Neurosci.*, **5**, 2254-2268.

FIGURES

Figure 5.1. Threshold corticothalamic stimulation for eliciting EPSPs and spindles in RE neurons. (A) intracellular recording from RE neuron in the rostral pole during spontaneously occurring spindles. Inset at right, expanded low-threshold spike burst, showing accelerando-decelerando pattern. Small artifacts represent minimal stimulation of corticothalamic fibers (internal capsule) at 1 Hz. (B) l*eft*, single EPSP evoked by threshold stimulation (120 μA; note absence of longer latency components in the evoked EPSP). *Right,* spindle oscillation elicited by threshold stimulation (180 μA). Inset, threshold intensities for induction of EPSPs (153 ± 27 μA) and spindles (241 ± 51 μA) in RE neurons (n = 12). Difference significant at * $p < 0.05$. (C) superimposed evoked responses (n = 3) at threshold intensities for EPSPs (*left*) and spindle generation (*right*). At rest (-78 mV), EPSPs were evoked at 120 μA (*left*), while at 180 μA (*right*) the response depended on the V_m (see main text). Scale bars for insets in *A* and *C*, 20 mV, 20 ms.

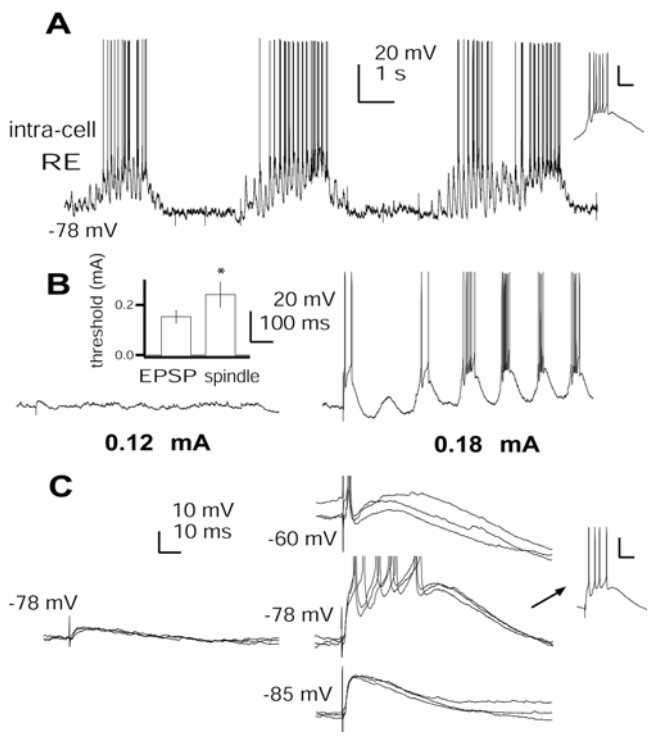
A
20 mV
1 s
intra-cell
RE
-78 mV
B
threshold (mA)
0.2
0.0
*
EPSP spindle
20 mV
100 ms
0.12 mA
0.18 mA
C
10 mV
10 ms
-60 mV
-78 mV
-78 mV
-85 mV

Figure 5.2. Early and late components in cortically evoked EPSPs of RE neurons. (A) intensity dependence of cortically evoked EPSPs. *Left*, averages (*a*-*b*-*c*; *n* = 10) and single responses (*d*-*e*) to stimuli of increasing intensity (*a*, 130 μA; *b*, 150 μA; *c*, 170 μA; *d*, 180 μA; *e*, 180 μA). *Right up*, probability of action potential generation as a function of stimulation intensity. Solid line represents the best sigmoid fitting ($p_{0.5}$ reached at 150 μA). Each point in the plot was extracted from multiple stimuli (*n* = 20); the fraction of stimuli eliciting action potentials normalized by one was considered as the spike probability for each stimulation intensity. *Right down*, intensity dependence of response amplitude and area. Note linear increase in both as stimulation intensity increased. Solid and dotted lines represent the best linear fitting for amplitude and area, respectively. Each point is the average extracted from 10 individual responses. (B) l*eft*, superimposed evoked EPSPs (*n* = 5) recorded at resting V_m (-76 mV). Top five traces show a typical fast, early response (*a*) followed by a secondary, much slower, later component (*b*). Bottom five traces depict EPSPs where later component (*b*) was absent in the same neuron, though neither V_m nor stimulation intensity were changed. *Right*, average (*n* = 30) of evoked EPSPs showing either one, early component (solid line) or both, early and late components (dotted line). EPSPs presenting both early (*a*) and late (*b*) components were seen in 70 % of EPSPs (*n* = 150) for the depicted neuron. Amplitude and area of EPSPs displaying just the early component were 3.5 ± 0.6 mV and 62.2 mV*ms. Amplitude and area of EPSPs displaying both early and late components were 3.6 ± 0.3 mV and 109.3 mV*ms. Stimulation intensity 200 μA.

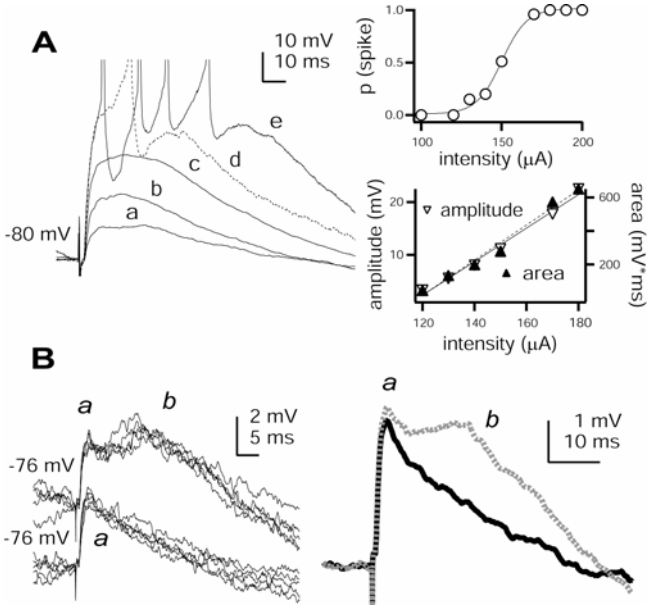
A
10 mV
10 ms
e
d
c
b
a
-80 mV
p (spike)
1.0
0.5
0.0
100
150
200
intensity (μA)
amplitude (mV)
20
10
amplitude
area
600
200
area (mV*ms)
120
140
160
180
intensity (μA)
B
a
b
2 mV
5 ms
-76 mV
-76 mV
a
a
b
1 mV
10 ms

Figure 5.3. Voltage-dependence of cortically-evoked EPSPs and voltage sensitivity of the late component to QX-314. (A) *left*, superimposed evoked EPSPs (*n* = 3) recorded at resting V_m (-78 mV) at the beginning (top) and after seven minutes (bottom) of recording with QX-314 (50 mM) in the pipette. *Right*, average (*n* = 10) of evoked EPSPs showing the effect of QX-314 on the late component of the response (see main text). Amplitude was measured as the difference between the resting V_m (1 ms before stimulation) and the peak of the early response. Depolarization area was calculated as the integral under the response up to 50 ms. Stimulation intensity 150 μA. (B) averages (*n* = 20) of evoked EPSPs at different V_ms for control recordings with K^+-acetate (left) and recordings with QX-314 (right). Note the presence of early (*a*) and late (*b*) components, the last one increasing with depolarization in control recordings, and the decrease of the late component upon depolarization in recordings with QX-314. (C) QX-314 affects the amplitude and depolarization area of cortically evoked EPSPs. Voltage dependence of response amplitude and area, respectively, for 5 neurons recorded under QX-314 (20-60 min) and for 7 neurons recorded with K^+-acetate, as control. Note that QX-314 starts to exert a significant effect at –80 mV, which increased with depolarization. Values were normalized to the one measured at the most hyperpolarized V_m (-110 mV) and individual points from different neurons were grouped in 10-mV intervals (-110 mV to -70 mV). Stimulation intensity 300 μA.

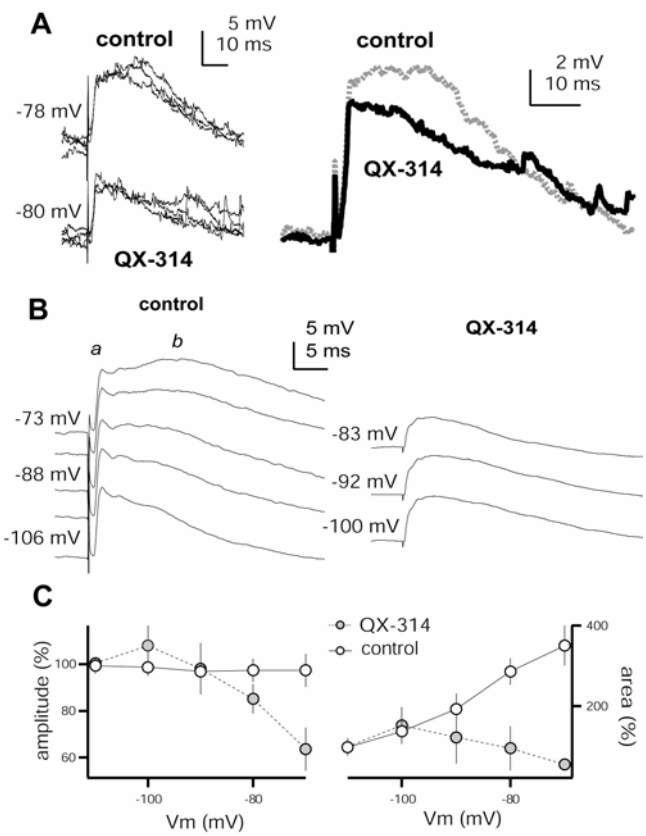
A
control
5 mV
10 ms
-78 mV
-80 mV
QX-314
control
2 mV
10 ms
QX-314
B
control
a
b
5 mV
5 ms
QX-314
-73 mV
-88 mV
-106 mV
-83 mV
-92 mV
-100 mV
C
QX-314
control
amplitude (%)
100
80
60
-100
-80
Vm (mV)
400
200
area (%)
-100
-80
Vm (mV)

Figure 5.4. Properties of suprathreshold EPSPs in RE neurons. (A) cortically evoked suprathreshold responses at different V_ms. Early (*a*) and late (*b*) components of responses are depicted. Dotted line at -65 mV shows a full action potential triggered by the early (*a*) component. (B) *left*, probability of action potential generation as a function of V_m. Dotted and solid lines represent the best sigmoid fitting for components *a* and *b*, respectively; where $V_{0.5}$ was -64.2 mV (*a*) and -71.6 mV (*b*). *Middle*, voltage dependence of response slope, for both early and late components of EPSPs. Note only slight decrease for *a* (scale, right axis) and exponential increase for *b* (scale, left axis). *Right*, spike latency as a function of V_m. Note constant value for *a*, and exponential decrease for *b*. Each point is calculated from 10 single trials in all plots. Stimulation intensity 300 μA.

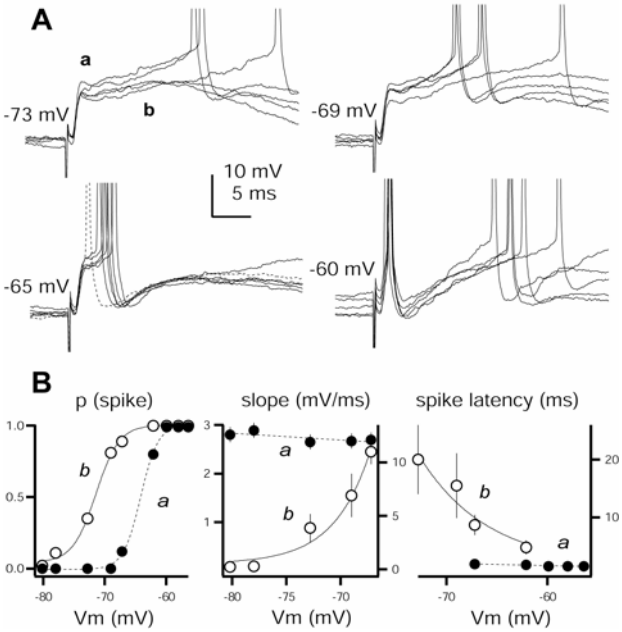
A
a
b
-73 mV
-69 mV
10 mV
5 ms
-65 mV
-60 mV
B
p (spike)
slope (mV/ms)
spike latency (ms)
1.0
0.5
0.0
3
2
1
10
5
0
20
10
b
a
-80
-70
-60
-75
Vm (mV)

Figure 5.5. Temporal summation of cortically evoked EPSPs. (A) average (*n* = 5, in a-c) of trains of EPSPs evoked by stimuli at 100 Hz, except for the single traces displaying truncated action potentials (*a*, -91 mV; *b*, -86 mV; *c*; -82 mV; *d*, -76 mV; *e*, -63 mV). (B) temporal summation of EPSPs was obtained by dividing amplitude of last (fifth) EPSP by the first one. Note that summation starts at -82 mV. V_m change shifts EPSP to trigger spike in the train. At -76 mV, only the last (fifth) EPSP can reach threshold for spike generation due to temporal summation. At -53 mV, the first EPSP elicits an action potential. Stimulation intensity 300 μA.

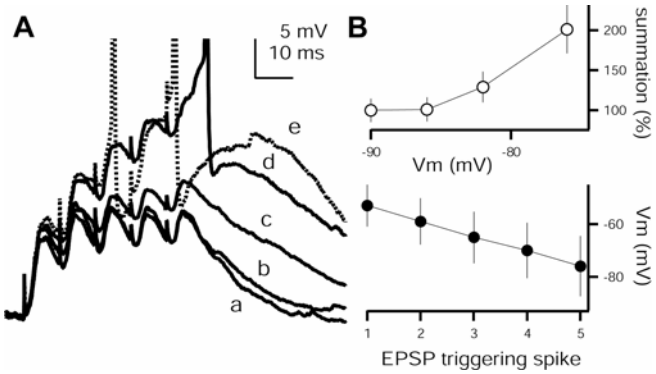
A
5 mV
10 ms
e
d
c
b
a
B
summation (%)
200
150
100
-90
-80
Vm (mV)
Vm (mV)
-60
-80
1
2
3
4
5
EPSP triggering spike

6. Intrinsic Chemical Synapses and their Role in Network Oscillations

PROLONGED HYPERPOLARIZING POTENTIALS PRECEDE SPINDLE OSCILLATIONS IN THE THALAMIC RETICULAR NUCLEUS

Pablo Fuentealba, Igor Timofeev and Mircea Steriade (2004). *Proceeding of the Nacional Academy of Science USA* 101(26):9816-9821.

RESUMÉ

Des enregistrements intracellulaires des neurones RE *in vivo* ont révélé la présence de potentiels hyperpolarisants prolongés (HP) précédant les fuseaux dans un sous-groupe (30%) de neurones du noyau thalamique réticulaire (RE). Ces HP (6-10 mV, 200-300 ms) étaient présentes seulement avant le début des ondes fuseaux spontanées. Les vagues corticothalamiques étaient aussi effectives dans la génération de telles HP suivies des fuseaux dans les neurones RE. Une baisse atteignant jusqu'à 40% dans la résistance d'entrée apparente (R_{in}) était associée à ces HP suggérant un processus actif plutôt qu'une *disfacilitation*. De plus, le potentiel de renverse était d'environ -100 mV pour les HP provoquées et spontanées, ce qui est cohérent avec une activation de conductances K^+ lentes. L'ajout de QX-314 dans les pipettes d'enregistrements a diminué l'amplitude et la fréquence des HP, ce qui suggère une participation de la protéine-G dépendante des courants K^+ dans la génération des hyperpolarisations. Des enregistrements intracellulaires et extracellulaires simultanés dans le noyau RE ont démontré que quelques neurones RE déchargeaient pendant les HP et par conséquent, pourraient être impliqués dans leurs générations. Les HP précédant les fuseaux pourraient jouer un rôle dans la transition de décharges en continu à des vagues de décharges des neurones RE à l'intérieur des limites du potentiel de membrane (-60 to -65 mV) lequel organise les conditions favorables pour la génération des vagues de décharges à seuil bas qui initient les séquences fuseaux. Ces données sont des arguments supplémentaires en faveur de la génération des fuseaux à l'intérieur du noyau thalamique RE.

ABSTRACT

The thalamic reticular (RE) nucleus is a key structure in the generation of spindles. Intracellular recordings of RE neurons *in vivo* revealed the presence of prolonged hyperpolarizing potentials preceding spindles in a subgroup (30%) of neurons. These hyperpolarizations (6-10 mV) lasted for 200-300 ms and were present just before the onset of spontaneously occurring spindle waves. Corticothalamic volleys were also effective in generating such hyperpolarizations followed by spindles in RE neurons. A drop of up to 40% in the apparent input resistance (R_{in}) was associated with these hyperpolarizing potentials, suggesting an active process rather than disfacilitation. Accordingly, the reversal potential was around -100 mV for both spontaneous and cortically elicited hyperpolarizations, consistent with the activation of slow K^+ conductances. QX-314 in the recording pipettes decreased both the amplitude and incidence of prolonged hyperpolarizations, suggesting the participation of G-protein dependent K^+ currents in the generation of hyperpolarizations. Simultaneous extracellular and intracellular recordings in the RE nucleus demonstrated that some RE neurons discharged during the hyperpolarizations and, thus, may be implicated in their generation. The prolonged hyperpolarizations preceding spindles may play a role in the transition from tonic to bursting firing of RE neurons within a range of membrane potential (-60 to -65 mV) at which they set favorable conditions for the generation of low-threshold spike-bursts that initiate spindle sequences. These data are further arguments for the generation of spindles within the thalamic RE nucleus.

INTRODUCTION

Spindles (7-15 Hz) are a hallmark oscillation during early sleep states. During the past two decades, a series of studies have demonstrated that spindles are generated within the thalamic reticular (RE) nucleus, which is uniquely composed of neurons using γ-aminobutyric acid (GABA) as neurotransmitter. Spindles are transferred to the cerebral cortex through the interactions between RE and thalamocortical neurons. Thus, experimental evidence has shown that spindles are abolished in thalamocortical systems after lesions of RE neurons or transections separating them from thalamocortical neurons (1) but survive in the RE nucleus deafferented from the dorsal thalamus and cerebral cortex (2). Computational studies agreed with the initiation of spindle rhythmicity in the isolated RE nucleus (3-5) and suggested that, at relatively hyperpolarized levels of membrane potential (V_m), as is the case during slow-wave sleep, the inhibitory postsynaptic potentials (IPSPs) between RE neurons can be reversed and $GABA_A$-mediated depolarizing potentials can generate persistent spatio-temporal patterns in the RE nucleus (6). The transfer of spindles from the RE nucleus, which is devoid of cortical projections, to the cerebral cortex is due to RE-cells' interactions with thalamocortical neurons (7-9).

The mechanisms underlying spindle initiation in the RE nucleus are not completely elucidated. Our hypothesis (2) predicted that hyperpolarization of RE-cells' dendrites through dendrodendritic synapses of GABAergic RE neurons (10-11) would de-inactivate a low-threshold Ca^{2+} conductance, triggering a Ca^{2+} spike followed by

GABA exocytosis and hyperpolarization in postsynaptic RE-cells' dendrites. The hyperpolarization in synaptically coupled dendrites was thought to initiate spindle oscillation and to spread it to adjacent elements. In essence, any idea aiming at explaining the genesis of spindles in the isolated network of RE neurons implicates the possibility that active RE neurons would hyperpolarize adjacent neurons and create an avalanche spread of the oscillation within the nucleus, with ultimate implication of target thalamocortical neurons. The source for activating a set of RE neurons that would hyperpolarize adjacent and/or more distant RE neurons may be any excitatory synaptic drive acting on these cells but primarily the neocortex that is known for being particularly potent in triggering (12) and synchronizing (13) spindles.

In the present experiments, using intracellular recordings *in vivo* in the rostrolateral sector of the cat RE nucleus, we show the presence of spontaneous as well as cortically elicited prolonged hyperpolarizing potentials leading to the onset of spindle oscillations in a sample (30%) of RE neurons. These hyperpolarizations were associated with a decrease in the apparent input resistance (R_{in}), thus suggesting an active inhibition rather than disfacilitation. Extracellularly recorded RE neurons in the vicinity of the intracellularly recorded neurons showed that their firing was temporally related with the hyperpolarization leading to spindles. We propose that the prolonged hyperpolarizations are part of the mechanisms that initiate spindles within the RE nucleus.

METHODS

Preparation.

Experiments were performed on adult cats (2.5-3.5 kg), anesthetized with pentobarbital (25 mg/kg, i.p.). When the cats showed ocular and EEG signs of deep anesthesia, the animals were paralyzed with gallamine triethiodide and artificially ventilated with control of the end-tidal CO_2 concentration at ~3.5%. Body temperature was maintained at 36-38^{o} C. The depth of anesthesia was continuously monitored by EEG and additional doses of anesthetics were administered at the slightest tendency toward activated (low-voltage and fast EEG) rhythms. At the end of experiments, animals were given a lethal dose of pentobarbital (50 mg/kg).

Recordings and stimulation.

Current-clamp intracellular recordings from thalamic RE and relay neurons were performed using glass micropipettes (DC resistance, 30-60 MΩ). To avoid breaking of recording micropipettes, the cortex and white matter overlying the head of the caudate nucleus were removed by suction. The pipettes entered ~3 mm through the caudate nucleus to reach the rostral pole or the rostrolateral sector of the thalamic RE nucleus. Pipettes were generally filled with 3 M solution of K-acetate and, in some experiments, with 50 mM of QX-314. The stability of intracellular recordings was ensured by cisternal drainage, bilateral pneumothorax, hip suspension, and by filling the hole over the thalamus with 4% agar solution. A high-impedance amplifier with active bridge circuitry

was used to record and inject current inside the cells. Most intracellular recordings included in the database lasted for periods longer than 30 min.

For simultaneous extracellular unit recordings, tungsten electrodes (10-15 MΩ; Frederick Haer, Bowdoinham, WA, USA) were inserted through the caudate nucleus, 0.5-1 mm rostrolateral to the intracellular recording micropipette. RE neurons were recognized by their long (>50 ms) and typical accelerando-decelerando spike-bursts in both intracellular and extracellular recordings (see Figs. 6.1*A* and 6.5*B*).

Electrical stimulation of corticothalamic fibers was performed by descending one or two bipolar stimulating electrodes to the internal capsule and applying current pulses (200 μs, 500-1000 μA, 0.5-1 Hz).

The apparent input resistance (R_{in}) was estimated as follows. Synaptic responses evoked by stimulation of cortical areas or corticothalamic fibers were recorded under different levels of membrane polarization obtained by current injection through the pipette (from –1 to +1 nA steady current). I-V curves were built by plotting the holding V_m against different levels of DC injected. Plots were made for multiple time intervals, generally in increments of 10 ms, before and after stimulation onset. For each plot, a linear function was fitted, whose slope was considered to be the apparent R_{in} for that particular time interval (see Fig. 6.1*C*). Next, a V_m vs. DC (I-V) plot was made for multiple time intervals, with reference to stimulation onset. The slope of the linear fitting in each plot represented the apparent R_{in} for the corresponding time interval.

Data analysis.

All data analysis was performed under Igor Pro 4.0 (Wavemetrics. Inc.). Values are expressed as mean ± SD, and t-tests were used to assess statistical differences, when necessary. Differences were considered as significant at $p<0.05$.

RESULTS

Spindle oscillations may be preceded by prolonged hyperpolarizations in RE cells

The intracellularly recorded RE neurons (*n* = 31) were able to generate spontaneously low-threshold spikes (LTSs) without current injection. The neuron depicted in Fig. 6.1*A* was recorded at a V_m of -79 mV and generated prolonged spike-bursts (>50 ms; inset in Fig. 6.1*A*) that occurred during spindle waves.

A subgroup of the recorded RE neurons (32%, 10 of 31) displayed prolonged hyperpolarizing potentials preceding spontaneously occurring spindle oscillations. One of those neurons is illustrated in Fig. 6.1*A* and shows simultaneous occurrence of spindles in the EEG and intracellular recording. The neuron displayed prolonged hyperpolarizations before every single spindle sequence. Generally, however, hyperpolarizations preceded spindles in only ~60% of cases (see below, Fig. 6.3*D*). The initial phase of the hyperpolarization was rather constant but the late part was variable, since rebound activity in the network was evident as depolarizing events with different amplitudes in the intracellular recording (arrowhead in superimposition, Fig. 6.1*A*). The activation of the hyperpolarization could be well fitted with a single exponential function (time constant, τ = 36 ms) and its duration was ~300 ms (Fig. 6.1*A*). The average τ for the activation of the hyperpolarization was 42 ± 4.8 ms (*n* = 5) and the duration 200-300 ms (*n* = 10).

The hyperpolarizations favored the occurrence of bursting behavior in RE cells. The neuron in Fig. 6.1*B* was slightly depolarized with positive current injection through

the pipette in order to induce continuous, tonic firing. This discharge pattern was present until the onset of spindle waves, when spontaneous membrane hyperpolarization was followed by robust bursting discharges. Therefore, hyperpolarization was able to switch the neuronal firing pattern from tonic to bursting, since it likely de-inactivated the Ca^{2+}-dependent T-current (14-17) so that incoming inputs, probably excitatory postsynaptic potentials (EPSPs) of cortical or dorsal thalamic origin, could elicit LTSs. Then, the hyperpolarization is a mechanism for switching discharge patterns in RE neurons from tonic to bursting (Fig. 6.1*B*), thus contributing to generation of spindling. Plotting the amount of hyperpolarization necessary to reach the threshold of postinhibitory rebound spike-bursts indicated that hyperpolarization is effective in controlling the transition from tonic to bursting discharges within a narrow band of V_m (-60 to -65 mV; data not shown).

Previous studies have shown that electrical stimulation of appropriate neocortical areas or corticothalamic fibers is effective in generating spindle oscillations (12, 18). The same type of electrical stimulation was also able to induce hyperpolarizations preceding spindles in all tested neurons (n = 5). In such cases, an initial EPSP preceded a prolonged hyperpolarization, which was followed by spindles (Fig. 6.1*C*). Averaged responses to corticothalamic stimulation demonstrated similar durations and amplitudes for spontaneous and evoked hyperpolarizations (compare panels *A* and *C* in Fig. 6.1). Recent *in vitro* data also indicate that focal stimulation of cortical layer VI produces di- or polysynaptic inhibitory currents in RE neurons (19).

During the prolonged hyperpolarizations, the apparent R_{in} of RE neurons could drop by 40% (32 ± 12%, *n* = 5; bottom right plot in Fig. 6.1*C*), suggesting it to be the result of active inhibition processes rather than disfacilitation in the network.

Voltage dependency of prolonged hyperpolarizations

To determine the voltage dependence of hyperpolarizations, different levels of V_m were attained in intracellular recordings by injecting steady current through the recording pipette. For each of such levels, the amplitude of hyperpolarizations was measured at the holding V_m. Figure 6.2 shows a representative example where a RE neuron was studied by this procedure. The left column displays the spindles that follow the spontaneous hyperpolarizations, marked by asterisks (panel *A*), while the right column shows expanded traces for hyperpolarizations at different V_ms (panel *B*). The hyperpolarization displayed higher amplitude as V_m was depolarized, which is consistent with the activation of inhibitory conductances. At more negative values of the V_m, the hyperpolarization became progressively smaller until it was virtually abolished around –100 mV to –105 mV (Fig. 6.2, *A*-*C*). The reversal potential (V_{rev}) was estimated by the extrapolation of a linear fitting to the I-V curve (Fig. 6.2*C*). Even though there was large variability in the voltage dependency of hyperpolarizations among different RE neurons, the V_{rev} remained similar in most cases (V_{rev} = -103 ± 4. 6 mV; *n* = 5), a value similar to the expected V_{rev} for K^+ in these cells (20, 21). Similar to the case of spontaneously occurring hyperpolarizations, the voltage dependency of evoked ones proved to be consistent with the activation of K^+ conductances: such hyperpolarizations reversed at similar V_m values compared to spontaneously occurring ones (V_{rev} = -101 ± 2.7 mV; *n* = 5) (Fig. 6.2*C*).

Ionic basis of prolonged hyperpolarizations

To elucidate some aspects of the ionic bases of prolonged hyperpolarizations, intracellular recordings were performed with the inclusion of QX-314 (50 mM) in the pipette. QX-314 is a blocker of multiple membrane conductances, including some K^+ currents (see Discussion). In the three neurons recorded under QX-314, in which hyperpolarizations preceding spindles could be detected, both the amplitude and incidence of hyperpolarizations were decreased. During the initial period of recording (2-5 min.), RE neurons displayed full action potentials coincident with spindle waves preceded by hyperpolarizations (control, Fig. 6.3*A*). As time elapsed (15-60 min.), QX-314 blocked Na^+ currents and, thus, decreased the spikes' amplitudes during spindles (QX-314, Fig. 6.3*A*). Not only the action potentials, but also the preceding hyperpolarizations were affected, showing decreased amplitudes (QX-314; Fig. 6.3*A*). Rebound activity occurring during the late part of hyperpolarizations was also affected by QX-314, displaying decreased incidence (Fig. 6.3*B*). Averages (n = 10) of hyperpolarizations selected from initial (control, Fig. 6.3*C*) and late (QX-314, Fig. 6.3*C*) periods of recordings with QX-314 showed a two-fold decrease in amplitude of hyperpolarizations preceding spontaneous spindles (Fig. 6.3*D*).

Prolonged hyperpolarizations may be preceded by cortically elicited EPSPs

RE neurons fired occasionally single spikes just before the onset of prolonged hyperpolarizations. In Fig. 6.4*A*, a RE neuron was depolarized by current injection (+0.3 nA) and discharged tonic spikes just before the onset of the prolonged hyperpolarizing

potential preceding spindles. When the same neuron was slightly hyperpolarized, due to membrane fluctuations, it displayed depolarizing potentials, likely EPSPs (Fig. 6.4*B*) that occasionally led to the action potentials that preceded the hyperpolarization (see Fig. 6.4*A*). Electrical stimulation of corticothalamic fibers was effective in mimicking the spontaneous behavior as, upon stimulation, EPSPs were evoked, followed by hyperpolarization and subsequent spindling (Fig. 6.4*C*).

The occurrence of spontaneous hyperpolarizations heralded ~60% of spindles recorded in RE neurons (Fig. 6.4*D*). However, in two RE neurons, such hyperpolarizations could be detected preceding every single spindle (see Fig. 6.1). On the other hand, evoked spindles were always preceded by hyperpolarizations (Fig. 6.4*D*) when corticothalamic fibers (Fig. 6.4*C*) or cortical areas (Fig. 6.1*C*) were stimulated. Only half of hyperpolarizations preceding spindles were initiated by an EPSP (Fig. 6.4*D*), suggesting that corticothalamic inputs are important for the generation of such hyperpolarizations, but not obligatory.

Network operations in the RE nucleus during hyperpolarizations preceding spindles

Although the present evidence pointed to the cerebral cortex as a probable source for the generation of hyperpolarizations (see Figs. 6.1*C* and 6.4*C*), their *direct* origin within the RE nucleus remained to be determined since both thalamic and cortical inputs to RE neurons are glutamatergic, therefore excitatory in nature. To support the hypothesis of intra-RE origin of these prolonged hyperpolarizing potentials, three pairs of simultaneous extracellular and intracellular recordings could be performed in the RE

nucleus, to study local activities within the RE network during the hyperpolarizations preceding spindle oscillations. One of such paired recordings is depicted in Fig. 6.5, showing the intracellular activity of one RE neuron and extracellular activities of at least two RE units. In most cases, at least one extracellularly recorded unit fired before the onset of the intracellular spindles, the discharge being temporally related with the prolonged hyperpolarization heralding the spindle sequence in the intracellularly recorded neuron (Fig. 6.5*A*-*B*). The hyperpolarizations preceding the first three spindle sequences in Fig. 6.5*A* were temporally associated with firing of one extracellularly recorded unit (*a*), while the last hyperpolarization was accompanied by firing of the second extracellularly recorded unit (*b*). These events are expanded in Fig. 6.5*B*.

Autocorrelograms for action potentials showed that intracellular and both extracellular units presented oscillatory activity in the range of spindle activities (7-14 Hz), as seen by clear presence of secondary peaks at ± 110 ms (~9 Hz, Fig. 6.5*C*). The crosscorrelation for spikes showed that both extracellularly recorded units fired in phase, usually one of them (*b*) preceding the firing of the other (*a*) (Fig. 6.5*D*). However, both units generally preceded the activity in the intracellular recording (Fig. 6.5*C*). Consistent with extracellular discharges preceding those in the intracellular recording, the extracellular recordings showed spiking activity at the beginning and throughout the prolonged hyperpolarizations (Fig. 6.5*D*). Therefore, the latter were correlated with action potential discharges in nearby and/or distant locations in the RE nucleus, suggesting that these potentials may be locally generated within the RE network.

DISCUSSION

We demonstrated the presence of a prolonged hyperpolarization that precedes spindle oscillations in one third of RE neurons. These hyperpolarizations *(a)* were detected in spontaneous spindle waves, but were also induced by activation of corticothalamic projections, in which case they were preceded by EPSPs; *(b)* were associated with decreased neuronal R_{in}, displayed V_{rev} around –100 mV, and were sensitive to intracellular QX-314, suggesting the implication of G-protein dependent K^+ currents; *(c)* may act as a switch between tonic and bursting discharge modes in RE neurons; and *(d)* their direct presynaptic origin could be local, due to the discharges of other RE neurons.

Both spontaneously occurring and evoked hyperpolarizations produced a significant drop in the R_{in} of RE neurons, suggesting the involvement of active conductances. Therefore, disfacilitation, like that occurring in cortical (22) and thalamic (23) neurons during the slow oscillation in natural sleep or anesthesia, can be discarded as a possible mechanism underlying the prolonged hyperpolarizations leading to spindles in RE neurons. The V_{rev} (around -100 mV) of RE-neurons' hyperpolarization suggests the activation of K^+ conductances (20, 21). The V_{rev} for $GABA_A$-mediated IPSPs in RE cells was estimated at -70 mV (6, 24, 25). At that range of V_m, the hyperpolarization preceding spindles displayed significant amplitude, thus discarding the role of $GABA_A$-mediated IPSPs in their generation. Moreover, the I-V relation for this hyperpolarization was linear for a large range of V_m values (-100 mV to -50 mV), implying a very little contribution, if

any, of $GABA_A$-mediated potentials at V_m more depolarized than -70 mV. QX-314 in the pipette decreased both their amplitude and incidence, consistent with the activation of K^+ conductances during the prolonged hyperpolarizations. QX-314 affects a wide range of membrane conductances, including the blockade of fast and persistent Na^+ currents (26), low- and high-voltage activated Ca^{2+} currents (27), K^+ currents (28, 29) as well as hyperpolarization-activated currents (30). It is unlikely that depolarizing (Ca^{2+} and Na^+) currents are implicated in the genesis of the prolonged hyperpolarizations. On the other hand, it has been shown that QX-314 also blocks G-protein-activated, inwardly rectifying K^+ channels (31). This opens the possibility that the prolonged hyperpolarization in RE neurons is an inhibitory potential activated by G-protein coupled to second messenger cascades (32). Candidates for such an effect are $GABA_B$ receptors (21) as well as peptidergic receptors for somatostatin (33) and neuropeptide Y (34), which are expressed by RE neurons (35, 36) and may initiate second-messenger cascades which end up in the activation of G-protein-activated, inwardly rectifying K^+ channels (32, 37, 38). The case of $GABA_B$ receptors might be controversial, since *in vitro* experiments have shown that young rodents express very little $GABA_B$ postsynaptic responses in RE neurons (21). However, those experiments did not assess a critical point, that is, how much $GABA_B$ conductance is activated during thalamic oscillations when large populations of neurons fire in synchrony (13, 18). And, experiments in ferret slices have shown that $GABA_B$ responses to glutamate applied in the perigeniculate sector of the RE nucleus are not so small, as the rebound spike-bursts were blocked by an antagonist of $GABA_B$ receptors (39). Therefore, the possibility that the RE nucleus expresses a significant $GABA_B$ response during spindle oscillations cannot be discarded. Since we cannot determine the

precise ionic bases of prolonged hyperpolarizations preceding spindles in RE neurons, we suggest that at least some of the above-mentioned receptors for GABA, somatostatin and neuropeptide Y may trigger these hyperpolarizations.

Experimental evidence and computational models have shown that soma and dendrites of RE neurons are electrically compartmentalized (40) and, because the RE-cells' soma must be strongly hyperpolarized to generate LTSs (41), the T-current is located in dendrites (16, 40). A similar reasoning suggests that the hyperpolarizations preceding spindles may have a dendritic origin, since in some cases strong soma depolarization did not increase their amplitude but abolished them, leaving instead a low-frequency discharge period (not shown). Indeed, G-protein-activated, inwardly rectifying K^+ channels (31) may mediate dendritic hyperpolarizations (34).

The simultaneous intra- and extracellular recordings in the present experiments demonstrated that some RE neurons fire spike-bursts that were temporally related to the hyperpolarizations in adjacent neurons. These data suggest that some hyperpolarizations leading to spindles are generated within the RE nucleus. Since corticothalamic excitatory volleys could also elicit such hyperpolarizations and knowing the propensity of cortex to evoke spindling (12, 13, 18), we propose that firing in some cortical neuronal pools may excite RE neurons, generating EPSPs and in some cases LTSs crowned by spike-bursts, which would generate prolonged hyperpolarizations in adjacent and/or distant RE neurons. There is indeed evidence for both dendrodendritic (10, 11) and axoaxonic synapses (42), which mediate inhibitory interactions in the RE nucleus (25, 39).

In sum, the present demonstration of prolonged hyperpolarizations leading to spindles and generated locally in the RE nucleus is in keeping with the proposal that spindles are initiated in the pacemaking RE nucleus (2, 7, 43).

REFERENCES

1. Steriade, M., Deschênes, M., Domich, L. & Mulle, C. (1985) *J. Neurophysiol.* **54**, 1473-1497.

2. Steriade, M., Domich, L., Oakson, G. & Deschênes, M. (1987) *J. Neurophysiol.* **57**, 260-273.

3. Wang, X.J. & Rinzel, J. (1993) *Neuroscience* **53**, 899-904.

4. Destexhe, A., Contreras, D., Sejnowski, T.J. & Steriade, M. (1994) *J. Neurophysiol.* **72**, 802-818.

5. Bazhenov, M., Timofeev, I., Steriade, M. & Sejnowski, T.J. (2000) *J. Neurophysiol.* **84**, 1076-1087.

6. Bazhenov, M., Timofeev, I., Steriade, M. & Sejnowski, T.J. (1999) *Nature Neurosci.* **2**, 168-174.

7. Steriade, M., McCormick, D.A. & Sejnowski, T.J. (1993) *Science* **262**, 679-685.

8. Von Krosigk, M., Bal, T. & McCormick, D.A. (1993) *Science* **261**, 361-364.

9. Bal, T., von Krosigk, M. & McCormick, D.A. (1995) *J. Physiol. (Lond)* **483**, 665-685.

10. Yen, C.T., Conley, M., Hendry, S.H.C. & Jones, E.G. (1985) *J. Neurosci.* **5**, 2254-2268.

11. Deschênes, M., Madariaga-Domich, A. & Steriade, M. (1985) *Brain Res.* **334**, 165-168.

12. Steriade, M., Wyzinski, P. & Apostol, V. (1972) In *Corticothalamic Projections and Sensorimotor Activities* (ed. T.L. Frigyesi, E. Rinvik & M.D. Yahr), pp. 221-272 (Raven Press, New York).

13. Contreras, D., Destexhe, A., Sejnowski, T.J. & Steriade, M. (1996) *Science* **274**, 771-774.

14. Llinás, R.R. (1988) *Science* **242**, 1654-1664.

15. Llinás, R.R. & Geijo-Barrientos, E. (1988) In *Cellular Thalamic Mechanisms* (ed. M. Bentivoglio and R. Spreafico), pp. 23-33 (Elsevier, Amsterdam).

16. Huguenard, J.R. (1996) *Annu. Rev. Physiol.* **58**, 329-348.

17. Gentet, L.J. & Ulrich, D. (2003) *J. Physiol. (Lond.)* **546**, 801-811.

18. Contreras, D. & Steriade, M. (1996) *J. Physiol. (Lond.)* **490**, 159-179.

19. Zhang, L. & Jones, E.G. (2004) *J. Neurophysiol.* **91**, 759-766.

20. Huguenard, J.R. & Prince, D.A. (1994) *J. Neurosci.* **14**, 5485-5502.

21. Ulrich, D. & Huguenard, J.R. (1996) *J. Physiol. (Lond.)* **493**, 845-854.

22. Steriade, M., Timofeev, I. & Grenier, F. (2001) *J. Neurophysiol.* **85**, 1969-1985.

23. Contreras, D., Timofeev, I. & Steriade, M. (1996) *J. Physiol. (Lond.)* **494**, 251-264.

24. Zhang, S.J., Huguenard, J.R. & Prince, D.A. (1997) *J. Neurophysiol.* **78**, 2280-2286.

25. Shu, Y. & McCormick, D.A. (2002) . *J. Neurophysiol.* **87**, 2571-2576.

26. Crill, W.E. (1996) *Annu. Rev. Physiol.* **58**, 349-362.

27. Talbot, M.J. & Sayer, R.J. (1996) *J. Neurophysiol.* **76**, 2120-2124.

28. Svoboda, K., Denk, W., Kleinfeld, D. & Tank, D.W. (1997) *Nature* **385**, 161-165.

29. Paré, D. & Lang, E.J. (1998) *Eur. J. Neurosci.* **10**, 3164-3170.

30. Perkins, K.L. & Wong, R.K. (1995) *J. Neurophysiol.* **73**, 911-915.

31. Andrade, R. (1991) *Eur. J. Pharmacol.* **199**, 259-262.

32. Hille, B. (1994) *Trends Neurosci.* **17**, 531-536.

33. Sun, Q.Q., Huguenard, J.R. & Prince, D.A. (2002) *J. Neurosci.* **22**, 5374-5386.

34. Sun, Q.Q., Huguenard, J.R. & Prince, D.A. (2001) *J. Physiol. (Lond.)* **531**, 67-79.

35. Graybiel, A.M. & Elde, R.P. (1983) *J. Neurosci.* **3**, 1408-1321.

36. Bendotti, C., Hohmann, Forloni, G., Reeves, R., Coyle, J.T. & Oster-Granite, M.L. (1990) *Dev. Brain Res.* **53**, 26-39.

37. Dolphin, A.C. (1998) *J. Physiol. (Lond)* **506**, 3-11.

38. Yamada, M., Inanobe, A. & Kurachi, Y. (1998) *Pharmacol. Rev.* **50**, 723-760.

39. Sanchez-Vives, M.V., Bal, T. & McCormick, D.A. (1997) *J. Neurosci.* **17**, 8894-8908.

40. Destexhe, A., Contreras, D., Steriade, M., Sejnowski, T.J. & Huguenard, J.R. (1996) *J. Neurosci.* **16**, 169-185.

41. Mulle, C, Madariaga, A. & Deschênes, M. (1986) *J. Neurosci.* **16**, 2134-2145.

42. Pinault, D., Smith, Y. & Deschênes, M. (1997) *J. Neurosci.* **17**, 3215-3233.

43. Steriade, M., Jones, E.G. & Llinás, R.R. (1990) *Thalamic Oscillations and Signaling* (Wiley-Interscience, New York).

FIGURES

Figure 6.1. Prolonged hyperpolarizing potentials (PHPs) precede spontaneous and evoked spindle oscillations. Barbiturate anesthesia in this and all subsequent figures. *A*, *top*, EEG from motor cortex (area 4) and intracellular recording of RE neuron from the rostral pole of the nucleus. Typical low-threshold spike-burst of RE cell expanded in inset. *Below left*, superimposition of PHPs (n = 5) shows constant activation phase followed by irregular late phase, frequently leading to rebound activities (*arrowhead*). *Below right*, averaged PHPs (n = 20). Activation phase (first 100 ms) was fitted with a monoexponential function (τ = 36 ms). *B*, *left*, another RE neuron depolarized by steady current injection (+0.5 nA) and displaying spontaneous PHPs. PHPs hyperpolarized V_m to -72 mV, were LTSs could be generated and spindles initiated. *Right*, expanded epochs showing PHPs. Triangles point to the onset of LTS responses. Traces are displaced for clarity. *C*, *left*, superimposed traces (n = 3) showing responses to stimulation of cortical area 4 (same neuron as in *A*). In all cases a sequence of EPSP-PHP-spindle was generated. *Right top*, average (n = 10) of early responses to cortical stimuli applied at resting V_m. *Right bottom*, time-evolution of R_{in} during PHP. Each point represents the slope of linear fitting to the V_m-DC relation calculated for each time point in the graphic**.** In this and subsequent figures, asterisks mark PHPs.

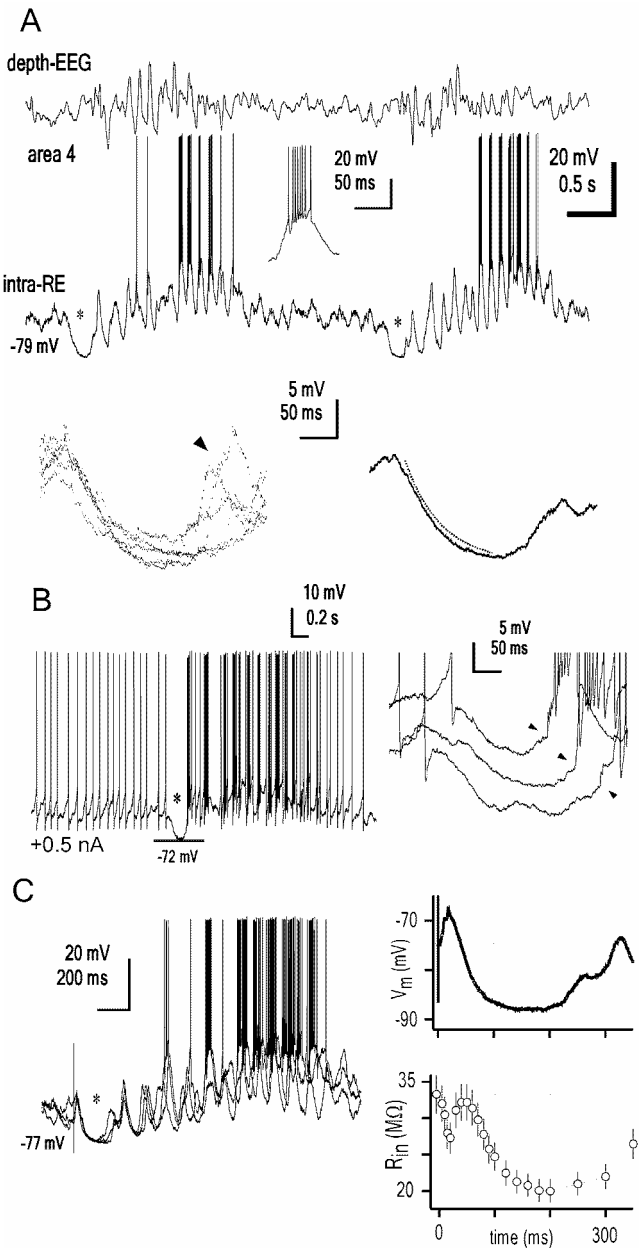
A
depth-EEG
area 4
20 mV
50 ms
20 mV
0.5 s
intra-RE
-79 mV
5 mV
50 ms
B
10 mV
0.2 s
5 mV
50 ms
+0.5 nA
-72 mV
C
20 mV
200 ms
-77 mV
-70
-90
Vm (mV)
35
20
Rin (MΩ)
0
time (ms)
300

Figure 6.2. Voltage dependency of spontaneous PHPs is consistent with a K^+ conductance. RE neuron displaying PHP and held at different V_m values by current injection in the pipette. *A* shows spindles and *B* shows expanded PHPs for the same periods. Values of injected current are indicated in *B*. *C*, estimation of the reversal potential (V_{rev}) for spontaneous (*left*) and evoked (*right*) PHP for various neurons (n = 5 in each plot). Solid line represents a linear fitting which predicts a V_{rev} of -103 mV and -101 mV for spontaneous and evoked PHPs, respectively.

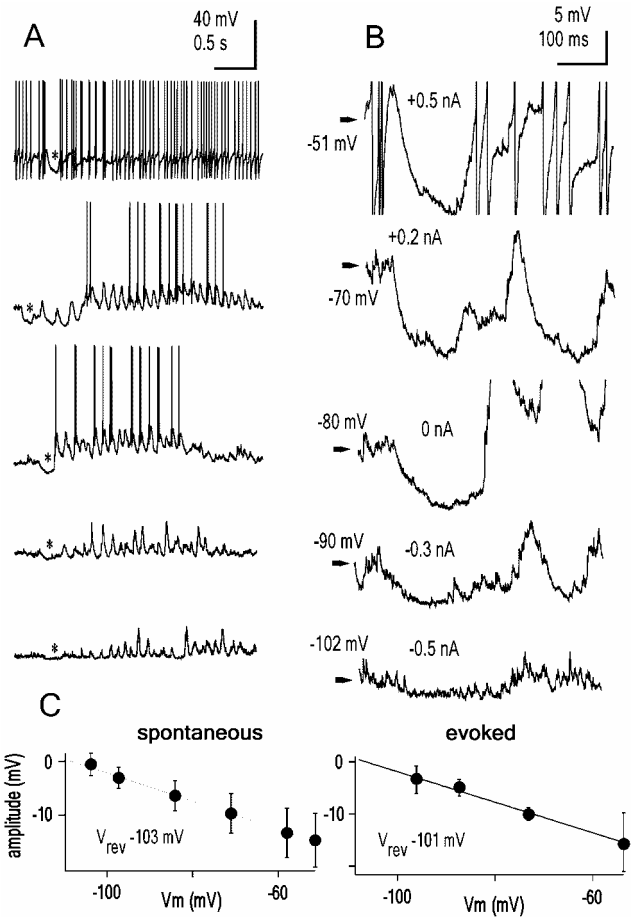
A
40 mV
0.5 s
B
5 mV
100 ms
+0.5 nA
-51 mV
+0.2 nA
-70 mV
-80 mV
0 nA
-90 mV
-0.3 nA
-102 mV
-0.5 nA
C
spontaneous
evoked
amplitude (mV)
0
-10
V_rev -103 mV
V_rev -101 mV
-100
Vm (mV)
-60

Figure 6.3. QX-314 decreased both the amplitude and incidence of PHPs. *A*, RE neuron recorded under QX-314 (50 mM). During the first 5 min (control), spikes and PHP displayed normal amplitudes, which decreased after 45 min (QX-314). *B*, superimposed PHPs (n = 6) from the neuron illustrated in *A*, in both conditions. *C*, averages (n = 10) from PHPs at the beginning (control) and towards the end (QX-314) of the recording. *D*, amplitude and incidence of PHPs for both conditions. ** $p<0.05$.

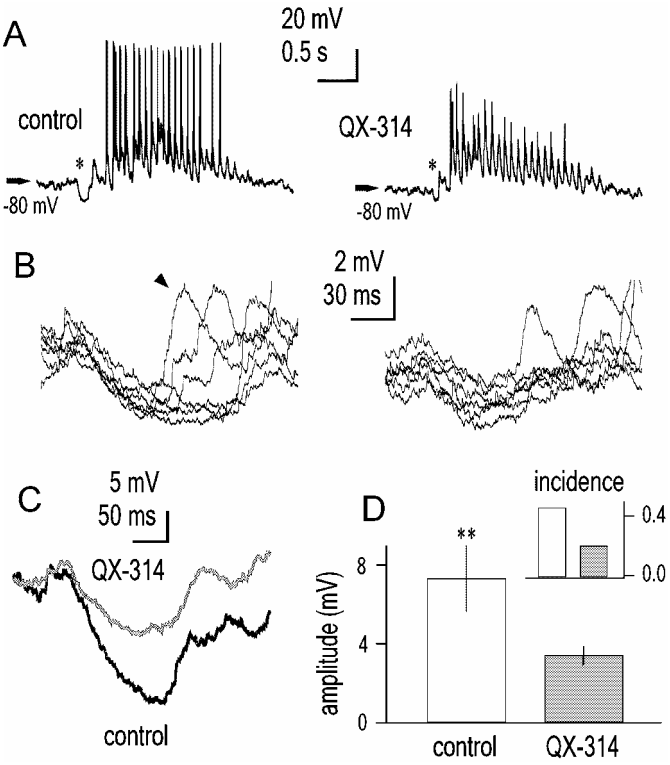
A
20 mV
0.5 s
control
QX-314
*
*
-80 mV
-80 mV
B
2 mV
30 ms
C
5 mV
50 ms
QX-314
control
D
incidence
0.4
0.0
**
8
4
0
amplitude (mV)
control
QX-314

Figure 6.4. Cortically evoked EPSP may precede PHPs. *A*, RE neuron depolarized by steady current injection (+0.5 nA) displayed single, tonic spikes preceding PHPs. *Left column* shows intracellular spindle and *right column* depicts three superimposed PHPs expanded. *B*, spontaneous fluctuations in V_m showed an EPSP (underlying single spike, as in *A*) when the cell was slightly hyperpolarized. *C*, corticothalamic stimulation could mimic the spontaneous sequence EPSP-PHP-spindle. *D*, summary for the recorded RE neurons displaying PHPs (n =10). *Left bars* indicate the proportion of spindles in each neuron which displayed PHPs (PHP, 57.2 ± 16.7%) and *right bars* depict fraction of those PHPs preceded by putative EPSPs (EPSP, 31.6 ± 18.4%). For each cell, the fraction was calculated from 30-to-50 spindle oscillations. Note that evoked spindles are always preceded by PHPs and EPSPs.

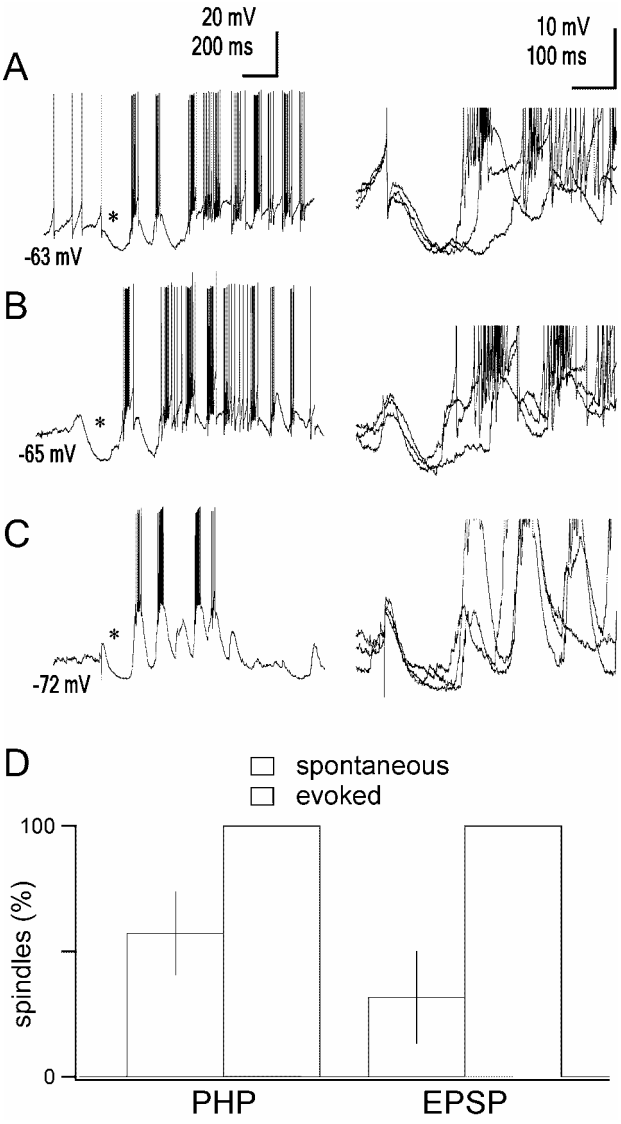
A
20 mV
200 ms
10 mV
100 ms
-63 mV
B
-65 mV
C
-72 mV
D
spontaneous
evoked
100
spindles (%)
0
PHP
EPSP

Figure 6.5. Distant RE neurons discharge during PHPs. *A*, simultaneous recording of intracellular (intra-cell) and extracellular (multi-unit) activities in the RE nucleus. Extracellular electrode was located ~1 mm anterior to the intracellular electrode. Note the presence of two units in the extracellular recording (*a* and *b*). *B*, expanded traces from epochs in *A*, indicated by arrows. *Left panel* displays the first spindle sequence in *A* for both intra- and extracellular recordings. Note discharge of one unit (*a*) during PHP, preceding spindles. *Right panel* depicts the last spindle sequence in *A*. Note the second unit (*b*) firing during PHP. Bottom traces depict typical accelerando-decelerando burst for both units, which identify them as RE neurons. *C*, autocorrelograms and crosscorrelograms of action potentials for intracellular and extracellular recordings. Bin size, 1 ms and 5 ms, for autocorrelograms and crosscorrelograms; respectively. *D*, five superimposed traces showing PHPs (*left*) and correlated discharge in both units for the same period (*right*). Time zero was set at the peak of depolarizing potentials preceding PHPs. Binsize = 10 ms.

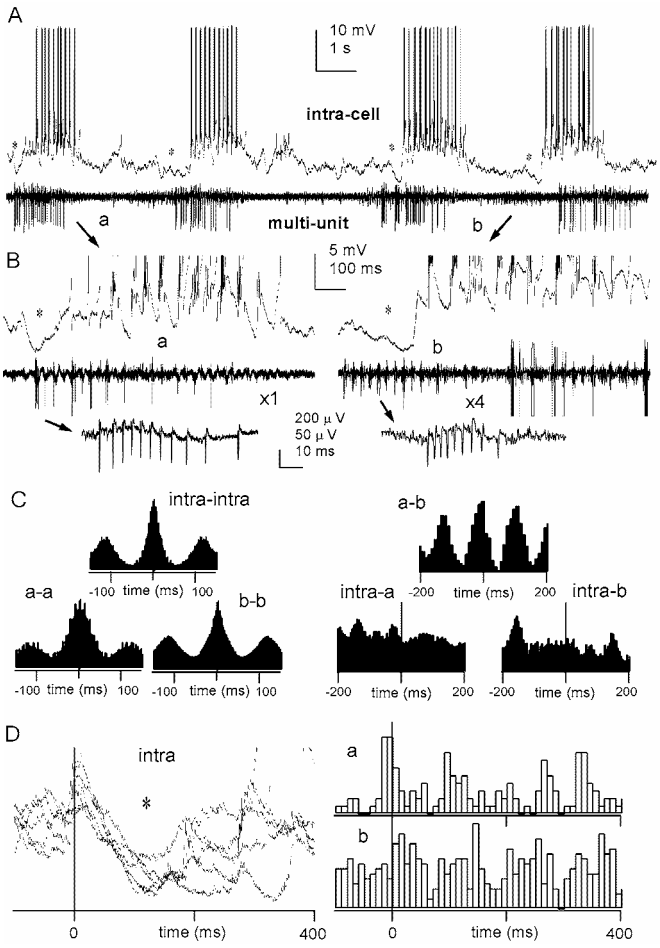
A
10 mV
1 s
intra-cell
multi-unit
a
b
B
5 mV
100 ms
a
b
x1
x4
200 µ V
50 µ V
10 ms
C
intra-intra
-100 time (ms) 100
a-a
b-b
-100 time (ms) 100
-100 time (ms) 100
a-b
-200 time (ms) 200
intra-a
intra-b
-200 time (ms) 200
-200 time (ms) 200
D
intra
0
time (ms)
400
a
b
0
time (ms)
400

7. Neuronal Integration of Synaptic Inputs in the Cortex

SYNAPTIC INTERACTIONS BETWEEN THALAMIC AND CORTICAL INPUTS ONTO CORTICAL NEURONS *IN VIVO*

Pablo Fuentealba, Sylvain Crochet, Igor Timofeev, and Mircea Steriade (2004) *Journal of Neurophysiology* 91:1990-1998.

RESUMÉ

Afin d'étudier les interactions entre les entrées thalamiques et corticales sur les neurones néocorticaux, nous avons utilisé des stimulations en paire de pulses (PPS) des entrées thalamiques et corticales qui convergeaient sur les neurones corticaux et thalamiques enregistrés intracellulairement sur des chats anesthésiés. Les PPS sur des voies homosynaptiques cortico-corticales produisaient une facilitation, une dépression ou aucun effet significatif, tandis que les réponses corticales aux entrées thalamocorticales étaient principalement facilitées. À l'opposé, les interactions hétérosynaptiques, produisaient généralement une diminution dans l'amplitude du pic et une aire de dépolarisation de l'EPSPs provoqué, avec un effet maximal à ~10 ms et durant de 60 ms à 100 ms. Tous les neurones testés par un stimulus thalamique suivit d'un stimulus cortical ont montré une diminution de la résistance d'entrée apparente (R_{in}), laquelle a suivit un temps de course en parallèle avec la diminution de la réponse, ce qui suggère que le drainage (*shunting*) est le facteur responsable de la diminution de l'EPSP. Seulement la moitié des neurones testés par un stimulus cortical suivit d'un stimulus thalamique ont montré un changement dans la R_{in}. Le drainage d'une décharge dans le thalamus pourrait compter pour ces cas dans lesquels la diminution de la réponse synaptique des neurones corticaux n'était pas associée à une diminution de la R_{in}, puisque les neurones thalamocorticaux montraient une diminution de la probabilité de décharges pendant la stimulation corticale. Ces résultats suggèrent un drainage de courte durée, mais forte intensité, entre les entrées thalamocorticales et corticales sur les neurones corticaux.

ABSTRACT

To study the interactions between thalamic and cortical inputs onto neocortical neurons, we used paired-pulse stimulation (PPS) of thalamic and cortical inputs as well as PPS of two cortical or two thalamic inputs that converged, at different time-intervals, onto intracellularly recorded cortical and thalamocortical neurons in anesthetized cats. PPS of homosynaptic cortico-cortical pathways produced facilitation, depression or no significant effects in cortical pathways, whereas cortical responses to thalamocortical inputs were mostly facilitated at both short and long intervals. By contrast, heterosynaptic interactions between either cortical and thalamic, or thalamic and cortical, inputs generally produced decreases in the peak amplitudes and depolarization area of evoked EPSPs, with maximal effect at ~10 ms and lasting from 60 ms to 100 ms. All neurons tested with thalamic followed by cortical stimuli showed a decrease in the apparent input resistance (R_{in}), whose time-course paralleled that of decreased responses, suggesting that shunting is the factor accounting for EPSP's decrease. Only half of neurons tested with cortical followed by thalamic stimuli displayed changes in R_{in}. Spike shunting in the thalamus may account for those cases in which decreased synaptic responsiveness of cortical neurons was not associated with decreased R_{in}, since thalamocortical neurons showed decreased firing probability during cortical stimulation. These results suggest a short-lasting but strong shunting between thalamocortical and cortical inputs onto cortical neurons.

INTRODUCTION

Each neocortical neuron receives inputs from multiple presynaptic sources, integrates them, and generates an output that is transmitted to other neuronal populations. The major inputs of neocortical neurons arise from other neocortical neurons and thalamic nuclei. Synchronous presynaptic inputs evoke excitatory and/or inhibitory postsynaptic potentials (EPSPs and IPSPs, respectively), whose amplitudes depend on multiple factors. *(a)* Intrinsic neuronal properties may modify the synaptic efficacy, as shown by amplification or reduction of EPSPs and IPSPs exerted by some ionic currents (Crill 1996; Llinás 1988; Marder, 1998; Stuart and Sakmann 1995). *(b)* Rhythmic synaptic volleys of neocortical origin produce frequency-dependent facilitation or depression (Buhl et al. 1997; Gupta et al. 2000; Markram et al. 1998; Reyes and Sakmann 1999; Thomson and Bannister 2003), whereas thalamic afferents generally depress (Gil et al. 1997, 1999). *(c)* Among the multiple extracellular factors that may affect responsiveness of postsynaptic neurons, the extracellular Ca^{2+} concentration is not stable (Massimini and Amzica, 2001) and its modifications influence synaptic efficacy. *(d)* The state of the thalamocortical network also contributes to the modulation of PSPs. Generally, states associated with membrane depolarization in anesthetized preparations are accompanied by low input resistance (R_{in}), which decreases PSPs due to the shunting effects associated with network activities (Borg-Graham et al. 1998; Contreras et al. 1996; Hirsch et al. 1998; Paré et al. 1998); however, in chronically implanted animals, the R_{in} is stable and increased during quiet waking (Steriade et al. 2001), probably due to

the enhanced release of some neuromodulators, among them acetylcholine that blocks K^+ conductances (Krnjević et al. 1971; McCormick 1992).

The effects of paired-pulse stimulation (PPS) on responsiveness of cortical neurons have been intensively studied *in vitro*. Most studies have been performed in slices from CA1-CA3 hippocampal fields (Bi and Poo 1999; Kamiya et al. 2002; Magee 2000). Fewer *in vitro* studies have been devoted to neocortex, using PPS in pathways from infragranular to supragranular layers, from layer IV to layer III in slices from the somatosensory cortex (Castro-Alamancos and Connors 1997), or recording layer III responses to white matter stimulation in visual cortex slices (Kirkwood et al. 1999). While *in vitro* studies on homosynaptic hippocampal pathways generally reported strong facilitation, data resulting from PPS in homosynaptic neocortical pathways reported depression (Volgushev et al. 1996) that was ascribed to a high probability of release in the majority of neocortical synapses (Castro-Alamancos and Connors 1997).

In the present study, we used intracellular recordings of neocortical neurons *in vivo* and investigated the effects of PPS in *heterosynaptic* pathways to determine the effects of convergence between single thalamic and cortical inputs onto target cortical and thalamic neurons. We also compared these effects to those exerted by interactions in *homosynaptic* (corticocortical and thalamocortical) pathways. The results show that, in contrast to the strong facilitation obtained with stimulation of homosynaptic thalamocortical pathways, shunting is the major effect by interacting thalamic with

cortical stimuli, being associated with both decreased input resistance and disfacilitatory mechanisms.

METHODS

Experiments were conducted on 35 adult cats, under anesthesia with pentobarbital (35 mg/kg, i.p.).

Preparation

The animals were paralyzed with gallamine triethiodide after the EEG showed typical signs of deep anesthesia, consisting of rhythmic sequences of spindle waves (7-14 Hz). Supplementary doses of anesthetics were administered at the slightest changes toward activated EEG patterns. The cats were ventilated artificially with the control of end-tidal CO_2 at 3.5-3.7%. The body temperature was maintained at 37-38^{o} C and the heart rate was ~90-100 beats/min. Stability of intracellular recordings was ensured by the drainage of cisterna magna, hip suspension, bilateral pneumothorax, and filling the hole made for recordings with a solution of 4% agar.

Recording and stimulation

Intracellular recordings from cortical suprasylvian association areas 5/7, cortical pericruciate motor areas 4/6, and thalamic ventrolateral (VL) nucleus, were performed using glass micropipettes filled with a solution of 3 M potassium-acetate. For thalamic recordings in VL nucleus, the middle suprasylvian gyrus was removed. A high-impedance amplifier with active bridge circuitry was used to record the membrane potential (V_m) and inject current into the neurons. Field potentials were recorded in the vicinity of impaled neurons, using coaxial electrodes with the tip (cortical depth) at ~0.8-

1 mm. For cortical stimulation, electrodes (similar to those used for field potential recordings) were inserted into the same area from which recordings were performed, while thalamic electrodes were inserted in appropriate nuclei (lateroposterior, LP, for recordings in areas 5/7; and VL for recordings in areas 4/6). In all cases, low intensity stimuli (50-200 μA) at frequencies of 0.33-to-1 Hz were used. The paired-pulse protocol was employed at intervals of 5-to-200 ms, generally in increments of 10 ms**.** For the paired-pulse protocol, the first pulse was considered the conditioned stimulus (*CS*) and the second one the testing stimulus (*TS*), which evoked a conditioned response (*CR*) and a testing response (*TR*), respectively. Most results are expressed as mean ± SD.

At the end of experiments, the cats were given a lethal dose of pentobarbital.

Data analysis

*Estimation of R_{in}***.** Synaptic responses evoked by either cortical (*Cx*) or thalamic (*Th*) stimulation were recorded under different levels of membrane polarization, obtained by current injection through the pipette (from –1 to +1 nA steady current). V_m was plotted against different levels of DC injected. Plots were made for multiple time intervals, in increments of 10 ms, after and before stimulation onset. For each plot, a linear function was fitted, whose slope was considered to be the apparent R_{in} for that particular time interval. This general method is exemplified in Fig. 7.2*C*, where the *CS* was a cortical stimulus. Responses were recorded under three different levels of membrane polarization (0 nA -81 mV, under +0.5 nA, and under -0.5 nA). Next, a V_m vs. DC plot was made for each of the following time intervals in reference to stimulation onset: -5 ms, 10 ms, 30 ms, 50 ms, 80 ms, 110 ms, 140 ms, 170 ms and 200 ms. The

slope of the linear fitting in each plot represented the apparent R_{in} for the corresponding time interval. All values were normalized to the first one (-5 ms), considered as control.

EPSP's amplitude. Amplitude was calculated as the difference between the value of V_m taken at 1 ms before the onset of stimulation and the peak of the response. Before starting the paired-pulse protocol, individual responses were characterized in their voltage dependence by steady current injection in the recording pipette, as stimulation continued (see Fig. 7.2*A*-*B*). A plot of amplitude vs. V_m was built for each response. In most cases, a linear function was well fitted to the plot, allowing an estimation of the V_{rev} for the recorded responses. Points belonging to the linear fitting were considered to be the "expected amplitude", since they indicate the theoretical amplitude that a response would present at a given V_m value. Later, the paired-pulse protocol was applied and measurements of amplitude were performed for the second *CR*. In such cases, the amplitude was measured by subtraction of the control *CR* (Fig. 7.4). In cases where subtraction was not possible, as in the presence of antidromic responses (Fig. 7.6), the amplitude was calculated from 1 ms before the onset of stimulation up to the peak of the response, as it was done for individual, control responses. Amplitude values obtained in such conditions were considered "measured amplitude". Finally, amplitude values were compared between those obtained during the paired-pulse protocol (measured) and those estimated from the linear fitting of individual responses (expected). In such way, amplitude values were corrected by V_m and not simply averaged, since amplitude was dependent on V_m. (Fig. 7.2*B*).

Depolarization area of the response. Area was considered as the integral of the response, from 1 ms before the onset of stimulation up to the time were V_m recovered the same value as before the onset of stimulation. Area was considered as "expected" and "measured", with the same criteria used for the amplitude. During paired-pulse protocol, area of the *CR* was obtained by subtraction of the control *CR*. In cases where subtraction was not possible, as in the presence of antidromic responses (Fig. 7.6), area was calculated from 1 ms before the onset of stimulation up to the time were V_m recovered the same value as before the onset of stimulation.

RESULTS

Database and neuronal identification

Out of over 120 neurons recorded intracellularly, we retained for analysis 43 neurons that could be investigated during long-term recordings (40 to 150 min), which allowed repeated applications (>30 in most cases) of conditioning stimuli (*CS*) and testing stimuli (*TS*) to neocortex and thalamus at different time-intervals. Of those 43 neurons, 31 were located in cortical areas 5/7, 6 in cortical areas 4/6, and 6 in the thalamic VL nucleus.

Cortical and thalamic neurons were identified by antidromic and synaptic activation. In all cases, recorded neurons were driven by thalamic and cortical inputs, which allowed the study of interactions between such inputs. Stimulation intensity was adjusted to avoid composite responses; thus, mostly monosynaptic EPSPs were investigated. Figure 7.1 depicts responses of a cortical area 7 neuron, driven by both thalamic and cortical inputs. Local (area 7) cortical stimulation evoked a short-latency, monosynaptic EPSP (Fig. 7.1*A*). Stimulation of thalamic LP nucleus elicited a short-latency, monosynaptic EPSP with similar characteristics (amplitude and duration) as the cortically evoked one (Fig. 7.1*B*). All recordings presented here were performed on electrophysiologically identified regular-spiking (RS) or intrinsically-bursting (IB) neurons. Some cortical neurons (7 of 37) were identified as corticothalamic by antidromic invasion from thalamic nuclei (see Fig. 7.6).

Thalamically evoked EPSPs and cortically evoked IPSPs could be detected in the same neuron (Fig. 7.2*A*). For each recorded neuron we estimated the voltage-current relations for EPSPs and IPSPs, from which we anticipated the reversal potential and the expected amplitude at each given level of the V_m (Fig. 7.2*B*). These values were used to compare the expected value of the evoked response with that obtained when *TS* was preceded by *CS*. Local cortical stimulation evoked an IPSPs in some cortical neurons that was always associated with a drop in R_{in}, lasting from 100 ms to 200 ms. Thalamic stimuli occasionally elicited a compound, slow depolarization that followed the early EPSP with a latency of ~ 20 ms (not shown). Such late components could result from feedback activation of recurrent axons and those cases were not considered for analysis in order to avoid additional variables in the analysis of interacting inputs.

Homosynaptic interactions of cortical or thalamic synaptic inputs onto cortical neurons

Cortically evoked EPSPs displayed a variety of results when stimuli were paired. In some cases (22%, 2 of 9 neurons), *CS* or *TS* paired at time intervals of 10 to 20 ms (i.e. 100 and 50 Hz) produced EPSP facilitation ranging from 15% to 25% (Fig. 7.3*A*). In other cases (33%, 3 of 9), the paired-pulse protocol induced a moderate depression (~30%) in EPSP's amplitude, while the remaining cases (44%, 4 of 9) showed no change at any time-interval (not shown). Interaction between cortical inputs occurred during a narrow time-window, since after 50 ms the response had recovered control values (plot in Fig. 7.3*A*). Generally, cortico-cortical responses were monosynaptic, as revealed by their

short and stable latencies (1.8 ± 0.5 ms, n = 10) as well as time to peak (8.0 ± 3.2 ms, n = 10).

On the other hand, the facilitation of the second response elicited by paired thalamocortical volleys was maximal at time intervals of 60 to 100 ms, but this potentiation affected the second component of the biphasic EPSP, whereas the early EPSP was diminished (Fig. 7.3*B*). While the early EPSP (arrowhead, *a*, in Fig. 7.3*B*) was of short latency (3.5 ± 1 ms) and the time to peak was 8.8 ± 1.1 ms, the second EPSP (arrowhead, *b*, in Fig. 7.3*B*) had longer latency and prolonged time to peak (18.4 ± 0.9 ms). It is known that the second component follows by ~3 ms the low-threshold spike-bursts in thalamocortical neurons during augmenting responses elicited by rhythmic stimuli at 7-15 Hz (Steriade et al., 1998).

Interactions between cortical and thalamic synaptic inputs onto cortical neurons

In 90% of cases, and contrasting with data on homosynaptic facilitation, synaptic responses were decreased by interacting cortical with thalamic stimuli that elicited EPSPs in target cortical cells. Thus, 18 of 20 neurons tested with cortical *CS* preceding thalamic *TS* at different interstimuli intervals (ISIs) showed decreased EPSPs (the remaining 2 neurons did not display changes in EPSPs' amplitudes). And, 15 of 17 neurons tested with the reversed interaction, namely, thalamic *CS* preceding cortical *TS*, similarly exhibited decreased synaptic excitability (one neuron showed facilitation and the excitability of the remaining one was unaffected).

Figure 7.4 illustrates typical examples of such interactions in two cortical neurons from area 4. The two plots in Fig. 7.5 show pooled responses resulting from cortical-thalamic and thalamic-cortical *CS-TS* interactions in ten cortical neurons. Changes in synaptic responses were determined by measuring the amplitudes and area of depolarization of EPSPs (see Fig. 7.4*A*). The neuron depicted in Fig. 7.4*A*, with *CS-TS* trials between cortical and thalamic volleys delivered at ISIs between 10 ms and 120 ms, showed slightly more than 40% decrease in EPSP's amplitude at 10 ms and progressively lower values of reduced response, until recovery took place at 120 ms. The area of depolarization showed a similar curve, while full recovery occurred earlier, at ~80 ms. Testing with reversed stimuli (Fig. 7.4*B*), namely, *CS-TS* trials between thalamic and cortical stimuli, showed that maximal reduction in the cortically-evoked EPSP was at an ISI of 20 ms and recovery took place at ~70 ms, while the evolution of changes in the depolarization area was quasi-identical to that shown in the above panel (Fig. 7.4*A*). These changes are supported by changes in EPSPs' amplitude and depolarization area, resulting from pooled neuronal responses (n = 10) with the two types of *CS-TS* trials, cortical and thalamic as well as thalamic and cortical (Fig. 7.5).

Relations between decreased responses in heterosynaptic interactions and changes in input resistance

In 15 neurons, we examined the relations between changes in synaptic excitability during PPS and the apparent R_{in}. All five neurons tested with thalamic-cortical paired stimuli showed a decreased R_{in}, whose temporal evolution matched the depressed amplitudes of EPSPs evoked by the cortical *TS*. On the other hand, in five of ten neurons

tested with cortical-thalamic paired stimuli decreased R_{in} was observed, whereas the decreased amplitude and depolarization area of thalamically evoked EPSPs were the same as mentioned in the above section. These data are exemplified below.

Figure 7.6 depicts a corticothalamic neuron that displayed, after antidromic invasion by stimulating the thalamus (see expanded identification in inset of panel *A*), EPSPs that occasionally triggered action potentials. In the same neuron, cortical stimulation elicited EPSPs. The amplitude of cortical (*TS*)-evoked EPSP underwent maximal decrease at an interval of 10 ms and fully recovered at 50 ms following the *CS* delivered to the thalamic LP nucleus. The changes in R_{in} paralleled that of EPSP's decrease. Virtually identical aspects were seen in the other 4 neurons investigated with thalamic-cortical paired stimuli.

One of the 5 neurons in which the reversed interaction (cortical-thalamic) was used and the decreased EPSP's amplitude was *not* associated with diminished R_{in} is shown in Fig. 7.7. Although the decreased amplitude and depolarization area of the thalamic-evoked EPSP was comparable to that seen in the preceding figure, no concomitant changes in R_{in} were detected in this and the other 4 neurons belonging to the same category.

Cortical stimulation decreases firing in thalamic relay cells and induces disfacilitation in the feedback thalamocortical pathway

Although corticothalamic projections use glutamate as neurotransmitter that excites both thalamic reticular and thalamocortical neurons, electrical stimuli applied to neocortex or naturally synchronous volleys fired by cortical neurons during slow-wave sleep give rise to powerful excitation in GABAergic reticular neurons that, in turn, produces overwhelming inhibition of target thalamocortical neurons, associated with rhythmic IPSP-rebound spindle sequence (see Fig. 1 in Steriade 2000). We investigated the effects of corticothalamic volleys on thalamocortical neurons (n = 6) for possible answers to the question of decreased synaptic responses in the cortex, in the absence of changes in R_{in} (see Fig. 7.8).

The intrinsic excitability of thalamocortical neuron and the effect of corticothalamic volleys on its firing ability are illustrated in Figure 7.8. The inset in panel *A* shows two of the major intrinsic properties of such neurons: hyperpolarizing current steps produced a depolarizing sag leading to a low-threshold spike-burst (reviewed in Chapter 5 of Steriade et al. 1997). The cortical stimulus induced an early excitation, followed by slight but long-lasting (90 ms) hyperpolarization associated with silenced firing, while thalamic stimulus produced early synaptic excitation giving rise to action potentials (panels *A*-*B*). Preceding thalamic by cortical volleys at different ISIs led to 50-60% reduction in the firing probability of thalamocortical neuron, which lasted for 40 ms and progressively recovered control values (panels *C*-*D*). The time course of the reduction in firing probability of the thalamocortical neurons was similar to the decrease of EPSPs of cortical neurons (see Figs. 7.4, 7.5 and 7.7).

Similar effects, consisting of abolishing or reduction of the firing probability of thalamocortical cells, were observed during cortical-evoked rhythmic IPSPs of spindle sequences (n = 3). However, in such instances the time course of the effect was much longer, lasting for the entire duration of the spindle sequence (Fig. 7.9). A thalamic neuron displayed antidromic activation (arrow in Fig. 7.9*A*) followed by a spindle sequence. In the same neuron, thalamic-evoked EPSPs invariably leading to single action potentials (top right panel) were transformed into subthreshold EPSPs at ISIs up to 0.8 s after the onset of the cortical-evoked spindle (Fig. 7.9*B*). The same EPSP was able to elicit a low-threshold rebound spike-burst toward the end of the spindle (ISI 1.1 s) even when the membrane potential was not significantly different, and recovered the control pattern only after cessation of spindles (ISI 1.5 s). A summary of this temporal succession is shown in Fig. 7.9*C*.

DISCUSSION

Our data show that *(a)* PPS of intracortical pathways produced a variety of results, including facilitation, depression and no change; (*b*) PPS of thalamocortical pathways produced compound responses, with the early component being depressed and the second one giving rise to incremental responses; (*c*) at variance with these results using responses in homosynaptic circuits, interactions between heterosynaptic (cortical and thalamic or thalamic and cortical volleys) produced decreased peak amplitudes and depolarization area of *TS*-evoked EPSP, with maximal effect at ~10 ms and lasting from 60 ms to 100 ms; *(d)* all neurons tested with thalamic-cortical stimuli showed decreased R_{in} whose time-course paralleled that of decreased synaptic excitability, whereas only half of neurons tested with cortical-thalamic stimuli displayed changes in R_{in}; and *(e)* firing probability of thalamic relay neurons was dramatically reduced for ~100 ms following cortical stimuli, which may induce disfacilitation in cortical networks and account for those cases in which decreased excitability was not associated with decreased R_{in}.

The present *in vivo* intracellular study was performed on cortical neurons driven by both cortical and thalamic inputs. Synaptic responses were evoked by stimulation of either cortical local areas or related thalamic nuclei. Generally, such responses were short-latency, monosynaptic EPSPs, in view of their short and invariant latency. The EPSPs evoked in cortical neurons by stimulation of cortical pathways *in vivo* or *in vitro* are commonly followed by a long-lasting inhibition, resulting from fast and inhibitory

components that have been attributed to inhibitory GABAergic neurons. In the present experiments, low-intensity stimulation allowed cortical stimuli in most cases not to engage inhibitory networks, since no IPSP activation was seen during or after the repolarizing phase of the initial EPSP (Figs. 7.1, 7.4, 7.6); even though in those cases resting conditions were quite hyperpolarized (V_m <-73 mV), identification of the response by changing the V_m showed the absence of inhibitory components in such cases. However, in other cases an EPSP-IPSP sequence was activated, characteristic of cortical networks (Fig. 7.2*C*). Thalamic volleys were efficient in triggering a simple or composite EPSP, which was commonly followed by a rebound after 100-150 ms (Fig. 7.3*B*) that could occasionally develop into a spindle sequence. However, the time scale of that process (>100 ms) was very different from the short time reported here for interactions between *CR* and *TR*.

Facilitation or depression of cortical synaptic responses are thought to be due to calcium-dependent changes in the probability of transmitter release, observed at both excitatory and inhibitory synapses (Fisher et al., 1997; Zucker, 1999). In the present study, PPS of intracortical pathways induced a variety of results, including facilitation, depression or no change that can be explained in terms the heterogeneous of release probability at involved synapses in the cortex. In fact, it has been proposed that the release factor is the main determining factor for the direction of short-term plasticity, synapses with low release probability displaying predominantly facilitation and high probability synapses exhibiting predominantly depression (Thomson, 2000; Thomson et al., 1995). The main result of PPS in thalamocortical pathway was depression of the

initial component of EPSP, which may be similar to the heterosynaptic effect produced by conditioning thalamic volleys on cortically evoked responses. On the other hand, a progressive and higher facilitation was seen at time-intervals longer than 60 ms, which are explained by the mechanism of thalamocortical augmenting responses (Steriade et al. 1998). In fact, the results presented here showed for all cortical neurons stimulated from thalamic pathways maximal amplitude of the second EPSP at ~100 ms (105 ± 15 ms), consistent with stimulation within the frequency (10 Hz) of spindles, which is typically used for induced augmenting potentials. Rhythmic volleys produce augmenting responses during the pulse-trains but also facilitation outlasting the stimulation period, and the self-sustained activity displays patterns and frequencies similar to those of evoked responses, reminiscent of "memory" processes in thalamocortical neuronal loops (Steriade 1999). Our results partially corroborate those in experiments with homosynaptic PPS visual cortex slices, in which however depressed EPSPs were only elicited by stimuli that presumably elicited single-axon EPSPs, but not with larger EPSPs that were facilitated by PPS (Volgushev et al., 1995).

While the majority of tested cortical neurons displayed the expected reduction in R_{in} that was associated with the depressed synaptic excitability, some thalamic neurons did not show such a decrease in R_{in}. In those cases, their disfacilitation could be invoked as cortical *CS* produced IPSPs in some cortical neurons that stopped firing and, consequently, no longer excited target thalamic relay neurons, thus creating a period of disfacilitation. This interpretation is congruent with our previous studies (Bazhenov et al. 1998; Timofeev et al. 1996; Timofeev and Steriade 1997) in which low intensity

prethalamic stimuli were unable to induce firing of thalamocortical neurons during periods of disfacilitation.

The present results have functional implications for understanding information processing during sensation of multiple qualities of the same object. In the visual system, the processing of one quality of information significantly diminishes or might even be lost if another quality of sensory information is simultaneously processed (Hillis et al. 2002). Our data suggest that the primary source for that loss of information processing is due to active inhibition followed by a period of disfacilitation, and both these processes decrease the network ability to respond to incoming excitatory signals. It is likely that similar mechanisms would provide the neuronal basis for contrast discrimination and other phenomena involving responses of a large neuronal network.

REFERENCES

Bazhenov M, Timofeev I, Steriade M, and Sejnowski TJ. Computational models of thalamocortical augmenting responses. *J Neurosci* 18: 6444-6465, 1998.

Bi GQ and Poo MM. Distributed synaptic modification in neural networks induced by patterned stimulation. *Nature* 401: 792-796, 1999.

Borg-Graham LJ, Monier C, and Fregnac Y. Visual input evokes transient and strong shunting inhibition in visual cortical neurons. *Nature* 393: 369-373, 1998.

Buhl EH, Tamás G, Szilagyi T, Stricker C, Paulsen O, and Somogyi P. Effect, number and location of synapses made by single pyramidal cells onto aspiny interneurones of cat visual cortex. *J Physiol* 500: 689-713, 1997.

Castro-Alamancos MA and Connors BW. Distinct forms of short-term plasticity at excitatory synapses of hippocampus and neocortex. *Proc Natl Acad Sci USA* 94: 4161-4166, 1997.

Contreras D, Timofeev I, and Steriade M. Mechanisms of long-lasting hyperpolarizations underlying slow sleep oscillations in cat corticothalamic networks. *J Physiol* 494: 251-264, 1996.

Crill WE. (1996) Persistent sodium current in mammalian central neurons. *Ann Rev Physiol* 58: 349-362, 1996.

Fisher SA, Fisher TM, and Carew TJ. Multiple overlapping processes underlying short-term synaptic enhancement. *Trends Neurosci* 20: 170-177, 1997.

Gil Z, Connors BW, and Amitai Y. Differential regulation of neocortical synapses by neuromodulators and activity. *Neuron* 19: 679-686, 1997.

Gil Z, Connors BW, and Amitai Y. Efficacy of thalamocortical and intracortical synaptic connections: quanta, innervation, and reliability. *Neuron* 23: 385-397, 1999.

Gupta A, Wang Y, and Markram H. Organizing principles for a diversity of GABAergic interneurons and synapses in the neocortex. *Science* 287: 273-278, 2000.

Hillis JM, Ernst MO, Banks MS, and Landy MS. Comining sensory information: mandatory fusion within, but not between, senses. *Science* 298: 1627-1630, 2002.

Hirsch JA, Alonso JM, Reid RC, and Martinez LM. Synaptic integration in striate cortical simple cells. *J Neurosci* 18: 9517-9528, 1998.

Kamiya H, Ozawa S, and Manabe T. Kainate receptor-dependent short-term plasticity of presynaptic Ca^{2+} influx at the hippocampal mossy fiber synapses. *J Neurosci* 22: 9237-9243, 2002.

Kirkwood A, Rozas C, Kirkwood J, Perez F, Bear MF. Modulation of long-term synaptic depression in visual cortex by acetylcholine and norepinephrine. *J Neurosci* 19: 1599-1609, 1999.

Krnjević K, Pumain R, and Renaud L. The mechanisms of excitation by acetylcholine in the cerebral cortex. *J Physiol* 215: 247-268, 1971.

Llinás RR. The intrinsic electrophysiological properties of mammalian neurons: insights into central nervous system function. *Science* 242: 1654-1664, 1988.

Magee JC. Dendritic integration of excitatory synaptic input. *Nat Rev Neurosci* 1: 181-190, 2000.

Marder E. From biophysics to models of network function. *Annu Rev Neurosci* 21: 25-45, 1998.

Markram H, Wang Y, and Tsodyks M. Differential signaling via the same axon of neocortical pyramidal neurons. *Proc Natl Acad Sci USA* 95: 5323-5328, 1998.

Massimini M and Amzica F. Extracellular calcium fluctuations and intracellular potentials in the cortex during slow sleep oscillation. *J Neurophysiol* 85: 1346-1350, 2001.

Paré D, Shink E, Gaudreau H, Destexhe A, and Lang EJ. Impact of spontaneous synaptic activity on the resting properties of cat neocortical pyramidal neurons in vivo. *J Neurophysiol* 79: 1450-1460, 1998.

Reyes A and Sakmann B. Developmental switch in the short-term modification of unitary EPSPs evoked in layer 2/3 and layer 5 pyramidal neurons of rat neocortex. *J Neurosci* 19: 3827-3835, 1999.

Steriade M. Coherent oscillations and short-term plasticity in corticothalamic networks. *Trends Neurosci* 22: 337-345, 1999.

Steriade M. Corticothalamic resonance, states of vigilance and mentation. *Neuroscience* 101: 243-276, 2000.

Steriade M, Jones EG, McCormick DA. *Thalamus* (vol. 1, *Organisation and Function*). Oxford: Elsevier, 1997.

Steriade M, Timofeev I, Grenier F, and Dürmüller N. Role of thalamic and cortical neurons in augmenting responses: dual intracellular recordings *in vivo*. *J Neurosci* 18: 6425-6443, 1998.

Stuart G and Sakmann B. Amplification of EPSPs by axosomatic sodium channels in neocortical pyramidal neurons. *Neuron* 15: 1065-1076, 1995.

Thomson AM. Facilitation, augmentation and potentiation at central synapses. *Trends Neurosci* 23: 305-312, 2000.

Thomson AM and Bannister AP. Interlaminar connections in the neocortex. *Cereb Cortex* 13: 5-14, 2003.

Thomson AM, West DC, and Deuchars J. Properties of single axon excitatory postsynaptic potentials elicited in spiny interneurons by action potentials in pyramidal neurons in slices of rat neocortex. *Neuroscience* 69: 727-738, 1995.

Timofeev I, Contreras D, and Steriade M. Synaptic responsiveness of cortical and thalamic neurons during various phases of slow sleep oscillation in cat. *J Physiol* 494: 265-278, 1996.

Timofeev I and Steriade M. Fast (mainly 30-100 Hz) oscillations in the cat cerebellothalamic pathway and their synchronization with cortical potentials. *J Physiol* 504: 153-168, 1997.

Volgushev M, Voronin LL, Chistiakova M, Artola A, and Singer W. All-or-none excitatory postsynaptic potentials in the rat visual cortex. *Eur J Neurosci* 7: 1751-1760, 1995.

FIGURES

Figure 7.1. Electrophysiological identification of cortical neuron and its responses to thalamic and cortical inputs. Barbiturate anesthesia in this and all subsequent figures. *A-B*, two traces represent depth-EEG and intracellular recording from area 7 during the spindle oscillation (7-14 Hz). Seven stimuli to closely located site in cortical area 7 (*A*) or thalamic lateroposterior (LP) nucleus (*B*) were applied during active (spindles) and silent (interspindle-lulls) phases of the spindle oscillation. In *A*, 5 superimposed traces illustrate *Cx*-evoked intracellular responses, consisting of short-latency, monosynaptic EPSPs. In *B*, EPSPs elicited in cortical neurons by stimulating LP thalamic nucleus (5 superimposed traces). Notice EPSPs to be also short-latency and monosynaptic. In this and following figures, V_m is indicated by horizontal arrows; thalamic (*Th*) and cortical (*Cx*) stimuli artifacts are marked by triangles and filled circles, respectively.

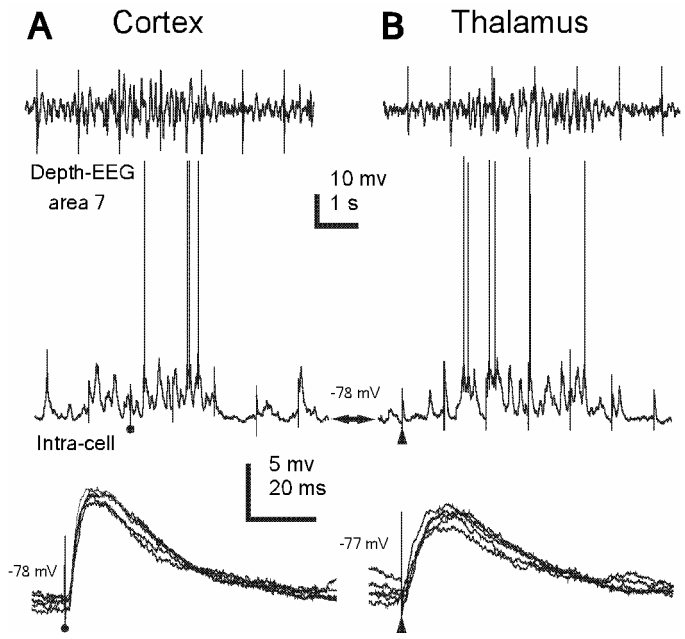
A
Cortex
B
Thalamus
Depth-EEG
area 7
10 mv
1 s
-78 mV
Intra-cell
5 mv
20 ms
-78 mV
-77 mV

Figure 7.2. Identification of thalamically and cortically evoked EPSPs and IPSPs in cortical neurons. *A*, the same cortical neuron recorded from area 5 responded with EPSP to *Th* (LP nucleus) stimulation and with IPSP to *Cx* stimulation in an adjacent site within area 5. *B*, estimation of EPSPs' and IPSPs' reversal potential. IPSP reversed at –76 mV and EPSP reversed close to 0 mV. *C*, PSPs at different V_ms, in area 5 neuron by stimulating the same cortical area. The plot shows the decreased R_{in}, lasting for ~150 ms (expressed as percentage of the initial value of R_{in}, before stimulation), associated with the cortically evoked IPSP.

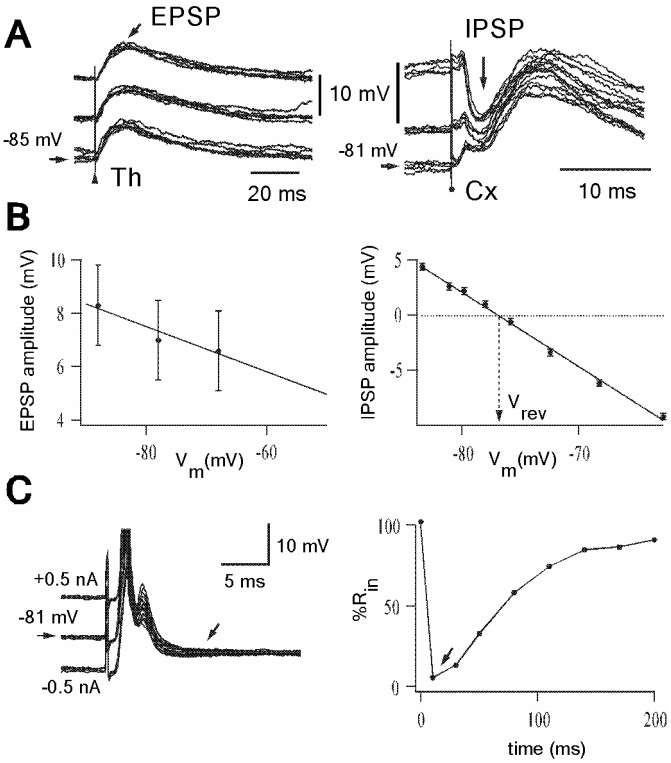
A
EPSP
IPSP
10 mV
-85 mV
-81 mV
Th
Cx
20 ms
10 ms
B
EPSP amplitude (mV)
IPSP amplitude (mV)
V_m(mV)
V_rev
C
10 mV
5 ms
+0.5 nA
-81 mV
-0.5 nA
%R_in
time (ms)

Figure 7.3. Interaction in cortical neurons between homosynaptic, cortical and thalamic volleys delivered at different time-intervals. One neuron recorded from area 4, with conditioning and testing stimuli applied in the same pathway. A, effect of paired-pulse protocol on Cx-evoked EPSPs. Three panels show averaged responses (n = 20) to two cortical stimuli paired at different intervals. Plot displays results for various pooled neurons (n = 8; mean ± SD). B, effect of paired-pulse protocol on Th-evoked EPSPs. Three panels show averaged responses (n = 20) to two thalamic stimuli paired at different intervals. Plot displays results for various pooled neurons (n = 10; mean ± SD).

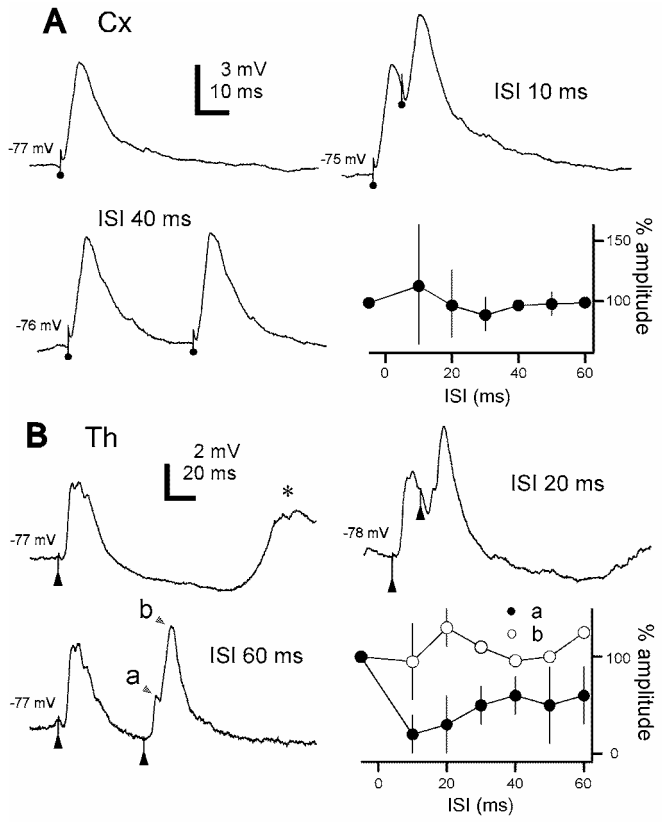
A
Cx
3 mV
10 ms
-77 mV
ISI 10 ms
-75 mV
ISI 40 ms
-76 mV
% amplitude
150
100
0
20
40
60
ISI (ms)
B
Th
2 mV
20 ms
*
-77 mV
ISI 20 ms
-78 mV
b
a
ISI 60 ms
-77 mV
a
b
% amplitude
100
0
0
20
40
60
ISI (ms)

Figure. 7.4. Interactions in cortical neurons between heterosynaptic, Cx and Th volleys delivered at different time-intervals. Two (A and B) different neurons recorded from area 4, with conditioning and testing stimuli applied to cortical area 4 and thalamic ventrolateral (VL) nucleus. A, effects of Cx-evoked EPSPs on Th-evoked EPSPs. Top left, averaged responses (n = 30) to single Cx and Th stimuli. The other panels represent interactions between Cx and Th volleys separated by 10 ms, 50 ms and 100 ms. Amplitude of EPSP and area of depolarization of conditioned (Th-evoked) response are shown between the two bottom plots. Left and right plots illustrate the time evolution of the amplitude and area of depolarization of Th-evoked EPSP when preceded by Cx stimulus at different interstimuli intervals (ISI). The straight line represents the expected response (see Figure 7.2B) and closed circles show the measured value with conditioning Cx inputs, expressed as percentage. The amplitude and depolarization area of the response are expressed as percentage of the expected value. B, another cortical neuron, with similar experimental design as in A; in this case, however, reversed stimuli were used, namely, the Th stimulus preceded the Cx stimulus at different time intervals. Plots were constructed as in panel A.

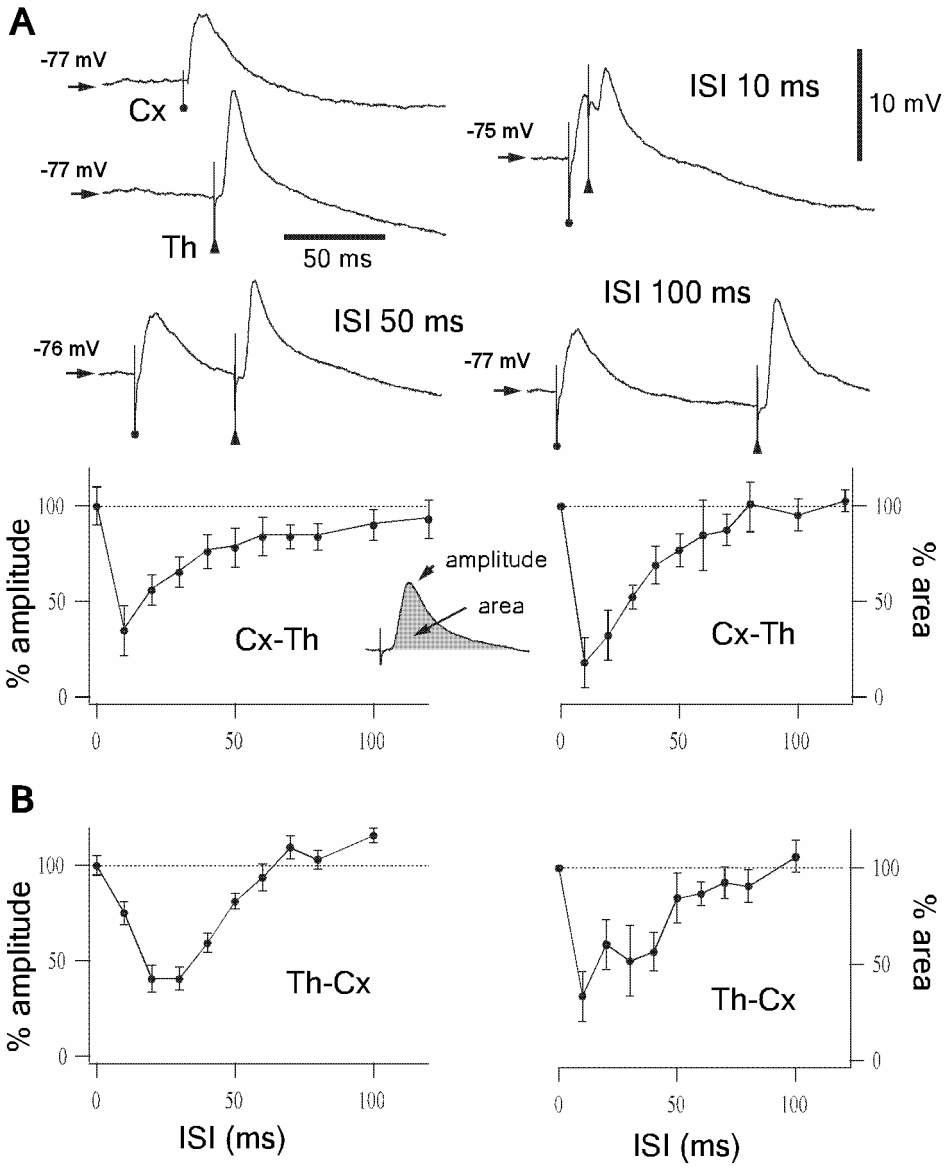
A
-77 mV
Cx
-77 mV
Th
50 ms
ISI 10 ms
10 mV
-75 mV
ISI 50 ms
-76 mV
ISI 100 ms
-77 mV
% amplitude
Cx-Th
amplitude
area
% area
Cx-Th
B
% amplitude
Th-Cx
ISI (ms)
% area
Th-Cx
ISI (ms)

Figure 7.5. Interactions in cortical neurons between heterosynaptic volleys for multiple neurons. Plots resulting from analysis of various neurons (n = 10), showing amplitude of EPSPs and area of depolarization of the conditioned response (similar to plots depicted in Fig. 7.4).

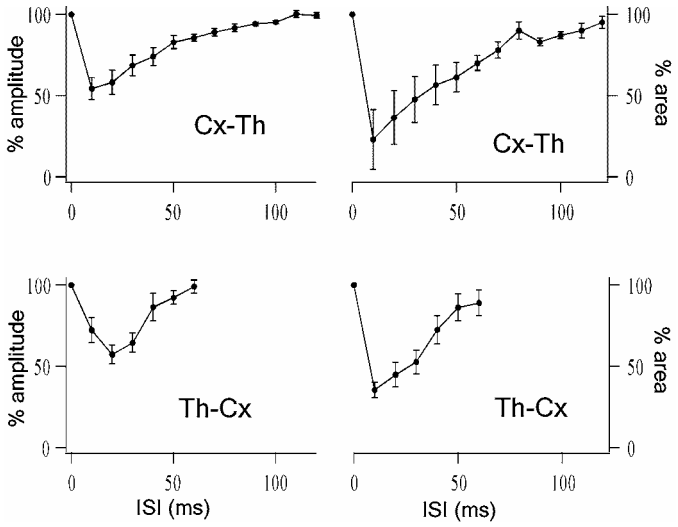
% amplitude
Cx-Th
% area
Cx-Th
% amplitude
Th-Cx
% area
Th-Cx
ISI (ms)
ISI (ms)
0
50
100

Figure 7.6. The *Th*-induced reduction in *Cx*-evoked EPSP's amplitude and depolarization area is accompanied by decrease in R_{in} in corticothalamic neuron recorded from area 5. *A*, top left panel shows superimposed traces of responses evoked by *Th* (LP nucleus) stimulus (antidromic spike followed by EPSP; see inset for expanded antidromic spike) and *Cx*-evoked EPSP in the same area 5 neuron. Three other panels show interactions between *Th*- and *Cx*-evoked activities at three ISI (10 ms, 30 ms and 50 ms). *B*, bottom plots show (left) the time evolution of the R_{in} elicited in the cortical cell by the conditioning *Th* stimulus and of the EPSP's amplitude evoked by *Cx* stimulus (expressed as percentage of the expected value). Note that the amplitude of the EPSP recovered earlier than the R_{in}. Right plot shows evolution of depolarization area.

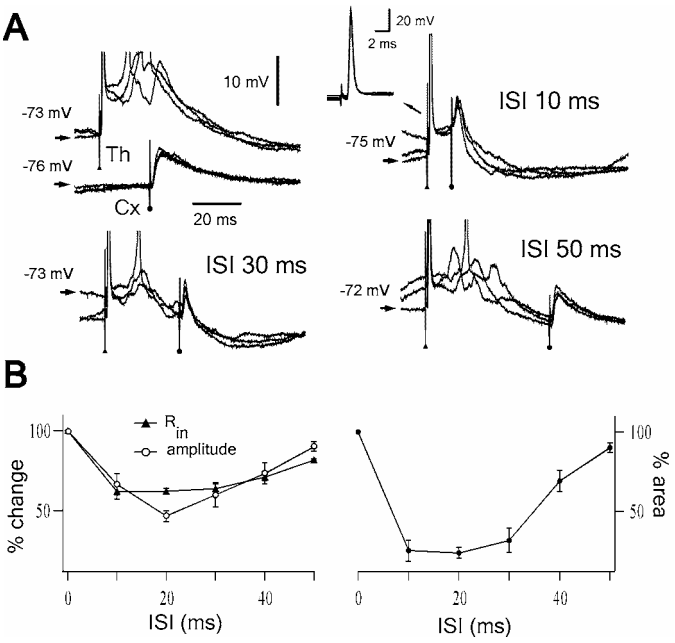
A
10 mV
-73 mV
-76 mV
Th
Cx
20 ms
20 mV
2 ms
ISI 10 ms
-75 mV
ISI 30 ms
-73 mV
ISI 50 ms
-72 mV
B
R in
amplitude
% change
100
50
0
20
40
ISI (ms)
% area
100
50
0
20
40
ISI (ms)

Figure 7.7. The Cx-induced reduction in amplitude and depolarization area of Th-evoked EPSP is not always associated with reduction in R_{in}. A, upper left panel shows superimposition of Cx- and Th-evoked EPSPs in area 6 neuron (Th stimulus to VL nucleus). The other panels depict interaction between conditioning Cx (area 5) and following Th (CL) inputs at different ISI (10 ms, 30 ms and 50 ms). B, left plot shows the time evolution of the R_{in} elicited by conditioning Cx stimulus (triangle) and of the amplitude of EPSP evoked by testing Th stimulus (open circle). Right plot displays the time course of the EPSP's area evoked by testing Th stimulus (circles).

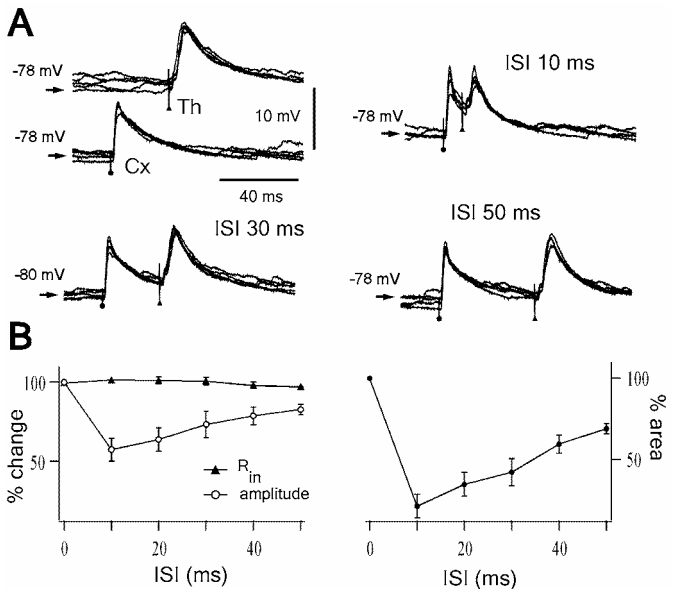
A
-78 mV
Th
10 mV
-78 mV
Cx
40 ms
ISI 10 ms
-78 mV
ISI 30 ms
-80 mV
ISI 50 ms
-78 mV
B
100
50
% change
R in
amplitude
0
20
40
ISI (ms)
100
50
% area
0
20
40
ISI (ms)

Figure 7.8. Conditioning *Cx* stimulation reduces the probability of action potentials evoked in thalamocortical neuron by local *Th* stimulation. Recording in VL nucleus, stimulation in area 4 and VL nucleus. *A*, top traces illustrate superimposed responses in VL neuron evoked by area 4 stimulation. Note long-lasting, slight hyperpolarization. Inset shows the response to a hyperpolarizing current step: depolarizing sag leading to low-threshold spike-burst. *B*, superimposed responses to *Cx* (left) and *Th* (right) stimuli. Note invariable presence of action potentials in response to *Th* stimuli. *C*, conditioning-testing (*Cx*-*Th*) stimulation at two time-intervals (40 ms and 100 ms). Bottom plot shows the decreased probability of eliciting action potentials in thalamic VL neuron when *Th* stimulus is paired with a preceding *Cx* volley.

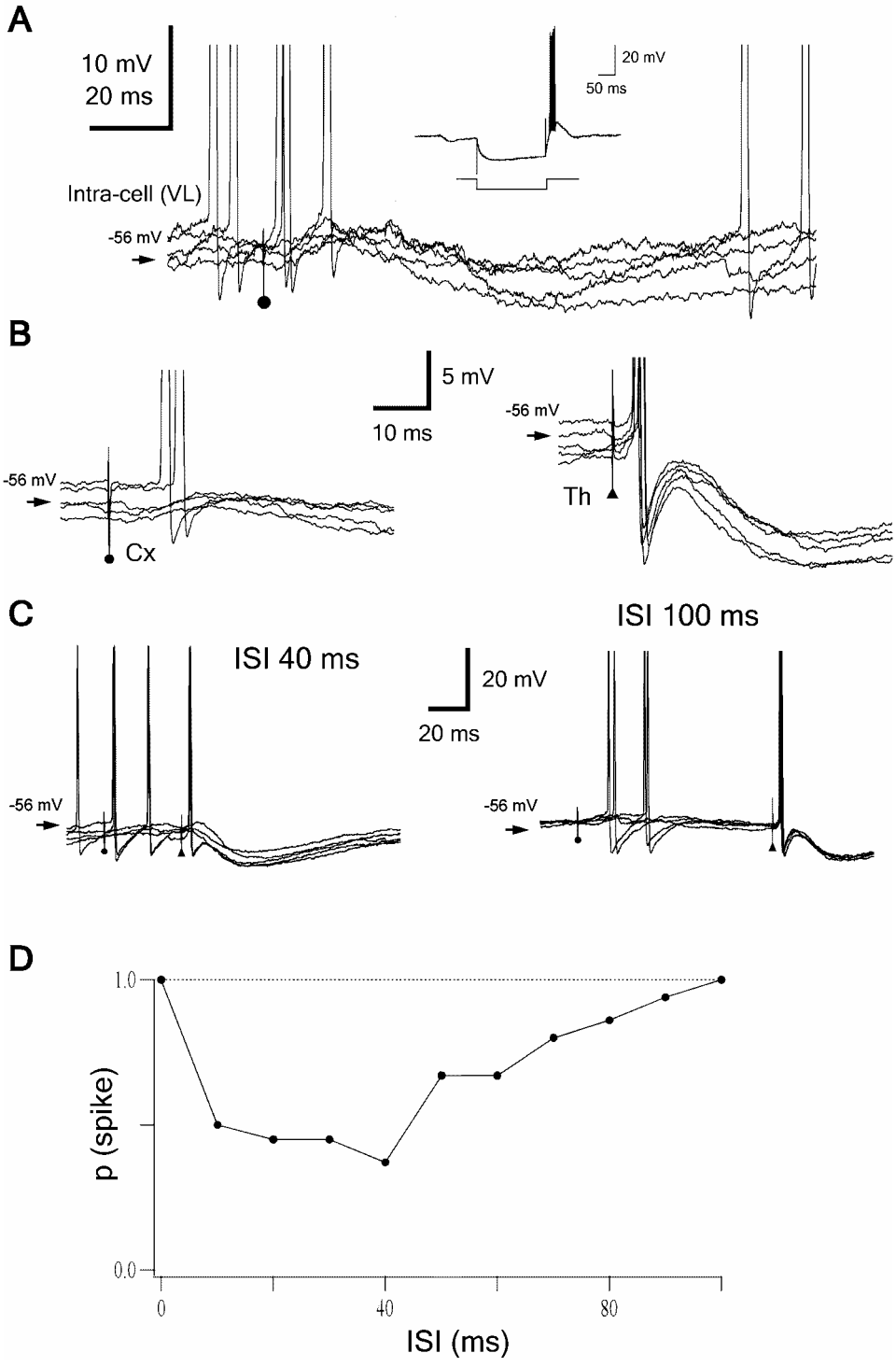
A
10 mV
20 ms
20 mV
50 ms
Intra-cell (VL)
-56 mV
B
5 mV
10 ms
-56 mV
Cx
-56 mV
Th
C
ISI 40 ms
-56 mV
ISI 100 ms
20 mV
20 ms
-56 mV
D
1.0
0.0
p (spike)
0
40
80
ISI (ms)

Figure 7.9. Evolution of *Cx*-induced decreased excitability of antidromically identified thalamocortical neuron during spindle sequence elicited by *Cx* stimulus. Recording and stimulation within VL nucleus. *Cx* stimulus applied to area 4. *A*, spindle sequence elicited by *Cx* stimulus. Insets show antidromic invasion of VL neuron from area 4 (left), and *Th*-induced EPSP leading to action potential in VL neuron (right). *B*, *Th*-evoked EPSPs at different ISI following the onset of spindle sequence (0.3 s, 0.8 s, 1.1 s and 1.5s), as indicated with arrows in the above depicted (minimized) spindles). Note abolition of action potential at 0.3 s and 0.8 s (evoked in *A*), rebound low-threshold spike-burst at 1.1 s (the end of spindle), and recovery of the control response with single action potential at 1.5 s (after cessation of spindle sequence). *C*, plot showing the probability of single spike (spike) and low-threshold spike (LTS) at different time intervals following a cortical stimulus.

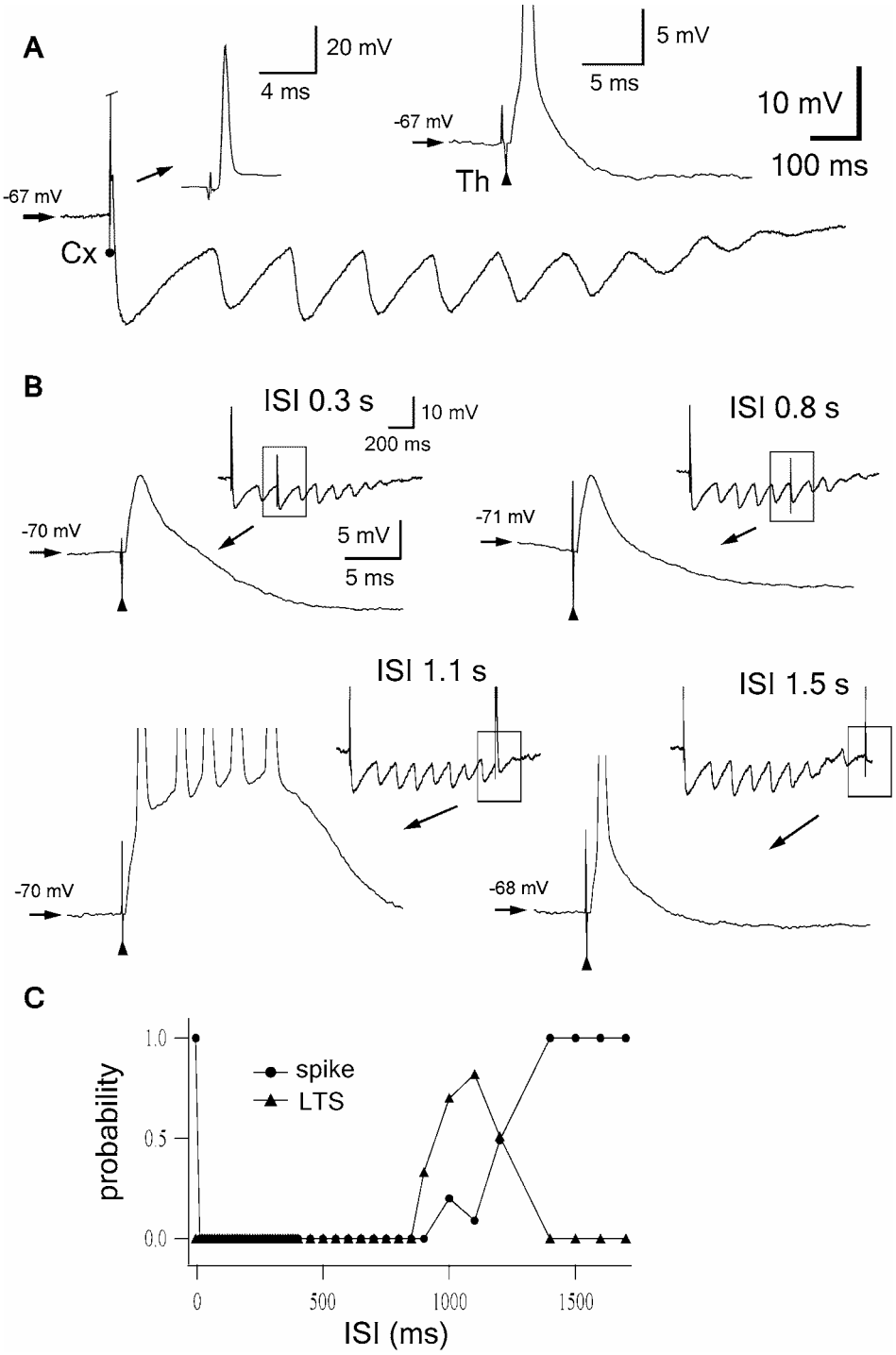
A
20 mV
4 ms
5 mV
5 ms
10 mV
100 ms
-67 mV
-67 mV
Th
Cx
B
ISI 0.3 s
10 mV
200 ms
5 mV
5 ms
-70 mV
ISI 0.8 s
-71 mV
ISI 1.1 s
-70 mV
ISI 1.5 s
-68 mV
C
spike
LTS
probability
1.0
0.5
0.0
0
500
1000
1500
ISI (ms)

8. Modulation of Neuronal Output by Dendritic Potentials in the Cortex

SELECTIVE AMPLIFICATION OF NEOCORTICAL NEURONAL OUTPUT BY FAST PREPOTENTIALS *IN VIVO*

Sylvain Crochet, Pablo Fuentelba, Igor Timofeev and Mircea Steriade (2004). *Cerebral Cortex(in press).*

RESUMÉ

La propagation des potentiels postsynaptiques au corps cellulaire est cruciale dans la détermination de la sortie neuronale. En utilisant des enregistrements intracellulaires sur des chats anesthésiés et non-anesthésiés, naturellement éveillés et naturellement endormis, nous avons trouvé des évidences pour la génération d'évènements rapides, tout ou rien, enregistré dans le corps cellulaire dans environ 20% des cellules à décharges régulières et des cellules à décharges par bouffées de potentiels d'action. Ces évènements, nommés prépotentiels rapides (FPPs), étaient supprimés par une hyperpolarisation du neurone ou par une inhibition de la transmission synaptique en perfusant un liquide cérébro-spinal artificiel sans ions Ca^{2+}. Les FPPs pouvaient être provoqués par une activation spécifique des entrées corticales et pouvaient ainsi être permettre aux neurones de décharger à des niveaux de potentiel de membrane plus hyperpolarisés. Ainsi, les FPPs représentent un mécanisme puissant pour augmenter la sortie des neurones néorcorticaux en réponse à des entrées données. Nous avons trouvé des évidences supplémentaires pour la modulation de la génération des FPPs à travers le cycle éveil-sommeil, ce qui indique des changements importants dans les propriétés intégratives des neurones néocorticaux dans différents états de vigilance. Nous suggérons que les FPPs représentent des décharges atténuées générées dans des points chauds (*hot spots*) de l'arbre dendritique et constitue un puissant mécanisme pour renforcer les connections fonctionnelles entre les éléments spécifiques des réseaux corticaux.

ABSTRACT

Neocortical cells integrate inputs from thousands of presynaptic neurons distributed along their dendritic arbors. Propagation of postsynaptic potentials to the soma is crucial in determining neuronal output. Using intracellular recordings in anesthetized and non-anesthetized, naturally awake and sleeping cats, we found evidence for generation of fast, all-or-none events recorded at the soma in about 20% of regular-spiking and intrinsically-bursting neurons. These events, termed fast prepotentials (FPPs), were suppressed by hyperpolarizing the neurons or by inhibiting synaptic transmission with perfusion of Ca^{2+}-free artificial cerebrospinal fluid. FPPs could be evoked by activation of specific cortical inputs and allowed neurons to fire at more hyperpolarized levels of membrane potentials. Thus, FPPs represent a powerful mechanism to boost the output of neocortical neurons in response to given inputs. We further found evidence for modulation of FPPs generation across the waking-sleep cycle, indicating important changes in the integrative properties of neocortical neurons in different states of vigilance. We suggest that FPPs represent attenuated spikes generated in hot spots of the dendritic arbor and constitute a powerful mechanism to reinforce the functional connections between specific elements of the cortical networks.

INTRODUCTION

Neocortical neurons operate as integrators of presynaptic neuronal activity. Each of them receives thousands of excitatory and inhibitory inputs, the majority of which arise in local circuits, which are mainly targeting their dendritic arbors (Szentágothai, 1965; Cragg, 1967; Gruner et al., 1974; DeFelipe and Fariñas, 1992; Peters, 1994). Postsynaptic potentials (PSPs) from many dendritic branches propagate to, and are integrated at, the soma and axon hillock, where they are transduced into output spike-trains (Yuste and Tank, 1996; Magee, 2000; Reyes, 2001; Williams and Stuart, 2003). Pyramidal-shaped neurons possess branched dendrites that can span virtually all layers, so that some presynaptic terminals are located close to the soma whereas others are situated in remote locations. An important issue concerning synaptic integration is how distant PSPs propagate to, and impact on, the soma.

The propagation of PSPs along the dendrites of cortical cells has been extensively studied during the last decade (Johnston et al., 1996; Yuste and Tank, 1996; Magee, 2000; Reyes, 2001; Hausser and Mel, 2003; Williams and Stuart, 2003). According to the passive cable theory, synaptic inputs would attenuate in a distance-dependent manner along the dendritic arbor, so that proximal inputs have a stronger somatic impact than distal ones (Rall, 1967, 1977; Spruston et al., 1994). This attenuation is partially compensated by an increase in the local amplitude of EPSPs, resulting from both an increase in local input resistance and a decrease in local capacitance with distance from the soma (Jaffe and Carnevale, 1999; Magee, 2000; Magee and Cook, 2000; Williams

and Stuart, 2002). Although a relative increase in AMPA receptor density has been found in the distal dendrites of neocortical pyramidal cells (Dodt et al., 1998), the somatic amplitude of unitary EPSPs decrease with the distance of their generation site to the soma (Magee and Cook, 2000; Williams and Stuart, 2002). Thus, the synaptic currents underlying EPSPs do not fully compensate for the filtering due to the passive properties of the dendritic membrane, as is the case in hippocampal pyramidal cells (Magee and Cook, 2000; Smith et al., 2003). On the other hand, the dendrites of pyramidal neurons are provided with voltage- and Ca^{2+}-dependent conductances that actively participate in the propagation or attenuation of PSPs (Johnston et al., 1996; Reyes, 2001).

Regenerative potentials in the dendrites of neocortical neurons have been mainly studied in pyramidal cells *in vitro*. A wide variety of dendritic potentials has been found to be initiated in the apical arbor, including fast Na^+ spikes, slow Ca^{2+} spikes or complex Na^+-Ca^{2+} potentials (Kim and Connors, 1993; Schiller et al., 1997; Schwindt and Crill, 1997; Stuart et al., 1997; Schwindt and Crill, 1998; Larkum et al., 1999b, 2001). Simultaneous dendritic and somatic recordings have revealed that dendritic spikes generally attenuate when they propagate to the soma (Schiller et al., 1997; Stuart et al., 1997; Larkum et al., 2001). Recent studies have also revealed the generation of Na^+ and Ca^{2+} spikes in apical dendrites of pyramidal neocortical cells *in vivo* (Helmchen et al., 1999; Svoboda et al., 1999; Zhu and Connors, 1999; Larkum and Zhu, 2002). Both experimental data (Larkum and Zhu, 2002) and modeling studies (Rhodes and Llinás, 2001; Rudolph and Destexhe, 2003) suggest that the *in vivo* condition could be more favorable for active propagation of dendritic regenerative potentials. Indeed, the active

propagation of dendritic spikes *in vivo* could be facilitated by a more depolarized level of membrane potential (V_m) and depolarizing fluctuations due to synaptic background could occasionally boost the impact of dendritic spikes.

In the present study, we show that ~20% of regular-spiking (RS) or intrinsically-bursting (IB) neocortical neurons display fast and high-amplitude events recorded at the soma, which were different from EPSPs. These sharp events, previously described as FPPs in the hippocampal (Spencer and Kandel, 1961), neocortical (Deschênes, 1981) and thalamocortical (Steriade et al., 1991; Timofeev and Steriade, 1997) neurons presumably represent fast Na^+ dendritic spikes that could be evoked by activation of specific cortical inputs. FPPs were able to enhance significantly the somatic impact of such inputs, thus resulting in an important boosting of the neuronal output. We also show that, in chronically implanted animals, the generation of FPPs is actively modulated across natural states of vigilance.

METHODS

Animal preparation

Experiments were performed in adult cats under anesthesia as well as in chronically implanted, naturally waking and sleeping adult cats. The experimental protocols were approved by the Committee for Animal Care and Protection of Laval University (permission nr. 2002-007) and also conformed to the policy of the American Physiological Society. Every effort was made to minimize animal suffering, and only the minimum number of animals necessary to obtain reliable data was utilized.

For acute experiments, 34 adult cats (2.5-4 kg) were anesthetized with pentobarbital (Somnotol, 35 mg/kg, i.p.) (n = 29) or ketamine-xylazine (10-15 mg/kg and 2-3 mg/kg i.m., respectively) (n = 5). The animals were paralyzed with gallamine triethiodide after the electroencephalogram (EEG) showed typical signs of deep general anesthesia and supplementary doses of anesthetics were administered at the slightest changes toward activated EEG patterns. The cats were ventilated artificially with the control of end-tidal CO_2 at 3.5-3.7%. The body temperature was maintained at 37-38^{o}C and the heart rate was ~90-100 beats/min. Stability of intracellular recordings was ensured by hip suspension, drainage of cisterna magna, bilateral pneumothorax, and filling the hole made in the scull with a solution of 4% agar.

Experiments on non-anesthetized animals were conducted on 8 adult cats, chronically implanted as previously described (Steriade et al., 2001; Timofeev et al., 2001). Briefly, surgical procedures for chronic implantation of recording and stimulating electrodes were carried out under deep barbiturate anesthesia (Somnotol, 35 mg/kg, i.p.), followed by two to three administrations, every 12 h, of buprenorphine (0.03 mg/kg, i.m.) to prevent pain. Penicillin (500,000 units i.m.) was injected during three consecutive days. During surgery, the cats were implanted with electrodes for electro-oculogram (EOG), electromyogram (EMG) from neck muscles, and intracortical EEG recordings. In addition, one to three chambers allowing the intracellular penetrations of micropipettes were placed over various neocortical areas. Acrylic dental cement was used to fix on the skull the electrodes and recording chambers and a previously described system (Steriade and Glenn, 1982) allowed head fixation without pain or pressure during recording sessions.

At the end of experiments, the cats were given a lethal dose of pentobarbital.

Intracellular recordings and stimulation

Intracellular recordings were performed using glass micropipettes filled with a solution of 3 M potassium-acetate (KAc) and direct current (DC) resistances between 25 and 75 MΩ. A high-impedance amplifier with active bridge circuitry was used to record the V_m and inject current into the neurons.

In acute experiments field potentials were recorded at 3-6 mm from the impaled neurons, using bipolar coaxial electrodes, with the ring at the pial surface and the tip at

the cortical depth, separated by 0.8-1 mm. Stimulating electrodes (1 or 2, similar to those used for field potential recordings) were inserted in the vicinity of micropipettes and into related thalamic nuclei. Cortical neurons were recorded from areas 5, 7 or 21 of intact cortex and in small isolated cortical slab (7 mm x 12 mm) from suprasylvian association areas 5 and 7. The preparation of cortical slabs is described elsewhere (Timofeev et al., 2000).

Chronically implanted cats were trained to sleep in the stereotaxic apparatus for 4-5 days after surgery. Intracellular recordings began when the cat displayed normal sleep-waking cycles. After small perforation of the dura, a glass micropipette was inserted in the cortex and the recording chamber was filled with warm sterile solution of 4% agar. Two to three recording sessions, lasting for 1-3 h, were performed daily; seven to ten days of recordings could be made in each chamber.

Microdialysis

Local change in extracellular Ca^{2+} concentration ($[Ca^{2+}]_o$) in the cortex was achieved using the reverse microdialysis method. The membrane of the microdialysis probe (2 mm length, 0.22 mm diameter, from EICOM, Kyoto, Japan) was inserted in the cortex and the recording micropipettes were placed at 0.2-0.3 mm from the membrane. The microdialysis probe was perfused with the following artificial cerebrospinal fluids (ACSF) (concentration in mM): control (NaCl 124, KCl, 2.5, $NaHCO_3$ 26, NaH_2PO_4 1.25, $MgSO_4$ 2, $MgCl_2$ 1, $CaCl_2$ 1); high Ca^{2+} (NaCl 124, KCl, 2.5, $NaHCO_3$ 26, NaH_2PO_4 1.25, $MgSO_4$ 2, $MgCl_2$ 0, $CaCl_2$ 5); and Ca^{2+} free (NaCl 125, KCl, 2.5,

$NaHCO_3$ 26, NaH_2PO_4 0, $MgSO_4$ 2, $MgCl_2$ 1, $CaCl_2$ 0, $MnCl_2$ 1). The actual $[Ca^{2+}]_o$ at the recording site was measured with a Ca^{2+}-sensitive microelectrodes (Diamond General, Ann Arbor, MI, USA).

Data analysis

Signals were recorded with a 16-channel Vision data acquisition system (Nicolet, Madison, WI, USA) at a sampling rate of 20 KHz. Analyses were performed off-line on a personal computer using IgorPro software (WaveMetrics, Lake Oswego, OR, USA). For the analysis of spontaneous synaptic activity, intracellular recordings were filtered off-line between 0 Hz and 1000 Hz to eliminate high-frequency electronic noise. The peak-to-peak amplitude of residual noise in the intracellular recordings was measured during periods of absence of spontaneous synaptic activity (i.e. during inter-spindle lulls under barbiturate anesthesia). The maximal noise amplitude ranged between 0.1 and 0.2 mV. All spontaneous depolarizing events (presumably EPSPs) with amplitude higher than 0.2 mV were then extracted automatically using a custom-written routine in IgorPro. The events were detected as positive peaks in the first derivative of the intracellular signal. The detection of non-monotony in the rising phase of each event allowed the discrimination of compound events that appeared as single peaks in the intracellular signal. The depolarizing slope of each event was fitted with a sigmoid function. The amplitude and maximum slope were determined between the beginning and the end of the rising phase of detected events. The rise-time was measured between 10 and 90 % of peak amplitude. For determination of fast prepotentials (FPPs) and action potentials (APs) threshold, we measured the membrane potential (V_m) for each individual FPP and

AP at the initiation point, determined in the averaged traces. For APs, the initiation point was determined in averaged APs that were not initiated by FPPs. The distinction between the initial FPP and the following AP was very clear in the first derivative of the signal as shown in Fig. 8.1A. The initiation V_m was then measured for all APs at the same time before the peak of the AP. Pooled data are expressed as mean ± SEM. When relevant, statistical analysis was carried out using two-tailed *t*-test.

RESULTS

Characterization of FPPs in neocortical neurons

We analyzed the features of spontaneous postsynaptic events in electrophysiologically identified regular-spiking (RS) and intrinsically-bursting (IB) neocortical neurons (McCormick et al., 1985; Connors and Gutnick, 1990; Nuñez et al., 1993) recorded under barbiturate anesthesia. Depolarizing events of amplitude higher than 0.2 mV were extracted automatically from intracellular recordings (see Material and Methods). The number of events extracted varied from cell to cell between 7000 and 21000 (mean 10654 ± 411) for 1 min of recording.

(a) Spontaneous EPSPs were characterized by low-amplitude and slow-rising phase. Overall, 78.7 ± 1.4% of events had amplitude lower than 0.5 mV and 87.6 ± 2.0% had maximal slope slower than 1 V/s. In 78% of cells (65/83) no event with amplitude higher than 5 mV or maximum rising slope faster than 6 V/s was detected.

(b) However, in 22% of the cells (18/83), some high-amplitude and fast-rising events were extracted. These events appeared as a population distinct from spontaneous EPSPs, as revealed by plotting the amplitude versus the maximal slope for all events (Fig. 8.1, middle panel right). Their mean amplitude ranged from cell to cell between 3.6 and 10.2 mV, with an average value of 6.16 ± 0.14 mV, and their mean maximal slope ranged from 8 to 20 V/s, with an average value of 12.97 ± 0.30 V/s. The rise-time of these events (0.49 ± 0.009 ms) was significantly shorter than the rise time of the faster EPSPs (1.09 ±

0.041 ms, $P<0.001$) and significantly longer than the rise time of full-blown APs (0.28 ± 0.008 m, $P<0.001$). Their falling phase was characterized by a biphasic decay best fitted by a double exponential: the τ of the initial fast decay was 0.79 ± 0.03 ms, while the τ of slower decay was 6.93 ± 0.29 ms. Because of these features, fast-rising events were very similar to the FPPs initially described in hippocampal neurons by Spencer and Kandel (1961), and hereafter we will call them FPPs.

All neurons in which FPPs were detected had APs longer than 0.6 ms at half amplitude (mean = 0.81 ± 0.01 ms). The cortical depth distribution of neurons was calculated from the depth of the recording indicated by the micro-driver and corrected according to the angle of the pipette within the cortex (Fig. 8.2). The neurons displaying FPPs were distributed mainly between 200 and 800 μm, and between 1200 and 1600 μm, indicating that most of them were recorded in layers II/III and V/VI. The input resistance of neurons displaying FPPs (17.43 ± 0.95 MΩ) was not significantly different from that of neurons without FPPs (18.44 ± 1.00 MΩ, $P>0.8$).

FPPs appeared as all-or-none events that crowned spontaneously occurring EPSPs. They appeared either in isolation or led to full-blown APs (see overlay in Fig. 8.1). The essential condition for FPP generation was a relatively depolarized V_m and the presence of synaptic activity. Actually, hyperpolarizing the cell by intracellular injection of current suppressed FPPs (Fig. 8.3). However, depolarizing current pulses could not elicit FPPs during periods without spontaneous synaptic activity (i.e. interspindle lull in barbiturate anesthesia) but, instead, induced trains of APs. In Fig. 8.3, the cell was held at

two V_m levels by injection of hyperpolarizing current pulses. The histogram of V_m (gray) shows a bimodal distribution resulting from current pulses, with FPPs initiated only at V_ms more depolarized than –70 mV. In this neuron, the mean threshold for the generation of FPPs was –66 mV. In the 18 neurons with FPPs, we compared the V_m at the initiation of FPPs and the V_m at initiation of APs. The threshold for FPPs' generation was different from cell to cell and varied from –72 mV to –62 mV (mean: 67.2 ± 0.2 mV), but was always more hyperpolarized than the threshold for axonal APs initiation (55.9 ± 0.1 mV, $P<0.001$) (see below). In all 18 neurons, holding the cell below the threshold for FPPs' generation completely suppressed their appearance.

In order to determine the dependence of FPPs' generation on synaptic transmission, we used the reverse microdialysis technique to change the extracellular concentration of calcium $[Ca^{2+}]_o$ in the vicinity of the recorded neurons. The actual $[Ca^{2+}]_o$ at the recording site was measured with a Ca^{2+}-sensitive electrode. The baseline control $[Ca^{2+}]_o$ was 1.2 mM, as previously described *in vivo* (Massimini and Amzica, 2001); 10 to 15 min after perfusion of the microdialysis probe with high Ca^{2+} ACSF, the $[Ca^{2+}]_o$ reached a stable level of 3 mM; after 20 min of perfusion with the Ca^{2+}-free ACSF, the $[Ca^{2+}]_o$ stabilized at 0.6 mM. Two RS and one IB neurons displaying FPPs could be recorded under different conditions of $[Ca^{2+}]_o$. An example is depicted in Fig. 8.4. Increasing $[Ca^{2+}]_o$ markedly enhanced the background of synaptic activity and the incidence of FPPs, from 0.68 ± 0.04 Hz to 1.18 ± 0.07 Hz ($P<0.05$). In low Ca^{2+} condition, the spontaneous synaptic activity was strongly reduced and FPPs were almost completely suppressed (0.03 ± 0.00, $P<0.01$). The same effect was observed in the three

neurons. The change in FPPs incidence was not related to change in neuronal firing, since the mean firing rate of neurons (calculated for 10 neurons recorded in three conditions) was slightly, but not significantly, decreased in high Ca^{2+} condition (0.75 ± 0.23, P>0.3) and increased in low Ca^{2+} condition (1.41 ± 0.33, P>0.6), as compared to control condition (1.08 ± 0.15). No significant change in V_m was observed between the three conditions (Fig. 8.4). The slight change in firing rate was due the change in the firing threshold for APs, as shown in Fig. 8.4. Thus FPPs' generation appeared to be strongly dependant on synaptic transmission.

We examined the possibility of FPPs' generation within local cortical circuits and analyzed the spontaneous activity of RS or IB neurons recorded in isolated cortical slabs from the suprasylvian association cortex. FPPs were found in 15% (3/20) of such neurons, thus indicating that FPPs could be generated in response to activation of inputs arising from local cortical networks. The FPPs recorded in isolated cortical slabs shared common features with those recorded in intact cortex, i.e., they were all-or-none events, associated with intense synaptic activity during spontaneous or elicited active periods (Fig. 8.5A), and their generation was voltage dependent (Fig. 8.5B).

Selective amplification of cortical inputs

In 13 out of 18 neurons, we tested the efficacy of cortical and/or thalamic inputs to evoked FPPs. FPPs could be elicited by cortical simulation in 8 of the 13 neurons. In general, responses to cortical stimulation consisted in a depolarization-hyperpolarization sequence, the first depolarization being composed of a summation of EPSPs. The early

depolarization was crowned by an FPP when the response reached the threshold for their generation (Fig. 8.4). Interestingly, *the generation of FPPs selectively depended on the stimulated pathway*. At variance with an earlier study that pointed to thalamic inputs generating FPPs' in cortical neurons (Deschênes, 1981), cortical stimulation evoked FPPs while thalamic stimuli, applied to intralaminar centrolateral or lateral posterior nuclei, did not elicit FPPs in the same neuron, even when the response reached the threshold for FPP generation (Fig. 8.6A). This was observed in the 4 neurons in which we tested both thalamic and cortical stimulation.

In other 4 neurons, we compared the potency of cortical stimuli applied at different sites to evoke FPPs. Stimuli were applied alternatively through two electrodes (see Material and Methods) inserted in the ipsilateral cortex, at 1-2 mm from the recorded neuron and separated by 2-3 mm. The intensity of stimulation was adjusted for each electrode to induce EPSPs of similar amplitude, when subthreshold for FPP. Figure 8.6B shows the responses of another cortical neuron to stimuli applied through two different cortical electrodes. Stimuli delivered to the first electrode evoked an EPSP that was crowned by an FPP when it reached the threshold (left), whereas stimuli applied to the second electrode evoked a similar responses but no FPP (right). To be sure that the second stimulation did not fail to evoke FPPs because of more depolarized threshold for FPP generation, we held the cell at a more depolarized level of V_m while stimulating through the second electrode. At more depolarized V_m, the EPSP eventually evoked an AP (not shown) but no FPP was observed. The consequence of FPPs' generation in response to cortical stimulation was a non-linearity in the voltage-response relationship,

as revealed by plotting the maximum V_m reached by the evoked response versus the V_m before stimulation. As shown in Fig. 8.4B (bottom), the progression of the V_m reached by the response increased linearly with the initial V_m (blue open triangles) until it reached the threshold for FPP generation. Then, the FPPs induced a jump in the V_m reached by the response (blue filled triangles). On the other hand, the V_m reached by the response to stimuli applied through the second electrode increased linearly even above the threshold for FPP generation (green open circles).

Besides its dependence upon synaptic inputs, the generation of FPPs was also dependent on the temporal sequence of the inputs. In 2 out of 5 neurons, a single cortical stimulus was ineffective in initiating an FPP but, when paired at short time interval (~10 ms), an FPP crowned the second EPSP (Fig. 8.6C). This effect was not only due to a more depolarized V_m since a single stimulus could not evoke an FPP even when the response passed over the threshold for FPP generation.

An important function of FPPs appeared to be their contribution to the output of cortical neurons, i.e. the generation of full-blown APs. As shown in Fig. 8.7A, APs could be initiated in the same neuron following the summation of several EPSPs, whereas only one FPP was necessary to reach the firing threshold from the same V_m level. However, as can be see in Fig. 8.7 (expanded traces in A and averaged traces in B), the firing threshold for APs was the same whether the AP was initiating from summated EPSPs or from one FPP. Indeed, FPPs are events of high amplitude generated at V_ms 5 to 10 mV more hyperpolarized than the firing threshold for full-blown APs (see histograms in Fig.

8.5B). Consequently, FPPs facilitate neuronal firing at more hyperpolarized levels. This is of special importance for the integrative properties of cortical neurons.

Since FPPs are generated in response to the activation of specific inputs (see again Fig. 8.6, A-B), they can boost selectively the output of the neuron in response to those inputs. In the neuron depicted in Fig. 8.8, cortical stimulation evoked a sequence of depolarization-hyperpolarizing potentials and, when the neuron was more depolarized, early EPSPs were crowned by FPP. At slightly more depolarized potential, the FPP led to full-blown AP and, when the cell was more depolarized, the AP rode directly on the EPSPs. We calculated the probability for the evoked response to elicit an AP (output) as a function of the initial V_m when FPPs were generated. We then extrapolated the output-V_m function for the same response when no FPP was generated. In both cases, the output-V_m relation was best fitted by a sigmoid function. As seen in the bottom graph of Fig. 8.8, the generation of FPP shifted the output-V_m curve to more hyperpolarized levels. Thus, FPPs allowed the neuron to fire in response to the same synaptic input at V_ms more hyperpolarized by ~5 mV.

Modulation of FPPs generation across behavioral states

Finally, we investigated the possibility that the incidence of FPPs is modulated by natural states of vigilance and analyzed intracellular recordings of RS and IB neurons in awake and sleeping cats. FPPs were found in 10 out of 56 neurons (18%) in different states of vigilance. FPPs were present in all behavioral states but their frequency was different and depended on the V_m variations (Fig. 8.9). During slow-wave sleep (SWS),

the mean V_m was more hyperpolarized and the incidence of FPPs was the lowest. During waking and paradoxical sleep (PS; or REM sleep), the V_m was equally more depolarized and the frequency of FPPs was higher in both these states than in SWS, reaching the highest values in PS. We measured the incidence of FPPs in 8 neurons, during different states of vigilance. The incidence of FPPs was the lowest during SWS (4.4 ± 0.95 Hz) and was significantly higher during waking (15.02 ± 1.18 Hz, $p<0.01$) and PS (28.97 ± 4.40 Hz, $P<0.01$). Despite a similar V_m level, the incidence of FPPs during PS was significantly higher than during waking ($P<0.05$), suggesting that neuromodulators implicated in the regulation of behavioral states may modulate the generation of FPPs.

DISCUSSION

In the present paper we report the presence of fast and high-amplitude events, FPPs, recorded from the soma of about 20 % of RS and IB neocortical neurons. The FPPs were all-or-none events, suppressed by hyperpolarization, and always associated with synaptic background activity. They were evoked by activation of specific local cortical inputs and exerted a powerful and selective boosting of cortical neuronal output. Finally, we found that the incidence of FPPs was modulated by natural states of vigilance.

Nature and origin of FPPs

FPPs were first described in the hippocampus (Spencer and Kandel, 1961) and later also found in neocortical (Deschênes, 1981), thalamocortical (Steriade et al., 1991; Timofeev and Steriade, 1997) and other central neurons. They were interpreted to either represent attenuated dendritic spikes (Turner et al., 1993; Ariav et al., 2003) or reflect APs in electrotonically coupled neurons (Llinás et al., 1974; MacVicar and Dudek, 1981; Valiante et al., 1995; Gibson et al., 1999; Hughes et al., 2002; Landisman et al., 2002). Although *in vitro* studies have revealed abundant electrical coupling via gap-junctions between both pyramidal neurons and interneurons in immature neocortex (Peinado et al., 1993; Bittman et al., 2002), electrophysiological evidence for electrical coupling in adult animal has been only found between local interneurons but not between pyramidal neurons (Connors et al., 1983; Galarreta and Hestrin, 1999; Gibson et al., 1999). In the present study, FPPs were recorded in RS and IB neurons with relatively wide APs (mean duration at half amplitude: 0.82 ± 0.01 ms), indicating that these neurons were most

likely not interneurons. In a few experiments, we stained the recorded neurons with intracellular injection of Neurobiotine. One neuron that displayed FPPs was stained and was identified as a pyramidal-shaped layer III neuron (data not shown). Recent experiments in the hippocampus demonstrated the generation of spikelets of 1 to 10 mV in amplitude mediated by axo-axonal gap junctions between pyramidal cells (Schmitz et al., 2001). However, to the best of our knowledge, there is no evidence for electrical coupling between axons of pyramidal neurons in the neocortex. On the other hand, the possibility that electrical coupling between neocortical pyramidal neurons may persist in adult animals has been raised by molecular studies. Thus, connexin36 might be expressed by a subset of pyramidal neurons (Deans et al., 2001) and the expression of mRNA for another type of connexin (43) has been found in pyramidal cells of mature neocortex (Simburger et al., 1997).

In the present study, the generation of FPPs was voltage-dependent and always associated with synaptic activity. Similarly, the generation of dendritic spikes recorded from pyramidal neocortical or hippocampal neurons *in vitro* has been shown to be voltage-dependent (Kim and Connors, 1993; Schwindt and Crill, 1997; Schiller et al., 2000; Ariav et al., 2003). Finally, we found that FPPs were suppressed when synaptic transmission is inhibited by perfusion of Ca^{2+}-free ACSF and their incidence increased with perfusion of high-Ca^{2+} ACSF. These observations do not support the idea that FPPs represent APs in electronically coupled neurons, since electrical coupling is not affected or even enhanced in low-Ca^{2+} conditions (Perez-Velazquez et al., 1994; Valiante et al., 1995; Draguhn et al., 1998; Mann-Metzer and Yarom, 1999). Thus, although we cannot

completely discard the possibility that FPPs represent APs in electrotonically coupled neurons, our results strongly suggest that they are more likely dendritic regenerative potentials. It is also unlikely that the neurons that displayed FPPs in our study were recorded at dendritic levels: *(a)* first, none of them showed characteristic features of established dendritic recordings *in vitro* or *in vivo*, such as plateau potentials or complex spikes (Kim and Connors, 1993; Steriade et al., 1996; Helmchen et al., 1999; Zhu and Connors, 1999; Larkum and Zhu, 2002); *(b)* second, all cells generated trains of full-blown, overshooting APs of constant amplitudes in response to depolarizing current pulses, whereas backpropagating axonal APs recorded in the dendrites of cortical neurons *in vivo* show strong attenuation and broadening with distance from the soma (Svoboda et al., 1999; Waters et al., 2003). We therefore think that our recordings were performed at somatic levels of cortical neurons and thus suggest that FPPs represent attenuated dendritic spikes.

As to the mechanisms underlying the generation of FPPs, it is well established that the dendrites of cortical pyramidal cells can sustain active regenerative potentials under certain conditions. Na^+, Ca^{2+} and NMDA-generated spikes have been demonstrated in the apical and basal dendrites of cortical pyramidal neurons (Magee et al., 1998; Hausser et al., 2000; Schiller and Schiller, 2001; Hausser and Mel, 2003; Williams and Stuart, 2003). Because of the slow time course of Ca^{2+} and NMDA spikes (Kim and Connors, 1993; Schiller et al., 1997; Schwindt and Crill, 1997; Larkum et al., 1999a; Schiller et al., 2000; Larkum et al., 2001; Larkum and Zhu, 2002), we assume that at least the earliest sharp component of the FPPs represent a Na^+ spike whose generation has

been shown in the apical dendrites of neocortical and hippocampal pyramidal cells (Kim and Connors, 1993; Stuart et al., 1997; Golding and Spruston, 1998; Schwindt and Crill, 1998) and in the basal dendrites of hippocampal pyramidal neurons as well (Ariav et al., 2003). However, Na^+ spikes generated in apical dendrites are most of the time associated with Ca^{2+} spikes and strongly attenuate while propagating to the soma (Schiller et al., 1997; Stuart et al., 1997; Larkum et al., 2001). As a result, when simultaneously recorded at the dendrite and soma *in vitro*, dendritic Na^+ spikes do not appear as fast potentials at the soma. Moreover, we were able to block the generation of FPPs by injection of hyperpolarizing current at the soma. *In vitro* data demonstrate that alteration of somatic membrane potential by direct current injection can affect the membrane potential of the dendrites at least out to 300-400 μm from the soma (Schwindt and Crill, 1995). The high conductance state of cortical neurons *in vivo* probably further limits the dendritic impact of somatic current injection, suggesting that FPPs are not generated far from the soma, i.e. in proximal apical or basal dendrites of pyramidal cells. Another possibility is that FPPs were generated in distal apical dendrites and then propagated actively to the soma. This possibility was suggested in modeling studies showing that under *in vivo*-like conditions, a depolarized V_m increases the probability of generation and propagation of dendritic spikes (Rhodes and Llinás, 2001; Rudolph and Destexhe, 2003). In this condition, hyperpolarizing the soma could block the propagation FPPs (Larkum et al., 2001). However, their relatively small amplitude at the soma, compared to the amplitude of regenerative potentials generated in the dendrites, does not support the idea of an active propagation in this case.

In hippocampal pyramidal cells *in vitro*, co-activation of clustered neighboring inputs on basal dendrites can elicit a local spike that consists in fast Na^+ and slow NMDA components (Ariav et al., 2003). These dendritic spikes, recorded at the soma, have a shape very similar to the FPPs described here and are similarly suppressed by injection of hyperpolarizing current at the soma. But in layer V neocortical pyramidal cells *in vitro*, only the slow NMDA spike was evoked by the activation of basal dendrites (Schiller et al., 2000). However, in our experiments, many neurons with FPPs were localized in layers II/III or VI. It is thus possible that Na^+ spikes, similar to those generated in the basal dendrites of hippocampal neurons, can be generated in the basal dendrites of some subpopulation of neocortical pyramidal cells in other layers. Therefore, we suggest that FPPs represent dendritic Na^+ spikes generated in the basal dendrites of neocortical pyramidal cells. The biphasic decay of the FPPs may reflect an underlying slow component due either to Ca^{2+} or NMDA conductances.

The generation of dendritic spikes is supposed to occur when synaptic inputs are activated simultaneously and/or converge at the same dendritic region. In neocortical pyramidal neurons, supralinear summation of EPSPs due to active dendritic processes has been found to occur in a time window shorter than 30 ms (Nettleton and Spain, 2000). Local spikes in the basal dendrites of both neocortical or hippocampal pyramidal cells can be initiated by co-activation of clustered neighboring basal inputs (Schiller et al., 2000; Ariav et al., 2003). Based on the local amplitude of EPSPs recorded *in vitro*, Williams and Stuart (2002) have found that the synchronized activation of 4 to 30 presynaptic neurons is required for the initiation of dendritic spikes. Thus, initiation of

local spikes is expected to occur either if inputs carrying related information selectively innervate the same dendritic segments (Archie and Mel, 2000; Poirazi and Mel, 2001) or if the network activity is synchronized (Kamondi et al., 1998; Helmchen et al., 1999). In keeping with this idea, we found that FPPs could be evoked by gross cortical stimulations, which activate simultaneously a pool of neurons and fibers or by paired stimuli at high frequency. Thus, only converging coincident inputs or closely time-spaced inputs could generate FPPs, suggesting that FPPs are likely generated in response to an important depolarization of a particular dendritic segment. Interestingly, the activation of different cortical inputs had various effects on the generation of FPPs, even when the subthreshold evoked responses were very similar (see Fig. 8.6). This observation point out to the input-specific generation of FPPs that might be due either to the location of these inputs (apical or basal dendrites) or to the convergence of the simultaneously activated inputs (clustered or spread on the dendritic arbors). The input-dependent generation of FPPs may also be due to non-uniformly distributed glutamate receptors that form hot spots of response to glutamate on dendritic arbors. Synaptic inputs impinging upon these regions would have a higher probability to elicit dendritic spikes (Frick et al., 2001).

Functional implication of FPPs for the integrative properties of cortical neurons

Active regenerative dendritic potentials have mainly been studied in the apical dendrites of neocortical and hippocampal pyramidal cells. Physiological and modeling studies have shown that forward-propagating dendritic spikes can boost the influence of synapses in distal dendrites on their way to the soma, thereby circumventing the

attenuation produced by the passive cable properties of dendrites (Cauller and Connors, 1994; Schwindt and Crill, 1998; Larkum et al., 2001; Williams and Stuart, 2002; Rudolph and Destexhe, 2003). It is assumed that dendritic spikes strongly attenuate as they propagate forward and appear at the soma as slow events undistinguishable from other postsynaptic potentials (Schiller et al., 1997; Stuart et al., 1997; Golding and Spruston, 1998; Larkum et al., 2001). However, in the present study we found that FPPs were significantly higher in amplitude and had faster rising phase than other spontaneous depolarizing events recorded at the soma. FPPs induced a non-linearity in the integrative properties of cortical neurons (see Fig. 8.6B), thus providing additional computational properties to the neurons by markedly enhancing the somatic impact of cortical inputs. We further demonstrate that the boosting of EPSPs by FPPs results in a functional hierarchy of the inputs by a selective enhancement of the output of cortical neurons for given inputs. Thus, FPPs may reinforce the functional links between specific elements of the cortical network. This hypothesis is of interest since we demonstrated, using dual intracellular recordings of synaptically connected neurons *in vivo*, that the somatic impact of individual cortical inputs during active states of the network is very weak due to a high conductance state and high failure rate (Timofeev and Crochet, 2002). FPPs might also enhance neuronal output in response to simultaneous arriving inputs. Indeed, the generation of dendritic spikes might require coincident activation of different inputs and may thus play an important role for coincidence detection of cortical inputs.

As demonstrated recently in hippocampal neurons, Na^+ dendritic spikes could serve to improve the precision and the stability of the timing of axonal APs, mainly by

reducing the temporal jitter of evoked APs (Ariav et al., 2003). This was apparently not the case for FPPs in the present study because *(a)* the generation of FPPs themselves showed relatively high temporal variability (not shown); and *(b)* once an FPP is generated, the timing of the AP was also variable (see Figs. 8.1 and 8.5A). Physiological studies have also suggested that forward-propagating Ca^{2+} spikes could be involved in the generation of burst firing in cortical neurons (Larkum et al., 1999a-b; Schwindt and Crill, 1999; Williams and Stuart, 1999). In contrast to Ca^{2+} spikes initiated in apical dendrites, we found that FPPs did not evoke a burst of axonal APs, but rather single AP. This is expected from the fast decay of the FPPs, which are more likely generated by a Na^{+} conductance and which contrast with the broad Ca^{2+} spikes evoked in apical dendrites.

Dendritic excitability is regulated by neuromodulators such as serotonin, acetylcholine or noradrenaline (Hoffman and Johnston, 1999; Carr et al., 2002). These neuromodulators are released by ascending activating systems that originate in the brainstem and basal forebrain, and play a major role in the control of behavioral states (Steriade and McCarley, 1990). In line with these observations, we found evidence for a modulation of FPPs generation across behavioral states of vigilance. In all recorded neurons, we found changes in the incidence of spontaneous FPPs associated with shifts from a state of vigilance to another. The incidence of FPPs appeared to be the lowest during SWS and the highest during PS. The decrease in FPPs incidence during SWS was expected because of V_m hyperpolarization during this state (Steriade et al., 2001) due to decreased firing rates in thalamocortical (Glenn and Steriade, 1982) and other corticipetal systems during SWS, compared to both waking and PS. The increased incidence of FPPs

in PS compared to waking (Fig. 8.9) fits in well with the higher firing rates, during PS, of mesopontine cholinergic neurons with identified projections to intralaminar and lateroposterior thalamic nuclei (Steriade et al., 1990), which are the main afferents of cortical association areas at which level the present recordings were made. Thus, neuromodulators are able to control the integrative properties of cortical neurons across behavioral states.

Concluding remarks

This study revealed that about 20 % of RS and IB neocortical neurons are able to generate FPPs. The electrophysiological features of these events strongly suggest that they represent forward propagated Na^+ dendritic spikes attenuated at the soma. We propose that FPPs represent dendritic spikes generated by coincident inputs converging on the same dendritic segment. These dendritic spikes strongly affect the integrative properties of cortical neurons and may serve to reinforce the functional links between *specific elements of the cortical network* or for coincidence detection as well. Finally, the generation FPPs appeared to be regulated across behavioral states, indicating important changes in the integrative properties of cortical neurons during states of vigilance.

REFERENCES

Archie KA, Mel BW (2000) A model for intradendritic computation of binocular disparity. Nat Neurosci 3:54-63.

Ariav G, Polsky A, Schiller J (2003) Submillisecond precision of the input-output transformation function mediated by fast sodium dendritic spikes in basal dendrites of CA1 pyramidal neurons. J Neurosci 23:7750-7758.

Bittman K, Becker DL, Cicirata F, Parnavelas JG (2002) Connexin expression in homotypic and heterotypic cell coupling in the developing cerebral cortex. J Comp Neurol 443:201-212.

Carr DB, Cooper DC, Ulrich SL, Spruston N, Surmeier DJ (2002) Serotonin receptor activation inhibits sodium current and dendritic excitability in prefrontal cortex via a protein kinase C-dependent mechanism. J Neurosci 22:6846-6855.

Cauller LJ, Connors BW (1994) Synaptic physiology of horizontal afferents to layer I in slices of rat SI neocortex. J Neurosci 14:751-762.

Connors BW, Gutnick MJ (1990) Intrinsic firing patterns of diverse neocortical neurons. Trends Neurosci 13:99-104.

Connors BW, Benardo LS, Prince DA (1983) Coupling between neurons of the developing rat neocortex. J Neurosci 3:773-782.

Cragg B (1967) The density of synapses and neurones in the motor and visual areas of the cerebral cortex. J Anat 101:639-654.

Deans MR, Gibson JR, Sellitto C, Connors BW, Paul DL (2001) Synchronous activity of inhibitory networks in neocortex requires electrical synapses containing connexin 36. Neuron 31:477-485.

DeFelipe J, Fariñas I (1992) The pyramidal neuron of the cerebral cortex: morphological and chemical characteristics of the synaptic inputs. Prog Neurobiol 39:563-607.

Deschênes M (1981) Dendritic spikes induced in fast pyramidal tract neurons by thalamic stimulation. Exp Brain Res 43:304-308.

Dodt HU, Frick A, Kampe K, Zieglgansberger W (1998) NMDA and AMPA receptors on neocortical neurons are differentially distributed. Eur J Neurosci 10:3351-3357.

Draguhn A, Traub RD, Schmitz D, Jefferys JG (1998) Electrical coupling underlies high-frequency oscillations in the hippocampus in vitro. Nature 394:189-192.

Frick A, Zieglgansberger W, Dodt HU (2001) Glutamate receptors form hot spots on apical dendrites of neocortical pyramidal neurons. J Neurophysiol 86:1412-1421.

Galarreta M, Hestrin S (1999) A network of fast-spiking cells in the neocortex connected by electrical synapses. Nature 402:72-75.

Gibson JR, Beierlein M, Connors BW (1999) Two networks of electrically coupled inhibitory neurons in neocortex. Nature 402:75-79.

Glenn LL, Steriade M (1982) Discharge rates and excitability of cortically projecting intralaminar thalamic neurons during waking and sleep states. J Neurosci 2:1287-1404.

Golding NL, Spruston N (1998) Dendritic sodium spikes are variable triggers of axonal action potentials in hippocampal CA1 pyramidal neurons. Neuron 21:1189-1200.

Gruner JE, Hirsch JC, Sotelo C (1974) Ultrastructural features of the isolated suprasylvian gyrus in the cat. J Comp Neurol 154:1-27.

Hausser M, Mel B (2003) Dendrites: bug or feature? Curr Opin Neurobiol 13:372-383.

Hausser M, Spruston N, Stuart GJ (2000) Diversity and dynamics of dendritic signaling. Science 290:739-744.

Helmchen F, Svoboda K, Denk W, Tank DW (1999) In vivo dendritic calcium dynamics in deep-layer cortical pyramidal neurons. Nat Neurosci 2:989-996.

Hoffman DA, Johnston D (1999) Neuromodulation of dendritic action potentials. J Neurophysiol 81:408-411.

Hughes SW, Blethyn KL, Cope DW, Crunelli V (2002) Properties and origin of spikelets in thalamocortical neurones in vitro. Neuroscience 110:395-401.

Jaffe DB, Carnevale NT (1999) Passive normalization of synaptic integration influenced by dendritic architecture. J Neurophysiol 82:3268-3285.

Johnston D, Magee JC, Colbert CM, Cristie BR (1996) Active properties of neuronal dendrites. Annu Rev Neurosci 19:165-186.

Kamondi A, Acsady L, Buzsaki G (1998) Dendritic spikes are enhanced by cooperative network activity in the intact hippocampus. J Neurosci 18:3919-3928.

Kim HG, Connors BW (1993) Apical dendrites of the neocortex: correlation between sodium- and calcium-dependent spiking and pyramidal cell morphology. J Neurosci 13:5301-5311.

Landisman CE, Long MA, Beierlein M, Deans MR, Paul DL, Connors BW (2002) Electrical synapses in the thalamic reticular nucleus. J Neurosci 22:1002-1009.

Larkum ME, Zhu JJ (2002) Signaling of layer 1 and whisker-evoked Ca2+ and Na+ action potentials in distal and terminal dendrites of rat neocortical pyramidal neurons in vitro and in vivo. J Neurosci 22:6991-7005.

Larkum ME, Kaiser KM, Sakmann B (1999a) Calcium electrogenesis in distal apical dendrites of layer 5 pyramidal cells at a critical frequency of back-propagating action potentials. Proc Natl Acad Sci USA 96:14600-14604.

Larkum ME, Zhu JJ, Sakmann B (1999b) A new cellular mechanism for coupling inputs arriving at different cortical layers. Nature 398:338-341.

Larkum ME, Zhu JJ, Sakmann B (2001) Dendritic mechanisms underlying the coupling of the dendritic with the axonal action potential initiation zone of adult rat layer 5 pyramidal neurons. J Physiol 533:447-466.

Llinás R, Baker R, Sotelo C (1974) Electrotonic coupling between neurons in cat inferior olive. J Neurophysiol 37:560-571.

MacVicar BA, Dudek FE (1981) Electrotonic coupling between pyramidal cells: a direct demonstration in rat hippocampal slices. Science 213:782-785.

Magee J, Hoffman D, Colbert C, Johnston D (1998) Electrical and calcium signaling in dendrites of hippocampal pyramidal neurons. Annu Rev Physiol 60:327-346.

Magee JC (2000) Dendritic integration of excitatory synaptic input. Nat Rev Neurosci 1:181-190.

Magee JC, Cook EP (2000) Somatic EPSP amplitude is independent of synapse location in hippocampal pyramidal neurons. Nat Neurosci 3:895-903.

Mann-Metzer P, Yarom Y (1999) Electrotonic coupling interacts with intrinsic properties to generate synchronized activity in cerebellar networks of inhibitory interneurons. J Neurosci 19:3298-3306.

Massimini M, Amzica F (2001) Extracellular calcium fluctuations and intracellular potentials in the cortex during the slow sleep oscillation. J Neurophysiol 85:1346-1350.

McCormick DA, Connors BW, Lighthall JW, Prince DA (1985) Comparative electrophysiology of pyramidal and sparsely spiny stellate neurons of the neocortex. J Neurophysiol 54:782-806.

Nettleton JS, Spain WJ (2000) Linear to supralinear summation of AMPA-mediated EPSPs in neocortical pyramidal neurons. J Neurophysiol 83:3310-3322.

Nunez A, Amzica F, Steriade M (1993) Electrophysiology of cat association cortical cells in vivo: intrinsic properties and synaptic responses. J Neurophysiol 70:418-430.

Peinado A, Yuste R, Katz LC (1993) Extensive dye coupling between rat neocortical neurons during the period of circuit formation. Neuron 10:103-114.

Perez-Velazquez JL, Valiante TA, Carlen PL (1994) Modulation of gap junctional mechanisms during calcium-free induced field burst activity: a possible role for electrotonic coupling in epileptogenesis. J Neurosci 14:4308-4317.

Peters A (1994) Number of neurons and synapses in primary visual cortex. In: Cerebral Cortex, Further Aspects of Cortical Function; Including Hippocampus (Jones E, Peters A, eds), pp 267-294. New York: Plenum.

Poirazi P, Mel BW (2001) Impact of active dendrites and structural plasticity on the memory capacity of neural tissue. Neuron 29:779-796.

Rall W (1967) Distinguishing theoretical synaptic potentials computed for different soma-dendritic distributions of synaptic input. J Neurophysiol 30:1138-1168.

Rall W (1977) Core conductor theory and cable properties of neurons. In: Handbook of Physiology. The Nervous System. Cellular Biology of Neurons. (Kandel ER, Brookhart JM, Mountcastle VB, eds), pp 39-97. Bethesda: American Physiological Society.

Reyes A (2001) Influence of dendritic conductances on the input-output properties of neurons. Annu Rev Neurosci 24:653-675.

Rhodes PA, Llinás RR (2001) Apical tuft input efficacy in layer 5 pyramidal cells from rat visual cortex. J Physiol 536:167-187.

Rudolph M, Destexhe A (2003) A fast-conducting, stochastic integrative mode for neocortical neurons in vivo. J Neurosci 23:2466-2476.

Schiller J, Schiller Y (2001) NMDA receptor-mediated dendritic spikes and coincident signal amplification. Curr Opin Neurobiol 11:343-348.

Schiller J, Schiller Y, Stuart G, Sakmann B (1997) Calcium action potentials restricted to distal apical dendrites of rat neocortical pyramidal neurons. J Physiol 505:605-616.

Schiller J, Major G, Koester HJ, Schiller Y (2000) NMDA spikes in basal dendrites of cortical pyramidal neurons. Nature 404:285-289.

Schmitz D, Schuchmann S, Fisahn A, Draguhn A, Buhl EH, Petrasch-Parwez E, Dermietzel R, Heinemann U, Traub RD (2001) Axo-axonal coupling. a novel mechanism for ultrafast neuronal communication. Neuron 31:831-840.

Schwindt P, Crill W (1999) Mechanisms underlying burst and regular spiking evoked by dendritic depolarization in layer 5 cortical pyramidal neurons. J Neurophysiol 81:1341-1354.

Schwindt PC, Crill WE (1995) Amplification of synaptic current by persistent sodium conductance in apical dendrite of neocortical neurons. J Neurophysiol 74:2220-2224.

Schwindt PC, Crill WE (1997) Local and propagated dendritic action potentials evoked by glutamate iontophoresis on rat neocortical pyramidal neurons. J Neurophysiol 77:2466-2483.

Schwindt PC, Crill WE (1998) Synaptically evoked dendritic action potentials in rat neocortical pyramidal neurons. J Neurophysiol 79:2432-2446.

Simburger E, Stang A, Kremer M, Dermiezel R (1997) Expression of connexin43 mRNA in adult rodent brain. Histochem Cell Biol 107:127-137.

Smith MA, Ellis-Davies GC, Magee JC (2003) Mechanism of the distance-dependent scaling of Schaffer collateral synapses in rat CA1 pyramidal neurons. J Physiol 548:245-258.

Spencer W, Kandel E (1961) Electrophysiology of hippocampal neurons. IV. Fast prepotentials. J Neurophysiol 24:272-285.

Spruston N, Jaffe DB, Johnston D (1994) Dendritic attenuation of synaptic potentials and currents: the role of passive membrane properties. Trends Neurosci 17:161-166.

Steriade M, Glenn LL (1982) Neocortical and caudate projections of intralaminar thalamic neurons and their synaptic excitation from midbrain reticular core. J Neurophysiol 48:352-371.

Steriade M, McCarley RW (1990) Brainstem Control of Wakefulness and Sleep. New York: Plenum Press.

Steriade M, Datta S, Paré D, Oakson G, Curró Dossi R (1990) Neuronal activities in brainstem cholinergic nuclei related to tonic activation processes in thalamocortical systems. J Neurosci 10:2541-2559.

Steriade M, Curró Dossi R, Paré D, Oakson G (1991) Fast oscillations (20-40 Hz) in thalamocortical systems and their potentiation by mesopontine cholinergic nuclei in the cat. Proc Natl Acad Sci USA 88:4396-4400.

Steriade M, Amzica F, Contreras D (1996) Synchronization of fast (30-40 Hz) spontaneous cortical rhythms during brain activation. J Neurosci 16:392-417.

Steriade M, Timofeev I, Grenier F (2001) Natural waking and sleep states: a view from inside neocortical neurons. J Neurophysiol 85:1969-1985.

Stuart G, Schiller J, Sakmann B (1997) Action potential initiation and propagation in rat neocortical pyramidal neurons. J Physiol 505:617-632.

Svoboda K, Helmchen F, Denk W, Tank DW (1999) Spread of dendritic excitation in layer 2/3 pyramidal neurons in rat barrel cortex in vivo. Nat Neurosci 2:65-73.

Szentágothai J (1965) The use of degeneration methods in the investigation of short neuronal connections. In: Degeneration patterns in the nervous system, progress in brain research. (Singer M, Schadé P, eds), pp 1-32. Amsterdam: Elsevier.

Timofeev I, Steriade M (1997) Fast (mainly 30-100 Hz) oscillations in the cat cerebellothalamic pathway and their synchronization with cortical potentials. J Physiol 504:153-168.

Timofeev I, Crochet S (2002) Activity-dependent modulation of synaptic responses in vivo. Soc Neurosci Abstr 32: 345.16.

Timofeev I, Grenier F, Steriade M (2001) Disfacilitation and active inhibition in the neocortex during the natural sleep-wake cycle: an intracellular study. Proc Natl Acad Sci USA 98:1924-1929.

Timofeev I, Grenier F, Bazhenov M, Sejnowski TJ, Steriade M (2000) Origin of slow cortical oscillations in deafferented cortical slabs. Cereb Cortex 10:1185-1199.

Turner RW, Meyers DE, Barker JL (1993) Fast pre-potential generation in rat hippocampal CA1 pyramidal neurons. Neuroscience 53:949-959.

Valiante TA, Perez Velazquez JL, Jahromi SS, Carlen PL (1995) Coupling potentials in CA1 neurons during calcium-free-induced field burst activity. J Neurosci 15:6946-6956.

Waters J, Larkum M, Sakmann B, Helmchen F (2003) Supralinear Ca2+ influx into dendritic tufts of layer 2/3 neocortical pyramidal neurons in vitro and in vivo. J Neurosci 23:8558-8567.

Williams SR, Stuart GJ (1999) Mechanisms and consequences of action potential burst firing in rat neocortical pyramidal neurons. J Physiol 521:467-482.

Williams SR, Stuart GJ (2002) Dependence of EPSP efficacy on synapse location in neocortical pyramidal neurons. Science 295:1907-1910.

Williams SR, Stuart GJ (2003) Role of dendritic synapse location in the control of action potential output. Trends Neurosci 26:147-154.

Yuste R, Tank DW (1996) Dendritic integration in mammalian neurons, a century after Cajal. Neuron 16:701-716.

Zhu JJ, Connors BW (1999) Intrinsic firing patterns and whisker-evoked synaptic responses of neurons in the rat barrel cortex. J Neurophysiol 81:1171-1183.

FIGURES

Figure 8.1. Fast prepotentials (FPPs) in regular spiking (RS) neocortical neurons *in vivo*. Barbiturate anesthesia. Top left, electroencephalogram (EEG) and intracellular recording in area 5. The neuron was electrophysiologically identified as RS (top right). A part of the intracellular recording is expanded below (arrow). Different depolarizing events extracted are indicated in green (EPSPs) and blue (FPPs). Plotting the amplitude vs. the maximum slope for the selected events (middle panel, right) revealed an FPP population characterized by high-amplitude and fast-rising phase (dashed blue line). The bottom panel shows, on the left, an overlay of four EPSPs leading to FPPs in isolation or leading to full-blown action potential (AP). At right, the superimposition of averaged APs (red trace, truncated), FPPs (blue trace), and 'fast' (max. slope >3 V/s) EPSPs (green trace).

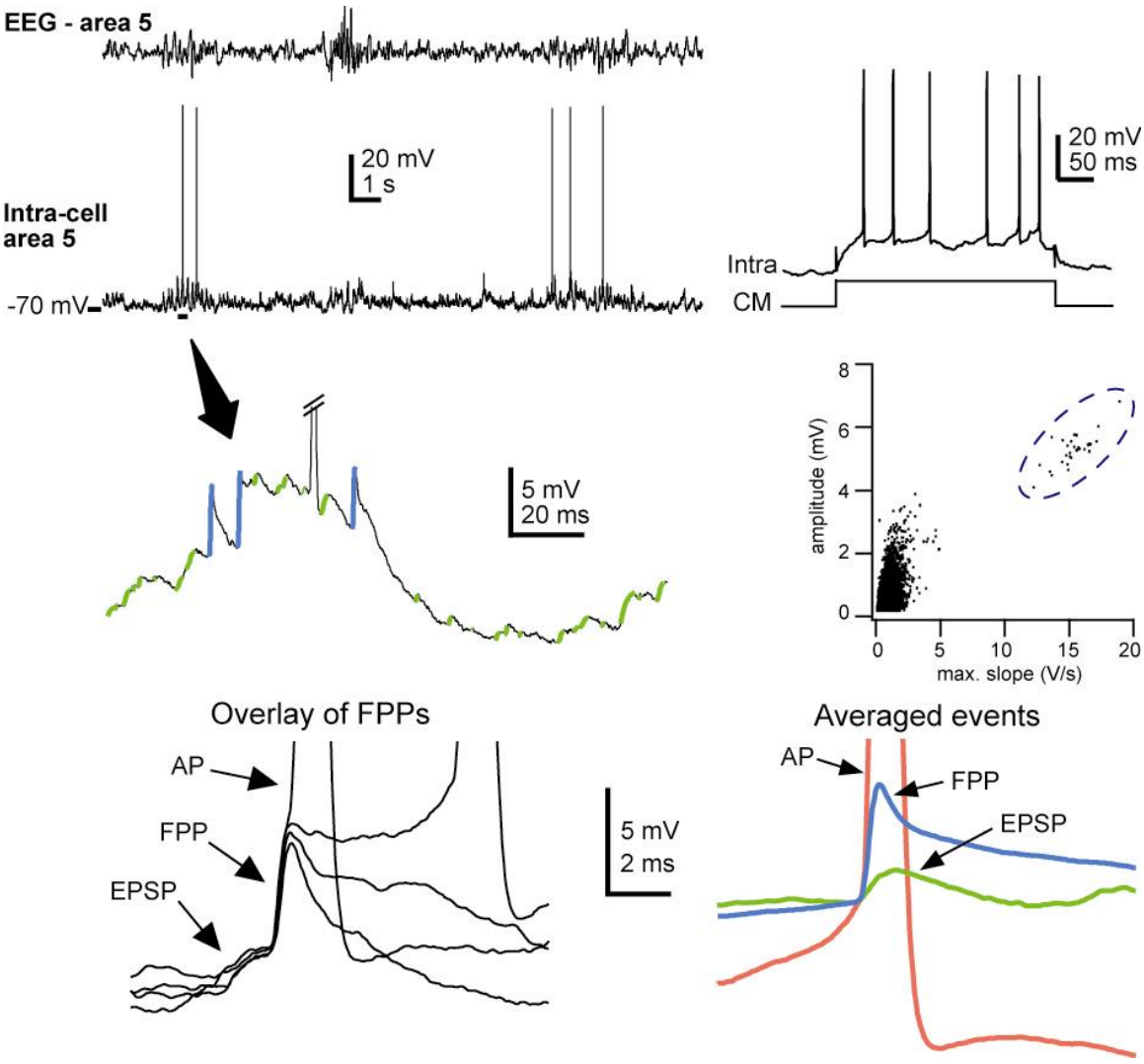
EEG - area 5
20 mV
1 s
Intra-cell
area 5
-70 mV
20 mV
50 ms
Intra
CM
5 mV
20 ms
amplitude (mV)
max. slope (V/s)
Overlay of FPPs
AP
FPP
EPSP
5 mV
2 ms
Averaged events
AP
FPP
EPSP

Figure 8.2. Depth distribution of regular-spiking (RS) and intrinsically-bursting (IB) neurons recorded in the intact cortex of anesthetized cats (association areas 5 and 7). Histograms show the depth distribution for the neurons in which no FPP were detected (left) and for the neurons with FPPs (right). The depth of the recorded neurons was corrected according to the angle of the pipette.

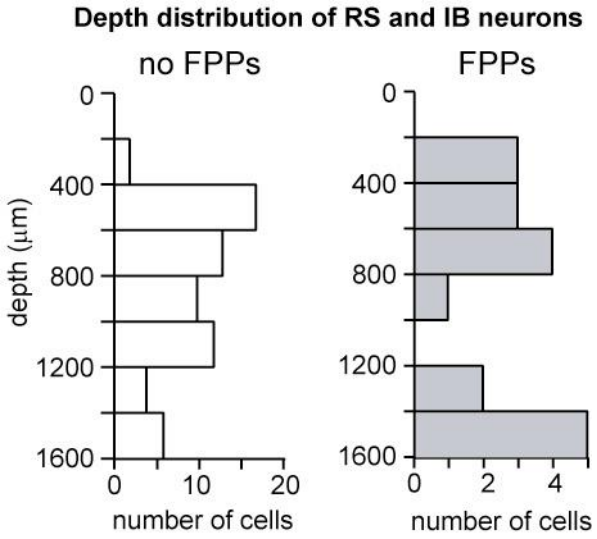
Depth distribution of RS and IB neurons
no FPPs
FPPs
depth (μm)
0
400
800
1200
1600
0
10
20
number of cells
0
2
4
number of cells

Figure 8.3. FPPs' generation is voltage dependent. Four traces in the top panel depict EEG from the depth of cortical area 5, intracellular recording from the same area, its first derivative, and the current monitor (CM). Barbiturate anesthesia. The cell was held at two V_m levels by injection of hyperpolarizing current pulses. The presence of FPPs is revealed by peaks in the derivative signal (peaks corresponding to APs are truncated); note their absence when the V_m is below –70 mV. The bottom left histograms show the V_m (gray) and the V_m for FPP initiation (FPP threshold, black line). Averaged FPPs is shown in the bottom right panel. The dashed line represents the mean threshold.

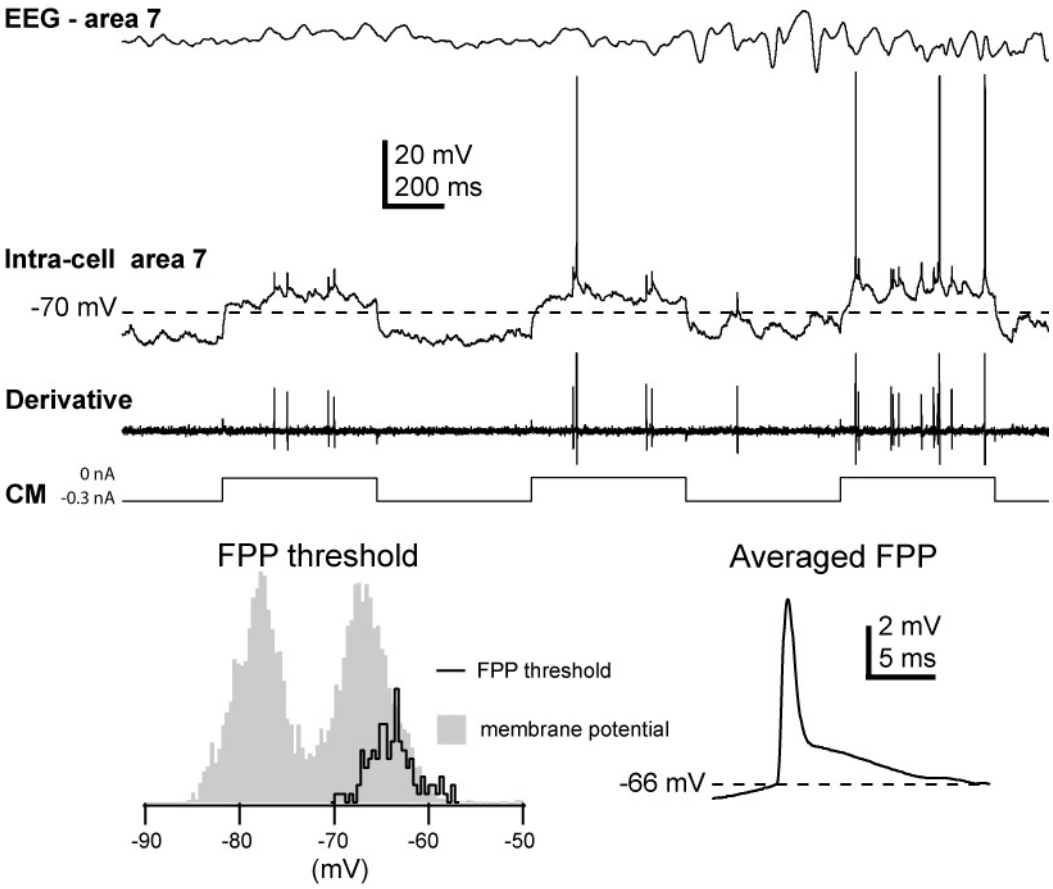
EEG - area 7
20 mV
200 ms
Intra-cell area 7
-70 mV
Derivative
CM
0 nA
-0.3 nA
FPP threshold
FPP threshold
membrane potential
-90
-80
-70
-60
-50
(mV)
Averaged FPP
2 mV
5 ms
-66 mV

Figure 8.4. FPPs' generation depends on synaptic transmission. Barbiturate anesthesia. The upper panel shows the EEG and intracellular recording of a cortical neuron in three conditions of extracellular Ca^{2+} ($[Ca^{2+}]_o$). The same neurons were recorded while a microdialysis probe inserted in the vicinity of the pipette was perfused with normal artificial cerebrospinal fluid (ACSF) (control, *Cont*), with ACSF enriched in Ca^{2+} (High Ca^{2+}, *H Ca*) and with Ca^{2+} free ACSF (low Ca^{2+}, *L Ca*). Note the increase and decrease of the background synaptic activity in H Ca and L Ca conditions respectively. The middle panel shows the superimposition of APs and FPPs for the three conditions. Note the presence of FPPs in isolation, FPPs of leading to APs, and APs arising from summation of EPSPs in *Cont* and *H Ca* conditions while in *L Ca* condition all APs arose from EPSPs. Note also the change in firing threshold for axo-somatic APs. The left bottom panel shows the mean incidence (± SEM) of FPPs in the three conditions of extracellular Ca^{2+} calculated for the neuron depicted in the upper panels. The middle and rigth bottom histograms show the mean firing rates and mean V_ms (± SEM) calculated for 10 cortical neurons in the three conditions. Asterisks represent significant difference: *, $P<0.05$ and **, $P<0.01$.

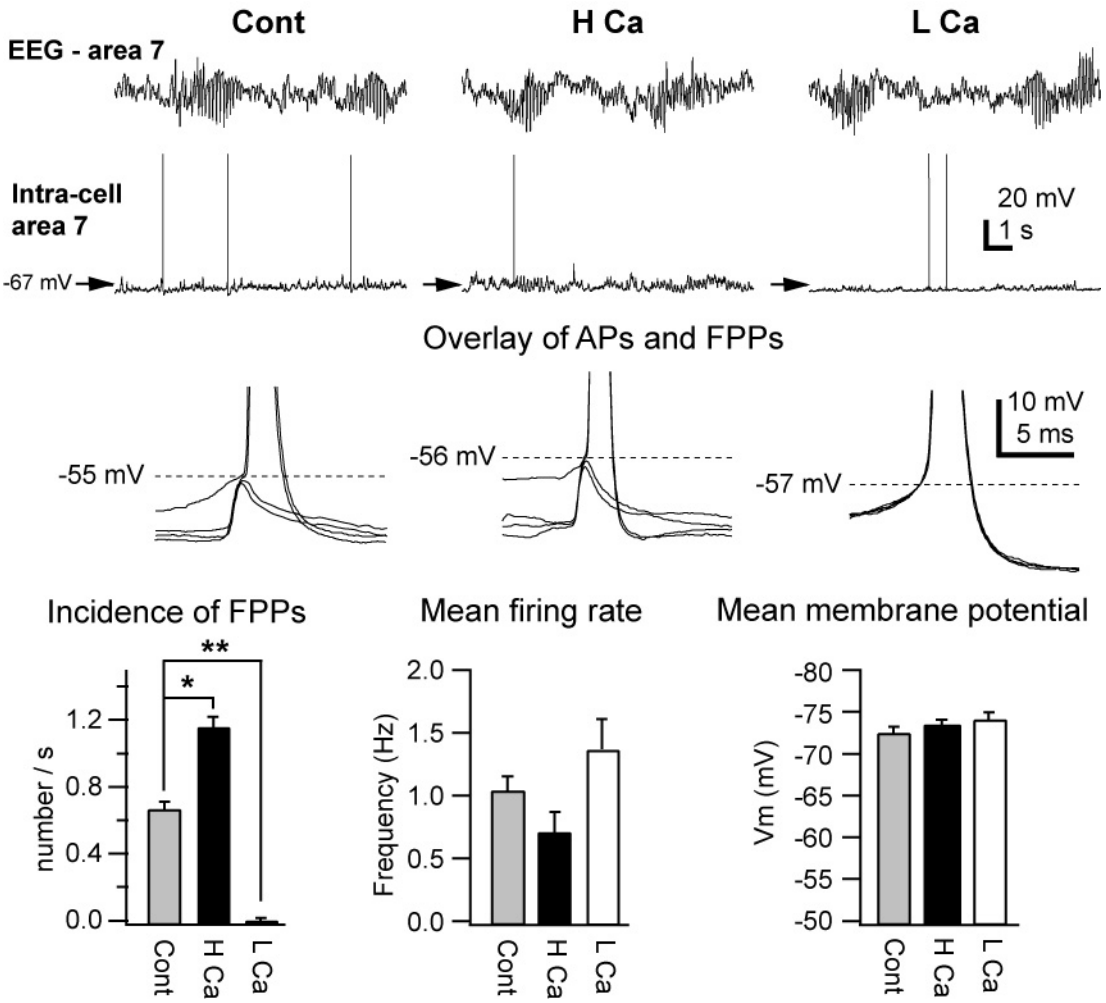
Cont
H Ca
L Ca
EEG - area 7
Intra-cell
area 7
-67 mV
20 mV
1 s
Overlay of APs and FPPs
-55 mV
-56 mV
-57 mV
10 mV
5 ms
Incidence of FPPs
Mean firing rate
Mean membrane potential
number / s
Frequency (Hz)
Vm (mV)
**
*
Cont
H Ca
L Ca

Figure 8.5. FPPs are present in isolated cortical slab. Ketamine-xylazine anesthesia. *A*, local field potential and intracellular recording in small isolated cortical slab from areas 5-7, showing one spontaneous and two cortically evoked (▲ marks cortical stimuli) active periods. FPPs are present during active periods associated with intense synaptic activity. The lower panel depicts a superimposition of four FPPs in isolation or leading to full-blown APs (left) and averaged FPPs (right). *B,* active periods were evoked in isolated slab by cortical stimuli every 3 s (▲), while holding the cell at different V_m levels by injection of DC current. FPPs (arrowheads) were present during active periods only when V_m reached the threshold for their generation (bottom left) and their frequency increased with the depolarization of the neuron (bottom right). Baseline V_m is V_m just before cortical stimulation; FPPs' frequency is expressed as the mean number of FPPs (± SEM) by second of active periods. Asterisks represent significant difference with previous V_m level: **, $P<0.01$ and ***, $P<0.001$.

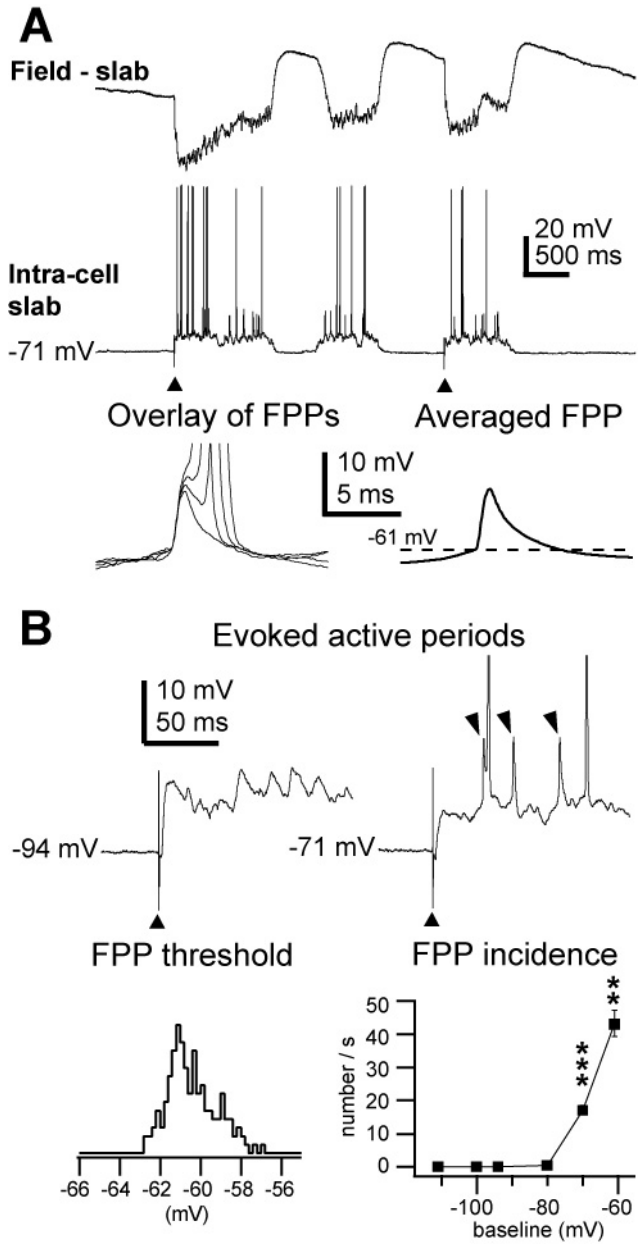
A
Field - slab
20 mV
500 ms
Intra-cell
slab
-71 mV
Overlay of FPPs
Averaged FPP
10 mV
5 ms
-61 mV
B
Evoked active periods
10 mV
50 ms
-94 mV
-71 mV
FPP threshold
FPP incidence
-66 -64 -62 -60 -58 -56
(mV)
number / s
50
40
30
20
10
0
***
***
-100 -80 -60
baseline (mV)

Figure 8.6. FPPs can be evoked by specific cortical inputs. Barbiturate anesthesia. *A*, cortical stimulation evoked a sequence of depolarization-hyperpolarizing potential; the early depolarization was crowned with a FPP when it reached the threshold for FPP generation. In the same neuron, stimulation of thalamic intralaminar centrolateral (CL) nucleus evoked a slow depolarizing response with long latency that never evoked an FPP, even when it passed over the threshold. *B*, another neuron. FPP was evoked by cortical stimulation through one electrode (Cx1), whereas stimulation with another cortical electrode (Cx2) was not able to elicit a FPP. The bottom panel shows the V_m at the peak of the evoked responses (response V_m) as a function of the V_m before stimulation (baseline membrane potential). Blue triangles, stimulation through the first cortical electrode (Cx1); green circles, stimulation through the second cortical electrode (Cx2). Note the linear progression of the response to stimulation of the first electrode (open triangles) until it reaches the threshold for FPP generation, and the jump in the response V_m when FPPs were generated (plain triangles). The response to stimulation through the second electrode followed a linear progression even above the threshold for FPP generation. *C*, cortical neuron in which single cortical stimulation (left) did not evoke an FPP, whereas paired stimuli at 10-ms interval (right) evoked an FPP (arrow) that crowned the second EPSP (superimposed three responses in each case). Note that in one case the FPP led to a full blown AP (AP truncated).

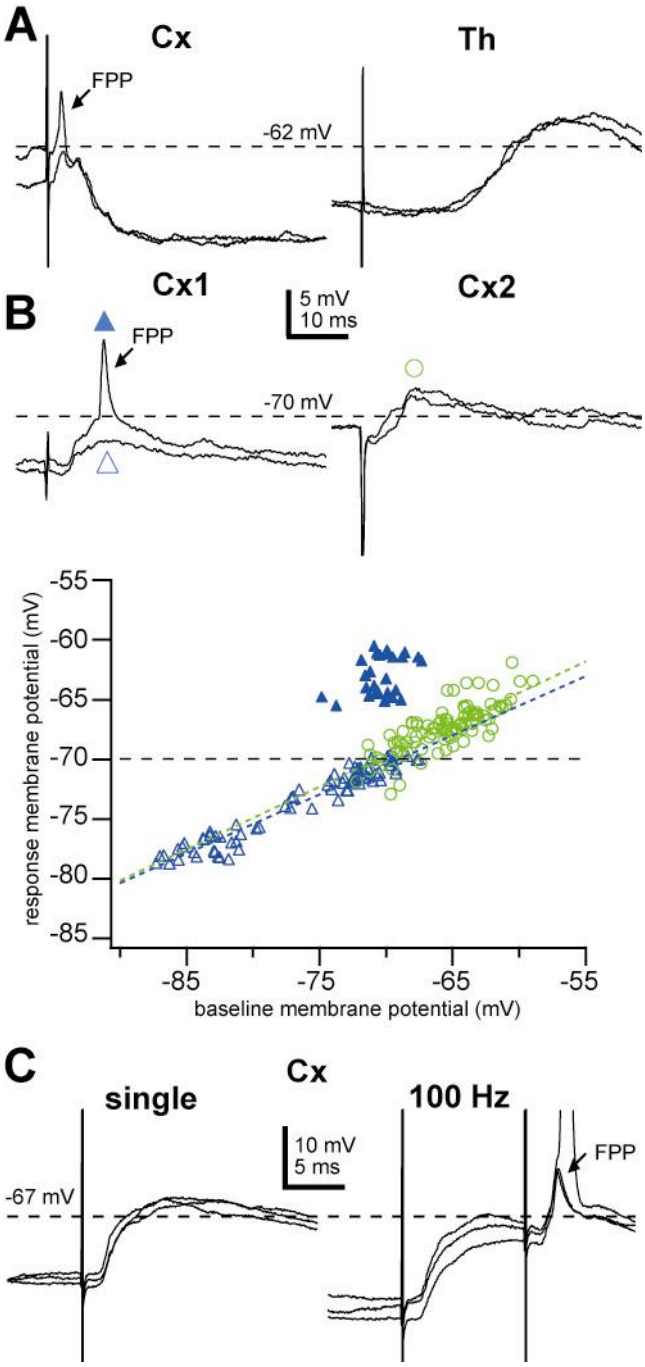
A
Cx
Th
FPP
-62 mV
B
Cx1
Cx2
5 mV
10 ms
FPP
-70 mV
response membrane potential (mV)
-55
-60
-65
-70
-75
-80
-85
-85
-75
-65
-55
baseline membrane potential (mV)
C
single
Cx
100 Hz
10 mV
5 ms
-67 mV
FPP

Figure 8.7. FPPs allow neuronal firing at more hyperpolarized levels. Barbiturate anesthesia. *A*, a short period of intracellular recording (APs truncated) shows two FPPs in isolation, one FPP leading to full-blown AP, and one AP elicited by summation of EPSPs. Parts indicated by arrows are expanded below with the derivative of the intracellular signal showing a peak preceding the AP (middle) or in isolation (right). Note that the summation of several EPSPs is necessary to reach firing threshold while one FPP is sufficient from the same level of V_m. *B*, left panel depicts a superimposition of averaged APs elicited by summation of EPSPs (red), AP elicited by FPP (black) and FPP in isolation (blue). The right panel shows histograms for the amplitude of FPPs (up) as well as for the threshold for APs (red) and FPPs (blue) (down). Histograms were fitted with Gaussian functions (thick lines). Note that FPPs were initiated at a level of depolarization nearly 5 mV below the usual firing level and that their mean amplitude was above 5 mV, thus allowing the cell to fire at more hyperpolarized V_m.

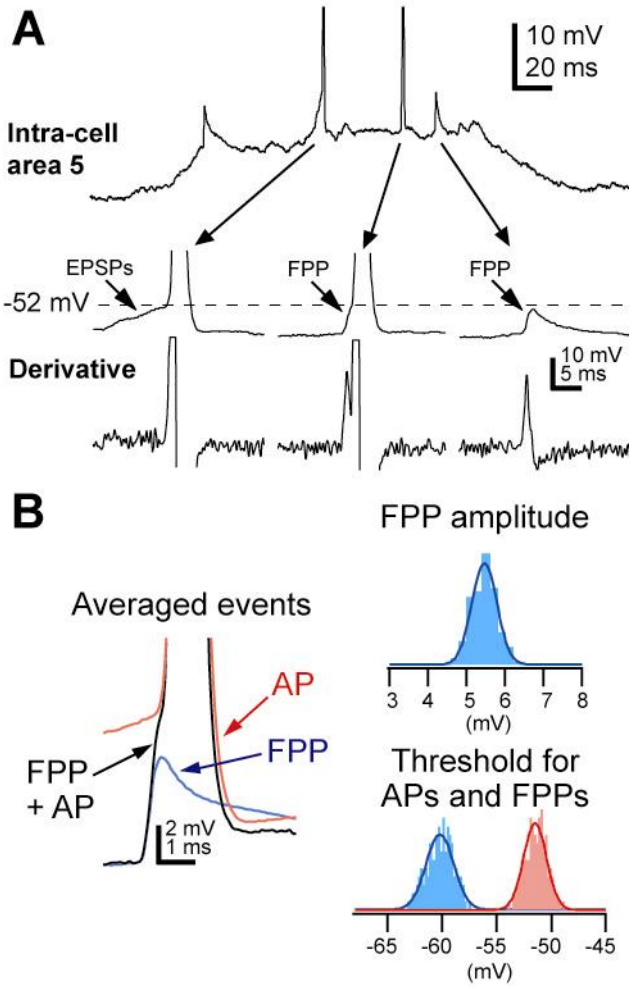
A
10 mV
20 ms
Intra-cell
area 5
EPSPs
FPP
FPP
-52 mV
Derivative
10 mV
5 ms
B
FPP amplitude
Averaged events
AP
FPP
FPP
+ AP
2 mV
1 ms
3 4 5 6 7 8
(mV)
Threshold for
APs and FPPs
-65 -60 -55 -50 -45
(mV)

Figure 8.8. FPPs boost the output of cortical neurons. Barbiturate anesthesia. Top panel, overlay of four cortically evoked responses at different V_m levels. At hyperpolarized levels, the cortical stimulation evoked an EPSP followed by an IPSP; when the cell was more depolarized, the EPSP reached the threshold for FPP generation and an FPP crowned the EPSP; when the cell was slightly more depolarized, the FPP reached the firing threshold and elicited an AP; finally, at more depolarized level, an AP could be elicited directly from the EPSP. Blue and green traces represent, respectively, the responses that evoked an FPP and the responses that did not. The middle panel represents the maximum V_m reached by the response in function of the V_m just before stimulation. Green circles and blue triangles represent responses without and with an FPP, respectively. Plain symbols indicate APs overshooting at about 10 mV. In the bottom panel, the probability for the cortical stimulation to evoke an AP in function of the V_m, when an FPP is generated (blue triangles) or not (green circles). The response curves obtained were fitted with sigmoid functions. Note that FPP generation shifts the response curve by 5 mV to more hyperpolarized levels.

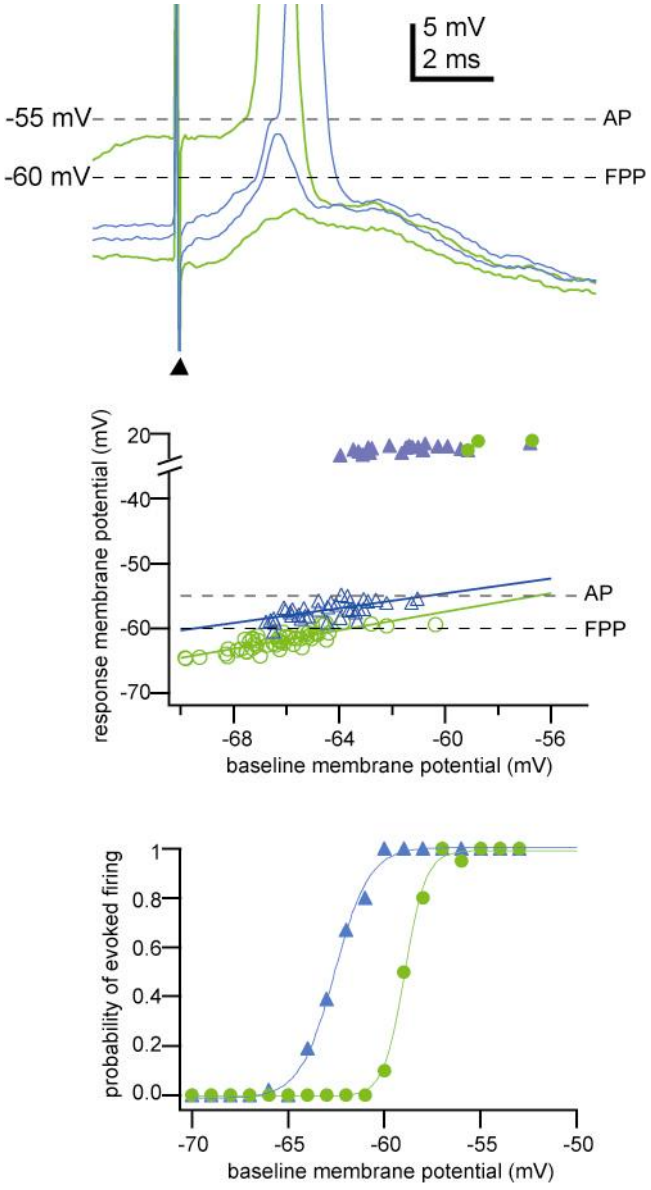
5 mV
2 ms
-55 mV
-60 mV
AP
FPP
response membrane potential (mV)
20
-40
-50
-60
-70
-68
-64
-60
-56
baseline membrane potential (mV)
AP
FPP
probability of evoked firing
1
0.8
0.6
0.4
0.2
0.0
-70
-65
-60
-55
-50
baseline membrane potential (mV)

Figure 8.9. FPP generation is regulated across the states of vigilance. Four traces in the top panel depict electromyogram (EMG), electro-oculogram (EOG), EEG from the depth of right cortical area 3 (somatosensory), and intracellular recording from left area 3. The same neuron was recorded during waking (W), slow-wave sleep (SWS) and paradoxical sleep (PS). Parts of the intracellular recording marked by horizontal bars are expanded bellow. The derivative of the intracellular signal revealed the presence of FPPs (APs are truncated in intracellular recording and its derivative). Note the absence of FPP when the cell is more hyperpolarized than –65 mV. The left bottom panel shows averaged FPPs. The middle bottom panel shows the distribution of V_m of the neuron depicted in the three behavioral states (W, red; SWS, green and PS, blue). The right bottom panel shows the mean incidence of FPPs in the three behavioral states calculated for 8 neurons. Asterisks represent significant difference: *, $P<0.05$ and **, $P<0.01$.

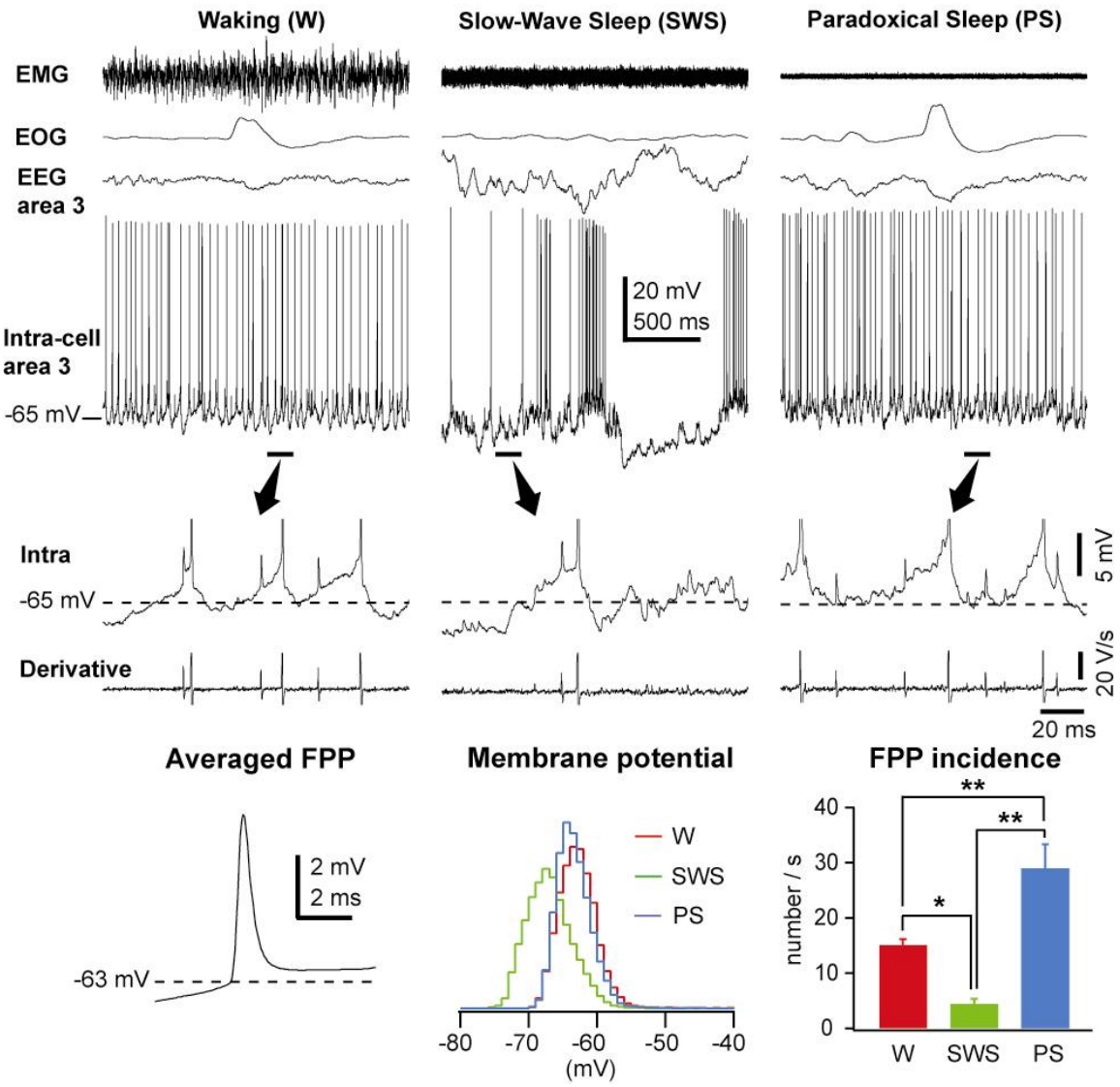
Waking (W)
Slow-Wave Sleep (SWS)
Paradoxical Sleep (PS)
EMG
EOG
EEG
area 3
Intra-cell
area 3
-65 mV
20 mV
500 ms
Intra
-65 mV
Derivative
5 mV
20 V/s
20 ms
Averaged FPP
2 mV
2 ms
-63 mV
Membrane potential
W
SWS
PS
-80
-70
-60
-50
-40
(mV)
FPP incidence
**
**
*
40
30
20
10
0
number / s
W
SWS
PS

9. DISCUSSION

In the present work the membrane properties of RE neurons, both intrinsic and synaptic, have been studied in an *in vivo* model. We also discussed their importance for network oscillations in the thalamic network. The results have demonstrated new features in the membrane properties of RE neurons, and their implication for the generation, spreading, modulation and synchronization of spindle oscillations in the RE and thalamic networks. Thus, the study had assessed bottom-up relations (from cellular to network level) as well as top-down interactions (from network to cellular level). These results were presented and discussed in detail in the preceding sections. This section will present a general discussion of the findings and an integrated model of them.

The study dealt mainly with five different topics, all of them tightly related, since they implied the RE nucleus and its essential role in thalamic spindle oscillations. The topics studied were:

1. Electrical synapses and their role in network oscillations.
2. Intrinsic membrane bistability and their role in network oscillations.
3. Membrane properties and their modulation by network activity.
4. Synaptic membrane responsiveness and its integrative properties.
5. Intrinsic chemical synapses and their role in network oscillations.

The main results of the present study can be summarized as follows:

a) RE neurons display electrical synapses mediated by gap junctions, which have a role in the propagation of spindle activities in the RE network.
b) Some RE neurons express an intrinsic conductance that produces membrane bistability, which affects both membrane integrative properties and general spindling pattern in thalamic networks.
c) Intrinsic membrane properties of RE neurons are powerfully modulated by network activities.
d) Cortico-RE EPSPs show a secondary depolarizing component that is highly relevant for integrative membrane properties of RE neurons.
e) Prolonged-hyperpolarizing potentials precede spindle waves, likely acting as primers for the initiation of the rhythm in the thalamus.

9.1. Technical considerations

All the results here presented were obtained from preparations *in vivo*, where the structure and connectivity of the central nervous system remains intact (Domich et al., 1986; Steriade et al., 1986; Steriade, 2001). Even more, the ionic conditions, which are of supreme importance in any electrophysiological study, were not mainly affected by the method of study here employed (Steriade, 2001). Therefore, it can be safely ascertained that the present results are close to physiological conditions under which the RE nucleus operates and spindle waves normally occur (Domich et al., 1986; Steriade et al., 1986; Steriade et al., 1997).

About the quality of the recordings it is also important to clarify some points. *In vivo* intracellular recordings in the RE nucleus are especially difficult to perform (Mulle et al., 1986), likely due to the structure of the nucleus, which is a very thin layer (0.5 mm) of cells, massively traversed by thalamocortical and corticothalamic axons (Jones, 1975a; Yen et al., 1985). Additionally, most neurons present somas quite small (20-30 μm, (Yen et al., 1985)) when compared to other brain regions, and their spatial orientation is parallel to the recording micropipette, due to the vertical-lateral orientation of the RE nucleus (Jones, 1975a; Yen et al., 1985), making it difficult not only to impale, but to maintain stable recordings for long periods (Mulle et al., 1986; Contreras et al., 1993).

Nevertheless, our results are based mostly on long-duration recordings (30-180 min.) that assured their quality. First, most recordings were stable, e.g. did not show abrupt changes in membrane potential. Second, action potentials were overshooting, with amplitudes in the range of 60-70 mV. Third, the resting membrane potential was quite hyperpolarized (~-75 mV) and neurons did not fire during those periods. Most studies in slices have presented intracellular recordings of RE neurons where the resting membrane potential is quite hyperpolarized, in the range of -70 mV to -80 mV. Experiments performed in recent years under *in vivo* conditions with patch clamp recordings, have found relatively low-rate discharges in cortical neurons, suggesting that sharp electrodes produce perturbations in neuronal membranes, which depolarize the membrane potential and increase the neuronal firing rate (Waters et al., 2003). Our results obtained in the RE nucleus with sharp electrodes showed in all cases quite hyperpolarized values of membrane potential, suggesting that the recording microelectrode did not produce alterations in neuronal membranes. Moreover, the discharge frequencies obtained under both extra- and intracellular recordings were quite similar, precluding the possibility that the recording technique would damage or alter the membrane constitution of RE neurons.

One important difference between *in vivo* and *in vitro* studies is the neuronal apparent input resistance (R_{in}). In fact, experiments performed in slices have reported values of R_{in} one order of magnitude higher than those found using *in vivo* preparations (Mulle et al., 1986; Contreras et al., 1993; McCormick et al., 1995; Cox et al., 1997; Zhang et al., 1997). The explanation of this difference does not reside in the physical alteration of neuronal membranes produced by sharp electrodes, which is not supposed to

occur with patch-clamp electrodes; but on the ongoing level of network activity. As explained above, probably the major virtue of *in vivo* preparations is the presence of auto-sustained, reverberant network activity in any brain region, but especially cortex, thalamus and RE nucleus (Steriade, 2001). Such activity is especially rich and complex in the thalamocortical system (Steriade et al., 1997; Steriade, 2001).

Therefore, *in vivo* preparations have the virtue of maintaining the experimental conditions close to the physiological ones. However, in this kind of preparations it is not possible to study in detail the ionic composition of both synaptic and intrinsic neuronal responses; or to determine the specific properties of receptors involved in the transduction cascades. In the same way, the use of optic techniques and voltage-sensitive dyes is limited (Devor and Yarom, 2002; Leznik et al., 2002; Petersen et al., 2003). Thus, *in vivo* preparation have a highly qualitative value, since they closely represent physiological conditions; however their quantitative power of resolution is poor, given that they cannot shed light on many of the molecular elements involved in the subject of study.

9.2. Towards an integrated model of thalamic oscillations

All the presented results are closely related and relevant for the understanding of the functioning of the RE nucleus in the complex thalamocortical network as well as for its relation to spindle oscillations. Spindles are transferred to the cerebral cortex through the interactions between RE and thalamocortical neurons (Steriade et al., 1993b; McCormick and Bal, 1997). Thus, experimental evidence has shown that spindles are abolished in thalamocortical systems after lesions of RE neurons or transections separating them from thalamocortical neurons (Steriade et al., 1985) but survive in the RE nucleus deafferented from the dorsal thalamus and cerebral cortex (Steriade et al., 1987a). Computational studies agreed with the initiation of spindle rhythmicity in the isolated RE nucleus (Wang and Rinzel, 1993; Destexhe et al., 1994a; Bazhenov et al., 2000) and suggested that, at relatively hyperpolarized levels of membrane potential, as is the case during slow-wave sleep, the IPSPs between RE neurons can be reversed and $GABA_A$-mediated depolarizing potentials can generate persistent spatio-temporal patterns in the RE nucleus (Bazhenov et al., 1999). These experiments provided the first proposal of a mechanism for the initiation of spindles in the RE network. The transfer of spindles from the RE nucleus, which is devoid of cortical projections, to the cerebral cortex is due to RE-cells' interactions with thalamocortical neurons (Steriade et al., 1993b; von Krosigk et al., 1993; Bal et al., 1995a, b).

Electrical coupling might mediate synchronization of thalamic oscillations

Our results show that RE neurons investigated *in vivo* display small but rapidly rising and decaying potentials, termed spikelets in recent *in vitro* studies on RE (Landisman et al., 2002) and thalamocortical (Hughes et al., 2002) neurons, which are a sign of electrotonic coupling. In the absence of definitive dual intracellular recordings from neighboring RE neurons, the evidence indicate that spikelets recorded in our experiments were not synaptically triggered events. Additionally, spikelets are not dependent on synaptic inputs from cortex, as is the case of dendritic spikes that are most efficiently triggered by cortico-RE volleys (Contreras et al., 1993), since they occurred without changes in incidence and shape/amplitude in decorticated animals. As well, recordings with KCl-filled micropipettes, to reverse $GABA_A$-receptor-mediated potentials, did not affect their characteristic features.

Although electrotonic coupling has been described in a variety of central structures in mammals, at least for neocortex it is common in early stages of circuit formation and decreases during later development (Connors et al., 1983; Peinado et al., 1983). Among the exceptions to this rule are the inferior olive in which the morphological correlate of the electrotonic coupling, gap junctions, is present at birth (Bourrat and Sotelo, 1983) and RE neurons in which spikelets were recorded in our experiments on adult cats. In these two structures, the role of electrotonic coupling may be that of a synchronizing device.

Experimental and modeling studies have shown that electrotonic coupling underlies the rhythmicity of complex spike activity in the olivo-cerebellar pathway (Welsh and Llinás, 1997; Makarenko and Llinás, 1998; Loewenstein et al., 2001). A combination of electrical and chemical synapses among local-circuit basket inhibitory neurons has been proposed to entrain fast rhythms, in the gamma frequency range, in rat neocortex (Tamas et al., 2000), and electrical synapses are also thought to generate gamma oscillations in the hippocampus (Draguhn et al., 1998; Traub et al., 1999a; Traub et al., 1999b).

As to the RE nucleus, besides chemical synapses among these GABAergic neurons, which have been implicated in the generation and synchronization of spindle rhythms in experimental (Steriade et al., 1987a) and modeling (Destexhe et al., 1994a; Bazhenov et al., 1999; Bazhenov et al., 2000) studies, electrotonic coupling may be an additional factor in this synchronizing processes. In fact, our computer simulations showed that activity in the RE nucleus can spread not only between pairs of neighboring electrotonically coupled neurons but also at greater distances. This spreading activity could not be due to single spikelets because they are not able to trigger action potentials. However, LTSs may be able to activate a neighbor cell and thus contribute to the propagation and synchronization of spindle activity. This could be expected due to the low-pass properties of gap junctions (Landisman et al., 2002), which strongly filter fast signals (such as action potentials) but not slower signals (as LTSs). Besides a role in spreading slow activities in the RE nucleus, predicted by modeling studies, we propose

that electrical coupling in the RE nucleus may be functionally relevant for the synchronization of thalamic oscillations.

Intrinsic properties can generate membrane bistability and shape thalamic spindle oscillations

The active state in bistable RE neurons has the characteristics of plateau potentials**.** Such behavior could be generated either by intrinsic membrane properties or a particular synaptic activity in the thalamocortical network. The membrane bistability that we reported seems to be intrinsically generated, as is the case described in multiple structures in the central nervous system, as the spinal cord (Bennett et al., 1998), cerebellum (Llinás and Sugimori, 1980a, b), dorsal thalamus (Williams et al., 1997; Toth et al., 1998; Hughes et al., 1999), neocortex (Schwindt and Crill, 1999), olfactory bulb (Heyward et al., 2001), and hippocampus (Chuang et al., 2000; Fricker and Miles, 2000). That membrane bistability is an intrinsic, voltage-dependent property of RE neurons was indicated by its presence only at the resting membrane potential, through induction of prolonged depolarizing plateaus by brief intracellular current pulses, and by termination of these plateaus by hyperpolarizing current pulses. Our results indicate that intrinsic mechanisms are involved in the generation, maintenance, and termination of active states during membrane bistability. While the active state represents a depolarized plateau potential that may be de-activated by hyperpolarization, the silent state is maintained until sufficient depolarization occurs to initiate an active depolarization toward the active state. The transition from the silent to the active state proceeds exponentially. Our data

showed that small-amplitude EPSPs are ineffective in spike generation during the silent state. However, when EPSPs are strong enough, they give rise to action potentials even during the silent state, and the transition to an active state may occur.

The two different modes of membrane bistability are associated with different degrees of neuronal responsiveness. The active state is around the threshold for action potential generation, while the silent state is subthreshold. A broader range of depolarizing inputs' amplitudes may be processed during the silent state, without the generation of a short-latency and stereotyped spike, than in the active state. On the other hand, small-amplitude EPSPs, which are ineffective during the silent state, may well trigger action potentials during the active state. When excitatory inputs occurring during the silent state are strong enough, transition to the active state might occur. Such transition amplifies the voltage change produced by transient depolarizing signals.

Actually, corticofugal volleys elicit complex depolarizing responses in RE neurons, composed by several EPSPs followed by all-or-none events resembling dendritic spikes or, in less numerous RE neurons, presumably unitary dendritic spikes (Contreras et al., 1993). The dendritic spikes may contribute to the generation of spindle oscillations by boosting distal inputs and depolarizing the soma as well as by triggering dendritic low-threshold spikes (Huguenard and Prince, 1992; Destexhe et al., 1996; Huguenard, 1996) that are crucial in the generation of spindle oscillations. Thus, although an intrinsic membrane property, bistability may strongly be modulated by synaptic activity.

Membrane bistability in a subgroup of RE neurons may play an important role in different patterns of spindles displayed by thalamocortical neurons. Consequently, any change in the bursting pattern of RE neurons would affect their targets, thalamic relay neurons. Our intracellular recordings of thalamocortical cells showed at least two different patterns during spontaneously occurring spindles. Although simultaneous recordings of RE and thalamocortical neurons have not been performed in the present experiments, the two patterns displayed may be related to the actions exerted by non-bistable and bistable RE neurons, respectively. Indeed, non-bistable neurons fired stronger bursts, with higher intra-bursts frequencies, which are assumed to generate deeper and longer IPSPs in TC neurons, giving rise to the usual frequency range of spindles under barbiturate anesthesia, ~7-10 Hz. By contrast, IPSPs with lower amplitudes and higher frequency, up to 20 Hz, are likely to be mainly generated by single action potentials in RE neurons, as they occur during the depolarizing plateau in bistable cells. In either case, the crucial role of RE neurons in initiating spindles, even in the absence of feed-back excitatory effects from thalamocortical neurons, is shown by the absence of rebound bursts with fast action potentials after the first three or four IPSPs in relay cells (Timofeev et al., 2001). Supporting these results, computational models of thalamic networks, including bistable RE neurons, showed a significant shaping of thalamic oscillations in thalamocortical neurons by bistable RE neurons. While spindles are initiated in the RE nucleus (Steriade et al., 1985; Steriade et al., 1986; Steriade et al., 1987a), this oscillation is maintained by reciprocal actions between RE and

thalamocortical neurons (Steriade et al., 1993a; von Krosigk et al., 1993; Bal et al., 1995a, b).

Therefore, one single intrinsic membrane property can have important effects on the network behavior, as is the case of membrane bistability which may sculpt the shape of spindle in thalamic networks. However, the other way around is also true, since ongoing synaptic activity can modulate the dynamics of intrinsic membrane bistability in single cells in the RE nucleus.

Membrane properties are modulated during thalamic oscillations

Our experimental results have shown that spindle oscillations modulate membrane properties of RE neurons during spindle waves, by producing several effects: an average depolarization of membrane potential (10-20 mV), increased membrane fluctuations (1-3 mV to 10 mV) and decreased R_{in} (up to 80%). All these three were mainly due to the sequential activation of powerful LTSs in those neurons (Mulle et al., 1986; Huguenard and Prince, 1992; Contreras and Steriade, 1995). Membrane fluctuations were increased by almost one order of magnitude during spindle waves, but this effect was not entirely due to LTSs occurring during spindles, since fast activities, as constituted by EPSPs and spikelets (Kim et al., 1997; Landisman et al., 2002) were also enhanced. This is consistent with our results which demonstrate a role for spreading and synchronization of activity in the RE nucleus by electrical connections, as those mediated by gap junctions (see below).

The effect of synaptic background activity on ongoing cellular activity has previously been studied, especially for the cortex, with computational models (Ho and Destexhe, 2000; Destexhe et al., 2003; Fellous et al., 2003), through the generation of different artificial states of background noise *in vitro* (Stacey and Durand, 2001; McCormick et al., 2003; Mitchell and Silver, 2003), and through the activation of synaptic potentials or local suppression of network activity *in vivo* (Destexhe et al., 1996; Timofeev et al., 1996). Those studies showed that membrane depolarization and small to moderate membrane fluctuations may facilitate the responsiveness to synaptic inputs, especially those of lower amplitude. Our results showed that volleys of synaptic activity can result in significant changes in neuronal excitability and responsiveness in RE neurons.

Even if spindles were not to be considered as cortical high-conductance states, they are clearly active network states. Active network states imply a series of consequences for integrative properties of neurons. One consequence is that responsiveness of neurons is markedly different in the presence of fluctuating background synaptic activity. Due to the presence of membrane potential fluctuations, neurons respond stochastically to a given stimulus, and their behavior is best described by probability functions; this has been demonstrated for cortical cells (Ho and Destexhe, 2000). Consistent with these observations in the cortex, our experiments showed that RE neurons respond to cortical activation in a way that is well fitted by probability functions. Another effect of active network states is on temporal processing. The reduction of the

space constant in states of high conductance is accompanied by a marked reduction in the membrane time constant (Destexhe et al., 2003). This result was apparent in our experimental data, since active responses were faster to injected positive current pulses. As it has been proposed, the reduced time constant should favor finer temporal discrimination of distant synaptic inputs. Modeling studies have predicted that cortical neurons can resolve higher frequency inputs in active membrane states than when silent; therefore, cortical cells in high-conductance states can efficiently track synaptic inputs (Destexhe et al., 2003). It is expected that a similar case might be found in RE neurons, though evidence should be provided by future experiments.

Thus, our results support the idea that synaptic and intrinsic activities in the RE network is highly modulated at the cellular level by thalamic oscillations, which are generated by the RE nucleus itself.

Integrative properties during synaptic responsiveness are relevant for the generation and maintenance of spindle waves

We detected a secondary depolarizing component in cortically-evoked EPSPs of RE neurons, as was also previously reported (Contreras et al., 1993). In the present study, this component occasionally occurred as an all-or-none event, appearing ~5 ms after the peak of the response, in cases of small amplitude EPSPs. Higher amplitude EPSPs presented always a secondary depolarizing component. The secondary depolarizing component of the EPSP was voltage dependent, as it was present at membrane potentials

as hyperpolarized as -100 mV, linearly increased with depolarization, and gave rise to action potentials as the membrane potential was close to firing threshold. Besides its voltage dependency, the secondary depolarizing component was sensitive to QX-314 in the recording pipette. The effect of QX-314 was also voltage dependent since it did not affect responses at voltages more negative than -80 mV. QX-314 is a blocker of many conductances; however, given the hyperpolarized membrane potential at which QX-314 exerted its effect, the secondary depolarizing component was probably due to the dendritic activation of T-current. The secondary component of evoked responses seems to be important for the integrative properties of RE neurons since it modulated both the neuronal output and its precise timing. Indeed, the secondary component was able to boost spike generation in RE neurons at membrane potentials more negative by 5-10 mV and to generate single or multiple spikes within a variable time window, as compared to stereotyped spikes generated by the peak of the early component of EPSPs when it reached the threshold. Consistent with an integrative role of the secondary depolarization, high-frequency stimulation induced temporal summation of evoked responses in a voltage dependent manner. Thus, even though cortical inputs are prevailing in the RE nucleus (Jones, 1975a; Liu and Jones, 1999) and may seem to control the activity of RE neurons (Contreras and Steriade, 1995, 1996), there is an intrinsic component in the membrane properties of those cells, which allow them to finely regulate their output.

The presence and contribution of persistent Na^+ currents cannot be discarded since its range of activation is close to the threshold for spike generation (5-10 mV below) and it is also blocked by QX-314 (Crill, 1996). Besides, studies in inhibitory

neurons from the hippocampus have demonstrated the presence and importance of active dendritic Na^+ conductances (Martina et al., 2000). It is thus possible that a joint contribution of Ca^{2+} and Na^+ dendritic currents acts in RE neurons for integration of cortical inputs.

Another effect of QX-314 on evoked responses was the two- to three-fold decrease in the rising slope. The rising phase of any active response depends on both its location in the dendritic tree and the active conductances that regulate its conduction to the soma (Rall, 1995; Magee, 2000). In our experiments, electrical stimulation of corticothalamic fibers frequently elicited fast-rising responses (5-10 mV/ms slope) in RE neurons. Recent experiments have shown that cortically evoked EPSPs are mainly AMPA-receptor-dependent, with a negligible element of NMDA-receptor response, which is virtually absent at hyperpolarized levels of membrane potential (-70 mV, (Gentet and Ulrich, 2004)). Even though the effect of QX-314 on the rising phase was not voltage dependent, a clear reduction was seen at different voltages in all cases, suggesting an additive contribution of active conductances to the AMPA component in the response.

The voltage dependent dendritic channel distribution in RE neurons provides them with important properties for integration of cortical inputs. We suggest that, in comparison with the effects these inputs exert on thalamocortical neurons, at which level dendritic currents generate high-frequency rhythms (Pedroarena and Llinás, 1997) that define brain alertness, the parallel activation of RE-cells' dendrites by synchronized

cortical volleys produces low-frequency oscillations (Contreras et al., 1993; Contreras and Steriade, 1996) that characterize the disconnected state of slow-wave sleep.

Hyperpolarizing potentials might initiate spindle oscillations in the thalamus

We have provided evidence for the presence of prolonged hyperpolarizing potentials (PHPs) preceding spindle oscillations in RE neurons. Though spindle oscillations in thalamic networks have longed been studied, the mechanism of its initiation has not been clearly elucidated. It has been proposed on the basis of *in vivo* studies and computational models that RE nucleus is able to generate by itself spindle waves, due mainly to the action of reversed $GABA_A$-IPSPs, which would trigger LTSs and bursting discharges, recruiting other neurons in the RE network (Bazhenov et al., 1999; Bazhenov et al., 2000). Our present results, provide evidence for an additional, non-exclusive mechanism for spindle initiation in the RE nucleus.

PHPs were present spontaneously in one third of the neurons studied (10 of 32), and in those cells, it was detected in ~60% of spindles, in apparently random fashion. Activation of corticothalamic afferents was able to elicit PHPs with similar characteristics as spontaneous ones (amplitude and duration), but in all those cases it was preceded by evoked EPSPs. The spontaneous PHP was itself occasionally headed by EPSPs (~30%) whose origin could therefore be attributed to corticothalamic inputs. These results suggest the possibility that PHPs might have, at least in some cases, a cortical origin.

Both spontaneous and evoked PHPs produced a significant drop in the R_{in} of RE neurons, suggesting the involvement of active inhibition processes. Therefore, disfacilitation processes, like those occurring during slow-oscillation activities (Steriade et al., 2001) were discarded as possible origin of the long hyperpolarizations heading spindles. The reversal potential of PHPs was quite hyperpolarized (~-100 mV), suggesting the activation of K^+ conductances (Huguenard and Prince, 1994; Ulrich and Huguenard, 1996b). The reversal potential for $GABA_A$-mediated IPSPs in the RE nucleus has been estimated in ~-70 mV (Zhang et al., 1997; Shu and McCormick, 2002). However, PHPs displayed significant amplitude at that range of membrane potential, discarding the possibility of $GABA_A$-mediated IPSPs implicated in the generation of PHPs. Moreover, the I-V relation for PHPs was linear for a large range of membrane potential values (-110 mV to -50 mV), implying a very little contribution, if not any, of $GABA_A$ potentials at membrane potentials more depolarized than -70 mV. Consistent with the activation of K^+ conductances during PHPs, QX-314 (50 mM) in the pipette decreased both their amplitude and incidence. QX-314 affects a wide range of membrane conductances, however, given the fact that PHPs are inhibitory potentials; it is unlikely that depolarizing currents (Ca^{2+} and Na^+) are implicated in the genesis of PHPs. On the other hand, it has been described that QX-314 blocks also G-protein-activated, inwardly rectifying K^+ (GIRK) channels (Andrade, 1991). This fact opens the possibility that PHP is an inhibitory potential activated by membrane metabotropic receptors coupled to second messenger cascades (Hille, 1992, 1994). Candidates for such an effect are $GABA_B$ receptors (Ulrich and Huguenard, 1996a), as well as the peptidergic receptors for

somatostatin (SST) (Sun et al., 2002) and neuropeptide Y (NPY) (Sun et al., 2001a; Sun et al., 2001b). All these molecules are expressed by RE neurons, as well as their respective agonists (Graybiel and Elde, 1983; Bendotti et al., 1990; Hoyer et al., 1995; Ulrich and Huguenard, 1996b; Sun et al., 2001a). Additionally, all these molecules initiate second-messenger cascades which end up in the activation of GIRK channels (Hille, 1994; Dolphin, 1998; Yamada et al., 1998). The case of $GABA_B$ receptors might be controversial, since experiments in slices have shown that rodents express very little $GABA_B$ responses in the RE nucleus (Ulrich and Huguenard, 1996b), contrary to the case of thalamocortical neurons, where $GABA_B$ responses are quite large (Ulrich and Huguenard, 1996b). Baclofen application to thalamic cells activated a K^+ conductance that was four times smaller in RE neurons with relay neurons (Ulrich and Huguenard, 1996b). These data suggested that the number of available $GABA_B$ receptors on RE neurons is smaller, and that the slow IPSPs that occur in only a subpopulation of RE neurons may remain subthreshold for LTS generation. However, these experiments performed *in vitro* did not asses the critical point, which is to know how much $GABA_B$ conductance is activated during thalamic oscillations, in which large populations of neurons fire in synchrony (Contreras et al., 1996a; Contreras and Steriade, 1996). Also, experiments in ferret slices have shown not so small $GABA_B$ components in response to glutamate applied in the perigeniculate nucleus (Sanchez-Vives and McCormick, 1997). In those experiments early bursting rebounds were blocked by the application of CGP 35348, and antagonist of $GABA_B$ receptors (Sanchez-Vives and McCormick, 1997). Therefore, the possibility that the RE nucleus expresses a significant $GABA_B$ response during spindle oscillations cannot be discarded. From our experiments it is not possible to

asses the precise ionic bases of PHP in RE neurons, but we can propose that at least one of the mentioned receptors (GABA, SST and NPY) constitutes the molecular basis of PHPs in the RE nucleus.

Computational models as well as experimental evidence have suggested strong electrical compartmentalization between dendrites and soma in RE neurons (Mulle et al., 1986; Destexhe et al., 1996). It is therefore reasonable to expect that an input to the distal dendrites would not have a dramatic effect on the soma, if its transfer to the soma depends only on passive properties. In the same way, current injection in the soma might well exert a local effect and not reach the dendrites. Early experiments in the RE nucleus showed that neurons have to be strongly hyperpolarized in the soma in order to be able to de-inactivate T-current and generate LTSs (Mulle et al., 1986). This was interpreted as distal location of T-current from the soma, likely dendritic. Indeed, later experiments proved the dendritic location of T-current in RE neurons (Destexhe et al., 1996). A similar reasoning suggested that PHP might well have a dendritic origin, since strong soma depolarization did not always increased PHP amplitude, but abolished it leaving instead a low-frequency discharge period. GIRK channels could be preferentially located in dendrites where they might mediate dendritic hyperpolarizations (Sun et al., 2001b). This is consistent with the idea of dendritic genesis of PHPs.

Our simultaneous intracellular and extracellular recordings proved that some neurons in the RE network were able to discharge during intracellularly recorded PHPs. These results suggest, although they do not directly demonstrate, that PHPs are locally

generated in the RE nucleus. The main inputs to the RE nucleus arise from dorsal thalamic nuclei, but especially from the cortical areas (Liu and Jones, 1999). However, all of them are of excitatory nature (Liu and Jones, 1999), and cannot be responsible for the direct generation of PHPs. The possibility of a disynaptic cortico-RE origin was supported by our results.

We propose that some cortical neuronal assembles may fire synchronously, thus activating RE neurons by their collaterals to the thalamus. Those RE neurons receiving projections from the cortex will display EPSPs of variable amplitudes, in some cases eliciting powerful LTSs. Indeed, our experiments show that to electrical stimulation of corticothalamic fibers induces responses which vary widely from cell to cell, even though the same stimulation parameters are conserved. Thus, a fraction of RE neurons will be excited and discharge over their neighbors, generating in some cases PHPs. In fact, there is evidence in RE neurons for the presence of both axo-axonic and dendro-dendritic synapses (Pinault et al., 1997), which mediate inhibitory interactions (Sanchez-Vives and McCormick, 1997; Shu and McCormick, 2002). Thus, the activation of PHPs might be relevant for the generation of spindle oscillations since these long-lasting potentials can hyperpolarize RE membranes to de-inactivate T-current, and thus elicit spike-bursts, essential for spindle oscillations (Steriade et al., 1990).

Dynamics of thalamic oscillations

Our results support the idea that thalamic spindles are highly integrated oscillations, since all properties of RE neurons described in the present series of articles showed to be relevant in one way or another for the occurrence of spindle waves in the thalamus. Each of the topics presented throughout these studies seem to be related to the internal dynamics of thalamic activity and the coordination of these different topics generate a contribution to a common result which is spindle oscillations.

The model we propose is not closed or exclusive, since it supports the large line of work dedicated to elucidate the cellular basis and functional significance of spindles, as highly coordinated and complex corticothalamic oscillations, initiated in the RE nucleus, maintained by RE-thalamic interactions, and later on transferred to the cortex.

The presentation of the model will start on an arbitrary point. However, given the cyclic nature of these oscillations any point in the circuit could be chosen to proceed.

Thus, in an initial step, the simultaneous activation of a significant number of corticothalamic inputs will generate EPSPs of variable amplitude in RE neurons, depending on the current state of activity and the synaptic contacts made on that particular sector of the RE nucleus. The existing state of activity in conjunction with the integrative properties of the secondary depolarizing component of the EPSP, will then determine the output for every single cell receiving the cortical input. As a result, some RE neurons will display a subthreshold EPSP, while others will present a suprathreshold

EPSP, whose spiking output might well be controlled by the properties of the secondary depolarization. If the cortical volley is strong enough, some other RE neurons will display an EPSP which will develop into a LTS, with several consequences on the neighboring cells (1, Fig. 9.1).

Some RE neurons are connected synaptically with some of their neighbors (~10%). Therefore, a presynaptic LTS will be transmitted not only to the relay nuclei from the dorsal thalamus, but also to some RE neurons were it will generate a prominent and prolonged hyperpolarization. Such hyperpolarizing potential generated by inhibitory neurons from the RE nucleus itself will deinactivate in some cases the T-current of the target neurons. In this way, a favorable environment for the generation and propagation of spindle activity will be attained in the RE nucleus (2, Fig. 9.1).

In addition to intrinsic chemical synaptic contacts, RE neurons also present electrical synapses which could display an important role in the propagation of thalamic oscillation. As LTSs are generated in RE neurons, neighboring cells connected by means of gap junctions will suffer a change in activity. Spike-to-spike synchronization is precluded due to the low-pass filter properties of gap junctions; however slow activities as the depolarizing envelope of LTSs is well transmitted through electrotonic contacts. Therefore, spindle waves could not only be propagated by electrical synapses but also synchronized to long distances (3, Fig. 9.1).

Coming back to the cortically generated EPSPs, which can generate multiple responses in target RE neurons, they can also produce the transition to a sustained active state in a subpopulation of cells. This sustained active state was shown to be related with the presence of membrane bistability, due to the generation of two clear-cut membrane modes in RE neurons recorded at resting conditions. Such a behavior is a consequence of intrinsic membrane properties of RE neurons and is relevant for the integration of incoming inputs. Most important however is the relevance for network activities in the thalamus. The activation of membrane bistability in some RE neurons seems to be sufficient to shape the general form of spindles not only in RE neurons, but also in thalamocortical neurons, the major targets of the RE nucleus and the secondary element in the generation of thalamic oscillations. Thus, while thalamocortical neurons receiving inputs from canonical RE neurons would display the typical waxing and waning pattern of sequential IPSPs during spindles; some thalamocortical neurons will receive also inputs from bistable RE neurons, and in those cases their spindling pattern should be different, affecting the general properties of the network oscillations (4, Fig. 9.1).

Finally, all these properties of RE neurons which are related to spindles are modulated by this oscillation. In fact, both synaptic and intrinsic membrane properties of RE neurons are modulated by spindles, both being enhanced during active network states. This suggests that the spindle rhythm is not necessarily a condition of low brain activity as has been classically considered, but it represents an internal, active state with its own dynamics (5, Fig. 9.1).

9.3. Figures

Figure 9.1. Integrated model of sleep spindle oscillations in the thalamic reticular nucleus. 1, Corticothalamic collaterals provide excitatory drive to RE neurons. A wave of excitation arising in the cortex may activate specific sectors in the RE nucleus. The spiking output will depend on the integrative properties of those cells, governed by the secondary depolarizing component of the cortico-reticular EPSPs. 2, Intrinsic chemical synapses in the RE nucleus can generate oscillatory rhythms. If it is strong enough, the activation of some RE neurons can generate rebound excitation in surrounding areas by de-inactivation of T-current in other RE neurons. Such a rebound excitation can be at the basis of spindle waves. 3, Electrical synapses in the RE nucleus. Gap junctions between RE neurons might have a role in spreading and synchronizing spindle oscillations in the thalamic network. 4, Corticothalamic collaterals provide excitatory drive to bistable RE neurons. A subpopulation of RE neurons is capable of expressing membrane bistability due to intrinsic properties, likely the expression of $Na_{(p)}$-current. Membrane bistability in RE neurons could have functional implications in shaping thalamic oscillation in the thalamus, both in RE and thalamocortical neurons. 5, Network oscillations modulate the membrane properties the cellular elements which generate the rhythms. Spindle waves exert a feedback modulation on RE neurons, affecting their membrane properties during periods of activity.

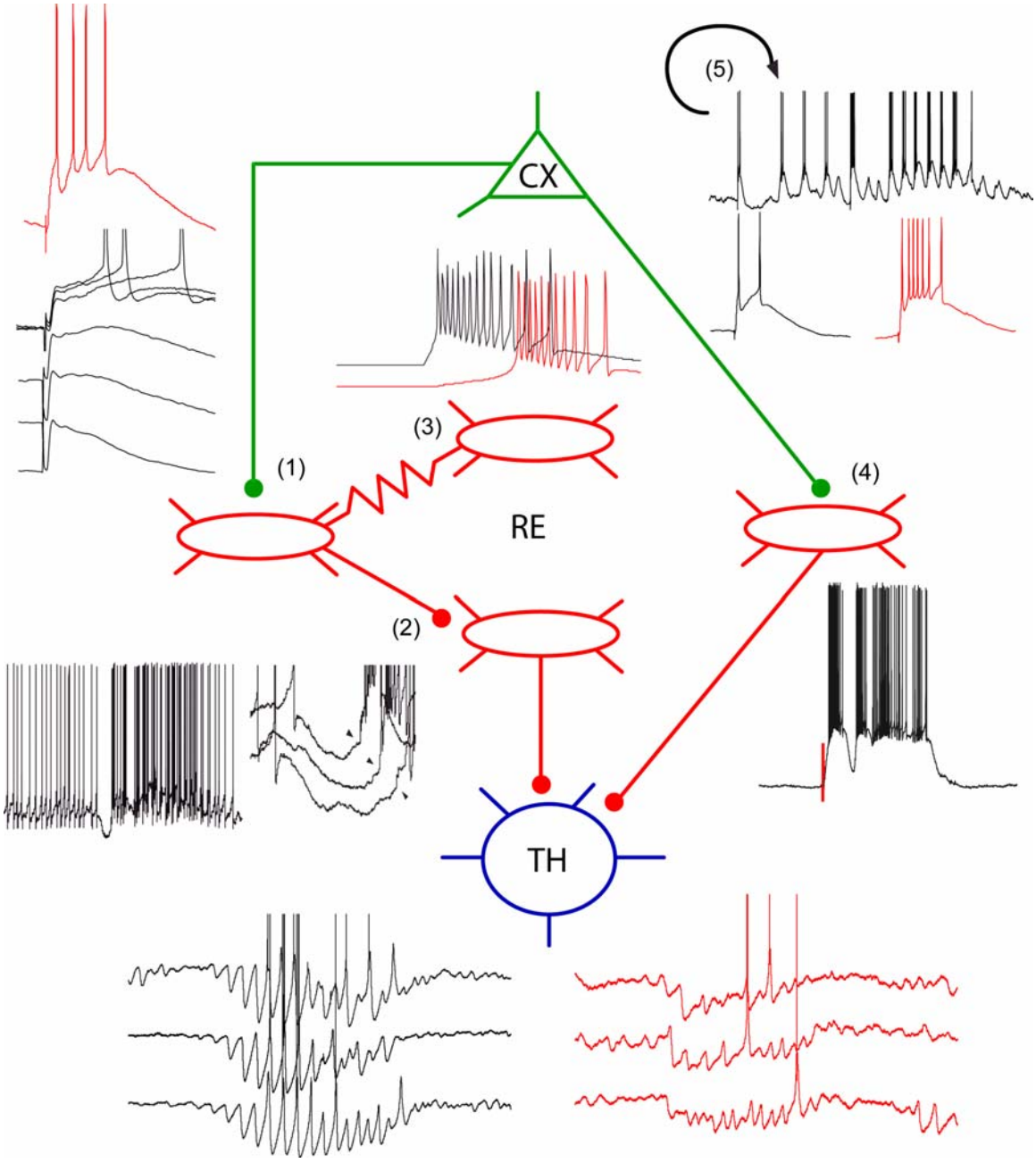
(5)
CX
(3)
(1)
RE
(4)
(2)
TH

BIBLIOGRAPHY

Agmon A, Yang LT, Jones EG, and O'Dowd DK. Topological precision in the thalamic projection to neonatal mouse barrel cortex. *J Neurosci* 15: 549-561, 1995.

Amzica F and Steriade M. Short- and long-range neuronal synchronization of the slow (< 1 Hz) cortical oscillation. *J Neurophysiol* 73: 20-38, 1995.

Amzica F and Steriade M. The K-complex: its slow (<1-Hz) rhythmicity and relation to delta waves. *Neurology* 49: 952-959, 1997.

Andrade R. Blockade of neurotransmitter-activated K+ conductance by QX-314 in the rat hippocampus. *Eur J Pharmacol* 199: 259-262, 1991.

Asanuma C and Porter LL. Light and electron microscopic evidence for a GABAergic projection from the caudal basal forebrain to the thalamic reticular nucleus in rats. *J Comp Neurol* 302: 159-172, 1990.

Asanuma C. GABAergic and pallidal terminals in the thalamic reticular nucleus of squirrel monkeys. *Exp Brain Res* 101: 439-451, 1994.

Avanzini G, de Curtis M, Panzica F, and Spreafico R. Intrinsic properties of nucleus reticularis thalami neurones of the rat studied in vitro. *J Physiol* 416: 111-122, 1989.

Bal T and McCormick DA. Mechanisms of oscillatory activity in guinea-pig nucleus reticularis thalami in vitro: a mammalian pacemaker. *J Physiol* 468: 669-691, 1993.

Bal T, von Krosigk M, and McCormick DA. Role of the ferret perigeniculate nucleus in the generation of synchronized oscillations in vitro. *J Physiol* 483 (Pt 3): 665-685, 1995a.

Bal T, von Krosigk M, and McCormick DA. Synaptic and membrane mechanisms underlying synchronized oscillations in the ferret lateral geniculate nucleus in vitro. *J Physiol* 483 (Pt 3): 641-663, 1995b.

Bal T and McCormick DA. What stops synchronized thalamocortical oscillations? *Neuron* 17: 297-308, 1996.

Barret JN. Motoneurons dendrites: role in synaptic integration. *Fred. Proc.* 34: 1398-1407, 1975.

Bazhenov M, Timofeev I, Steriade M, and Sejnowski TJ. Self-sustained rhythmic activity in the thalamic reticular nucleus mediated by depolarizing GABAA receptor potentials. *Nat Neurosci* 2: 168-174, 1999.

Bazhenov M, Timofeev I, Steriade M, and Sejnowski T. Spiking-bursting activity in the thalamic reticular nucleus initiates sequences of spindle oscillations in thalamic networks. *J Neurophysiol* 84: 1076-1087, 2000.

Bendotti C, Hohmann C, Forloni G, Reeves R, Coyle JT, and Oster-Granite ML. Developmental expression of somatostatin in mouse brain. II. In situ hybridization. *Brain Res Dev Brain Res* 53: 26-39, 1990.

Benevento LA, Rezak M, and Santos A. An autoradiographic study of the projections of the pretectum in the rhesus monkey (Macaca mulatta): evidence for sensorimotor links to the thalamus and oculomotor nuclei. *Brain Res* 127: 197-218, 1977.

Bennett DJ, Hultborn H, Fedirchuk B, and Gorassini M. Synaptic activation of plateaus in hindlimb motoneurons of decerebrate cats. *J Neurophysiol* 80: 2023-2037, 1998.

Berman N. Connections of the pretectum in the cat. *J Comp Neurol* 174: 227-254, 1977.

Bickford ME, Gunluk AE, Van Horn SC, and Sherman SM. GABAergic projection from the basal forebrain to the visual sector of the thalamic reticular nucleus in the cat. *J Comp Neurol* 348: 481-510, 1994.

Bourassa J, Pinault D, and Deschênes M. Corticothalamic projections from the cortical barrel field to the somatosensory thalamus in rats: a single-fibre study using biocytin as an anterograde tracer. *Eur J Neurosci* 7: 19-30, 1995.

Bourrat F and Sotelo C. Postnatal development of the inferior olivary complex in the rat. I. An electron microscopic study of the medial accessory olive. *Brain Res* 284: 291-310, 1983.

Brunton J and Charpak S. Heterogeneity of cell firing properties and opioid sensitivity in the thalamic reticular nucleus. *Neuroscience* 78: 303-307, 1997.

Chuang SC, Bianchi R, and Wong RK. Group I mGluR activation turns on a voltage-gated inward current in hippocampal pyramidal cells. *J Neurophysiol* 83: 2844-2853, 2000.

Cicirata F, Angaut P, Serapide MF, and Panto MR. Functional organization of the direct and indirect projection via the reticularis thalami nuclear complex from the motor cortex to the thalamic nucleus ventralis lateralis. *Exp Brain Res* 79: 325-337, 1990.

Cleland BG, Dubin MW, and Levick WR. Simultaneous recording of input and output of lateral geniculate neurones. *Nat New Biol* 231: 191-192, 1971.

Clemence AE and Mitrofanis J. Cytoarchitectonic heterogeneities in the thalamic reticular nucleus of cats and ferrets. *J Comp Neurol* 322: 167-180, 1992.

Conley M and Diamond IT. Organization of the Visual Sector of the Thalamic Reticular Nucleus in Galago. *Eur J Neurosci* 2: 211-226, 1990.

Conley M, Kupersmith AC, and Diamond IT. The Organization of Projections from Subdivisions of the Auditory Cortex and Thalamus to the Auditory Sector of the Thalamic Reticular Nucleus in Galago. *Eur J Neurosci* 3: 1089-1103, 1991.

Connors BW, Benardo LS, and Prince DA. Coupling between neurons of the developing rat neocortex. *J Neurosci* 3: 773-782, 1983.

Contreras D, Curro Dossi R, and Steriade M. Bursting and tonic discharges in two classes of reticular thalamic neurons. *J Neurophysiol* 68: 973-977, 1992.

Contreras D, Curro Dossi R, and Steriade M. Electrophysiological properties of cat reticular thalamic neurones in vivo. *J Physiol* 470: 273-294, 1993.

Contreras D and Steriade M. Cellular basis of EEG slow rhythms: a study of dynamic corticothalamic relationships. *J Neurosci* 15: 604-622, 1995.

Contreras D, Destexhe A, Sejnowski TJ, and Steriade M. Control of spatiotemporal coherence of a thalamic oscillation by corticothalamic feedback. *Science* 274: 771-774, 1996a.

Contreras D and Steriade M. Spindle oscillation in cats: the role of corticothalamic feedback in a thalamically generated rhythm. *J Physiol* 490 (Pt 1): 159-179, 1996.

Contreras D, Timofeev I, and Steriade M. Mechanisms of long-lasting hyperpolarizations underlying slow sleep oscillations in cat corticothalamic networks. *J Physiol* 494: 251-264, 1996b.

Contreras D, Destexhe A, Sejnowski TJ, and Steriade M. Spatiotemporal patterns of spindle oscillations in cortex and thalamus. *J Neurosci* 17: 1179-1196, 1997.

Cornwall J, Cooper JD, and Phillipson OT. Projections to the rostral reticular thalamic nucleus in the rat. *Exp Brain Res* 80: 157-171, 1990.

Cox CL, Huguenard JR, and Prince DA. Heterogeneous axonal arborizations of rat thalamic reticular neurons in the ventrobasal nucleus. *J Comp Neurol* 366: 416-430, 1996.

Cox CL, Huguenard JR, and Prince DA. Nucleus reticularis neurons mediate diverse inhibitory effects in thalamus. *Proc Natl Acad Sci U S A* 94: 8854-8859, 1997.

Crabtree JW. Prenatal development of retinocollicular projections in the rabbit: an HRP study. *J Comp Neurol* 286: 504-513, 1989.

Crabtree JW and Killackey HP. The Topographic Organization and Axis of Projection within the Visual Sector of the Rabbit's Thalamic Reticular Nucleus. *Eur J Neurosci* 1: 94-109, 1989.

Crabtree JW. The Somatotopic Organization Within the Cat's Thalamic Reticular Nucleus. *Eur J Neurosci* 4: 1352-1361, 1992.

Crabtree JW. Organization in the somatosensory sector of the cat's thalamic reticular nucleus. *J Comp Neurol* 366: 207-222, 1996.

Crabtree JW. Intrathalamic sensory connections mediated by the thalamic reticular nucleus. *Cell Mol Life Sci* 56: 683-700, 1999.

Crick F. Function of the thalamic reticular complex: the searchlight hypothesis. *Proc Natl Acad Sci U S A* 81: 4586-4590, 1984.

Crill WE. Persistent sodium current in mammalian central neurons. *Annu Rev Physiol* 58: 349-362, 1996.

Cucchiaro JB, Uhlrich DJ, and Sherman SM. Electron-microscopic analysis of synaptic input from the perigeniculate nucleus to the A-laminae of the lateral geniculate nucleus in cats. *J Comp Neurol* 310: 316-336, 1991.

Cucchiaro JB, Uhlrich DJ, and Sherman SM. Ultrastructure of synapses from the pretectum in the A-laminae of the cat's lateral geniculate nucleus. *J Comp Neurol* 334: 618-630, 1993.

Deschênes M, Madariaga-Domich A, and Steriade M. Dendrodendritic synapses in the cat reticularis thalami nucleus: a structural basis for thalamic spindle synchronization. *Brain Res* 334: 165-168, 1985.

Deschênes M, Bourassa J, Doan VD, and Parent A. A single-cell study of the axonal projections arising from the posterior intralaminar thalamic nuclei in the rat. *Eur J Neurosci* 8: 329-343, 1996.

Destexhe A, Contreras D, Sejnowski TJ, and Steriade M. A model of spindle rhythmicity in the isolated thalamic reticular nucleus. *J Neurophysiol* 72: 803-818, 1994a.

Destexhe A, Contreras D, Sejnowski TJ, and Steriade M. Modeling the control of reticular thalamic oscillations by neuromodulators. *Neuroreport* 5: 2217-2220, 1994b.

Destexhe A, Contreras D, Steriade M, Sejnowski TJ, and Huguenard JR. In vivo, in vitro, and computational analysis of dendritic calcium currents in thalamic reticular neurons. *J Neurosci* 16: 169-185, 1996.

Destexhe A and Paré D. Impact of network activity on the integrative properties of neocortical pyramidal neurons in vivo. *J Neurophysiol* 81: 1531-1547, 1999.

Destexhe A, Rudolph M, Fellous JM, and Sejnowski TJ. Fluctuating synaptic conductances recreate in vivo-like activity in neocortical neurons. *Neuroscience* 107: 13-24, 2001.

Destexhe A, Rudolph M, and Paré D. The high-conductance state of neocortical neurons in vivo. *Nat Rev Neurosci* 4: 739-751, 2003.

Devor A and Yarom Y. Generation and propagation of subthreshold waves in a network of inferior olivary neurons. *J Neurophysiol* 87: 3059-3069, 2002.

Dolphin AC. Mechanisms of modulation of voltage-dependent calcium channels by G proteins. *J Physiol* 506 (Pt 1): 3-11, 1998.

Domich L, Oakson G, and Steriade M. Thalamic burst patterns in the naturally sleeping cat: a comparison between cortically projecting and reticularis neurones. *J Physiol* 379: 429-449, 1986.

Draguhn A, Traub RD, Schmitz D, and Jefferys JG. Electrical coupling underlies high-frequency oscillations in the hippocampus in vitro. *Nature* 394: 189-192, 1998.

Dubin MW and Cleland BG. Organization of visual inputs to interneurons of lateral geniculate nucleus of the cat. *J Neurophysiol* 40: 410-427, 1977.

Edley SM and Graybiel AM. The afferent and efferent connections of the feline nucleus tegmenti pedunculopontinus, pars compacta. *J Comp Neurol* 217: 187-215, 1983.

Edwards SB and de Olmos JS. Autoradiographic studies of the projections of the midbrain reticular formation: ascending projections of nucleus cuneiformis. *J Comp Neurol* 165: 417-431, 1976.

Eysel UT, Pape HC, and Van Schayck R. Excitatory and differential disinhibitory actions of acetylcholine in the lateral geniculate nucleus of the cat. *J Physiol* 370: 233-254, 1986.

Fellous JM, Rudolph M, Destexhe A, and Sejnowski TJ. Synaptic background noise controls the input/output characteristics of single cells in an in vitro model of in vivo activity. *Neuroscience* 122: 811-829, 2003.

Fitzpatrick D, Penny GR, and Schmechel DE. Glutamic acid decarboxylase-immunoreactive neurons and terminals in the lateral geniculate nucleus of the cat. *J Neurosci* 4: 1809-1829, 1984.

Fricker D and Miles R. EPSP amplification and the precision of spike timing in hippocampal neurons. *Neuron* 28: 559-569, 2000.

Gentet LJ and Ulrich D. Strong, reliable and precise synaptic connections between thalamic relay cells and neurones of the nucleus reticularis in juvenile rats. *J Physiol* 546: 801-811, 2003.

Gentet LJ and Ulrich D. Electrophysiological characterization of synaptic connections between layer VI cortical cells and neurons of the nucleus reticularis thalami in juvenile rats. *Eur J Neurosci* 19: 625-633, 2004.

Graybiel AM and Elde RP. Somatostatin-like immunoreactivity characterizes neurons of the nucleus reticularis thalami in the cat and monkey. *J Neurosci* 3: 1308-1321, 1983.

Guillery RW. Anatomical evidence concerning the role of the thalamus in corticocortical communication: a brief review. *J Anat* 187 (Pt 3): 583-592, 1995.

Guillery RW, Feig SL, and Lozsadi DA. Paying attention to the thalamic reticular nucleus. *Trends Neurosci* 21: 28-32, 1998.

Hale PT, Sefton AJ, Baur LA, and Cottee LJ. Interrelations of the rat's thalamic reticular and dorsal lateral geniculate nuclei. *Exp Brain Res* 45: 217-229, 1982.

Harting JK, Van Lieshout DP, and Feig S. Connectional studies of the primate lateral geniculate nucleus: distribution of axons arising from the thalamic reticular nucleus of Galago crassicaudatus. *J Comp Neurol* 310: 411-427, 1991.

Hartings JA, Temereanca S, and Simons DJ. High responsiveness and direction sensitivity of neurons in the rat thalamic reticular nucleus to vibrissa deflections. *J Neurophysiol* 83: 2791-2801, 2000.

Hendrickson AE, Ogren MP, Vaughn JE, Barber RP, and Wu JY. Light and electron microscopic immunocytochemical localization of glutamic acid decarboxylase in monkey geniculate complex: evidence for gabaergic neurons and synapses. *J Neurosci* 3: 1245-1262, 1983.

Hendry SH, Jones EG, Hockfield S, and McKay RD. Neuronal populations stained with the monoclonal antibody Cat-301 in the mammalian cerebral cortex and thalamus. *J Neurosci* 8: 518-542, 1988.

Heyward P, Ennis M, Keller A, and Shipley MT. Membrane bistability in olfactory bulb mitral cells. *J Neurosci* 21: 5311-5320, 2001.

Hille B. *Ion Channels of Excitable Membranes*. Sunderland, MA: Sinauer, 1992.

Hille B. Modulation of ion-channel function by G-protein-coupled receptors. *Trends Neurosci* 17: 531-536, 1994.

Hirsch JC, Fourment A, and Marc ME. Electrophysiological study of the perigeniculate region during natural sleep in the cat. *Exp Neurol* 77: 436-454, 1982.

Ho N and Destexhe A. Synaptic background activity enhances the responsiveness of neocortical pyramidal neurons. *J Neurophysiol* 84: 1488-1496, 2000.

Houser CR, Vaughn JE, Barber RP, and Roberts E. GABA neurons are the major cell type of the nucleus reticularis thalami. *Brain Res* 200: 341-354, 1980.

Hoyer D, Bell GI, Berelowitz M, Epelbaum J, Feniuk W, Humphrey PP, O'Carroll AM, Patel YC, Schonbrunn A, Taylor JE, and et al. Classification and nomenclature of somatostatin receptors. *Trends Pharmacol Sci* 16: 86-88, 1995.

Hughes SW, Cope DW, Toth TI, Williams SR, and Crunelli V. All thalamocortical neurones possess a T-type Ca2+ 'window' current that enables the expression of bistability-mediated activities. *J Physiol* 517 (Pt 3): 805-815, 1999.

Hughes SW, Blethyn KL, Cope DW, and Crunelli V. Properties and origin of spikelets in thalamocortical neurones in vitro. *Neuroscience* 110: 395-401, 2002.

Huguenard JR and Prince DA. A novel T-type current underlies prolonged Ca(2+)-dependent burst firing in GABAergic neurons of rat thalamic reticular nucleus. *J Neurosci* 12: 3804-3817, 1992.

Huguenard JR and Prince DA. Intrathalamic rhythmicity studied in vitro: nominal T-current modulation causes robust antioscillatory effects. *J Neurosci* 14: 5485-5502, 1994.

Huguenard JR. Low-threshold calcium currents in central nervous system neurons. *Annu Rev Physiol* 58: 329-348, 1996.

Ide LS. The fine structure of the perigeniculate nucleus in the cat. *J Comp Neurol* 210: 317-334, 1982.

Jones EG. Some aspects of the organization of the thalamic reticular complex. *J Comp Neurol* 162: 285-308, 1975a.

Jones EG. Lamination and differential distribution of thalamic afferents within the sensory-motor cortex of the squirrel monkey. *J Comp Neurol* 160: 167-203, 1975b.

Jones EG. *The Thalamus*. New York: Plenum, 1985.

Jones EG. Thalamic circuitry and thalamocortical synchrony. *Philos Trans R Soc Lond B Biol Sci* 357: 1659-1673, 2002.

Jones HE and Sillito AM. The length-response properties of cells in the feline perigeniculate nucleus. *Eur J Neurosci* 6: 1199-1204, 1994.

Kim U, Bal T, and McCormick DA. Spindle waves are propagating synchronized oscillations in the ferret LGNd in vitro. *J Neurophysiol* 74: 1301-1323, 1995.

Kim U, Sanchez-Vives MV, and McCormick DA. Functional dynamics of GABAergic inhibition in the thalamus. *Science* 278: 130-134, 1997.

Kim U and McCormick DA. Functional and ionic properties of a slow afterhyperpolarization in ferret perigeniculate neurons in vitro. *J Neurophysiol* 80: 1222-1235, 1998.

Kultas-Ilinsky K, Yi H, and Ilinsky IA. Nucleus reticularis thalami input to the anterior thalamic nuclei in the monkey: a light and electron microscopic study. *Neurosci Lett* 186: 25-28, 1995.

Landisman CE, Long MA, Beierlein M, Deans MR, Paul DL, and Connors BW. Electrical synapses in the thalamic reticular nucleus. *J Neurosci* 22: 1002-1009, 2002.

Lee KH and McCormick DA. Modulation of spindle oscillations by acetylcholine, cholecystokinin and 1S,3R-ACPD in the ferret lateral geniculate and perigeniculate nuclei in vitro. *Neuroscience* 77: 335-350, 1997.

Levey AI, Hallanger AE, and Wainer BH. Cholinergic nucleus basalis neurons may influence the cortex via the thalamus. *Neurosci Lett* 74: 7-13, 1987.

Leznik E, Makarenko V, and Llinás R. Electrotonically mediated oscillatory patterns in neuronal ensembles: an in vitro voltage-dependent dye-imaging study in the inferior olive. *J Neurosci* 22: 2804-2815, 2002.

Liu XB, Warren RA, and Jones EG. Synaptic distribution of afferents from reticular nucleus in ventroposterior nucleus of cat thalamus. *J Comp Neurol* 352: 187-202, 1995.

Liu XB and Jones EG. Predominance of corticothalamic synaptic inputs to thalamic reticular nucleus neurons in the rat. *J Comp Neurol* 414: 67-79, 1999.

Llinás R and Sugimori M. Electrophysiological properties of in vitro Purkinje cell dendrites in mammalian cerebellar slices. *J Physiol* 305: 197-213, 1980a.

Llinás R and Sugimori M. Electrophysiological properties of in vitro Purkinje cell somata in mammalian cerebellar slices. *J Physiol* 305: 171-195, 1980b.

Loewenstein Y, Yarom Y, and Sompolinsky H. The generation of oscillations in networks of electrically coupled cells. *Proc Natl Acad Sci U S A* 98: 8095-8100, 2001.

Long MA, Landisman CE, and Connors BW. Small clusters of electrically coupled neurons generate synchronous rhythms in the thalamic reticular nucleus. *J Neurosci* 24: 341-349, 2004.

Lozsadi DA. Organization of cortical afferents to the rostral, limbic sector of the rat thalamic reticular nucleus. *J Comp Neurol* 341: 520-533, 1994.

Lozsadi DA. Organization of connections between the thalamic reticular and the anterior thalamic nuclei in the rat. *J Comp Neurol* 358: 233-246, 1995.

Lubke J. Morphology of neurons in the thalamic reticular nucleus (TRN) of mammals as revealed by intracellular injections into fixed brain slices. *J Comp Neurol* 329: 458-471, 1993.

Magee JC. Dendritic integration of excitatory synaptic input. *Nat Rev Neurosci* 1: 181-190, 2000.

Makarenko V and Llinás R. Experimentally determined chaotic phase synchronization in a neuronal system. *Proc Natl Acad Sci U S A* 95: 15747-15752, 1998.

Martina M, Vida I, and Jonas P. Distal initiation and active propagation of action potentials in interneuron dendrites. *Science* 287: 295-300, 2000.

McCormick DA and Pape HC. Properties of a hyperpolarization-activated cation current and its role in rhythmic oscillation in thalamic relay neurones. *J Physiol* 431: 291-318, 1990.

McCormick DA, Trent F, and Ramoa AS. Postnatal development of synchronized network oscillations in the ferret dorsal lateral geniculate and perigeniculate nuclei. *J Neurosci* 15: 5739-5752, 1995.

McCormick DA and Bal T. Sleep and arousal: thalamocortical mechanisms. *Annu Rev Neurosci* 20: 185-215, 1997.

McCormick DA, Shu Y, Hasenstaub A, Sanchez-Vives M, Badoual M, and Bal T. Persistent cortical activity: mechanisms of generation and effects on neuronal excitability. *Cereb Cortex* 13: 1219-1231, 2003.

Mitchell SJ and Silver RA. Shunting inhibition modulates neuronal gain during synaptic excitation. *Neuron* 38: 433-445, 2003.

Mitrofanis J and Baker GE. Development of the thalamic reticular and perireticular nuclei in rats and their relationship to the course of growing corticofugal and corticopetal axons. *J Comp Neurol* 338: 575-587, 1993.

Mitrofanis J and Guillery RW. New views of the thalamic reticular nucleus in the adult and the developing brain. *Trends Neurosci* 16: 240-245, 1993.

Molinari M, Hendry SH, and Jones EG. Distributions of certain neuropeptides in the primate thalamus. *Brain Res* 426: 270-289, 1987.

Montero VM, Guillery RW, and Woolsey CN. Retinotopic organization within the thalamic reticular nucleus demonstrated by a double label autoradiographic technique. *Brain Res* 138: 407-421, 1977.

Montero VM. Ultrastructural identification of synaptic terminals from cortical axons and from collateral axons of geniculo-cortical relay cells in the perigeniculate nucleus of the cat. *Exp Brain Res* 75: 65-72, 1989.

Morris BJ. Neuronal localisation of neuropeptide Y gene expression in rat brain. *J Comp Neurol* 290: 358-368, 1989.

Mukhametov LM, Rizzolatti G, and Tradardi V. Spontaneous activity of neurones of nucleus reticularis thalami in freely moving cats. *J Physiol* 210: 651-667, 1970.

Mulle C, Madariaga A, and Deschênes M. Morphology and electrophysiological properties of reticularis thalami neurons in cat: in vivo study of a thalamic pacemaker. *J Neurosci* 6: 2134-2145, 1986.

Nauta HJ. Projections of the pallidal complex: an autoradiographic study in the cat. *Neuroscience* 4: 1853-1873, 1979.

Oertel WH, Graybiel AM, Mugnaini E, Elde RP, Schmechel DE, and Kopin IJ. Coexistence of glutamic acid decarboxylase- and somatostatin-like immunoreactivity in neurons of the feline nucleus reticularis thalami. *J Neurosci* 3: 1322-1332, 1983.

Ohara PT and Lieberman AR. The thalamic reticular nucleus of the adult rat: experimental anatomical studies. *J Neurocytol* 14: 365-411, 1985.

Paré D, Steriade M, Deschênes M, and Oakson G. Physiological characteristics of anterior thalamic nuclei, a group devoid of inputs from reticular thalamic nucleus. *J Neurophysiol* 57: 1669-1685, 1987.

Paré D, Smith Y, Parent A, and Steriade M. Projections of brainstem core cholinergic and non-cholinergic neurons of cat to intralaminar and reticular thalamic nuclei. *Neuroscience* 25: 69-86, 1988.

Paré D and Steriade M. The reticular thalamic nucleus projects to the contralateral dorsal thalamus in macaque monkey. *Neurosci Lett* 154: 96-100, 1993.

Parent A and Steriade M. Midbrain tegmental projections of nucleus reticularis thalami of cat and monkey: a retrograde transport and antidromic invasion study. *J Comp Neurol* 229: 548-558, 1984.

Partridge LD and Swandulla D. Calcium-activated non-specific cation channels. *Trends Neurosci* 11: 69-72, 1988.

Pedroarena C and Llinás R. Dendritic calcium conductances generate high-frequency oscillation in thalamocortical neurons. *Proc Natl Acad Sci U S A* 94: 724-728, 1997.

Peinado JM, Gomez-Capilla JA, Mora F, and Osorio C. Putative amino acid neurotransmitters and the nucleus dorsomedialis thalamus-prefrontal cortex pathway in the rat. *Brain Res Bull* 10: 421-424, 1983.

Penny GR, Conley M, Schmechel DE, and Diamond IT. The distribution of glutamic acid decarboxylase immunoreactivity in the diencephalon of the opossum and rabbit. *J Comp Neurol* 228: 38-56, 1984.

Petersen CC, Grinvald A, and Sakmann B. Spatiotemporal dynamics of sensory responses in layer 2/3 of rat barrel cortex measured in vivo by voltage-sensitive dye imaging combined with whole-cell voltage recordings and neuron reconstructions. *J Neurosci* 23: 1298-1309, 2003.

Pinault D, Bourassa J, and Deschênes M. The axonal arborization of single thalamic reticular neurons in the somatosensory thalamus of the rat. *Eur J Neurosci* 7: 31-40, 1995a.

Pinault D, Bourassa J, and Deschênes M. Thalamic reticular input to the rat visual thalamus: a single fiber study using biocytin as an anterograde tracer. *Brain Res* 670: 147-152, 1995b.

Pinault D, Smith Y, and Deschênes M. Dendrodendritic and axoaxonic synapses in the thalamic reticular nucleus of the adult rat. *J Neurosci* 17: 3215-3233, 1997.

Pinault D and Deschênes M. Projection and innervation patterns of individual thalamic reticular axons in the thalamus of the adult rat: a three-dimensional, graphic, and morphometric analysis. *J Comp Neurol* 391: 180-203, 1998a.

Pinault D and Deschênes M. Anatomical evidence for a mechanism of lateral inhibition in the rat thalamus. *Eur J Neurosci* 10: 3462-3469, 1998b.

Raczkowski D and Fitzpatrick D. Organization of cholinergic synapses in the cat's dorsal lateral geniculate and perigeniculate nuclei. *J Comp Neurol* 288: 676-690, 1989.

Rall W. *The Theoretical Foundation of Dendritic Function*: MA:MIT Press, 1995.

Rinvik E, Ottersen OP, and Storm-Mathisen J. Gamma-aminobutyrate-like immunoreactivity in the thalamus of the cat. *Neuroscience* 21: 781-805, 1987.

Robson JA and Martin-Elkins CL. The effects of monocular deprivation on the size of GAD+ neurons in the cat's dorsal lateral geniculate nucleus. *J Comp Neurol* 239: 62-74, 1985.

Rose JE. Some modern aspects of the functional anatomy of the thalamus. *Monatsschr Psychiatr Neurol* 120: 378-387, 1950.

Sanchez-Vives MV and McCormick DA. Functional properties of perigeniculate inhibition of dorsal lateral geniculate nucleus thalamocortical neurons in vitro. *J Neurosci* 17: 8880-8893, 1997.

Scheibel ME and Scheibel AB. The organization of the nucleus reticularis thalami: a Golgi study. *Brain Res* 1: 43-62, 1966.

Scheibel ME and Scheibel AB. Structural organization of nonspecific thalamic nuclei and their projection toward cortex. *Brain Res* 6: 60-94, 1967.

Schiller J, Major G, Koester HJ, and Schiller Y. NMDA spikes in basal dendrites of cortical pyramidal neurons. *Nature* 404: 285-289, 2000.

Schwindt P and Crill W. Mechanisms underlying burst and regular spiking evoked by dendritic depolarization in layer 5 cortical pyramidal neurons. *J Neurophysiol* 81: 1341-1354, 1999.

Shibata H. Topographic organization of subcortical projections to the anterior thalamic nuclei in the rat. *J Comp Neurol* 323: 117-127, 1992.

Shosaku A and Sumitomo I. Auditory neurons in the rat thalamic reticular nucleus. *Exp Brain Res* 49: 432-442, 1983.

Shosaku A, Kayama Y, and Sumitomo I. Somatotopic organization in the rat thalamic reticular nucleus. *Brain Res* 311: 57-63, 1984.

Shosaku A. A comparison of receptive field properties of vibrissa neurons between the rat thalamic reticular and ventro-basal nuclei. *Brain Res* 347: 36-40, 1985.

Shu Y and McCormick DA. Inhibitory interactions between ferret thalamic reticular neurons. *J Neurophysiol* 87: 2571-2576, 2002.

Sillito AM and Kemp JA. The influence of GABAergic inhibitory processes on the receptive field structure of X and Y cells in cat dorsal lateral geniculate nucleus (dLGN). *Brain Res* 277: 63-77, 1983.

Singer W. Control of thalamic transmission by corticofugal and ascending reticular pathways in the visual system. *Physiol Rev* 57: 386-420, 1977.

Spreafico R, de Curtis M, Frassoni C, and Avanzini G. Electrophysiological characteristics of morphologically identified reticular thalamic neurons from rat slices. *Neuroscience* 27: 629-638, 1988.

Stacey WC and Durand DM. Synaptic noise improves detection of subthreshold signals in hippocampal CA1 neurons. *J Neurophysiol* 86: 1104-1112, 2001.

Steriade M and Wyzinski P. Cortically elicited activities in thalamic reticularis neurons. *Brain Res* 42: 514-520, 1972.

Steriade M, Oakson G, and Ropert N. Firing rates and patterns of midbrain reticular neurons during steady and transitional states of the sleep-waking cycle. *Exp Brain Res* 46: 37-51, 1982.

Steriade M, Parent A, and Hada J. Thalamic projections of nucleus reticularis thalami of cat: a study using retrograde transport of horseradish peroxidase and fluorescent tracers. *J Comp Neurol* 229: 531-547, 1984.

Steriade M, Deschênes M, Domich L, and Mulle C. Abolition of spindle oscillations in thalamic neurons disconnected from nucleus reticularis thalami. *J Neurophysiol* 54: 1473-1497, 1985.

Steriade M, Domich L, and Oakson G. Reticularis thalami neurons revisited: activity changes during shifts in states of vigilance. *J Neurosci* 6: 68-81, 1986.

Steriade M, Domich L, Oakson G, and Deschênes M. The deafferented reticular thalamic nucleus generates spindle rhythmicity. *J Neurophysiol* 57: 260-273, 1987a.

Steriade M, Parent A, Paré D, and Smith Y. Cholinergic and non-cholinergic neurons of cat basal forebrain project to reticular and mediodorsal thalamic nuclei. *Brain Res* 408: 372-376, 1987b.

Steriade M, Jones EG, and Llinás RR. *Thalamic oscillations and signaling*. New York: Wiley-Interscience, 1990.

Steriade M, Curro Dossi R, and Contreras D. Electrophysiological properties of intralaminar thalamocortical cells discharging rhythmic (approximately 40 HZ) spike-bursts at approximately 1000 HZ during waking and rapid eye movement sleep. *Neuroscience* 56: 1-9, 1993a.

Steriade M, McCormick DA, and Sejnowski TJ. Thalamocortical oscillations in the sleeping and aroused brain. *Science* 262: 679-685, 1993b.

Steriade M and Contreras D. Relations between cortical and thalamic cellular events during transition from sleep patterns to paroxysmal activity. *J Neurosci* 15: 623-642, 1995.

Steriade M, Jones EG, and McCormick DA. *Thalamus*. Oxford: Elsevier Science Ltd., 1997.

Steriade M. *The intact and sliced bran*. MA: The MIT Press, 2001.

Steriade M, Timofeev I, and Grenier F. Natural waking and sleep states: a view from inside neocortical neurons. *J Neurophysiol* 85: 1969-1985, 2001.

Sugitani M. Electrophysiological and sensory properties of the thalamic reticular neurones related to somatic sensation in rats. *J Physiol* 290: 79-95, 1979.

Sun QQ, Akk G, Huguenard JR, and Prince DA. Differential regulation of GABA release and neuronal excitability mediated by neuropeptide Y1 and Y2 receptors in rat thalamic neurons. *J Physiol* 531: 81-94, 2001a.

Sun QQ, Huguenard JR, and Prince DA. Neuropeptide Y receptors differentially modulate G-protein-activated inwardly rectifying K+ channels and high-voltage-activated Ca2+ channels in rat thalamic neurons. *J Physiol* 531: 67-79, 2001b.

Sun QQ, Huguenard JR, and Prince DA. Somatostatin inhibits thalamic network oscillations in vitro: actions on the GABAergic neurons of the reticular nucleus. *J Neurosci* 22: 5374-5386, 2002.

Swandulla D and Lux HD. Activation of a nonspecific cation conductance by intracellular Ca2+ elevation in bursting pacemaker neurons of Helix pomatia. *J Neurophysiol* 54: 1430-1443, 1985.

Swanson LW and Hartman BK. The central adrenergic system. An immunofluorescence study of the location of cell bodies and their efferent connections in the rat utilizing dopamine-beta-hydroxylase as a marker. *J Comp Neurol* 163: 467-505, 1975.

Tamas G, Buhl EH, Lorincz A, and Somogyi P. Proximally targeted GABAergic synapses and gap junctions synchronize cortical interneurons. *Nat Neurosci* 3: 366-371, 2000.

Temereanca S and Simons DJ. Functional topography of corticothalamic feedback enhances thalamic spatial response tuning in the somatosensory whisker/barrel system. *Neuron* 41: 639-651, 2004.

Timofeev I, Contreras D, and Steriade M. Synaptic responsiveness of cortical and thalamic neurones during various phases of slow sleep oscillation in cat. *J Physiol* 494: 265-278, 1996.

Timofeev I and Steriade M. Cellular mechanisms underlying intrathalamic augmenting responses of reticular and relay neurons. *J Neurophysiol* 79: 2716-2729, 1998.

Timofeev I, Bazhenov M, Sejnowski TJ, and Steriade M. Contribution of intrinsic and synaptic factors in the desynchronization of thalamic oscillatory activity. *Thalamus & Related Systems* 1: 53-69, 2001.

Toth TI, Hughes SW, and Crunelli V. Analysis and biophysical interpretation of bistable behaviour in thalamocortical neurons. *Neuroscience* 87: 519-523, 1998.

Traub RD, Schmitz D, Jefferys JG, and Draguhn A. High-frequency population oscillations are predicted to occur in hippocampal pyramidal neuronal networks interconnected by axoaxonal gap junctions. *Neuroscience* 92: 407-426, 1999a.

Traub RD, Whittington MA, Buhl EH, Jefferys JG, and Faulkner HJ. On the mechanism of the gamma --> beta frequency shift in neuronal oscillations induced in rat hippocampal slices by tetanic stimulation. *J Neurosci* 19: 1088-1105, 1999b.

Uhlrich DJ, Cucchiaro JB, Humphrey AL, and Sherman SM. Morphology and axonal projection patterns of individual neurons in the cat perigeniculate nucleus. *J Neurophysiol* 65: 1528-1541, 1991.

Uhlrich DJ and Manning KA. Projection of individual axons from the pretectum to the dorsal lateral geniculate complex in the cat. *J Comp Neurol* 363: 147-159, 1995.

Ulrich D and Huguenard JR. GABAB receptor-mediated responses in GABAergic projection neurones of rat nucleus reticularis thalami in vitro. *J Physiol* 493 (Pt 3): 845-854, 1996a.

Ulrich D and Huguenard JR. Gamma-aminobutyric acid type B receptor-dependent burst-firing in thalamic neurons: a dynamic clamp study. *Proc Natl Acad Sci U S A* 93: 13245-13249, 1996b.

Villa AE. Physiological differentiation within the auditory part of the thalamic reticular nucleus of the cat. *Brain Res Brain Res Rev* 15: 25-40, 1990.

von Krosigk M, Bal T, and McCormick DA. Cellular mechanisms of a synchronized oscillation in the thalamus. *Science* 261: 361-364, 1993.

Wang XJ and Rinzel J. Spindle rhythmicity in the reticularis thalami nucleus: synchronization among mutually inhibitory neurons. *Neuroscience* 53: 899-904, 1993.

Warren RA and Jones EG. Glutamate activation of cat thalamic reticular nucleus: effects on response properties of ventroposterior neurons. *Exp Brain Res* 100: 215-226, 1994.

Waters J, Larkum M, Sakmann B, and Helmchen F. Supralinear Ca2+ influx into dendritic tufts of layer 2/3 neocortical pyramidal neurons in vitro and in vivo. *J Neurosci* 23: 8558-8567, 2003.

Welsh JP and Llinás R. Some organizing principles for the control of movement based on olivocerebellar physiology. *Prog Brain Res* 114: 449-461, 1997.

Williams SR, Toth TI, Turner JP, Hughes SW, and Crunelli V. The 'window' component of the low threshold Ca2+ current produces input signal amplification and bistability in cat and rat thalamocortical neurones. *J Physiol* 505 (Pt 3): 689-705, 1997.

Williamson AM, Ohara PT, and Ralston HJ, 3rd. Electron microscopic evidence that cortical terminals make direct contact onto cells of the thalamic reticular nucleus in the monkey. *Brain Res* 631: 175-179, 1993.

Williamson AM, Ohara PT, Ralston DD, Milroy AM, and Ralston HJ, 3rd. Analysis of gamma-aminobutyric acidergic synaptic contacts in the thalamic reticular nucleus of the monkey. *J Comp Neurol* 349: 182-192, 1994.

Woolf NJ and Butcher LL. Cholinergic systems in the rat brain: III. Projections from the pontomesencephalic tegmentum to the thalamus, tectum, basal ganglia, and basal forebrain. *Brain Res Bull* 16: 603-637, 1986.

Yamada M, Inanobe A, and Kurachi Y. G protein regulation of potassium ion channels. *Pharmacol Rev* 50: 723-760, 1998.

Yen CT, Conley M, Hendry SH, and Jones EG. The morphology of physiologically identified GABAergic neurons in the somatic sensory part of the thalamic reticular nucleus in the cat. *J Neurosci* 5: 2254-2268, 1985.

Zhang SJ, Huguenard JR, and Prince DA. GABAA receptor-mediated Cl- currents in rat thalamic reticular and relay neurons. *J Neurophysiol* 78: 2280-2286, 1997.